eman ta zabal zazu

Universidad
del País Vasco

Euskal Herriko
Unibertsitatea

A STUDY OF METAL-ORGANIC FRAMEWORK SORPTION PHENOMENA IN SOLUTION

Nagore Barroso García

PhD Thesis 2023

Supervisors:
Dr Oscar Castillo
Dr Stefan Wuttke

eman ta zabal zazu

Universidad
del País Vasco

Euskal Herriko
Unibertsitatea

A STUDY OF METAL-ORGANIC FRAMEWORK SORPTION PHENOMENA IN SOLUTION

Nagore Barroso García

2023

Supervisors: Dr Stefan Wuttke

Dr Oscar Castillo

Leioa, April 2023

Agradecimientos

Este es el fin de una etapa. Una etapa que empezó el día que decidí estudiar química, aunque jamás imaginé que escogería este camino. Todo empezó con un laboratorio vacío y cientos de cajas que desempaquetar. Tras poco más de tres años en el BCMaterials, una pandemia mundial y otras muchas cosas, ha llegado el día más esperado. Con esto cierro una etapa de mi vida, dura y de mucho sufrimiento, pero que me ha servido para crecer tanto profesional como personalmente y la que me ha ayudado a darme cuenta de cuál es mi verdadera pasión: la enseñanza.

En el camino me han acompañado muchas personas sin las cuales esto hubiera sido casi imposible y a las que quiero agradecer que hayan estado junto a mí. Para empezar, gracias a mis directores Oscar y Stefan, por mostrarme cuán grande puede ser la pasión por la ciencia y por orientarme en todo el proceso. Especialmente por haberme guiado tan bien y haber sabido sacar lo mejor de mi. Gracias a todos los que han formado parte del Wuttkegroup, por las excursiones, los group meeting y las comidas. Al personal de administración por la paciencia infinita, al grupo de escalada del que tanto aprendí en esas soleadas tardes que pasamos en Urduliz y a muchos más.

En lo personal, quiero agradecer a María, a Maider y a las Panchis por aguantarme y quererme siempre. A mis padres, por habernos sacado adelante con tanto esfuerzo y trabajo, por enseñarme todo lo que se y por hacer de mi la persona que soy hoy. A Ander, por protegerme, por confiar en mí más de lo que yo lo hago y por haber sido siempre un referente. A Laura y a Mari. A Aitor, por hacerme la vida más fácil y sobretodo, por tu empeño en querer entender mi mundo que ni yo misma entiendo. A mis abuelas/os, pero en especial quiero dedicarle esta tesis a mi abuelo, mi héroe. Hace tiempo que no estás aquí para ver todo lo que he conseguido, pero hoy sé que estarías orgullosa de mí.

«El éxito no es definitivo, el fracaso no es fatal: lo que cuenta es el valor de continuar»

— *Winston S. Churchill*

«A veces me falla el coraje y pienso que debo dejar de trabajar, vivir en el campo y dedicarme a la jardinería. Pero estoy atada por mil lazos, y no sé cuándo podré arreglar las cosas de otra manera. Tampoco sé si, aun escribiendo libros científicos, podría vivir sin el laboratorio»

— Marie Curie

«Aprendí que los principios dan miedo y los finales son tristes y que lo importante es caminar juntos»

— Mi Abuelo

Table of Contents

Abstract

Throughout history, the use of materials has been of great importance. The first civilizations were classified based on the type of materials that were mainly used; Stone Age, Copper Age, Bronze Age and Iron Age. This points out the great relevance that materials have had and still have in society highlighting the role of Materials Science, whose main objective is to investigate the relationship between the properties and the structure of materials and which has allowed us to study and expand the field. Among all the most relevant materials, porous materials stand out, whose first use dates back to the year 3000 BC., when the Egyptians and Sumerians first employed coal for medicinal use. Advances in science and technology gave way to new discoveries such as zeolites in the 18th century, porous polymeric networks at the beginning of the 20th century or hybrid inorganic-organic compounds. In this last group, metal-organic frameworks can be found (MOFs).

Research in the field of MOFs has increased considerably since their discovery at the end of the 90s. This fact is due to the great chemical versatility that they offer since there are infinite possible combinations between the metallic nodes and the organic connectors. This enables us to vary the properties and, therefore, define their possible applications. Reticular chemistry offers scientists a powerful tool that allows them to design and/or predict the possible structures of porous materials, mostly those with rigid and robust geometry. One of the most important characteristics of these materials is the great porosity and surface area that they present, making them unique in their field. On the other hand, its physical-chemical stability and the possibility of adapting the MOFs to the required needs, whether it is obtaining variable pore sizes or decorating with specific functional groups, will determine the application in different fields (storage and gas separation, water remediation, biomedical applications, sensors, catalysis…).

To all this, we must add the possibility of controlling both the size and the morphology of the particles, another determining factor in the translation of these materials towards specific applications. Due to this, it is of main importance to identify and control the variables (concentration, solvent, temperature, pH, surfactants...) that affect the shape and size of the material particles, with the aim of offering reproducible synthesis protocols.

Abstract

Although the use of these porous materials for different applications has been proposed over the years, the common thread of this thesis is the study of different MOFs for adsorption processes in solution that have been less developed than gas phase adsorption processes, for which there are already well-established protocols for their characterization. In the six chapters that make up this thesis, the three most relevant points of Materials Science converge: the synthesis, characterization and applicability of MOFs.

Chapter 1 is a general introduction in which porous materials and their evolution until the discovery of MOFs are put into context, as well as a detailed description of their properties and characteristics, also mentioning the relevance that nanoparticles are acquiring. Along with this, the most used synthesis methods are described emphasizing the control of the shape and size of the particles of these materials. Likewise, this first chapter addresses the characterization techniques that this type of material required. Finally, a review of the possible applications of these materials is made, which usually have as a common denominator: the interaction of the high internal surface of MOFs with the molecules or entities that enter their channels/pores for storage, separation of other molecules, transformation (catalysis), identification and quantification (sensory), among others.

Chapter 2 is devoted to the synthesis and characterization of MOFs prepared and presented in the thesis memory, where a detailed description of the synthesis protocols is offered, as well as the structural characteristics of each MOF. Due to the great importance of obtaining particles whose shape and size are well-defined, the main objective of the first part of the chapter is to study the effect of different parameters (time, modulator, solvents or the concentration of reagents) on the shape and size of the particles. For this, well-known MOFs made up of different metals (Zr, Zn, Co, and Fe) and organic linkers (2-methylimidazole, fumaric acid, and terephthalic or 2-aminoterephthalic acid) were selected: Zr-fumarate, UiO-66, UiO-66-NH$_2$, ZIF-8, ZIF-67 and MIL-88A. In the second part of the chapter, the synthesis and characterization for other different MOFs (MOF-74(Co, Ni, Cu), MIL-127(Fe), Cu-TDPAT, JUK-8, ZU-301) are summarized. In this case, such an in-depth study of the synthesis parameters was not carried out, but rather they were synthesized following previous protocols

existing in the scientific literature. Most of the MOFs reported in this chapter were specifically prepared to be used in *Chapter 3*, *Chapter 4* and *Chapter* 5 of this thesis.

In *Chapter 3,* a new characterization technique suitable for adsorption processes in solution with materials whose metallic centre is paramagnetic is developed. Currently, the characterization of the adsorption properties that take place in the gas phase is highly developed, while for the processes in solution, most of the techniques are based on an indirect determination of the adsorption based on the decrease in the amount of adsorbate present in solution. This can give rise to certain errors, as in the case of molecules that are not completely soluble. Despite being adsorbed, their concentration would remain constant due to the equilibrium formed with the solid state of the adsorbate. All this has led to the development of a new technique called Magnetic Sustentation, which is mainly based on determining the minimum magnetic field required to keep the particles of a paramagnetic MOF attached to the pole of the electromagnet while they are submerged in a liquid. This value, known as the critical magnetic field, is determined before and after the adsorption experiment. The observed variation can be correlated with the amount of adsorbate captured by the MOF. In the chapter, this new technique is explained in detail, the theoretical development of the equations that govern this phenomenon is made and the existence of a linear relationship between the percentage of adsorbed mass and the critical magnetic field is demonstrated. The experiments have been carried out using MIL-88A(Fe), MOF-74(Cu, Co) and ZIF-67(Co), using water as a solvent for the first MOF due to its stability in it and ethanol for the others. This chapter demonstrates the versatility of the technique since, in addition to offering us the possibility of directly quantifying the percentage captured and being independent of the nature of the adsorbate, it offers the possibility of using different solvents. Finally, the possibility of preparing adsorption isotherms has been demonstrated and they have been compared with the adsorption isotherms obtained by traditional methods of indirect determination such as UV-Vis spectroscopy to demonstrate the reliability of the new technique. In addition, when preparing adsorption isotherms for acetonitrile, a non-quantifiable adsorbate in UV-Vis, one of the great advantages of Magnetic Sustentation has been demonstrated: the total independence with respect to the properties of the adsorbate.

Abstract

Following this thread, *Chapter 4* focuses on the use of MIL-88A(Fe) which, in addition to being paramagnetic and allowing its characterization with the new technique described above, has a flexible structure. MIL-88A is one of the MOFs with the highest breathing (expansion/contraction capacity) that exists, and this, together with its stability in water, has allowed us to study the capture/recovery of alcohols from water. Today, alcohols are widely used in industry, which has created difficulties when it comes to separating them from water. Among the most widely used alcohols, methanol causes great concern. Although it is not a toxic substance *per se*, its degradation products (formaldehyde and formic acid) are toxic. Currently, most methods for separating alcohols and water require large amounts of energy. Because of that, the objective of this chapter is the study of the flexible behaviour of MIL-88A in the capture of short-chain aliphatic alcohols (methanol, ethanol, n-propanol, isopropyl alcohol, n-butyl alcohol, sec-butyl alcohol, isobutyl alcohol and *tert*-butyl alcohol). On the one hand, the amount of alcohol that the MOF is capable of adsorbing after being immersed for 24 h in a diluted aqueous solution of the different alcohols has been quantified. The results show an inversely linear trend of the mass of alcohol incorporated with respect to the molecular volume of the alcohol, reaching the highest values for methanol (19.7%) and the lowest for *n-butyl alcohol* (11.5%). However, for branched alcohols, with adsorption values lower than the previous ones, the dependence concerning the volume ceases to exist and a dependence concerning the cross-section of the alcohol is established. In order to understand these experimental results, various theoretical studies have been carried out to explain the differences in adsorption between linear and branched alcohols and the diffusion problems presented by these last molecules. On the other hand, competitive studies have been carried out between different alcohols, demonstrating a greater affinity for the more hydrophobic ones, despite their larger size. Likewise, being aware of the difficulty involved in recovering the powdered material after these adsorption experiments in the liquid phase, the possibility of embedding the powdered material in polymeric membranes has been studied. For this purpose, polyvinylidene fluoride (PVDF) has been selected due to its high chemical and thermal stability, ease of processing and hydrophobicity. In addition to the synthesis and characterization of membranes with different MOF mass percentages, their use has been tested for the adsorption of methanol and ethanol at very low concentrations. It has been demonstrated the synergistic effect

that exists between the polymeric matrix and the porous material, with values substantially superior to those expected from the adsorptive behaviour of each of the components separately.

In *Chapter 5* of the thesis, a pioneering study has been carried out in the field of porous materials and water remediation. For the first time, a systematic study of different MOFs for the capture of carbon dioxide and the generated carbonate species in water has been done to deal with the acidification of water caused by global warming. For the study, MOFs with high adsorption capacities (MOF-74(Ni), MIL-127(Fe), Cu-TDPAT, UiO-66-NH$_2$, UiO-66, JUK-8) with different properties such as open metal sites, chemisorption or flexibility and high selectivity (ZU-301) have been chosen. Due to the different species that carbon dioxide presents depending on the pH, the behaviour of all MOFs was studied at pH 2, 6.3, 8.0 and 10.0 where the main species are CO_2, HCO_3^-/CO_2, HCO_3^- and HCO_3^-/CO_3^{2-}, respectively. After determining the stability of the materials at all pHs, the adsorption capacity of each MOF within its pH stability zone was studied. Moreover, preliminary experiments for CO_2 removal from real-world water samples, collected from lakes, rivers and the Mediterranean Sea were performed as a way to gage the material behaviour in more complex environments.

Finally, *Chapter 6* summarizes the main conclusions derived from this research, in addition to possible future work, in which it would be interesting to focus in future research. In general, the importance of the three basic pillars of materials research has been demonstrated: synthesis, characterization and applicability. The synthesis of well-known MOFs have been optimized with the aim of offering reliable and modifiable protocols depending on the required characteristics. In addition, a characterization technique has been developed with the aim of offering alternatives to conventional techniques. In general, the potential of MOFs for adsorption processes in solution and especially, in water, to adsorb organic species –alcohols- or inorganic –carbon dioxide and carbonate ions- was evaluated.

Resumen

A lo largo de la historia, el uso de los materiales ha tenido una gran importancia, llegando a clasificar a las primeras civilizaciones en función del tipo de material que se usaba, siendo las principales eras la Edad de Piedra, la Edad de Cobre, la Edad de Bronce y la Edad de Hierro. Esto pone en valor la gran relevancia que han tenido y tienen los materiales en la sociedad, destacando así el papel de la Ciencia de materiales, cuyo objetivo principal reside en investigar la relación de las propiedades de un material con su estructura, la cual ha permitido estudiar y ampliar el campo de estudio. Entre todos los materiales destacan los materiales porosos, cuyos primeros usos se remontan al año 3000 a.c. dónde los egipcios y Sumerios usaron por primera vez el carbón para uso medicinal. El avance en ciencia y tecnología abrió paso a nuevos descubrimientos cómo las zeolitas en el siglo XVIII, las redes poliméricas porosas a principios del siglo XX o los compuestos inorgánicos-orgánicos híbridos. En este último grupo se encuentran las estructuras metal-orgánicas, comúnmente conocidas por su término anglosajón *Metal-Organic Frameworks* (MOFs).

La investigación en el campo de los MOFs ha aumentado considerablemente desde su descubrimiento a finales de los años 90. Este hecho se debe a la gran versatilidad química que ofrecen, ya que existen infinitas combinaciones posibles entre los nodos metálicos y los conectores orgánicos, siendo posible variar las propiedades y, por lo tanto, definir sus posibles aplicaciones. La química reticular ofrece una poderosa herramienta a los científicos que permite diseñar y/o predecir las posibles estructuras de los materiales porosos, mayormente los de geometría rígida y robusta. Una de las características más importantes de estos materiales es la gran porosidad y área superficial que presentan haciéndolos únicos en su campo. Por otro lado, su estabilidad físico-química y la posibilidad de adecuar los MOFs a las necesidades requeridas, ya sea obtener tamaño de poros variables o decorarlos con grupos funcionales específicos, determinarán su aplicación en diferentes ámbitos (almacenamiento y separación de gases, sensórica, catálisis…). A todo esto, hay que sumarle la posibilidad de controlar tanto el tamaño como la morfología de las partículas, otro factor determinante en la traslación de estos materiales hacia aplicaciones concretas. Debido a ello, es de principal importancia identificar y controlar las variables (concentración, disolvente, temperatura, pH,

surfactantes…) que afectan a la forma y tamaño de las partículas del material, con el objetivo de ofrecer protocolos de síntesis reproducibles.

Aunque a lo largo de los años se ha propuesto el uso de estos materiales porosos para diferentes aplicaciones, el hilo conductor de esta tesis es el estudio de diferentes MOFs en procesos de adsorción en disolución que han sido menos desarrollados que los procesos de adsorción en fase gaseosa para los que ya existen protocolos bien establecidos para su caracterización. En los seis capítulos que forman esta tesis convergen los tres puntos más relevantes en la Ciencia de Materiales: la síntesis, caracterización y la aplicabilidad de los MOFs.

El *Capítulo 1* es una introducción general en la cual se ponen en contexto los materiales porosos y su evolución hasta el descubrimiento de los MOFs, así como una detallada descripción de las propiedades y características de los mismos, mencionando también la relevancia que están adquiriendo las nanopartículas de estos materiales. Junto con ello, se describen los métodos de síntesis más usados haciendo hincapié en el control de la forma y tamaño de las partículas de estos materiales. Asimismo, en este primer capítulo se abordan las técnicas de caracterización que este tipo de materiales requieren. Finalmente, se hace un repaso de las posibles aplicaciones de estos materiales, que suelen tener como denominador común la interacción de la elevada superficie interna del material con las moléculas o entidades que ingresan en sus canales/poros para su almacenamiento, separación de otras moléculas, transformación (catálisis), identificación y cuantificación (sensórica) entre otras.

El *Capítulo 2*, está destinado a la síntesis y caracterización de los MOFs preparados y presentados en la memoria de tesis, donde se ofrece una detallada descripción de los protocolos de síntesis, así como de las características estructurales de cada MOF. Debido a la gran importancia de obtener partículas cuya forma y tamaño estén bien definidas, el objetivo principal de la primera parte del capítulo es estudiar el efecto de diferentes parámetros (tiempo, modulador, disolventes o la concentración de los reactivos) en la forma y tamaño de las partículas. Para ello, se seleccionaron MOFs muy conocidos formados por diferentes metales (Zr, Zn, Co y Fe) y conectores orgánicos (2-metilimidazol, ácido fumárico y ácido tereftálico o 2-aminotereftálico): Zr-fumarate, UiO-66, UiO-66-NH$_2$, ZIF-8, ZIF-67 and MIL-88A. En la segunda parte del capítulo, se

incluyen los resultados obtenidos para otros MOFs diferentes (MOF-74(Co, Ni, Cu), MIL-127(Fe), Cu-TDPAT, JUK-8, ZU-301) donde no se realizó un estudio tan en profundidad de los parámetros de síntesis, sino que fueron sintetizados siguiendo protocolos previos existentes en la literatura científica. La mayoría de los MOFs fueron preparados especificamente para ser utilizados en los *Capítulos 3, 4* y *5* de esta tesis.

En el *Capítulo 3*, se describe y desarrolla una nueva técnica de caracterización, apta para procesos de adsorción en disolución con materiales cuyo centro metálico sea paramagnético. Actualmente, la caracterización de las propiedades de adsorción que tienen lugar en fase gas están altamente desarrollados, mientras que, para los procesos en disolución, la mayoría de las técnicas se basan en una determinación indirecta de la adsorción basada en la disminución de la cantidad de adsorbato presente en disolución. Esto puede dar lugar a ciertos errores, como es el caso de moléculas que no sean completamente solubles, ya que, a pesar de ser adsorbidos, su concentración se mantendría constante debido al equilibrio formado con el estado sólido del adsorbato. Todo esto, ha motivado el desarrollo de una nueva técnica denominada Sustentación Magnética y que se basa principalmente en determinar el campo magnético mínimo requerido para mantener las partículas de un MOF paramagnético adheridas al polo del electroimán mientras se encuentran sumergidas en un líquido. Este valor, conocido como campo magnético crítico, es determinado antes y después del experimento de adsorción. La variación observada puede correlacionarse con la cantidad de adsorbato capturada por el MOF. En el capítulo, se explica en detalle esta novedosa técnica, se hace el desarrollo teórico de las ecuaciones que rigen este fenómeno y se demuestra la existencia de una relación lineal entre el porcentaje de la masa adsorbida y el campo magnético crítico. Los experimentos se han llevado a cabo con los MOFs: MIL-88A(Fe), MOF-74(Cu, Co) y ZIF-67(Co), usando agua como disolvente para el primer MOF debido a su estabilidad en ella y etanol para los otros. En este capítulo se demuestra la versatilidad de la técnica, ya que además de ofrecernos la posibilidad de cuantificar directamente el porcentaje capturado independientemente de la naturaleza del adsorbato, ofrece la posibilidad de usar diferentes disolventes. Finalmente, se ha demostrado la posibilidad de preparar isotermas de adsorción y se han comparado con las isotermas de adsorción obtenidas por métodos tradicionales de determinación indirecta como UV-Vis a fin de demostrar la fiabilidad de la nueva técnica. Además, al preparar isotermas de adsorción para

Resumen

acetonitrilo, un adsorbato no-cuantificable en UV-Vis, se ha demostrado una de las grandes ventajas de la Sustentación Magnética: la total independencia con respecto a las propiedades del adsorbato.

Siguiendo este hilo, el *Capítulo 4* se enfoca en el uso del MIL-88A(Fe) que además de ser paramagnético y permitir su caracterización con la nueva técnica descrita anteriormente, posee una estructura flexible. MIL-88A es uno de los MOFs con mayor capacidad de expansión/contracción que existe, y eso, junto con su estabilidad en agua, nos ha permitido estudiar la captura/recuperación de alcoholes en agua. Hoy en día, se hace un uso muy extendido de los alcoholes en la industria, lo que ha generado una dificultad a la hora de separarlos del agua. Entre los alcoholes más usados, el metanol causa grandes preocupaciones, ya que, aunque *per sé* no sea una sustancia toxica, sí lo son sus productos de degradación: el formaldehido y el ácido fórmico. Actualmente, la mayoría de los métodos de separación de alcoholes y agua requieren grandes cantidades de energía. Debido a ello, el objetivo de este capítulo es el estudio del comportamiento flexible del MIL-88A en la captura de alcoholes alifáticos de cadena corta (metanol, etanol, alcohol n- e isopropílico y alcohol n-*,* sec-, iso y *tert*-butílico). Por un lado, se ha cuantificado la cantidad de alcohol que el MOF es capaz de adsorber tras estar inmerso durante 24 h en una disolución acuosa diluida de los diferentes alcoholes. Los resultados muestran una tendencia inversamente lineal de la masa de alcohol incorporada con respecto al volumen molecular del alcohol, alcanzándose los valores más altos para metanol (19.7%) y los más bajos para el alcohol n-butílico (11.5%). Sin embargo, para los alcoholes ramificados, con valores de adsorción más bajos que los anteriores, la dependencia con respecto al volumen deja de existir y se establece una dependencia con respecto a la sección transversal del alcohol. Para entender estos resultados experimentales, se han realizaron diversos estudios teóricos que permiten atribuir las diferencias en la adsorción entre los alcoholes lineales y ramificados a los problemas de difusión que presentan estas últimas moléculas. Por otro lado, se han hecho estudios de competitividad entre diferentes alcoholes demostrando una mayor afinidad por los más hidrofóbicos, a pesar de su mayor tamaño. Asimismo, siendo conscientes de la dificultad que entraña la recuperación del material en polvo tras estos experimentos de adsorción en fase líquida, se ha estudiado la posibilidad de embeber el material en polvo en membranas poliméricas. Para ello se ha seleccionado el fluoruro de polivinilideno,

comúnmente conocido por sus siglas PVDF provenientes de su nombre en inglés, por su alta estabilidad química y térmica, facilidad de procesado e hidrofobicidad. Además de la síntesis y caracterización de membranas con diferente porcentaje en masa del MOF, se ha probado su uso para la adsorción de metanol y etanol a muy baja concentración, demostrando el efecto sinérgico que existe entre la matriz polimérica y el material poroso, con valores sustancialmente superiores a los esperables, en base al comportamiento adsorptivo de cada uno de los componentes por separado.

En el *Capítulo 5* de la tesis, se ha llevado a cabo un estudio pionero en el ámbito de los materiales porosos y remediación de aguas. Por primera vez, se ha hecho un estudio sistemático de diferentes MOFs para la captura del carbono dióxido e iones de carbonato presente en el agua para hacer frente a la acidificación de las aguas causada entre otras cosas por el calentamiento global. Para el estudio, se han seleccionado MOFs con altas capacidades de adsorción (MOF-74(Ni), MIL-127(Fe), Cu-TDPAT, UiO-66-NH$_2$, UiO-66, JUK-8) y alta selectividad (ZU-301). Debido a las diferentes especies que presenta el carbono dióxido en función del pH, se estudió el comportamiento de todos los MOFs a pH 2, 6.3, 8.0 y 10.0 dónde las especies mayoritarias son CO_2, HCO_3^-/CO_2, HCO_3^- y HCO_3^-/CO_3^2, respectivamente. Tras determinar la estabilidad de los materiales en el rango de pHs, se estudió la capacidad de adsorción de cada MOF dentro de su zona de estabilidad. Además, se realizaron experimentos preliminares para la eliminación de CO_2 de muestras de agua del mundo real, recolectadas de lagos, ríos y el mar Mediterráneo, para medir el comportamiento del material en entornos más complejos.

Finalmente, en el *Capítulo 6* se resumen las principales conclusiones derivadas de esta investigación, además del posible trabajo a futuro en el que sería interesante centrarse en próximas investigaciones. En general, se ha demostrado la importancia de los tres pilares básicos de la investigación de los materiales: síntesis, caracterización y aplicabilidad. Se han optimizado las síntesis de MOFs muy conocidos con el objetivo de ofrecer protocolos fiables y modificables en función de las características requeridas. Además, se ha desarrollado una técnica de caracterización con el objetivo de ofrecer alternativas a las técnicas convencionales. En general, se ha evaluado el potencial de los MOFs en procesos de adsorción en disolución y en especial, en agua, para adsorber especies orgánicas –alcoholes- o inorgánicas –carbono dióxido e iones de carbonato-.

Laburpena

Historian zehar, materialen erabilerak garrantzi handia izan du. Izan ere, erabilitako material motaren arabera lehen zibilizazioak sailkatuak izan dira, aro nagusiak Harri Aroa, Kobre Aroa, Brontze Aroa eta Burdin Aroa izanik. Honek materialek gizartean izan duten eta oraindik duten garrantzi handia nabarmentzen du Materialen Zientziaren eginkizuna azpimarratuz, zeinaren helburu nagusia material batek bere egiturarekin duen erlazioa ikertzea baita, ikerketa-eremua aztertzea eta zabaltzea ahalbidetu duena. Material esanguratsuenen artean, material porotsuak nabarmentzen dira. Lehen erabilerak egiptoarrek eta sumertarren esku egon ziren, ikatza sendagai gisa erabiltzen hasi zirelarik K.a. 3000. urte inguruan. Zientzia eta teknologiaren aurrerapenek aurkikuntza berriei lekua eman zieten, hala nola, zeolitak XVIII. mendean, sare polimeriko porotsuak XX. mendearen hasieran edo konposatu ez-organiko-organiko hibridoak. Azken talde honetan egitura metal-organikoak daude, *Metal-Organic Frameworks* (MOFs) termino anglosaxoiarekin ezagutzen direnak.

MOFen eremuko ikerketa nabarmen handitu da 90eko hamarkadaren amaieran aurkitu zirenetik, aldakortasun kimiko handiari zor zaiona, gehienbat. Izan ere, metalezko nodoen eta konektore organikoen artean konbinazio posibleak amaigabeak dira, zeinak propietateak moldatzeko aukera eskaintzen duten, horien balizko aplikazioak definitu ahal izateko. Kimika erretikularrak edo sare-kimikak tresna indartsu bat eskaintzen die zientzialariei, material porotsuen egitura diseinatzeko eta/edo aurreikusteko aukera ematen diena, gehienbat geometria zurrun eta sendoa duten materialetan. Material hauen ezaugarri azpimarragarrien artean, porositate eta azalera-eremu handiak aurki daitezke. Bestalde, bere egonkortasun fisiko-kimikoak eta MOFak eskatutako beharretara egokitzeko aukerak, hots poro-tamaina aldakorrak lortu edota talde funtzional espezifikoak erabiltzea, euren aplikazioa hainbat esparrutan baldintzatuko du (biltegiratzea eta gasen bereizketa, sentsoreak, katalisia, biomedikuntza, etab.).

Horri guztiari, partikulen tamaina zein morfologia kontrolatzeko aukera gehitu behar zaio, hori baita material horiek aplikazio zehatzetara eramateko beste faktore erabakigarri bat. Hori dela eta, garrantzitsua da materialaren partikulen forman eta tamainan eragiten duten aldagaiak (kontzentrazioa, disolbatzailea, tenperatura, pH,

surfaktanteak...) identifikatzea eta kontrolatzea, sintesi-protokolo erreproduzigarriak eskaintzeko helburuarekin.

Urteetan zehar material porotsu hauek aplikazio desberdinetarako erabiltzea proposatu diren arren, tesi honen helburu nagusia MOFen funtzionamendua disoluzioan gertatzen diren adsortzio-prozesuetan aztertzea da. Izan ere, gas-faseko adsortzio-prozesuak baino gutxiago garatu dira, azkenengoentzat karakterizatzeko ondo ezarritako protokoloak daudelarik. Tesi hau osatzen duten sei kapituluetan Materialen Zientziako hiru puntu garrantzitsuenak bat egiten dute: MOFen sintesia, karakterizazioa eta erabilgarritasuna.

1. kapitulua sarrera orokor bat da. Bertan, material porotsuak MOFak aurkitu arte pairatu duten bilakaera testuinguruan jartzen da. Gainera, haien propietate eta ezaugarrien deskribapen zehatza egiten da, MOF nanopartikulak hartzen ari diren garrantzia ere aipatuz. Horrekin batera, gehien erabiltzen diren sintesi-metodoak deskribatzen dira, material horien partikulen forma eta tamainaren kontrola azpimarratuz. Era berean, lehen kapitulu honetan MOFek behar dituzten karakterizazio-teknikak jorratzen dira. Azkenik, material hauen balizko aplikazioen berrikuspena egiten da, izendatzaile komun gisa materialaren barne-azalera handiaren eta kanaletan/poroetan sartzen diren molekulen edo entitateen arteko interakzioa duena.

2. kapitulua memorian prestatu eta aurkeztutako MOFen sintesia eta karakterizazioari eskaintzen zaio, non sintesi-protokoloen deskribapen zehatza eskaintzen den, baita MOF bakoitzaren egitura-ezaugarriak ere. Forma eta tamaina ondo zehaztuta duten partikulak lortzeak duen garrantzi handia dela eta, kapituluaren lehen zatiaren helburu nagusia parametro ezberdinek (denbora, modulatzailea, disolbatzaileak edo erreaktiboen kontzentrazioa) ezaugarri hauetan duten eragina aztertzea da. Horretarako, metal (Zr, Zn, Co eta Fe) eta molekula organiko desberdinez (2-metilimidazol, azido fumarikoa eta azido tereftaliko edo 2-aminotereftaliko) osatutako MOF oso ezagunak aukeratu dira: Zr-fumaratoa, UiO-66, UiO-66-NH$_2$, ZIF-8, ZIF-67 eta MIL-88A. Kapituluaren bigarren zatian, beste MOF batzuetarako lortutako emaitzak erakusten dira (MOF-74 (Co, Ni, Cu), MIL-127 (Fe), Cu-TDPAT, JUK-8, ZU-301). Kasu honetan, ez zen sintesi-parametroen azterketa hain sakona egin, baizik eta literatura zientifikoan aurretik zeuden protokoloei jarraiki sintetizatu ziren. MOF gehienak tesi honetan erabiltzeko prestatuak izan dira, *3., 4. eta 5. kapituluetan* erabiltzeko, hain zuzen ere.

3. kapituluan, karakterizazio-teknika berri bat deskribatzen eta garatzen da, zentro metalikoa paramagnetikoa duten materialekin disoluzioan gertatzen diren adsortzio-prozesuetarako egokia dena. Gaur egun, gas-fasean gertatzen diren adsortzio-propietateen karakterizazioa oso garatuta dago. Disoluzioan gertatzen diren prozesuetarako, berriz, teknika gehienak adsorbatoaren zeharkako determinazioan oinarritzen dira, disoluzioan dagoen adsorbato-kantitatearen murrizketan oinarrituta. Horrek akats batzuk sor ditzake guztiz disolbagarriak ez diren molekulen kasuan bezala; adsorbatoaren egoera solidoarekin osatutako oreka dela eta, haien kontzentrazioa konstante mantenduko litzatekelako adsorbatuak izan arren. Honen ondorioz, *Magnetic Sustentation* izeneko teknika berri bat garatu da. Teknika hau, batez ere, MOF paramagnetiko baten partikulak likido batean murgilduta dauden bitartean elektroimanaren polora itsatsiak mantentzeko behar den gutxieneko eremu magnetikoa zehaztean oinarritzen da. Balio hau, eremu magnetiko kritiko bezala ezagutzen dena, adsortzio-esperimentuaren aurretik eta ondoren zehazten da. Behatutako aldakuntza MOFak harrapatutako adsorbato-kantitatearekin lotu daiteke. Kapituluan, teknika berri hau zehatz-mehatz azaltzen da, fenomeno hau gobernatzen duten ekuazioen garapen teorikoa eginez eta adsorbatutako masa-ehunekoaren eta eremu magnetiko kritikoaren arteko erlazio lineala dagoela frogatuz. Esperimentuak MIL-88A(Fe), MOF-74(Cu, Co) eta ZIF-67(Co) MOFekin egin dira, MIL-88A(Fe)-rako ura disolbatzaile gisa aukeratuz bertan duen egonkortasunagatik eta etanola, aldiz, besteentzako. Kapitulu honek teknikaren aldakortasuna erakusten du, izan ere, harrapatutako ehunekoa zuzenean kuantifikatzeko aukera eskaintzeaz eta adsorbatoaren izaeratik independentea izateaz gain, disolbatzaile desberdinak erabiltzeko aukera eskaintzen du. Azkenik, adsortzio-isotermak prestatzeko aukera frogatu da eta zeharkako determinazioko metodo tradizionalen bidez lortutako adsortzio-isotermekin alderatu dira, hala nola ultramore-ikuskor (UM-ikus) espektroskopiarekin, teknika berriaren fidagarritasuna frogatzeko asmoz. Gainera, azetonitrilorako isotermak prestatzerakoan, UM-ikus-ean adsorbato ez-kuantifikagarria dena, *Magnetic Sustentation* teknikaren abantaila handietako bat frogatu da: adsorbatoaren propietateekiko erabateko independentzia.

Hari horri jarraiki, *4. kapitulua* MIL-88A(Fe) delakoaren erabileran zentratzen da, bere izaera paramagnetikoak garatutako teknika berriaren bidezko karakterizazioa ahalbidetzeaz gain, egitura malgua baitu. MIL-88A zabaltzeko/uzkurtzeko gaitasun

handiena duen MOFetako bat da, eta horrek, uretan duen egonkortasunarekin batera, uretan alkoholak harrapatzea/berreskuratzea ahalbidetu digu. Gaur egun, alkoholaren erabilera oso zabalduta dago industrian, eta horrek zailtasun handiak sortu ditu alkoholak uretatik bereizteko orduan. Gehien erabiltzen diren alkoholen artean, metanolak kezka handiak sortzen ditu; izan ere, nahiz eta substantzia toxikoa ez izan, haien degradazio-produktuak badira: formaldehidoa eta azido formikoa, alegia. Gaur egun, alkoholak eta ura bereizteko metodo gehienek energia-kantitate handiak eskatzen dituzte. Hori dela eta, kapitulu honen helburua da MIL-88Aren portaera malgua aztertzea kate laburreko alkohol alifatikoak harrapatzean (metanola, etanola, n-propil alkohola, isopropil alkohola, n-butil alkohola, sec-butil alkohola, isobutil alkohola eta *tert*-butil alkohola). Alde batetik, 24 orduz alkoholen disoluzio urtsu diluitu batean murgilduta egon ondoren, MOFak adsorbatu dezakeen alkohol kantitatea kuantifikatu da. Emaitzek absorbatutako alkohol-masak alkoholaren bolumen molekularrarekiko joera lineala erakusten dute, metanolerako balio altuenak (%19.7) eta *n*-butil alkoholerako baxuenak (%11.5) lortuz. Hala ere, adarkatutako alkoholetan (adsortzio-balioak aurrekoak baino baxuagoa dutenak), bolumenarekiko mendekotasuna desagertu egiten da eta alkoholaren zeharkako sekzioarekiko mendekotasuna ezartzen da. Emaitza esperimental horiek ulertzeko, hainbat azterketa teoriko egin dira, azken molekula horiek dituzten hedapen-arazoei lotutako alkohol linealen adsortzioan dauden aldeak azaltzeko. Bestalde, hainbat alkoholen arteko lehiakortasun-azterketak egin dira, hidrofobikoenek afinitate handiagoa dutela erakutsiz, nahiz eta handiagoak izan. Era berean, fase likidoko adsortzio-esperimentu horien ondoren hauts-materiala berreskuratzeak duen zailtasunaz jabetuta, materiala mintz polimerikoetan sartzeko aukera aztertu da. Horretarako, polibinilideno fluoruroa hautatu da, *polyvinylidene fluoride* edo PVDF bezala ezaguna, egonkortasun kimiko eta termiko handia, prozesatzeko erraztasuna eta hidrofobizitatea dituelako. MOFaren masa-portzentai desberdineko mintzen sintesiaz eta karakterizazioaz gain, metanola eta etanola oso kontzentrazio baxuan adsorbatzeko gai dela probatu da, matrize polimerikoaren eta material porotsuaren artean dagoen efektu sinergikoa frogatuz, osagai bakoitzaren adsortzio-portaeratik espero zitekeenak baino balio nabarmen handiagoekin.

Tesiaren *5. kapituluan*, bide-urratzailea den azterlan bat egin da material porotsuen eta uren erremediatzearen esparruan. Lehen aldiz, hainbat MOFen azterketa sistematikoa egin da, uretan dagoen karbono dioxidoa harrapatzeko, besteak beste berotze globalak

eragindako uren azidifikazioari aurre egiteko. Azterketarako, adsortzio-gaitasun handiko MOFak hautatu dira (MOF-74 (Ni), MIL-127(Fe), Cu-TDPAT, UiO-66-NH$_2$, UiO-66 eta JUK-8), eta selektibitate altuko hautatu dira (ZU-301). Karbono dioxidoaren espezieak pH-aren arabera aldatzen direnez, MOF guztiak pH 2, 6.3, 8.3 eta 10.0ra duten portaera aztertu da, non espezie nagusiak CO_2, HCO_3^-/CO_2, HCO_3^- eta HCO_3^-/CO_3^{2-} diren, hurrenez hurren. Materialen egonkortasuna pH guztietan zehaztu ondoren, pH-aren egonkortasun-eremuaren barruan MOF bakoitzaren adsortzio-gaitasuna aztertu zen. Gainera, mundu errealeko ur laginetatik CO_2-a kentzeko esperimentuak egin izan dira. Horretarako, aintziretatik, ibaietatik eta Mediterraneo itsasotik jasotako ur-laginetan materialaren portaera aztertu da, ingurune konplexuagoetan neurtzeko.

Azkenik, *6. kapituluan* ikerketa honetatik eratorritako ondorio nagusiak laburbiltzen dira, etorkizuneko lan posiblea aipatzeaz gain, hurrengo ikerketetan lantzeko interesgarria izango litzatekeen puntuak aipatuz. Oro har, materialen ikerketaren oinarrizko hiru zutabeen garrantzia frogatu da: sintesia, karakterizazioa eta erabilgarritasuna. Oso ezagunak diren MOFen sintesiak optimizatu ditu, eskatutako ezaugarrien arabera protokolo fidagarriak eta aldagarriak eskaintzeko helburuarekin. Gainera, karakterizazio-teknika bat garatu da teknika konbentzionalei alternatibak eskaintzeko helburuarekin. Oro har, MOFek disoluzioan eta, bereziki, uretan adsortzio-prozesuetan espezie organikoak – alkoholak – edo ez-organikoak – karbono dioxidoa – harrapatzeko duten ahalmena ebaluatu da.

Chapter

1

Chapter 1

## Introduction to Metal-Organic Frameworks (MOFs)

1.1 EVOLUTION OF POROUS MATERIALS

Porous materials have been used since immemorial times. Egyptians and Sumerians used one of the very first known porous materials (porous charcoal) around 3000 B.C. for medical treatments or the manufacture of bronze. The first citation of the use of charcoal for the adsorption of odour vapours can be found in the Ebers papyrus around 1500 BC[1]. Its use was extended to the early modern area due to its adsorptive properties for treating gastrointestinal diseases and water purification[2].

Advances in science and technology, lead to the discovery of new materials. In the 18th century, Baron Axel Fredik Cronsttedt, a Swedish chemist and founder of modern mineralogy, discovered a new class of porous materials when moisture was formed during the heating of stilbite mineral[3]. He named these materials as zeolites, derived from Greek, where *zeo* means to boil and *lithos* stone. Almost one century after the discovery of natural zeolites, levinite, the first synthetic zeolite was prepared[4]. At the beginning of the 20th century, porous polymer networks (PPNs), containing well-known geometries formed by rigid organic functional groups, emerged[5]. By that time, it was well known that coordination polymers could be highly crystalline. The interest in these materials together with the research in the field grew exponentially.

In the late 20th century, Susumu Kitawa[6] designed for the first time hybrid inorganic-organic porous materials. These materials are known as first-generation compounds due to the lack of stability of the porous structure when removing guest molecules,

which suffer an irreversible collapse of the structure. It was not until 1990s that Omar Yaghi[7] developed the first stable and permanent porous materials – second generation compounds-, called porous coordination polymers (PCPs) or metal-organic frameworks (MOFs). Porous materials with flexible frameworks, able to respond reversibly to an external physical or chemical stimulus, were discovered later and form the third generation[8,9] (Figure 1.1).

| First generation | Second generation | Third generation |
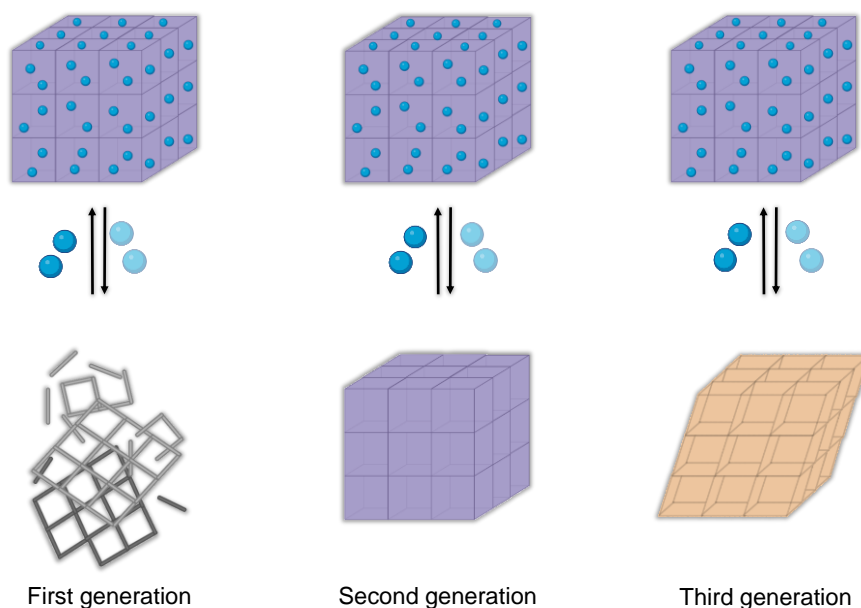
Figure 1.1. Materials of first, second and third generation before (top) and after (bottom) removal of guest molecules.
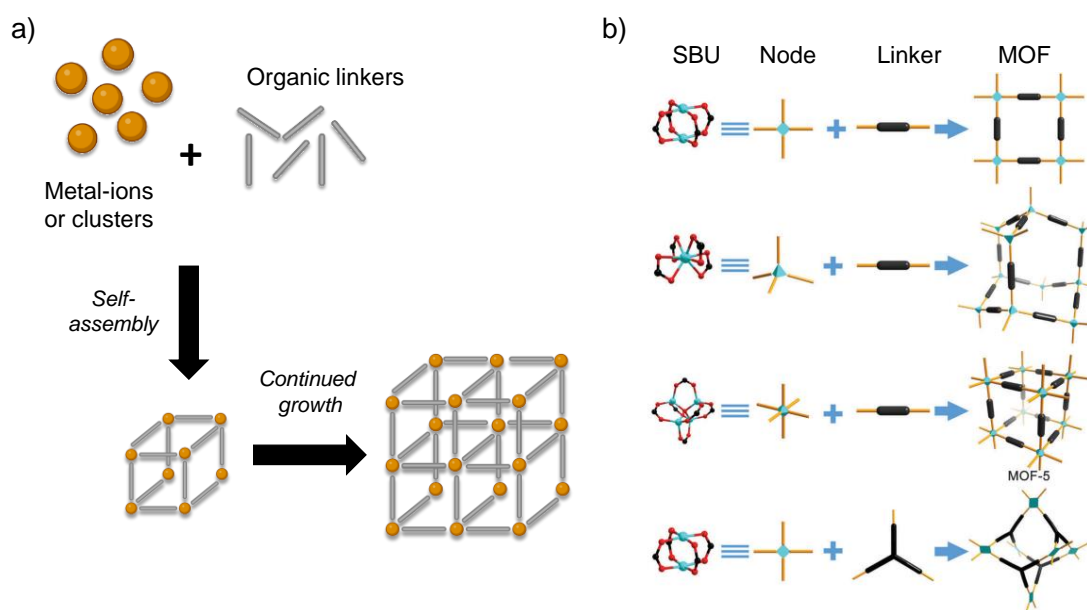
1.2 METAL-ORGANIC FRAMEWORKS

Although the synthesis of new materials has always been in the spotlight, until the 20th century, the discovery was serendipitous. Although this represented a breakthrough for solid-state materials, it limited the number of materials that could be prepared. Further research in the field of porous materials hinted at the connection between crystal structure and properties. This highlighted the importance of designing and developing new synthetic strategies to precisely control the structures and thus, obtain high porosity and tunable pore size. It is within this context that reticular chemistry emerged[10,11].

Reticular chemistry (from the Latin word *reticulum:* small net) focuses on connecting inorganic and organic molecular building blocks with strong directional bonds into crystalline extended structures and it has provided scientists with a powerful tool for designing covalent organic frameworks (COFs) and metal-organic frameworks (MOFs)[12,13]. The latter are a class of highly ordered crystalline materials formed by the assembly of inorganic ions or clusters (secondary building units) with organic linkers through strong coordination bonds (Figure 1.2a)[14].

Reticular synthesis was first proposed by Yaghi and co-workers[10] and allows predicting the structure of porous framework materials. Furthermore, it is noteworthy that the geometry and orientation of the organic unit for a specific inorganic building unit will direct the structure and thus, determine the topology of the resulting MOF. In Figure 1.2b a representation of the inorganic and organic building unit and the resulting structure of MOFs can be seen.

Figure 1.2. a) Metal-organic framework formation through strong coordination bond between organic and inorganic units and b) graphic illustration of metal-organic framework formation showing SBU and linkers topology, reproduced with permission from Lu *et al*[15].

Among the most outstanding properties of metal-organic frameworks, high surface areas (up to 10.000 m^2/g) and structural tunability can be highlighted[16]. The high chemical and structural diversity are one of the greatest advantages MOFs offer; on the one hand, the large number of combinations between secondary building units and

linkers have led to a drastic increase in the number of publications (Figure 1.3) and described structures, reporting up to 100.000 structures[17].
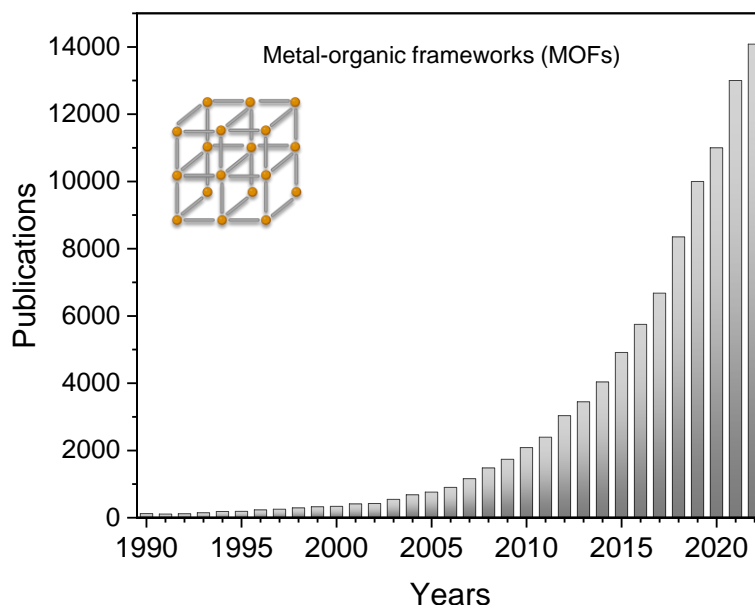

Figure 1.3. Number of MOF-related papers published from 1990 to 2022 (source: Web of Science).

Moreover, pore size can be tuned offering the possibility to obtain pores of different sizes. Even if the majority show microporosity (pore diameter < 2 nm), pore size can be tuned in exchange for obtaining mesopores (2-50 nm) and macropores (above 50 nm)[18]. For example, Wang *et al.*[19] prepared a series of mesoporous metalloporphyrin MOFs named PCN-600, which presented pore sizes of around 3 nm. Feng *et al.*[20] prepared a macroporous zeolitic imidazole framework (ZIF-8) with a pore diameter of 69 nm in order to improve enzyme immobilization efficiency and loading capacity. Changing pore size is not only a matter of structural study. It will also determine its applicability. Microporous MOFs are desirable for the adsorption of small molecules such as carbon dioxide that can be selectively adsorbed over nitrogen or methane (kinetic diameter: 3.3 Å CO_2, 3.6 Å N_2 and 3.8 Å CH_4) [21]. However, it is an undesirable feature for hosting large molecules due to the difficulties of incorporating them into the pores. Mass transfer and diffusion are also limited and their use in storage, catalysis or drug delivery is restricted.

1.3 METAL-ORGANIC FRAMEWORK NANOPARTICLES

Nanomaterials have always existed in human history but it was not until the 20th century when Richard Zsigmondy proposed the term nanometre for the first time. With this, he opened the door to an unexplored and fascinating world, but it was not until the 21st century that nanoscience and nanotechnology saw an increased interest[22]. Although the synthesis and post-synthetic modification of inorganic and organic nanoparticles are well-known, metal-organic framework nanoparticles (MOF NPs) still need to lay the groundwork for the development in the field[23], specifically in the synthesis, characterization and chemical control.

Historically, Professor Taniguchi first defined top-down approaches, which have been predominantly used in industry. Some years later, Eric K. Drexler, inspired by biology, described the bottom-up approach, where molecular assemblers could guide chemical reactions with atomic precision[24]. Currently, based on reticular chemistry, reticular nanoscience has emerged intending to create MOF NPs based on bottom-up assembly and offering the possibility of precisely controlling the geometry and atomic sequences[25] (Figure 1.4).
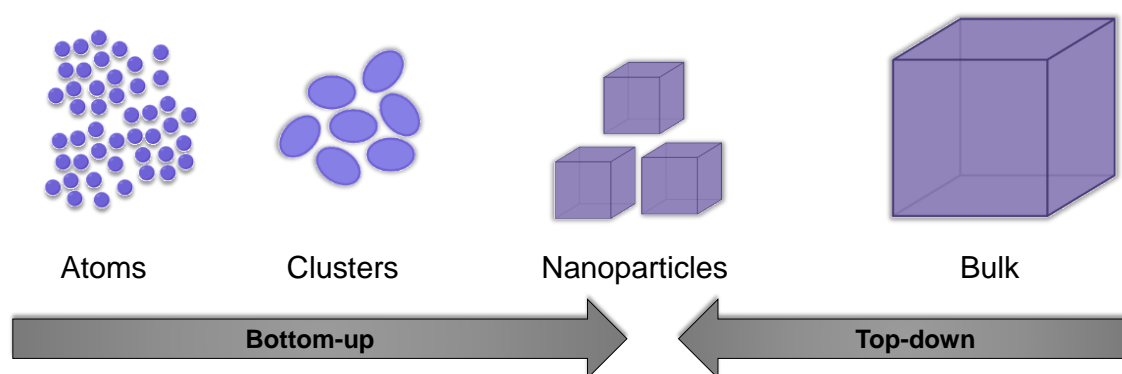
Figure 1.4. Schematic figure of the bottom-up and top-down approaches to form nanostructured materials.

One of the most outstanding characteristics of nanomaterials is the strong dependence of their properties on size, which has increased the interest to downsize materials to the nanoscale[26]. Although some properties of the nanoparticles remain unaltered compared to the bulk materials such as high porosity or the internal surface areas, other properties are enhanced such as their external surface area, which is drastically

increased. Moreover, new properties like short diffusion distances, higher chemical reactivity and surface defects are displayed[27]. In addition, some physical properties like optical, electrical or magnetic properties can emerge when materials size is reduced, which may improve the catalytic, separation and sensing activity of nano-sized MOFs[28]. The relevance of these applications will be discuss later in section 1.6.

1.4 SYNTHESIS OF METAL-ORGANIC FRAMEWORK

As previously described, reducing the size of MOFs to the nanoscale is a topic of great interest for the scientific community due to the new properties materials can acquired. Lately, many efforts have been made to have precise control of the size and morphology of MOF nanoparticles.

An interesting feature of preparing reticular nanoparticles compared to their bulk analogues is that they can be prepared in a shorter time and use less energy. For example, Chevreau *et al.*[29] prepared micrometric cubic MIL-127(Fe) of 2 μm through 16 hour solvothermal reaction, while they obtained 250 nm nanoparticles with microwave-assisted heating in 15 minutes. Moreover, internal and external surfaces can be tuned. The former, which normally is higher than the latter due to the high porosity, can be engineered via the framework and pore design, as well as by post-synthetic modification. This latter strategy can also be used to customize the external surface, which can be done selectively without altering the internal one[25].

For a better understanding of nanoMOFs synthesis, LaMer model is used, where nanoparticle nucleation and growth are divided into different stages (Figure 1.5)[30]. First, the dissolution of precursors leads to the formation of reactive monomers. Second, there is an increase in the concentration of reactive monomers surpassing nucleation concentration (C_{nuc}) and crystal seeds begin to form rapidly. Finally, there is a decrease in monomer concentration while nucleation and growth take place until the precursors and crystals reach equilibrium (C_{sat}).
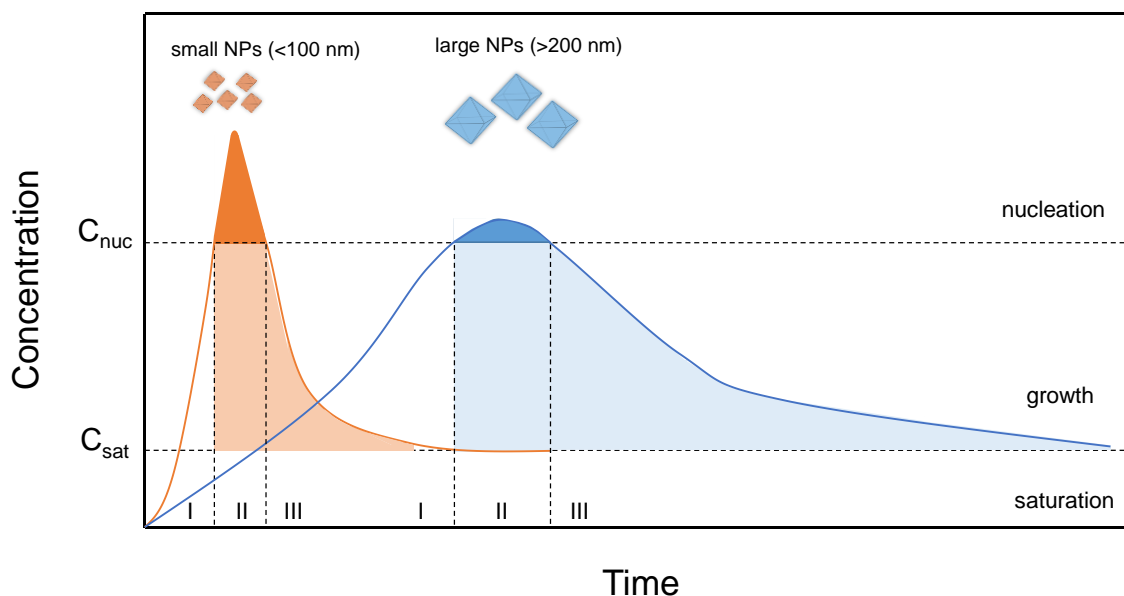
Figure 1.5. Schematic figure of the LaMer mechanism for nanoparticle formation (nucleation and growth).

According to Figure 1.5, nucleation period is the most critical step in nanoparticle formation, as it will define particle size; this is, the faster the nucleation the smaller the size. In this way, we can easily obtain small (1-100 nm) and large (200 nm-1 μm) nanoparticles[23]. LaMer process and thus, nanoparticle formation, can be highly influenced by different factors. For instance, the temperature effect has been widely studied on the size and distribution of MOF NPs[31]. The concentration of the starting reagents[32] or solvents[33] can also play an important role in morphology or size, respectively. Generally, the starting point of almost all synthetic strategies is the metal source (inorganic building unit, IBUs), the ligand (organic building unit, OBUs) and the solvent. Modulating agents are often used in order to precisely control morphology and crystallinity. In Figure 1.6, the most used strategies for MOF synthesis are illustrated.
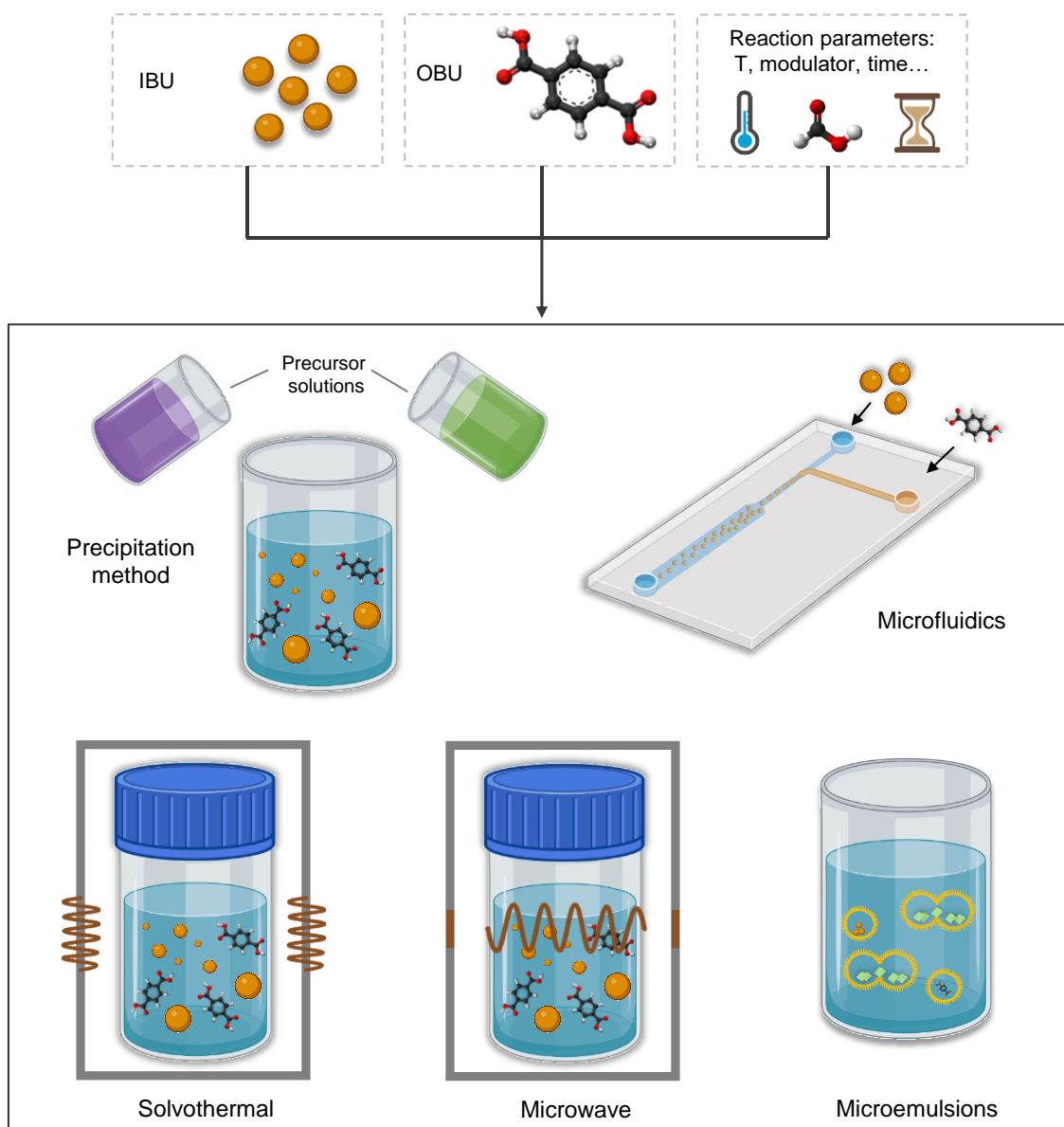
Figure 1.6. Schematic figure of some of the most used strategies for MOF synthesis.

Spontaneous precipitation is one of the simplest cases, where the two precursors' solutions are mixed and reacted at room temperature. For instance, Tranchemontagne *et al.*[34] developed a protocol for room temperature synthesis of four well-known MOFs: MOF-5, MOF-74, MOF-177 and MOF-199. On the contrary, there are not so many cases where this method is successful for the synthesis of MOF NPs. For example, Pan *et al.*[35] developed for the first time the first ZIF in an aqueous solution and at room temperature by mixing metal and organic solutions leading to 85 nm nanoparticles. Sophisticated modifications of this approach have also been proposed as was the case of HKUST-1, synthesized via freeze drying, where the reagents

solutions were cooled down and afterwards, the reaction mixture was warmed up to room temperature resulting in 100 nm size particles[36].

Solvothermal reaction has been one of the most common and widely used methods in MOF synthesis. Inorganic and organic precursors' solutions are mixed and heated under pressure in closed autoclaves, where the heat needs to progress from the outside to the inside of the vessel where the reagents are placed. For the synthesis, high-boiling organic solvents or water are used; the latter is also known as hydrothermal synthesis. Normally, high temperatures, long reaction times and moderate pressure are required and although single crystal formation is favoured due to the slow nucleation and rapid crystal growth, MOF NPs have also been synthesized with this method[37]. For example, Ganesh *et al.*[38] prepared Zr-fumarate nanoparticles solvothermally in a 24 hours reaction at 120 °C using formic acid as a modulator.

Conventional solvothermal heating does not allow controlling temperature gradient in the reaction medium, which leads to a heterogeneous distribution of the particles, while microwave-assisted heating overcomes this drawback by producing uniform nanosized crystals[37]. Contrary to solvothermal reactions, microwave heating process does not occur through a reaction vessel, but due to the coupling of microwave irradiation with molecular dipoles or ions present in the reaction medium. All this ensures homogeneous internal heating and therefore, results in narrow size distributions as well as homogeneous morphologies[39]. For instance, Simon *et al.*[40] prepared MIL-100(Fe) hydrothermally for 12 hours resulting in micron-sized octahedron shape particles, while García-Marquez *et al.*[41] obtained nanoparticles in a 6 minutes microwave reaction.

Microfluidics has been used since the 90s for nanoparticle synthesis[42], but it has not been until recently that it has become popular for MOF NPs synthesis. In a microfluidic reactor, the precursors' solutions are pressed through narrow channels placed on heated segments. Thanks to the small diameters of the channels, heat transfer is quite fast – 400 times higher than conventional heating- ensuring a precise control over nucleation and crystal growth[39]. In contrast to conventional heating methods, microfluidics stands out for the rapid heating and mass transfer, large

reaction interfaces, small amount of reagents needed and precise control of the synthesized nanoparticles, necessary for obtaining high-quality NPs[43,44].

Microemulsions, which are thermodynamically stable dispersions formed when two immiscible liquids or solutions are mixed in the presence of surfactants or emulsifiers, are another low-temperature method very useful to obtain monodispersed and uniform nanoparticles[45]. Nanoparticle size and crystallinity can be easily controlled due to the fact that each droplet is considered a nanoreactor allowing the growth and crystallization in a confined way[46]. Ye *et al.*[47] prepared micron-size Zn-MOFs in ionic liquid microemulsions, in order to overcome the main disadvantage of traditional methods by replacing the use of organic solvents with an environmentally friendly alternative. Shang *et al.*[48] prepared Lanthanum-MOF nanocrystals using ionic liquid microemulsions, where the morphology of the particle was controlled by changing the microstructure of the microemulsions. Sun *et al.*[49] prepared ZIF-8 and ZIF-67 by reverse microemulsion with uniform size distribution and extremely small particles of 10 nm.

As we have already seen through this section, there are several methods for the synthesis of MOFs. Therefore, understanding the characteristics and the advantages/disadvantages of each technique is crucial in order to meet the requirements in terms of size or morphology, since it will have a great impact on their properties and, therefore, on their application.

1.5 CHARACTERIZATION OF METAL-ORGANIC FRAMEWORKS

The most important aspects that need to be outlined when characterizing reticular materials are their crystallinity, morphology, particle size and porosity. In order to get this information, different techniques are needed. It is worth emphasizing that in all cases, the results must be analysed taking into account the characteristics of the instrument and the sample preparation procedure. The former will define the precision and accuracy of the analytical information, while the latter is crucial as different measurement conditions may affect data interpretation.

X-ray diffraction is one of the most important technique in the field of crystalline materials characterization. This technique is based on the diffraction provoked by X-ray radiation when it interacts with the electrons located in the atoms of a material. Depending on the incidence angle and the relative position of the atoms in the lattice constructive and destructive interferences can be produced. The formers can add up and form a strong constructive wave that follows Bragg's law (eq. 1.1)[50]:

$$n \cdot \lambda = 2d_{hkl} \cdot sen\theta \tag{1.1}$$

where, n is the diffraction order, λ is the wavelength of the incident X-rays, d_{hkl} is the interplanar distance (where h, k and l refer to Miller indices) and Θ is the glancing angle that forms the incident ray with the normal (Figure 1.7).
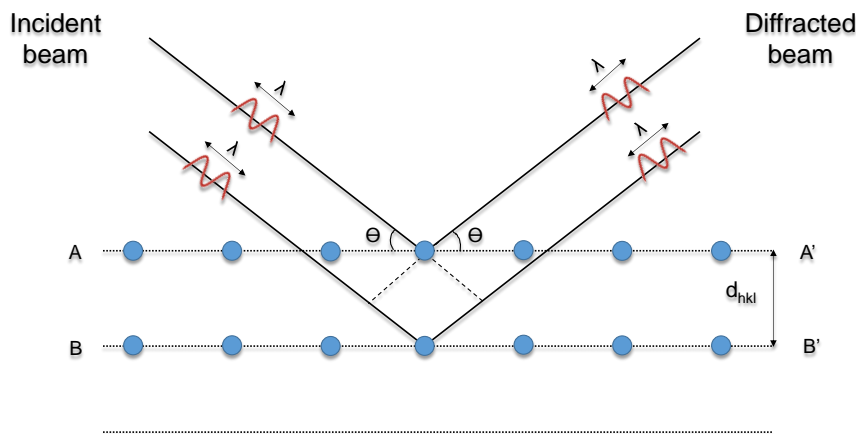
Figure 1.7. Schematic representation of X-ray diffraction technique.

A diffractogram with the characteristic peaks of the material is obtained, which allows identifying the compound by comparing the experimental and calculated patterns, as well as making degree-of-crystallinity (DOC) analysis to determine the number of amorphous compounds in a sample. It also offers the possibility to estimate the size of the crystallites (D) through the analysis of the diffraction profiles[51] from the Scherrer equation (eq. 1.2) and full width half maximum (FWHM).

$$D = \frac{K \cdot \lambda}{\beta_{hkl} \cdot cos\theta} \tag{1.2}$$

where K is a shape factor, λ is the wavelength of the incident X-rays, β_{hkl} is the line broadening at half the maximum intensity (FWHM) and Θ is the Bragg angle.

Transmission electron microscopy (TEM) can be used for nanoscale materials (normally < 200 nm) in order to get images with atomic resolution, which enables the study of morphology, topography and textural properties like crystal size and shape, as well as, the crystal structure[52]. This technique employs a short wavelength electron beam allowing to achieve subnanometer resolution[53]. On the contrary, sample preparation, measurement and analysis can be tedious work and sample limitations can exist. NPs need to be electron transparent and able to resist high vacuum and high-energy electron beam, which can damage the sample[54].

Scanning electron microscopy (SEM) allows imaging of the surface of a material through the detected secondary electrons emitted from the sample when it interacts with the incident electron beam. Moreover, the composition of the sample surface can also be investigated by detecting elastically backscattered electrons. One of the main requirements of this technique is that SEM samples need to be electrically conductive and nonconductive specimens are coated with an electrically conductive material, normally gold. The beam energy used in SEM is lower in comparison to TEM, which limits the penetrations of the beam in the sample limiting the study to the surface of the materials and preventing sample degradation. In addition, sample preparation, measurements and analysis are faster[55]. Overall, it allows not only measuring the particle size and distribution but also the morphology and composition of the particles.

Dynamic light scattering (DLS) is another used technique for particle size determination. Contrary to electron microscopy techniques, DLS measurements are performed in solution estimating the size from the Brownian diffusion. In this case, the laser beam is transmitted through the suspension, where the random thermal motion of the particles causes intensity changes in the scattered light. Particle size is calculated from the diffusion coefficient obtained from an autocorrelation analysis through the Stokes-Einstein equation (eq. 1.3):

$$D = \frac{k_B T}{6\pi\eta R_h} \tag{1.3}$$

where, D is the diffusion coefficient, k_B is the Boltzmann constant, T is the temperature at which the analysis is carried out, η is the kinematic viscosity of the solvent and R_h indicates the hydrodynamic radius of the particle. This technique offers

a fast measurement time, requires low amount of sample and it is compatible with a large variety of solvents. On the other hand, for non-spherical particles, the hydrodynamic radius can be different from the real particle size[56].

One of the intrinsic properties of MOFs is permanent porosity and hence, determining the surface area, pore volume and pore size distribution is essential to confirm their porosity. Gas adsorption, which is based on the amount of gas adsorbed in the surface of the material, is generally used in order to determine adsorption isotherms[57]. In order to understand the performance of a material, different adsorption models can be found, which are divided into two main groups: discrete and continuous distribution models[58].

Discrete distribution models. In the early 20th century, Irving Langmuir presented a model to describe the adsorption of gas molecules onto a solid surface at a constant temperature. This model assumes that all surface binding sites are similar and can only be occupied by one molecule, thus, forming a monolayer. In 1938, Brunauer, Emmett and Teller (BET) proposed a multilayer adsorption model, which is formed when additional gas molecules are adsorbed into the monolayer through intermolecular interactions. BET model makes three assumptions: (*i*) there is no interaction between solute molecules, (*ii*) the surface of the adsorbent is homogeneous and (*iii*) the adsorbed molecules provide adsorption sites forming multilayers.

Continuous distribution models. In 1906, Freundlich introduced a model, which related the amount of adsorbed gas with the amount of adsorbent and pressure at constant temperature providing a description for heterogeneous adsorption.

Figure 1.8 shows the different types of isotherms classified by IUPAC, which will show up according to the interactions and the pore size of the sample. Type I isotherm, commonly known as Langmuir isotherm, describes a chemisorption process in microporous materials. In the first stage, gas molecules are adsorbed forming a monolayer inside the micropores, which reach saturation quickly once they are filled. Type II describe the physisorption of gases on macro- or non-porous materials. The shape of the isotherm is the result of unrestricted monolayer-multilayer adsorption up to high pressures. In type III isotherms, adsorbent-adsorbate interactions are weak meaning that the adsorbate has to cover the surface before the second layer starts to

form. Adsorbed gas molecules are clustered around the most favourable sites of macro- or non-porous materials[59]. Type IV isotherms, which are mainly observed in mesoporous materials capillary condensation occurs. In the first step, a monolayer is created, followed by a plateau indicating that all energetically favourable sites have been occupied. At higher pressures, multilayers are formed. Type V isotherms typical of micro- and meso-porous adsorbents, reveal weak adsorbent-adsorbate interactions, similar to type III isotherms. The hysteresis in type IV and V can be correlated to the texture of the pores (*i.e.*, pore size distribution, geometry and connectivity)[60]. Type VI isotherms represent a layer-by-layer adsorption on a highly uniform nonporous surface[61].
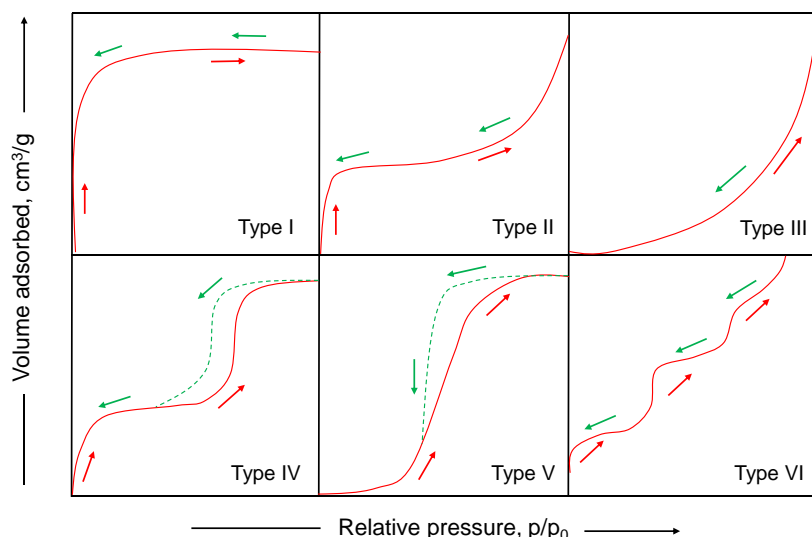
Figure 1.8. Different adsorption isotherms according to IUPAC's classification[62].

As described above, gas adsorption is a mature and well-studied technique, which allows not only to determine the pore volume or surface area but also to compare the behaviour of porous materials during the adsorption of different gaseous compounds like CO, CO_2 or CH_4[63]. On the contrary, nowadays, it is still difficult to find suitable techniques to characterize adsorption processes taking place in solution. One of the most widely spread techniques is ultraviolet-visible (UV-Vis) spectroscopy, based on the adsorption process of the light absorbed by a molecule at different wavelengths (in the UV-Vis range, 200 – 800 nm). The absorption causes the promotion of an electron (bonding electron of the molecules) to an excited state, which allows the identification of functional groups present in the molecules. The bands are wide due to the superposition of vibrational and electronic transitions. In addition, the intensity

of the bands is directly proportional to the concentration and the path length, according to Beer-Lambert law (eq. 1.4)[64]. Therefore, it can be used to determine the concentration of the absorbate in the solution:

$$A = \varepsilon \cdot C \cdot l \qquad (1.4)$$

where A is the absorbance, ε is the absorptivity of the attenuating species, C is the concentration of the attenuating species and l is the optical path length

The main advantages of UV-Vis spectroscopy are the low-cost, quickness of the measurements and versatility as it offers the possibility to use different solvents in the measurements. On the contrary, UV-Vis spectroscopy does not offer a direct measurement and quantification of the captured amount of targeted compounds by porous materials. Instead, it provides the amount remaining in the solution. Another drawback that can be found is that the molecules need to be active in ultraviolet, which in many cases limits the study of the adsorption process to active molecules (*i.e.*, double bounds).

In addition, nuclear magnetic resonance (NMR) is another useful technique, which relies on the change of the chemical environment, where nuclei under a constant and strong magnetic field are perturbed by a weak and oscillating magnetic field. Consequently, nuclei respond by producing electromagnetic signals with a determined frequency[65]. NMR spectroscopy is a very useful technique if the aim is to characterize the linkers used for MOF synthesis or quantify the percentage of a post-synthetically modification MOF. However and similarly to UV-Vis spectroscopy, adsorption processes in the solution can be indirectly quantified, determining the amount remaining in solution (this is, the amount not adsorbed), which can hinder the study of molecules that are not completely soluble.

High-performance liquid chromatography (HPLC) is one of the most used chromatographic methods for chemical analysis, separation and purification. Briefly, samples are injected into the column while the selected solvent is constantly poured through the column, where the different components of the sample flow down through the columns at different speeds depending on their chemical nature. While the compounds leave the column, they are sensed by a detector and the signal is plotted

against time. Among the main advantages of HPLC reusable and more effective columns compared to classical liquid chromatography can be found. Moreover, almost all the procedure is automatized, which leads to more precise control of the whole process. On the contrary, sample preparation, high cost of the columns and tedious work to find the right measurement conditions are highlighted[66]. HPLC can also be used to calculate the amount captured by an adsorbent, but similarly to the previously mentioned techniques, this process is done by comparing the amount of adsorbate remaining in the solution after the adsorption process to the initial mother solution.

1.6 APPLICATIONS OF METAL-ORGANIC FRAMEWORKS

The versatility of the two components nature of MOFs, IBUs and OBUs, provides these reticular materials with a great versatility in structural topologies, pore size, connectivity and chemical functionalization of their internal surface. This allows MOFs to be used in different applications since their properties can be tuned according to the requirements and placed them as better candidates compared to conventional materials, like activated carbon or zeolites[67]. Most of the applications are based on their intrinsic porosity, which allows MOFs to capture and host different molecules (Figure 1.9).
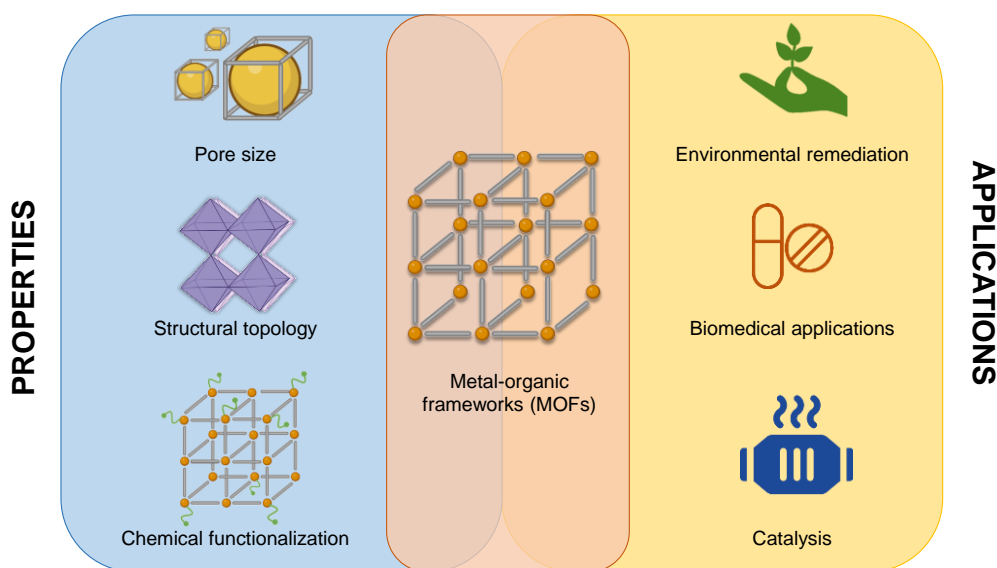

Figure 1.9. Relation between MOF properties and applications

1.6.1 Environmental remediation

Over the last decades, the increase in population, industrial development and the improvement of life quality and health care system has caused an increase in contamination levels[68]. Environmental pollution has been recognized as one of the most concerning global problems, as it can pose several risks not only to human health but also to ecosystems. Among the very diverse hazardous pollutants volatile organic compounds (VOCs), antibiotics and heavy metal ions can be found[67].

According to World Health Organization (WHO), water contamination is one of the biggest issues humankind needs to overcome. Around 1 billion people in the world can't get safe and clean water and about 2 million die due to polluted water[69]. Antibiotics, which can be defined as chemotherapeutic agents able to restrain or annul the growth of microorganisms, have been extensively used and their benefits are widely known as they can prevent infectious diseases[70]. The massive production of these products has led to several environmental problems *i.e.* water contamination. Antibiotics or generally, drugs, are not completely eliminated during sewage treatments and therefore, emitted into water. Although prescribing a lower dose can be an important step toward the reduction of the amount of antibiotics excreted[71], it needs to be applied together with other strategies such as the capture and removal of the pollutants. Azhar *et al.*[72] studied the adsorption of sulphonamide antibiotics, sulfachlorpyridazine, from wastewater for the first time using HKUST-1. Moreover, Zr-based MOFs were studied for the adsorption of diclofenac, one of the most frequent drug[73]. UiO-66 and functionalized UiO-66 (-SO_3H and -NH_2) were prepared and the adsorptive properties were compared to activated carbon, demonstrating a better performance of the pristine and functionalized Zr-MOFs. Likewise, they concluded that UiO-66-SO_3H had higher adsorption compared to pristine UiO-66 and at lower concentrations, the adsorption capacity was 13 times higher than activated carbon. The very well-known zeolitic imidazole ZIF-8 was used for the removal of a mixture of two very common antibiotics, tetracycline and oxytetracycline hydrochloride, reporting a capture of 91% and 83%, respectively[74].

Another source of water contamination is heavy metals, which can occur directly or indirectly in water. There are usually found in industrial manufacture or agriculture

as components of pesticides or herbicides. Some of the most typical heavy metals that can be found in water are arsenic (As), mercury (Hg), cadmium (Cd), chromium (Cr) and lead (Pb)[75]. For instance, Yang *et al.*[76] developed thiol-functionalized Zr-MOFs for the effective removal of Cr(VI), which can cause mutation and teratogenicity in humans and organisms. Thiol groups, not only serve as capture sites due to Cr(VI)-thiolate complex formation but also act as reductive sites for the degradation of Cr(VI) to Cr(III), whose lower toxicity makes these MOFs a safe-alternative for the removal of Cr(VI), as the leakage of the toxic heavy metal ion can be avoided. The same research group used these thiol Zr-MOF for the capture of divalent mercury. Hg(II) is highly dangerous due to its high water-solubility, non-biodegradable nature and high bioaccumulation, which can cause harm to the central nervous system, normally irreparable. They proved the fast kinetics, high adsorption capacity, selectivity, reusability and high working efficiency in a wide range of pH (0-7)[77]. Lead(II) is another harmful specie known for targeting almost all organs in the body, especially the central nervous system or causing positioning. Based on the adsorption mechanism, Hasankola *et al.*[78] synthesized Cu- and Zn-BTC MOFs and proved the effective ultrasound-assisted removal of Pb(II) from water in less than 30 minutes.

Environmental pollution and thus, remediation is not only focused on water but also on air pollution. In fact, during the last decades, there has been a shout-out to the massive production of greenhouse gases, which aggravates climate change[79]. Volatile organic compounds (VOCs) possess toxic and carcinogenic nature, which threaten human health with irreversible damage after long-time exposure. Moreover, they can damage ozone sphere or form photochemical smog due to the reaction with other air pollutants like NO_x and SO_x[80]. The annual emission of VOCs has increased drastically over the last years, leading to more strict politics in the direction of limiting the emissions of these gases. In order to overcome this worldwide issue, MOFs have been used as adsorbents to demonstrate their high adsorption capacity and viability for pollutant capture from the air. Chen *et al.*[81] reported for the first time the adsorption of four common VOCs (methanol, acetone, benzene and toluene) with a cobalt-adeninate MOF (Bio-MOF-11), which offered multiple Lewis-basic sites compared to other bio-MOFs. Sulphur hexafluoride (SF_6) and tetrafluoromethane (CF_4), used in the electrical industry as insulating gas and as an etchant in the semiconductor

industry, respectively, are two very powerful greenhouse gases capable of trapping more heat in the atmosphere compared to CO_2. Based on this, Senkovska *et al.*[82] investigated the adsorption capacities of different micro- and meso-porous MOFs at different pressures. At low pressures, microporous HKUST-1 and $Zn_4O(dmcpz)_3$ showed the best adsorption for SF_6 and CF_4, respectively. At high pressures, mesoporous MIL-101 and DUT-9 have the highest adsorption capacities for both gases.

On the whole, MOFs have proven to be a good alternative in environmental remediation, where water and air pollution are considered one of the most concerning global problems due to their great versatility and characteristics. Therefore, future research is envisaged on this topic.

1.6.2   Biomedical applications

During the last years, it has been shown that one of the main focus of MOF applications relies on biomedicine, where straightforward functionalization allow their use as transport vehicle for different imaging technique (*i.e.* magnetic resonance imaging)[83], drug delivery[84] or as cancer therapy[85]. The intrinsic porosity of MOFs offers the possibility of designing them as vehicles to trap, carry and deliver drug molecules. Therefore, different factors need to be considered in the design of these porous materials for biomedical applications. Particle size is an important factor especially in the administration route, as well as in the toxicity, biodistribution and lifetime of the particles in the body. For instance, it has been reported that particles larger than 200 nm are removed by macrophages[86]. The structure and morphology can influence the interaction with biological fluids and interfaces affecting their performance in the body[87]. Therefore, choosing adequate synthesis methods and characterization techniques is crucial in order to optimize synthesis of MOF NPs with homogenous size distributions and shapes.

In addition to the above-mentioned characteristics, biocompatibility and toxicity need to be studied in favour of avoiding immunological reactions. At first glance, one could think that metal source is the only factor to take into account in the design of non-toxic MOFs. Nevertheless, every single component of MOFs should be considered, as they could possess toxic organic molecules, *i.e.* ligands or solvents. Moreover,

ADME parameters –administration, distribution, metabolization and excretion- are strongly related to toxicity. The performance of MOFs in biomedical applications is also related to the biodegradability and stability of the framework. Particularly, in body fluids, where composition and pH value changes, MOFs bioerosion and drug release performances will strongly be affected and accordingly, it is a crucial factor to study[88].

Taking into account all these parameters, MOF NPs can be used for the storage and delivery of different bioactive agents. In order to develop efficient delivery systems, MOF NPs (or carriers) must fulfil some requirements. The release of the bioagent, as well as the degradation, needs to be studied and well controlled. Carriers should load drugs with high capacity and efficiency. Finally, carriers should allow surface modification and detection by imaging techniques. According to bioagent-carrier interaction, non-covalent and covalent delivery can be found. The former was the first drug-delivery-type developed system. Ferey *et al.*[89] used MIL-101 MOFs in order to study the loading and release of ibuprofen. The latter is based on covalently bonded bioagents to the carriers with the aim of avoiding interferences from the media and reversible processes. For example, MIL-101(Fe) was post-synthetically modified by functionalizing nanoparticles with amino groups, which allowed the loading of an anticancer drug, ethoxysuccinato-cisplatin (ESCP) through covalent bonds. They also demonstrated the utility of a silica thin layer coating for protecting the framework from degradation in PBS[90].

Gasotransmitters, small gas molecules freely permeable to cell membranes, which do not follow the traditional membrane receptor signalling mechanism, are a class of bioagents of interest. Nitric oxide (NO), an atmospheric pollutant with a worldwide industry concerned about its removal from the air, carbon monoxide (CO), named as the silent killer due to its binding affinity to iron and hydrogen sulphide (H_2S), a toxic gas known for its smell to rotten-eggs, are the most common gasostransmitters[88]. These gases are endogenously generated with specific molecular and cellular targeting and defined functions and therefore, this is one of the main reasons for the development of carriers and well-studied delivery systems[91]. As an example, Ma *et al.*[92] studied the loading and release of carbon monoxide in MIL-88B and NH_2-MIL-

88B concluding that CO binding occurred in the unsaturated coordination sites and that the release was subjected to the degradation of the frameworks.

As can be seen, the intrinsic characteristics of MOFs such as porosity or large surface areas, together with the possibility of reducing them to the nanoscale or tuning their shape have put them in the spotlight for their use in biomedicine. However, further studies need to be done to ensure their degradability, biocompatibility or toxicity before their use.

1.6.3 Catalysis

Catalysts are known to speed up chemical reactions due to the reduction of the transition state energy and thus, the activation energy. Consequently, their research in the field have grown not only in industrial processes (production of chemicals, petrochemistry or oil refining)[93] but also in biomedicine related applications (*i.e.* bioassay, imaging or therapeutics)[94]. Pristine or post-synthetically modified metal-organic frameworks are frequently utilized as heterogeneous catalysts. It was one of the earliest proposed and demonstrated applications for these materials[95,96]. One of the greatest advantages of MOFs toward conventional materials like zeolites is the great chemical variety, which allows not only to synthesize infinite structures but also to tune them. Porosity and all that it entails is one of the most important characteristics in catalysis. On the one hand, it is important to control the size, shape and uniformity of the pores since it allows a size-selective catalysis. In addition, transport and diffusion of substrates are favoured due to the open channels. For gas-phase catalysis, porosity should be retained, while for condensed-phase reactions, is not an essential factor. On the other hand, thermal and water stability are essential factors in order to ensure their activity[97,98]. In addition, MOF-5[99] and MOF-177[100] were reported for having extraordinary high surface areas and gas storage performances but suffered from low thermal stability, as well as sensitivity to moisture, which restricts their use as catalysts. Overall, as the use of MOFs as catalysts can be hampered because of their properties, it is important to characterize them properly.

Although the use of these crystalline materials as catalysts is still immature, a lot of progress has been done in the field and different strategies have been proposed in order to improve efficiency. Taking advantage of MOFs containing open metal sites

(OMS) is one of them. Jiang *et al*.[101] synthesized a sulfone-functionalized USTC-253 with exposed metal centres and defects sites. They proved an increased CO_2 uptake compared to the pristine MOF and proved to have good catalytic activity and recyclability in the cycloaddition of CO_2 and epoxide. Besides, functional linkers can be introduced in the framework, either during the synthesis process or via post-synthetic modification. Akiyama *et al*.[102] synthesized a series of functionalized MIL MOFs with $-NH_2$, $-(CH_3)_2$, $-NO_2$ and SO_3H. They proved that the Lewis acidity of OMSs and thus, the catalytic activity could be tuned by changing the functional group of the organic linker. In addition, they demonstrated the high conversion of glucose and selective production of fructose of SO_3H-MIL-101. Another approach is to embed functional nanoparticles inside MOFs cavities. Schröder *et al*.[103] loaded ruthenium nanoparticles into MOF-5 via gas-phase loading and following hydrogenolysis of a volatile compound. They proved the catalytic activity of Ru@MOF-5 in the oxidation of benzyl alcohol and the hydrogenation of benzene.

Overall, MOFs have shown good performances as heterogeneous catalysts due to their intrinsic properties and thus, their future as one of the most important type of heterogeneous catalysts can be anticipated.

1.7 SCOPE OF THE THESIS

The general aim of this thesis is to study the use of different Metal-Organic Frameworks (MOFs) for the adsorption of organic and inorganic species in solution. Within this general aim, the following objectives are drawn:

- To investigate the effect of different synthetic parameters such as reaction time, reagents concentration or modulators in the size and shape of some well-known MOFs: Zr-fumarate, UiO-66, ZIF-8, ZIF-67 and MIL-88A.
- To develop a new, rapid and direct characterization technique devoted to the quantification of adsorption processes taking place in solution for paramagnetic MOFs.

- To study the removal of short-chain alcohols in water using a flexible and paramagnetic MOF, as well as its integration in polymeric matrixes in order to see the possible synergy between the two components of the hybrid material.

- To explore the possibility of addresing ocean acidification by studying the performance of MOFs for the capture of carbon dioxide and the generated carbonate species in water.

In order to achieve these objectives the thesis has been structured in different chapters. *Chapter 1* is aimed to be a general introduction to Metal-Organic Frameworks (MOFs), where the evolution of porous materials until the discovery of MOFs is explained. Moreover, the importance of MOFs, which have provided researchers with a huge research field due to their great versatility not only in the applicability of the materials but also in the synthesis and properties, is shown. Finally, the importance of the synthesis, characterization and applications of MOFs is reported.

In *Chapter* 2, a systematic study can be found aimed to study the effect of different synthesis parameters in the size and shape of some well-known MOFs (Zr-fumarate, UiO-66, ZIF-8, ZIF-67 and MIL-88A).

In *Chapter 3,* a new and rapid characterization method for adsorption processes in solution (*i.e.* water and ethanol) is proposed based on the paramagnetic nature of the selected MOFs. The motivation for the development of the method was the difficulty to find techniques that could directly quantify in solution the amount of the captured absorbate.

Chapter 4 and *Chapter 5* are focused on possible applications of MOFs as adsorbents in aqueous environment. In *Chapter 4* the recovery of alcohols from water has been theoretically and experimentally studied using the paramagnetic and flexible MIL-88A(Fe) MOF. Moreover, competitive alcohol studies as well as the use of MIL-88A(Fe) as polymeric filler in order to address the possible synergies between the two components.

In *Chapter 5*, to the best of our knowledge, the first study of the capture of carbon dioxide and the generated carbonate species from water has been performed using porous materials with the aim of addressing a worldwide issue related to pollution.

For that, MOFs which have shown high adsorption capacity or selectivity with different features like undercoordinated metal sites, basic groups or flexible frameworks in the adsorption of carbon dioxide in the gas phase were chosen.

The final chapter is devoted to the general conclusions drawn from this doctoral thesis, where the improvements to this field are stated and in addition, some final remarks on future works are provided.

1.8 REFERENCES

(1) Cyril P. Bryan. *Ancient Egypcian Medicine: The Payrus Ebers*; Ares Publisher INC., **1974**.

(2) Ferhan Çeçen and Özgür Aktas. *Activated Carbon for Water and Wastewater Treatment: Integration of Adsorption and Biological Treatment*; John Wiley distributor; Wiley-VCH, **2011**.

(3) Margeta, K.; Farkaš, A.; Zeolites. *New Challenges: Introductory Chapter: Zeolites - From Discovery to New Applications on the Global Market*; IntechOpen, **2020**.

(4) Yaghi, O. M.; Kalmutzki, M. J.; Diercks, C. S. *Introduction to reticular chemistry: Metal-organic frameworks and covalent organic frameworks*; Wiley-VCH Verlag GmbH&Co. KGaA: Weinheim, **2019**.

(5) Day, G. S.; Drake, H. F.; Zhou, H.-C.; Ryder, M. R. *Commun. Chem.* **2021**, 4, 548.

(6) Munakata, M., Kuroda-Sowa, T., Maekawa, M., Honda, A. & Kitagawa, S. *J. Chem. Soc., Dalton Trans.* **1994**, 19, 2271–2275.

(7) Li, H., Eddaoudi, M., O'Keeffe, M. & Yaghi, O. M. *Nature* 1999, 402, 276–279.

(8) Kitagawa, S. *Acc. Chem. Res*. **2017**, 50, 514–516.

(9) Horike, S.; Shimomura, S.; Kitagawa, S. *Nat. Chem*. **2009**, 1, 695–704.

(10) Yaghi, O. M.; O'Keeffe, M.; Ockwig, N. W.; Chae, H. K.; Eddaoudi, Mohamed and Kim, Jaheon. *Nature* **2003**, 423, 705–714.

(11) Freund, R.; Zaremba, O.; Arnauts, G.; Ameloot, R.; Skorupskii, G.; Dincă, M.; Bavykina, A.; Gascon, J.; Ejsmont, A.; Goscianska, J.; Kalmutzki, M.; Lächelt, U.; Ploetz, E.; Diercks, C. S.; Wuttke, S. *Angew. Chem. Int. Ed*. **2021**, 60, 23975–24001.

(12) Ejsmont, A.; Andreo, J.; Lanza, A.; Galarda, A.; Macreadie, L.; Wuttke, S.; Canossa, S.; Ploetz, E.; Goscianska, *J. Coord. Chem. Rev*. **2021**, 430, 213655.

(13) Freund, R.; Canossa, S.; Cohen, S. M.; Yan, W.; Deng, H.; Guillerm, V.; Eddaoudi, M.; Madden, D. G.; Fairen-Jimenez, D.; Lyu, H.; Macreadie, L. K.; Ji, Z.; Zhang, Y.; Wang, B.; Haase, F.; Wöll, C.; Zaremba, O.; Andreo, J.; Wuttke, S.; Diercks, C. S. *Angew. Chem. Int. Ed*. **2021**, 60, 23946–23974.

(14) Butova, V. V.; Soldatov, M. A.; Guda, A. A.; Lomachenko, K. A.; Lamberti, C. *Russ. Chem. Rev*. **2016**, 85, 280–307.

(15) Lu, W.; Wei, Z.; Gu, Z.-Y.; Liu, T.-F.; Park, J.; Park, J.; Tian, J.; Zhang, M.; Zhang, Q.; Gentle, T.; Bosch, M.; Zhou, H.-C. *Chem. Soc. Rev*. **2014**, 43, 5561–5593.

(16) Moghadam, P. Z.; Li, A.; Wiggin, S. B.; Tao, A.; Maloney, A. G. P.; Wood, P. A.; Ward, S. C.; Fairen-Jimenez, D. *Chem. Mater*. **2017**, 29, 2618–2625.

(17) Ongari, D.; Talirz, L.; Smit, B. *ACS Cent. Sci*. **2020**, 6, 1890–1900.

(18) Jiao, L.; Seow, J. Y. R.; Skinner, W. S.; Wang, Z. U.; Jiang, H.-L. *Mater. Today* **2019**, 27, 43–68.

(19) Wang, K.; Feng, D.; Liu, T.-F.; Su, J.; Yuan, S.; Chen, Y.-P.; Bosch, M.; Zou, X.; Zhou, H.-C. *J. Am. Chem. Soc*. **2014**, 136, 13983–13986.

(20) Feng, Y.; Hu, H.; Wang, Z.; Du, Y.; Le Zhong; Zhang, C.; Jiang, Y.; Jia, S.; Cui, J. *J. Colloid Interface Sci*. **2021**, 590, 436–445.

(21) Li, B.; Wang, H.; Chen, B. *Chem. Asian J*. **2014**, 9, 1474–1498.

(22) Hulla, J. E.; Sahu, S. C.; Hayes, A. W. *Hum. Exp. Toxicol*. **2015**, 34, 1318–1321.

(23) Wang, S.; McGuirk, C. M.; d'Aquino, A.; Mason, J. A.; Mirkin, C. A. *Adv. Mater*. **2018**, 30, e1800202.

(24) Iqbal, P.; Preece, J. A.; Mendes, P. M. *Nanotechnology: The "Top-Down" and "Bottom-Up" Approaches. In Supramolecular Chemistry*; Gale, P. A., Steed, J. W., Eds.; John Wiley & Sons, Ltd: Chichester, UK, **2012**.

(25) Andreo, J.; Ettlinger, R.; Zaremba, O.; Peña, Q.; Lächelt, U.; Luis, R. F. de; Freund, R.; Canossa, S.; Ploetz, E.; Zhu, W.; Diercks, C. S.; Gröger, H.; Wuttke, S. *J. Am. Chem. Soc.*. **2022**, 144, 7531–7550.

(26) Marshall, C. R.; Staudhammer, S. A.; Brozek, C. K. *Chem. Sci*. **2019**, 10, 9396–9408.

(27) Haase, F.; Hirschle, P.; Freund, R.; Furukawa, S.; Ji, Z.; Wuttke, S. *Angew. Chem. Int. Ed.* **2020**, 59, 22350–22370.

(28) Carné, A.; Carbonell, C.; Imaz, I.; Maspoch, D. *Chem. Soc. Rev*. **2011**, 40, 291–305.

(29) Chevreau, H.; Permyakova, A.; Nouar, F.; Fabry, P.; Livage, C.; Ragon, F.; Garcia-Marquez, A.; Devic, T.; Steunou, N.; Serre, C.; Horcajada, P. *CrystEngComm* **2016**, 18, 4094–4101.

(30) Lamer, V. K.; Dinegar, R. H. *J. Am. Chem. Soc.* **1950**, 72, 4847–4854.

(31) Tsai, C.-W.; Langner, E. H.G. *Microporous Mesoporous Mater*. **2016**, 221, 8–13.

(32) Dang, S.; Song, S.; Feng, J.; Zhang, H. *Sci. China Chem*. **2015**, 58, 973–978.

(33) Lozano, L. A.; Iglesias, C. M.; Faroldi, B. M.C.; Ulla, M. A.; Zamaro, J. M. *J. Mater. Sci.* **2018**, 53, 1862–1873.

(34) Tranchemontagne, D. J.; Hunt, J. R.; Yaghi, O. M. *Tetrahedron* **2008**, 64, 8553–8557.

(35) Pan, Y.; Liu, Y.; Zeng, G.; Zhao, L.; Lai, Z. *Chem. Commun*. **2011**, 47, 2071–2073.

(36) Wee, L. H.; Lohe, M. R.; Janssens, N.; Kaskel, S.; Martens, J. A. *J. Mater. Chem*. **2012**, 22, 13742.

(37) Barros, B. S.; de Lima Neto, O. J.; de Oliveira Frós, A. C.; Kulesza, *J. ChemistrySelect* **2018**, 3, 7459–7471.

(38) Ganesh, M.; Hemalatha, P.; Peng, M. M.; Cha, W. S.; Jang, H. T. *Aerosol Air Qual. Res.* **2014**, 14, 1605–1612.

(39) Ploetz, E.; Engelke, H.; Lächelt, U.; Wuttke, S. *Adv. Funct. Mater.* **2020**, 30, 1909062.

(40) Simon, M. A.; Anggraeni, E.; Soetaredjo, F. E.; Santoso, S. P.; Irawaty, W.; Thanh, T. C.; Hartono, S. B.; Yuliana, M.; Ismadji, S. *Sci. Rep.* **2019**, 9, 16907.

(41) García Márquez, A.; Demessence, A.; Platero-Prats, A. E.; Heurtaux, D.; Horcajada, P.; Serre, C.; Chang, J.-S.; Férey, G.; La Peña-O'Shea, V. A. de; Boissière, C.; Grosso, D.; Sanchez, C. *Eur. J. Inorg. Chem.* **2012**, 5165–5174.

(42) Ma, J.; Lee, S. M.-Y.; Yi, C.; Li, C.-W. *Lab Chip* **2017**, 17, 209–226.

(43) Khan, I. U.; Serra, C. A.; Anton, N.; Vandamme, T. *J. Controlled Release* **2013**, 172, 1065–1074.

(44) Zhang, L.; Xia, Y. *Adv. Mater.* **2014**, 26, 2600–2606.

(45) Ganguli, A. K.; Ganguly, A.; Vaidya, S. *Chem. Soc. Rev.* **2010**, 39, 474–485.

(46) Zhang, L.; Wang, Y.; Tong, L.; Xia, Y. *Nano Lett.* **2014**, 14, 4189–4194.

(47) Ye, R.; Ni, M.; Xu, Y.; Chen, H.; Li, S. *RSC advances* **2018**, 8, 26237–26242.

(48) Shang, W.; Kang, X.; Ning, H.; Zhang, J.; Zhang, X.; Wu, Z.; Mo, G.; Xing, X.; Han, B. *Langmuir* **2013**, 29, 13168–13174.

(49) Sun, W.; Zhai, X.; Zhao, L. *Chem. Eng. J.* **2016**, 289, 59–64.

(50) Pope, C. G. *J. Chem. Educ.* **1997**, 74, 129–131.

(51) Gropp, C.; Canossa, S.; Wuttke, S.; Gándara, F.; Li, Q.; Gagliardi, L.; Yaghi, O. M. *ACS Cent. Sci.* **2020**, 6, 1255–1273.

(52) Subudhi, S.; Tripathy, S. P.; Parida, K. Catal. *Sci. Technol.* **2021**, 11, 392–415.

(53) Winey, M.; Meehl, J. B.; O'Toole, E. T.; Giddings, T. H. *Mol. Biol. Cell* **2014**, 25, 319–323.

(54) Anderson, W.; Kozak, D.; Coleman, V. A.; Jämting, Å. K.; Trau, M. *J. Colloid Interface Sci.* **2013**, 405, 322–330.

(55) Modena, M. M.; Rühle, B.; Burg, T. P.; Wuttke, S. *Adv. Mater.* **2019**, 31, e1901556.

(56) Pecora, R. *J. Nanopart. Res.* **2000**, 2, 123–131.

(57) Kumar, K. V.; Gadipelli, S.; Wood, B.; Ramisetty, K. A.; Stewart, A. A.; Howard, C. A.; Brett, D. J. L.; Rodriguez-Reinoso, F. *J. Mater. Chem. A* **2019**, 7, 10104–10137.

(58) Abu-Alsoud, G. F.; Hawboldt, K. A.; Bottaro, C. S. *ACS Appl. Mater. Interfaces* **2020**, 12, 11998–12009.

(59) Králik, M. *Chem. Pap.* **2014**, 68, 252.

(60) ALOthman, Z. *Materials* **2012**, 5, 2874–2902.

(61) Thommes, M.; Kaneko, K.; Neimark, A. V.; Olivier, J. P.; Rodriguez-Reinoso, F.; Rouquerol, J.; Sing, K. S.W. *Pure Appl. Chem.* **2015**, 87, 1051–1069.

(62) K. S. W. SING. *Pure Appl. Chem.* **1982**, 57, 2201–2218.

(63) Chowdhury, P.; Mekala, S.; Dreisbach, F.; Gumma, S. *Microporous Mesoporous Mater.* **2012**, 152, 246–252.

(64) H. Förster. *Mol. Sieves* **2004**, 4, 337–426.

(65) Schönhoff, M. *COCIS* **2013**, 18, 201–213.

(66) Hamilton, R. J.; Sewell, P. A. *Introduction to high performance liquid chromatography*, Eds., 2nd; Chapman and Hall Ltd: London, **1982**.

(67) Kumar, P.; Bansal, V.; Kim, K.-H.; Kwon, E. E. *J. Ind. Eng. Chem.* **2018**, 62, 130–145.

(68) Hooriabad Saboor, F.; Nasirpour, N.; Shahsavari, S.; Kazemian, H. *Chem. Asian J.* **2022**, 17, 1-23.

(69) Rani, L.; Kaushal, J.; Srivastav, A. L.; Mahajan, P. *Environ. Sci. Pollut. Res. Int.* **2020**, 27, 44771–44796.

(70) Gothwal, R.; Shashidhar, T. *CLEAN - Soil, Air, Water* **2015**, 43, 479–489.

(71) Daughton, C. G.; Ruhoy, I. S. Sci. *Total Environ*. **2013**, 443, 324–337.

(72) Azhar, M. R.; Abid, H. R.; Sun, H.; Periasamy, V.; Tadé, M. O.; Wang, S. *J. Colloid Interface Sci.* **2016**, 478, 344–352.

(73) Hasan, Z.; Khan, N. A.; Jhung, S. H. *Chem. Eng. J.* **2016**, 284, 1406–1413.

(74) Li, N.; Zhou, L.; Jin, X.; Owens, G.; Chen, Z. *J. Hazard. Mater*. **2019**, 366, 563–572.

(75) Rezania, S.; Taib, S. M.; Md Din, M. F.; Dahalan, F. A.; Kamyab, H. *J. Hazard. Mater.* **2016**, 318, 587–599.

(76) Yang, P.; Shu, Y.; Zhuang, Q.; Li, Y.; Gu, J. *Langmuir* **2019**, 35, 16226–16233.

(77) Yang, P.; Shu, Y.; Zhuang, Q.; Li, Y.; Gu, *J. Chem. Commun*. **2019**, 55, 12972–12975.

(78) Hasankola, Z. S.; Rahimi, R.; Safarifard, V. *Inorg. Chem. Commun*. **2019**, 107, 107474.

(79) Safaei, M.; Foroughi, M. M.; Ebrahimpoor, N.; Jahani, S.; Omidi, A.; Khatami, M. *TrAC, Trends Anal. Chem*. **2019**, 118, 401–425.

(80) Yang, C.; Miao, G.; Pi, Y.; Xia, Q.; Wu, J.; Li, Z.; Xiao, J. *Chem. Eng. J*. **2019**, 370, 1128–1153.

(81) Chen, R.; Yao, Z.; Han, N.; Ma, X.; Li, L.; Liu, S.; Sun, H.; Wang, S. *ACS omega* **2020**, 5, 15402–15408.

(82) Senkovska, I.; Barea, E.; Navarro, J. A. R.; Kaskel, S. *Microporous Mesoporous Mater*. **2012**, 156, 115–120.

(83) Chowdhury, M. A. *ChemBioEng Reviews* **2017**, 4, 225–239.

(84) Wu, M.-X.; Yang, Y.-W. *Adv. Mater*. **2017**, 29.

(85) Fu, C.; Zhou, H.; Tan, L.; Huang, Z.; Wu, Q.; Ren, X.; Ren, J.; Meng, X. *ACS nano* **2018**, 12, 2201–2210.

(86) Blanco, E.; Shen, H.; Ferrari, M. *Nat. Biotechnol*. **2015**, 33, 941–951.

(87) Ahmadi, M.; Ayyoubzadeh, S. M.; Ghorbani-Bidkorbeh, F.; Shahhosseini, S.; Dadashzadeh, S.; Asadian, E.; Mosayebnia, M.; Siavashy, S. *Heliyon* **2021**, 7, e06914.

(88) Horcajada, P.; Gref, R.; Baati, T.; Allan, P. K.; Maurin, G.; Couvreur, P.; Férey, G.; Morris, R. E.; Serre, C. *Chem. Rev*. **2012**, 112, 1232–1268.

(89) Férey, G.; Mellot-Draznieks, C.; Serre, C.; Millange, F.; Dutour, J.; Surblé, S.; Margiolaki, I. *Science* **2005**, 309, 2040–2042.

(90) Taylor-Pashow, K. M. L.; Della Rocca, J.; Xie, Z.; Tran, S.; Lin, W. *J. Am. Chem. Soc.* **2009**, 131, 14261–14263.

(91) Chen, W.; Wu, C. *Dalton Trans*. **2018**, 47, 2114–2133.

(92) Ma, M.; Noei, H.; Mienert, B.; Niesel, J.; Bill, E.; Muhler, M.; Fischer, R. A.; Wang, Y.; Schatzschneider, U.; Metzler-Nolte, N. *Chem. Eng. J*. **2013**, 19, 6785–6790.

(93) Martínez, C.; Corma, A. *Coord. Chem. Rev*. **2011**, 255, 1558–1580.

(94) Dong, H.; Fan, Y.; Zhang, W.; Gu, N.; Zhang, Y. *Bioconjug. Chem*. **2019**, 30, 1273–1296.

(95) B. F. Hoskins and Richard Robson. *J. Am. Chem. Soc.* **1990**, 112, 1546–1554.

(96) Fujita, M.; Kwon, Y. J.; Washizu, S.; Ogura, K. J *J. Am. Chem. Soc.* **1994**, 116, 1151–1152.

(97) Lee, J.; Farha, O. K.; Roberts, J.; Scheidt, K. A.; Nguyen, S. T.; Hupp, J. T. *Chem. Soc. Rev.* **2009**, 38, 1450–1459.

(98) Wang, Q.; Astruc, D. *Chem. Rev*. **2020**, 120, 1438–1511.

(99) Rosi, N. L.; Eckert, J.; Eddaoudi, M.; Vodak, D. T.; Kim, J.; O'Keeffe, M.; Yaghi, O. M. *Science* **2003**, 300, 1127–1129.

(100) Hee K. Chae, Diana Y. Siberio-Perez, Jaheon Kim, YongBok Go, Mohamed Eddaoudi, Adam J. Matzger, Michael O'Keeffe, Omar M. Yaghi1. *Nature* **2004**, 427, 521–523.

(101) Jiang, Z.-R.; Wang, H.; Hu, Y.; Lu, J.; Jiang, H.-L. *Che*mSusChem **2015**, 8, 878–885.

(102) Akiyama, G.; Matsuda, R.; Sato, H.; Kitagawa, S. *Chem. Asian J.* **2014**, 9, 2772–2777.

(103) Schröder, F.; Esken, D.; Cokoja, M.; van den Berg, M. W. E.; Lebedev, O. I.; van Tendeloo, G.; Walaszek, B.; Buntkowsky, G.; Limbach, H.-H.; Chaudret, B.; Fischer, R. A. *J. Am. Chem. Soc.* **2008**, 130, 6119–6130.

Chapter 2

Chapter 2

Synthesis and characterization of MOFs and MOF nanoparticles

2.1 INTRODUCTION

As previously described in *Chapter 1*, Metal-Organic Frameworks are a class of porous crystalline materials with large surface areas that have great advantages, mainly because of the possibility of tunning the framework to obtain different properties. Up to now, 100.000 articles have been published[1], which shows how the field of MOFs has developed since the discovery of the first porous material of this type[2]. This growth underlines the importance of materials science, whose main objective is to lead the way starting from the discovery and design of new materials to their possible applications, in order to address social challenges. This process is depicted in Figure 2.1.
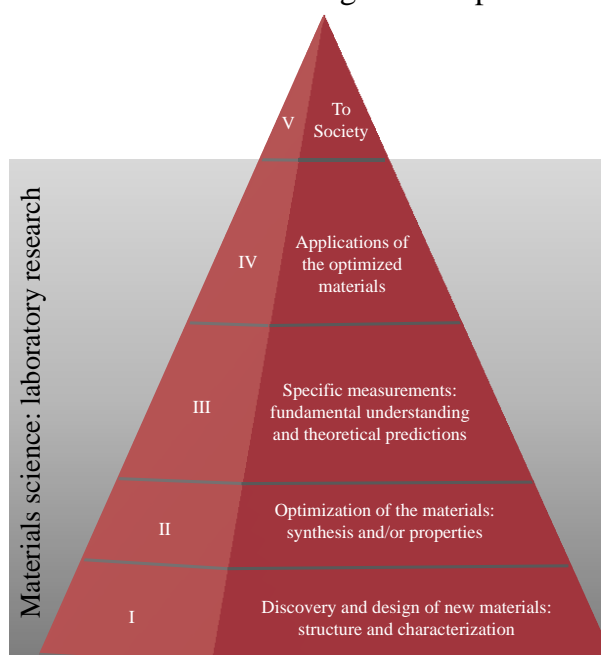
Figure 2.1. The materials synthesis pyramid: since the discovery and design of new materials to the implementation in society (stages I-V).

Even though new MOFs are discovered constantly, efforts to understand and improve the already existing ones are of reliable importance. The synthesis of MOFs is a very delicate process since a great variety of factors can affect the formation of the framework such as solvents, molar ratios of the precursors, synthesis methods, reaction times and temperature[3]. In addition, chemical designability allows not only to combine many different building blocks but also to selectively change a single structural parameter or functional group in order to tune the required properties according to the applications. As an example, isoreticular MOFs can be found, which are formed using different linkers (*i.e.* with different length between the coordinating functional groups or different side substituent.) and own similar topology[4]. Eddaoudi *et al.*[5] synthesized a class of isoreticular MOFs, named IRMOFs, with cubic topology using many ditopic carboxylate linkers. As a result, they obtained MOFs with different pore functionality and size, obtaining pores in the mesoporous range (> 20 Å). Another strategy that can be followed is the functionalization of the internal or external surface in reticular materials, where different approaches can be performed such as the introduction of covalent bonds to the linkers, electrostatic interactions between the framework and guest species or linker exchange[6,7].

Since nanoscience and nanotechnology were born, there has been an increasing interest to study materials at this length scale. Over the years, it was discovered that downsizing a material from the micro- to the nano-scale could completely change its properties[8]. In the case of MOFs, it has been proven that nanoparticles inherit some of the properties of their bulk precursor like high porosity or internal surface areas, while new properties characteristics from the nanoregime are displayed. Among them, short diffusion distances and enhanced adsorption kinetics can be outlined[9]. Although it is highly remarkable that the properties of MOFs can be designed as desired, it is important to control the synthesis of materials with high precision in order to obtain homogenous batches in size and in shape.

These requirements and the lack of optimized protocols motivated us to write this chapter with the main objective of briefly summarizing the synthesis and basic characterization, generally, powder X-ray diffraction, dynamic light scattering and scanning electron microscopy of all Metal-Organic Frameworks used along this PhD thesis. This chapter is divided in two different sections. In the first one, the effect of

some synthesis parameters on the size and shape of MOFs are studied. The aim is to show the optimization process to obtain well-shaped and homogeneous particles of some well-known MOFs: Zr-fumarate, UiO-66 and UiO-66-NH$_2$, isostructural zeolitic imidazole frameworks, ZIF-8 and ZIF-67 and flexible MIL-88A(Fe). For that, the effect of different factors like reaction times, modulators or molar ratios on the size and shape of the MOFs were investigated. In the second part, the characterization of MIL-127, M-MOF-74 (M = Ni, Co, Cu), Cu-TDPAT, JUK-8 and ZU-301 is shown following already reported protocols. Almost all the prepared MOFs will be used in the following chapters of the PhD thesis.

2.2 EXPERIMENTAL PROCEDURE

2.2.1 Chemicals

Iron(III) chloride hexahydrate (FeCl$_3$·6H$_2$O, 99+%), zinc acetate dihydrate (Zn(COO)$_2$·2H$_2$O, 98%), fumaric acid (99+%), zirconium(IV) chloride (ZrCl$_4$, 98%), terephthalic acid (TPA, 99+%), 2-aminoterephthalic acid (99%), 2- methylimidazole (98%), cetyltrimethylammonium bromide (CTAB, 99+%), benzoic acid (99.5%), oxalic acid (98%) and acetic acid (AA, 99.8%) were purchased from Acros Organics. Cobalt(II) nitrate hexahydrate (Co(NO$_3$)$_2$·6H$_2$O, 98%) was purchased from Carl Roth, zinc(II) carbonate (ZnCO$_3$, 97%) from Alfa Aesar. Copper(II) nitrate trihydrate (Cu(NO$_3$)$_2$·3H$_2$O, 99%), 2,5-dihydroxiterephthalic acid (DHTPA, 99%) and 3-methyl-1H-1,2,4-triazole (Mtz) from Fluorochem. Nickel(II) nitrate hexahydrate (Ni(NO$_3$)$_2$·6H$_2$O, extra pure) and propionic acid (PA, 98%) were purchased from Fisher Scientific. Copper(II) acetate hydrate (Cu(OAc)$_2$·H$_2$O, 98.1%) was purchased from BLDpharm and N,N-dimethylformamide (DMF, 99.9% GLR), formic acid (FA, 98%) and methanol (MeOH, 99.8%) from Labkem. Ethanol (EtOH, denatured) was purchased from Chem-labs. All reagents were used without further purification except for ethanol that was distilled in order to remove the denaturant.

2.2.2 Synthesis of metal-organic frameworks

Zr-fumarate. Zirconium chloride (0.120 mg, 0.51 mmol) and fumaric acid (0.181 mg, 1.54 mmol) were dissolved in a mixture of DMF (10 mL) and formic acid (0.95 mL). The mixture was placed in an oven at 110 °C for different reaction times (4, 8, 12, 18 and 24 h). Subsequently, it was allowed to cool down and the solid was recovered by centrifugation. It was washed by centrifugation (14000 rpm, 5 min, 12 mL) x 3 redispersing each time in DMF. Thin layer chromatography (TLC) was used in order to make sure that there is no more fumaric acid in the supernatant after the last centrifugation step in DMF. The crystal structure of Zr-fumarate is depicted in Figure 2.2.

a)

b)
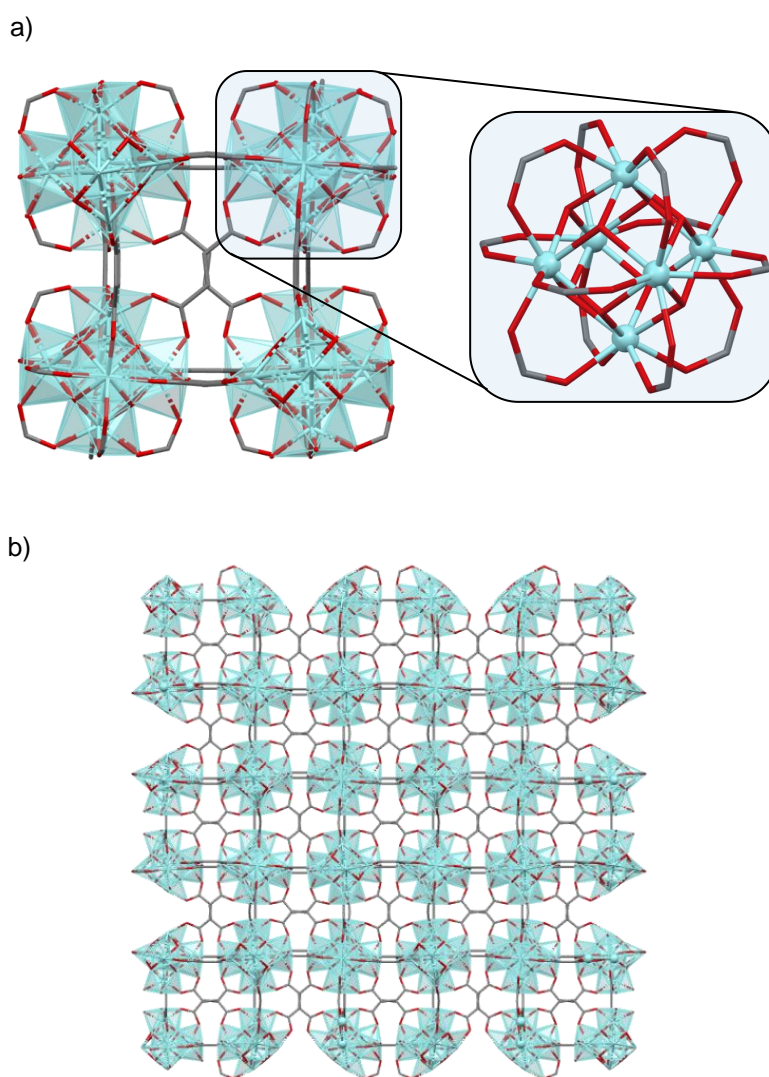
**Figure 2.2.** a) SBU found in Zr-fumarate $Zr_6O_4(OH)_4(C_4H_2O_4)_6$ [10] and b) crystal packing.

UiO-66 and UiO-66-NH₂(Zr). Zirconium chloride (0.886 g, 3.72 mmol) and terephthalic acid (0.623 g, 3.71 mmol) were dissolved in a mixture of DMF (100 mL) and modulators (formic acid, FA (14 mL, 37.10 mmol), acetic acid, AA (2.13 mL, 37.10 mmol) or propionic acid, PA (2.78 mL, 37.10 mmol)). In some cases, water (20 µL, 1.11 mmol) was added to the reaction mixture. The mixture was placed in an oven at 120 °C for 24 h.

For the amino-functionalized MOF the synthetic procedure was similar using 2-aminoterephthalic acid (0.681 g, 3.71 mmol) as a linker instead of terephthalic acid, DMF (100 mL) and formic acid (14 mL, 37.10 mmol) as a modulator.

In both cases, the resulting reaction mixture was allowed to cool down and the solid was recovered by centrifugation. It was washed by centrifugation (18000 rpm, 30 min, 84 mL) x 2 redispersing each time in DMF. Thin layer chromatography (TLC) was used in order to make sure that there is no more terephthalic acid in the supernatant after the last centrifugation step in DMF. In order to change the solvent, the sample is split into two tubes and centrifuged (18000 rpm, 1 h, 84 mL) x 3 in EtOH.

In order to study the effect of activation, UiO-66_FA_DMF was activated heating MOF samples at 150 °C for 20 minutes in a microwave reactor, with heavy stirring. After cooling to room temperature, the MOF was washed (18000 rpm, 1 h, 6 mL) x 3 H_2O and dry in the oven at 100 °C for 24 h. The crystal structure of UiO-66 is shown in Figure 2.3.

a)
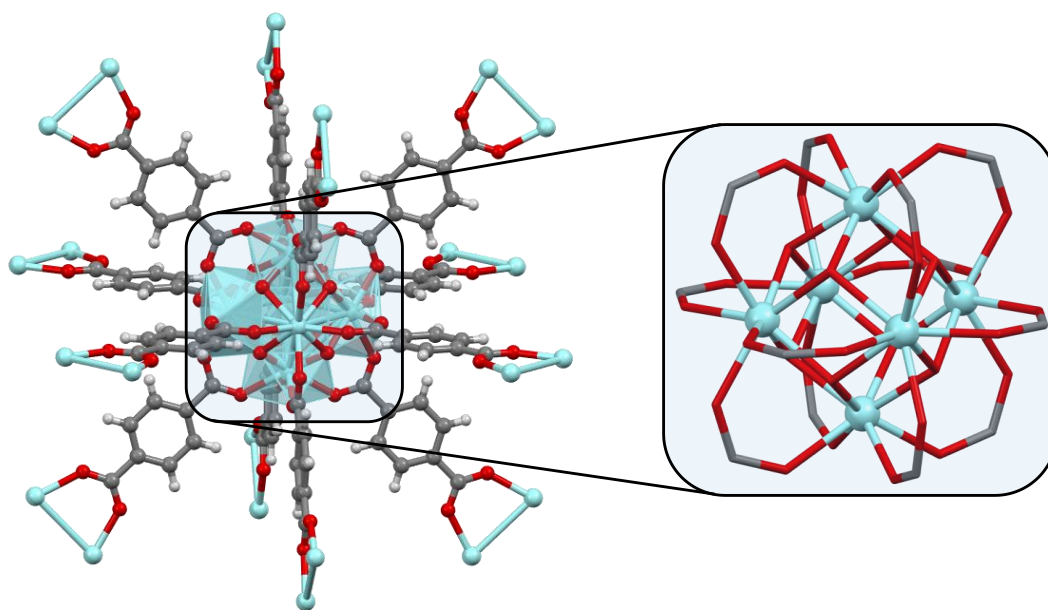
b)
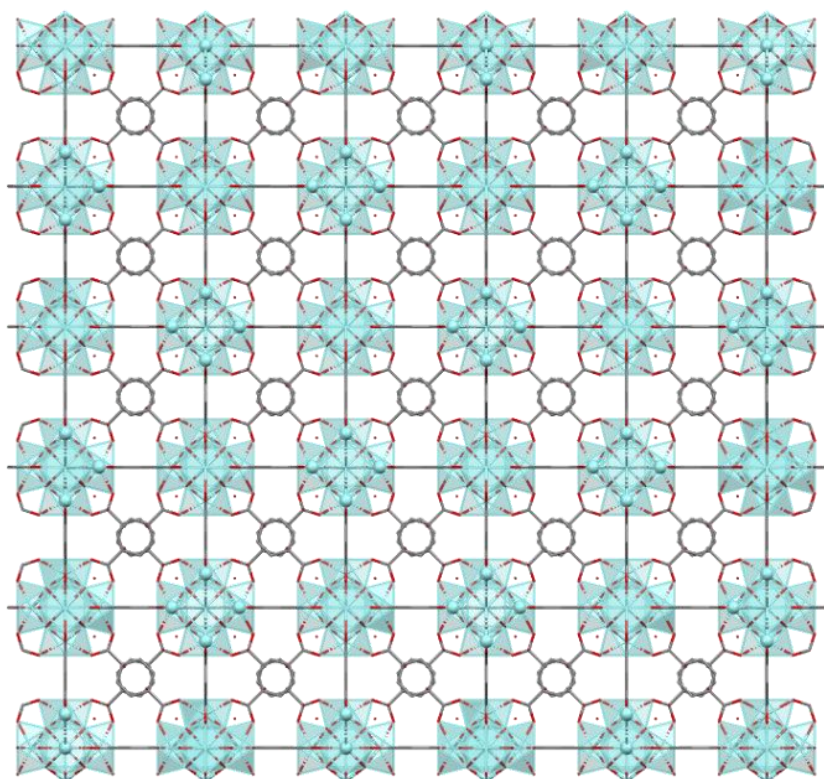
Figure 2.3. a) SBU found in UiO-66 [Zr$_6$O$_4$(OH)$_4$(BDC)$_6$][11] and b) crystal packing.

ZIF-8(Zn). For the synthesis of ZIF-8 two different methodologies were used. Procedure A: the metal salt aqueous solution was added to a mixture of linker/CTAB and procedure B: linker aqueous solution was added to a mixture of metal salt/CTAB solution.

ZIF-8 cubes, truncated cubes (TC) and truncated cubes-dodecahedrons (TC_TRD) were obtained using 1:9.7:0.0011 molar ratio of Zn:2-MeIm:CTAB. Briefly, 2-methylimidazole (4.36 g, 52.60 mmol) and CTAB (894 µL, 7.05 mM) were dissolved in water (20 mL). Then, zinc(II) acetate (1.21 g, 5.40 mmol) dissolved in water (19.11 mL) was added to the solution (procedure A) and stirred for 5 minutes (the clear solution turned white after a few seconds). The white suspension was left undisturbed for 15 minutes or 2 h in order to get cubes or truncated cubes (TC), respectively. Contrarily, when the same amount of reagents were used but procedure B was followed truncated cubes and dodecahedrons (TC-TRD) were obtained.

Truncated rhombic dodecahedron (TRD) ZIF-8 were synthesized with 1:9.7:0.011 molar ratio of Zn:2-MeIm:CTAB, as follows: 2-methylimidazole (5.362 g, 64.70 mmol) and CTAB (1.93 mL, 6.98 mM) were dissolved in water (30 mL). Then, zinc(II) acetate (1.50 g, 6.70 mmol) dissolved in water (18.07 mL) was added to the solution and stirred for 5 minutes (the clear solution turned white after a few seconds). The white suspension was left undisturbed for 2 h.

In all cases, ZIF-8 nanoparticles were recovered by centrifugation and washed by centrifugation (18 000 rpm, 15 min, 30 mL) x 5 in ethanol. The supernatant of each washing step was tested with 2-bromothymol blue until no linker could be detected by colour change.

ZIF-67(Co). Different syntheses were carried out in order to obtain particles of different sizes and shapes. Generally, a cobalt(II) nitrate aqueous solution was prepared and added to a mixture of 2-methylimidazole and CTAB aqueous solution. Different molar ratios were used and samples were labelled as follows: ZIF-67_Co:2-MeIm:CTAB, water (mL). The mixture was stirred for 13 minutes at room temperature (the clear solution turned purple, immediately) and the purple suspension was left undisturbed (3 h or 24 h) at room temperature. ZIF-67 nanoparticles were

recovered and washed by centrifugation (21500 rpm, 15 min, 36 mL) x 4 in methanol. The crystal structure of isostructural ZIF-8/-67 is shown in Figure 2.4.
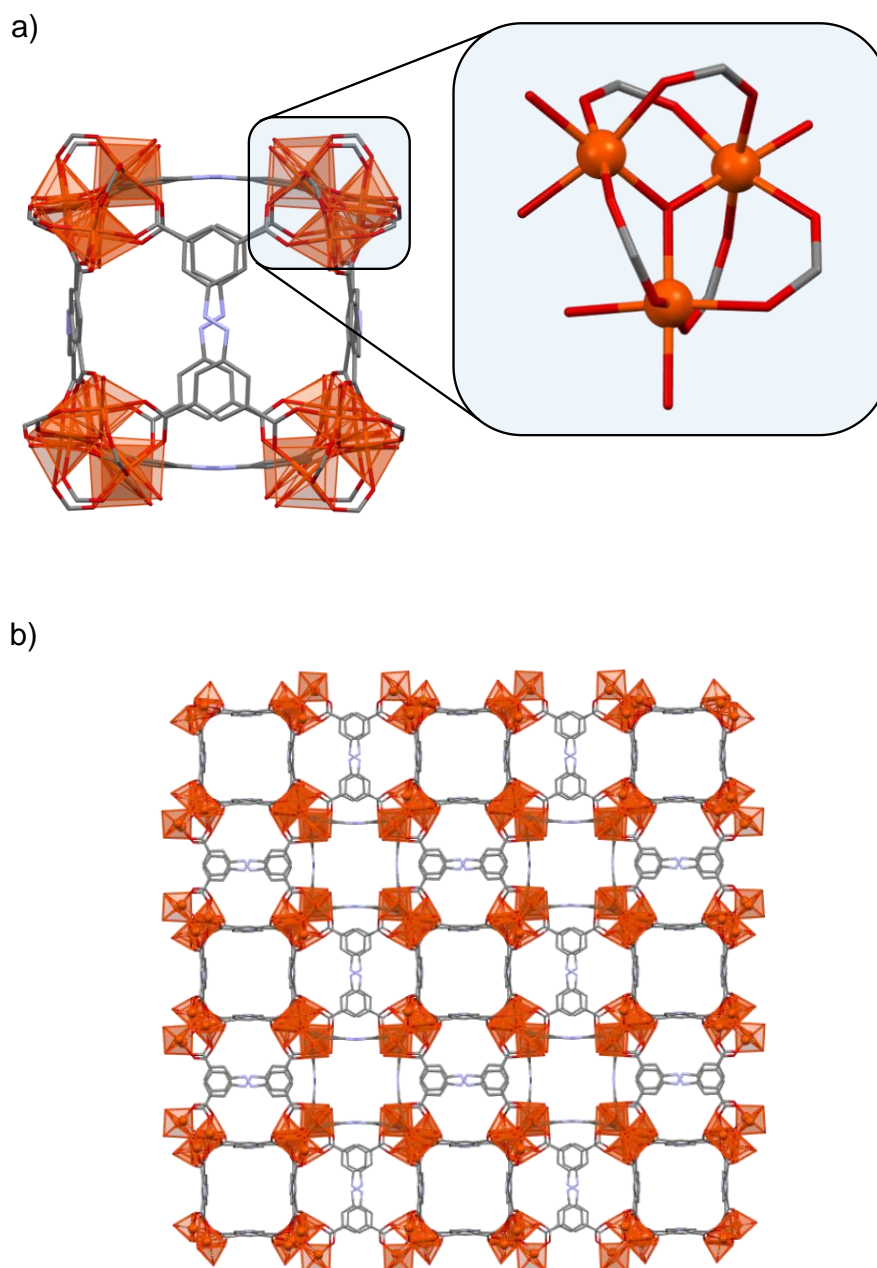
a)
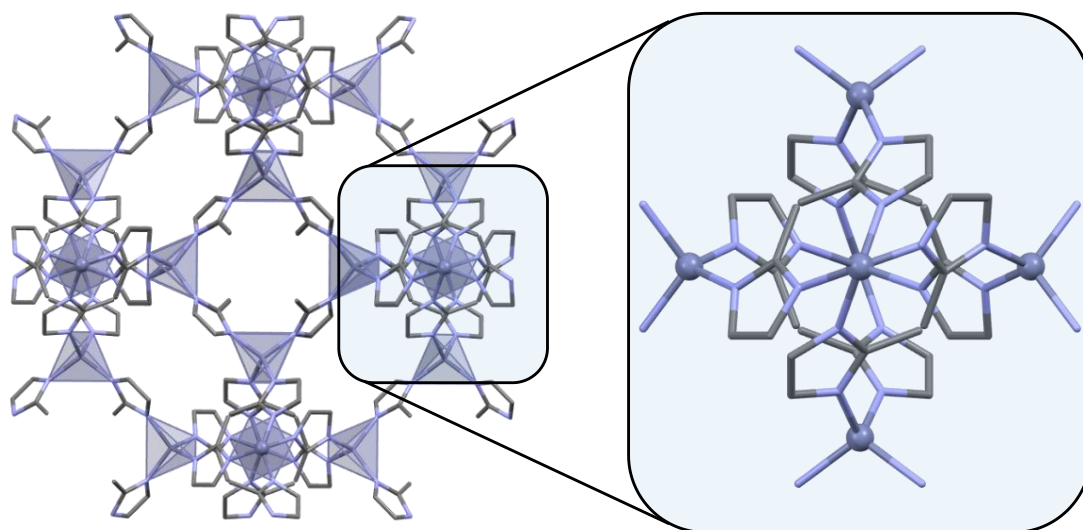
b)
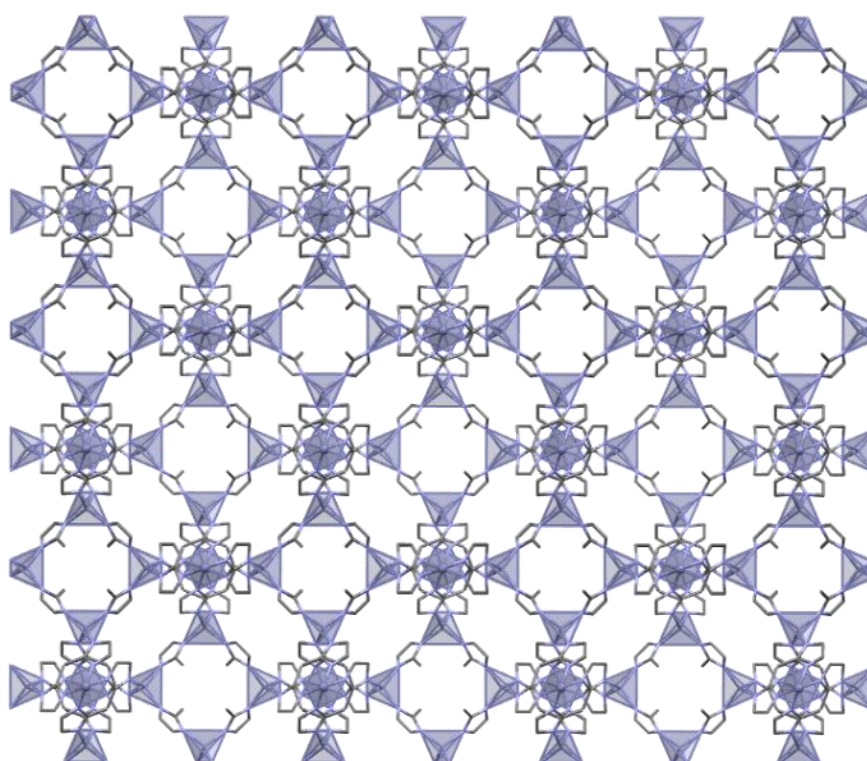
Figure 2.4. a) Details of the connectivity found in ZIF-8 and ZIF-67 $[M(2\text{-mIm})_2]_n$[12] and b) crystal packing enhancing the channel present in the crystal structure.

MIL-88A(Fe). MIL-88A(Fe) samples with different particle sizes were synthesized. For that, already reported protocols were used with some modifications[13,14]. Briefly, iron(III) chloride hexahydrate (1.381 g, 5.11 mmol) and fumaric acid (0.593 g, 5.11 mmol) were dissolved in a mixture of 25 mL of solvent: DMF (MIL-88A_DMF), 1:1 (v:v) DMF:water (MIL-88A_DMF:H_2O) and H_2O (MIL-88A_H_2O). The reaction mixture was placed in a preheated oven at 65 °C for a specific time: (MIL-88A_DMF and MIL-88A_H_2O for 12 hours and MIL-88A_DMF:H_2O for 4 hours. The compound was recovered by centrifugation and washed (15000 rpm, 15 min, 36 mL) x 2 in water and x 3 in ethanol. Crystal structure of MIL-88A is shown in Figure 2.5.
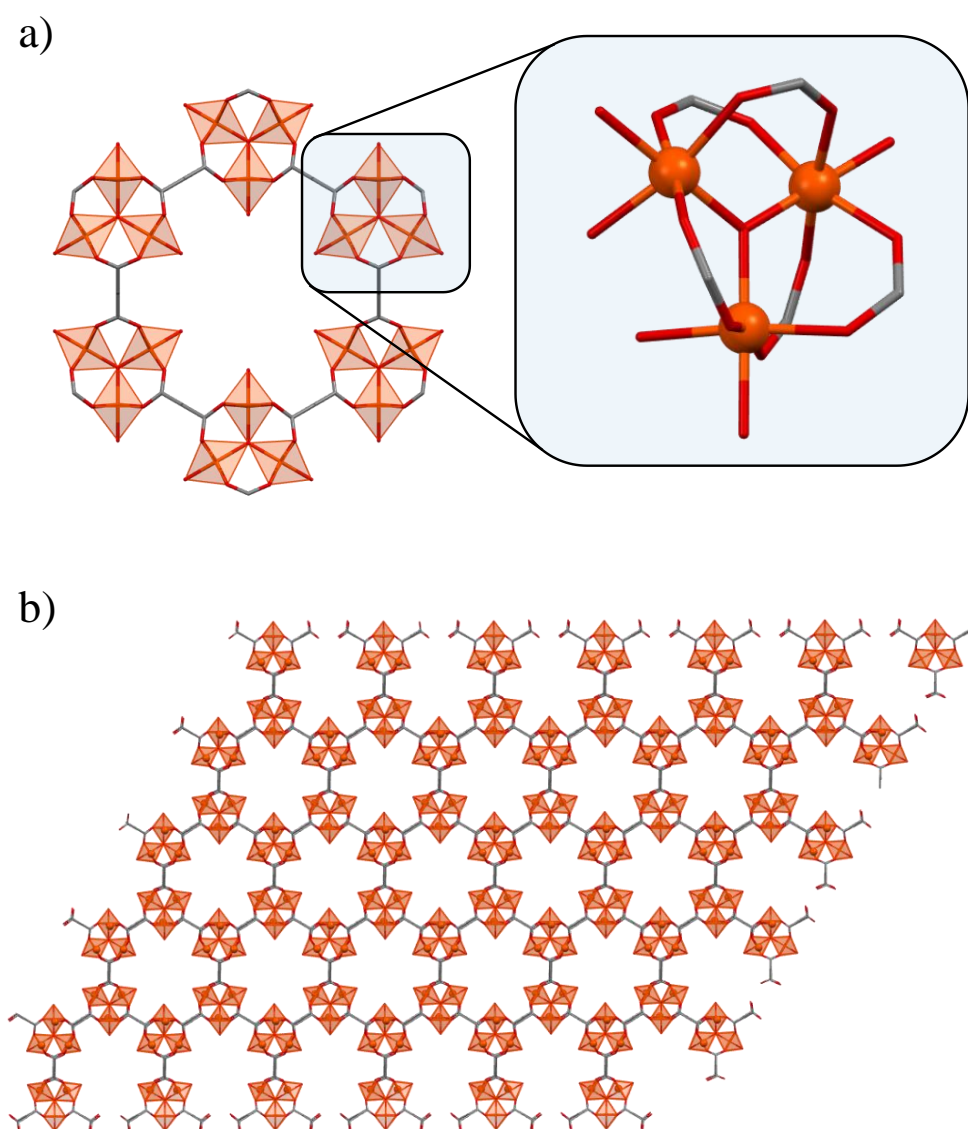
Figure 2.5. a) SBU found in MIL-88A [Fe$_3$O(H_2O)$_2$(fumarate)$_3$]$_n$[15] and b) crystal packing enhancing the channel present in the crystal structure.

MIL-127(Fe). MIL-127(Fe) was synthesized according to an already reported[16]. In a round bottom flask containing 50 mL of DMF, $FeCl_3 \cdot 6H_2O$ (34.40 g, 13.00 mmol) and H_4-TazBz (22.20 g, 62.00 mmol) were introduced. Then, the mixture was stirred under reflux for 24 h. The resulting brown solid was recovered by filtration, washed four times with 100 ml of DMF (the first two at 80 °C), twice with 100 mL of acetone and then dried under vacuum (Figure 2.6).

a)

b)

Figure 2.6. a) Details of the connectivity found in MIL-127 [$Fe_3O(H_2O)_2(C_{16}H_{10}N_2O_8)_{4/3}Cl)_n$[17]] and b) crystal packing enhancing the channel present in the crystal structure.

MOF-74(Ni). In a 500 ml round bottom flask, $Ni(NO_3)_2 \cdot 6H_2O$ (3.80 g, 13.00 mmol) and 2,5-dihydroxyterephthalic acid (1.15 g, 5.70 mmol) were suspended in 300 ml of a 1:1:1 DMF, EtOH and H_2O solvent mixture. The mixture cleared to a green solution at 80 ºC and was kept at 125 ºC for 1 hour. Then 0.5 ml of concentrated aqueous ammonia (30%) were added, and the flask was kept at 125 ºC for 48 hours. The resulting precipitate was filtered, and washed twice with DMF for 2 h at 80 ºC, then twice with water for 2 hours and twice with ethanol at room temperature for 1 day. The resulting olive green powder was dried in the air at room temperature.

MOF-74(Co). MOF-74(Co) was synthesized according to an already reported procedure[18]. Cobalt(II) nitrate hexahydrate (0.717 g, 2.41 mmol) was dissolved in a mixture of water, DMF, and ethanol (60 mL, 1:1:1, v:v:v) and then, 2,5-dihydroxyterephthalic acid (0.145 g, 0.73 mmol) was added. The reaction mixture was stirred for a few minutes at room temperature and the autoclave was sealed. The autoclave was put into an oven at 120 °C for 24 h. The solid was recovered by centrifugation and washed (15000 rpm, 30 min, 6 mL) x 3 in hot DMF. Afterwards, it was washed 3 times in ethanol and then stored in ethanol over two days.

MOF-74(Cu). MOF-74(Cu) was synthesized according to an already reported procedure[19]. Copper(II) acetate hydrate (0.204 g, 1.00 mmol) and 2,5-dihydroxyterephthalic acid (0.101 g, 0.51 mmol) were dissolved separately in 7.5 mL of methanol. Copper acetate solution was added dropwise to the linker solution and it was stirred at room temperature for 24 h. The solid was recovered by centrifugation and washed (15000 rpm, 30 min, 6 mL) x 3 in hot DMF. Afterwards, it was washed 3 times in ethanol and then stored in ethanol over two days.

The crystal structure of M-MOF-74 is depicted in Figure 2.7.

a)

b)
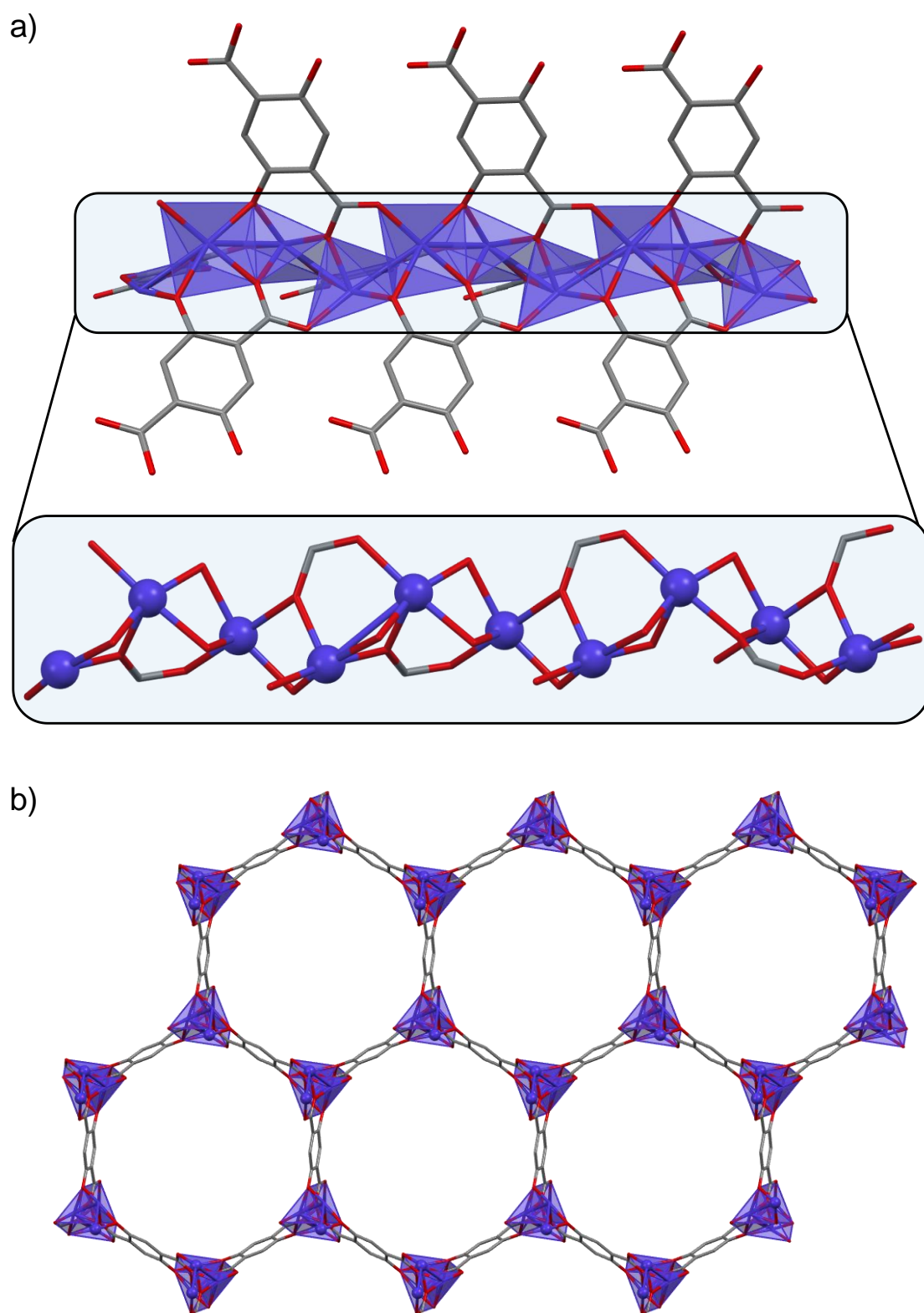
Figure 2.7. a) 1D SBU found in M-MOF-74 ([M_2(dhta)(H_2O)$_2$]$_n$ and b) crystal packing enhancing the channel present in the crystal structure.

Cu-TDPAT. Cu-TDPAT was synthesized according to an already reported procedure[20]. 2.416 g of $Cu(NO_3)_2 \cdot 3H_2O$ (10 mmol) and 1.236 g of H_6TDPAT (2 mmol) were suspended in 100 ml of DMF in a round bottom flask and sonicated for 5 minutes. The mixture was then heated at 100 ℃ for 24 hours. The turquoise precipitate was filtered from the greed solution and washed 2 times for 2 h with 50ml of DMF at 80 ℃ and twice again at room temperature. The solid was then dispersed twice in 50 ml of acetone for 2 and 24 hours respectively, before the final filtration and vacuum drying (Figure 2.8).

a)
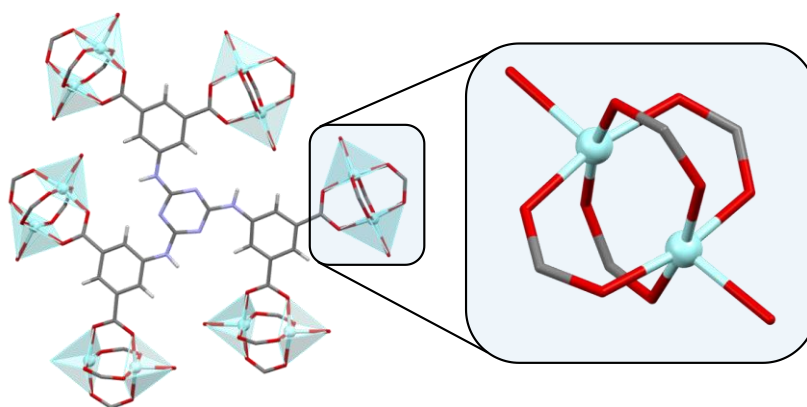
b)
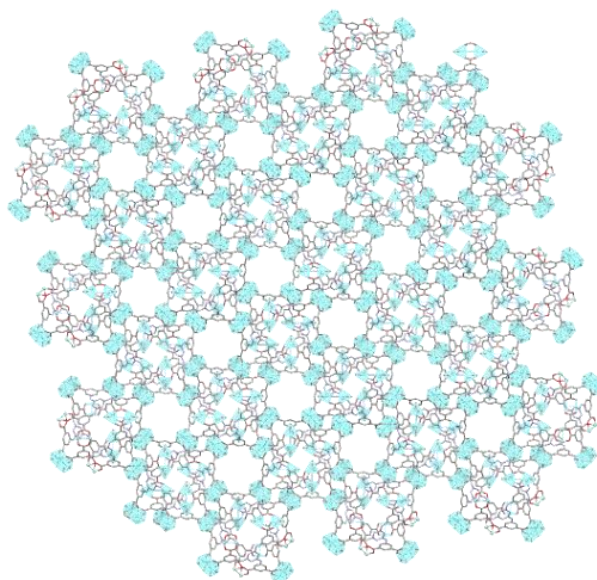
Figure 2.8. a) SBU found in Cu-TDPAT [Cu_3(TDPAT)(H_2O)$_3$]$_n$, in which H_6TDPAT was 2,4,6-tris(3,5-dicarboxylphenylamino)-1,3,5-triazine and b) crystal packing enhancing the cannel present in the crystal structure.

JUK-8. JUK-8 was synthesized according to an already reported procedure[21]. $Zn(NO_3)_2 \cdot 6H_2O$ (0.297 g, 1.00 mmol), [N'[1],N'[3]-bis[(E)-(pyridin-4-yl)methylidene]benzene-1,3-dicarbohydrazide]·EtOH·H$_2$O (pip·EtOH·H$_2$O) (0.372 g, 0.85 mmol) and 4,4'-oxybis(benzenedicarboxylic) acid (H$_2$oba) (258 mg, 1.00 mmol) were suspended in DMF (16 mL) and H$_2$O (1.8 mL) by sonication (5 min) and heated in a closed vial at 90 ºC for 4 days. Yellow crystals of JUK-8 were filtered off, washed with DMF and dried under vacuum at 60 ºC for 30 min (Figure 2.9).
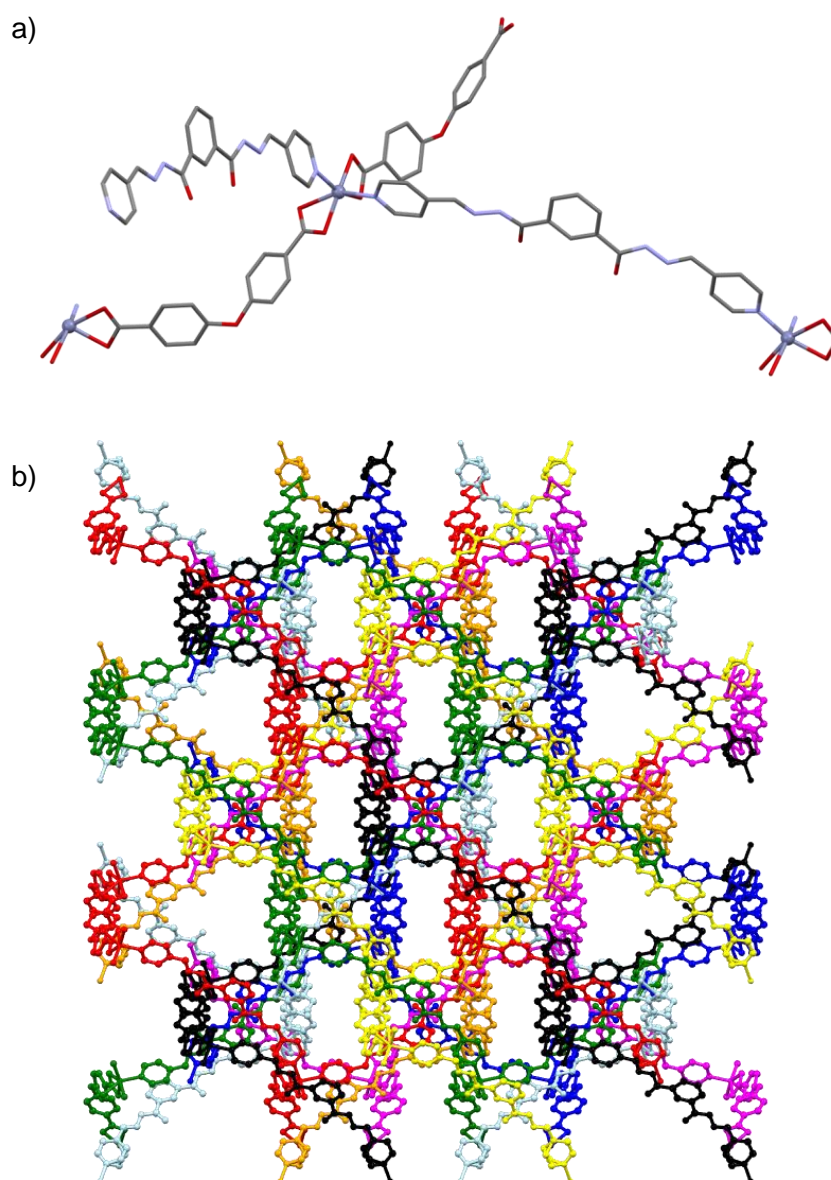
Figure 2.9. a) Details of the connectivity found in JUK-8 [Zn(oba)(pip)]$_n$[22], in which oba^{2-}= 4,4′-oxybis(benzenedicarboxylate), pip = 4-pyridyl-functionalized benzene-1,3-dicarbohydrazide and b) crystal packing enhancing the channel present in the crystal structure, where each subnet is depicted in a different colour.

ZU-301(Zn). ZU-301 was synthesized according to an already reported procedure[23]. Oxalic acid (0.603 g, 6.56 mmol), Mtz (2.40 g, 28.90 mol) and zinc(II) carbonate (0.60 g, 1.07 mmol) were added to a 100 mL stainless steel Teflon-lined autoclave, where methanol (54 mL) and water (9 mL) were previously incorporated. The mixture was stirred at room temperature for 30 minutes. The autoclave was sealed and placed in an oven at 180 °C for 48 h. Subsequently, it was allowed to cool down and the solid was recovered by centrifugation. It was washed by centrifugation (21500 rpm, 30 min, 24 mL) x 3 redispersing each time in H_2O. In order to change the solvent, the sample was centrifuged (21500 rpm, 1 h, 24 mL) x 3 in EtOH (Figure 2.10).

a)

b)
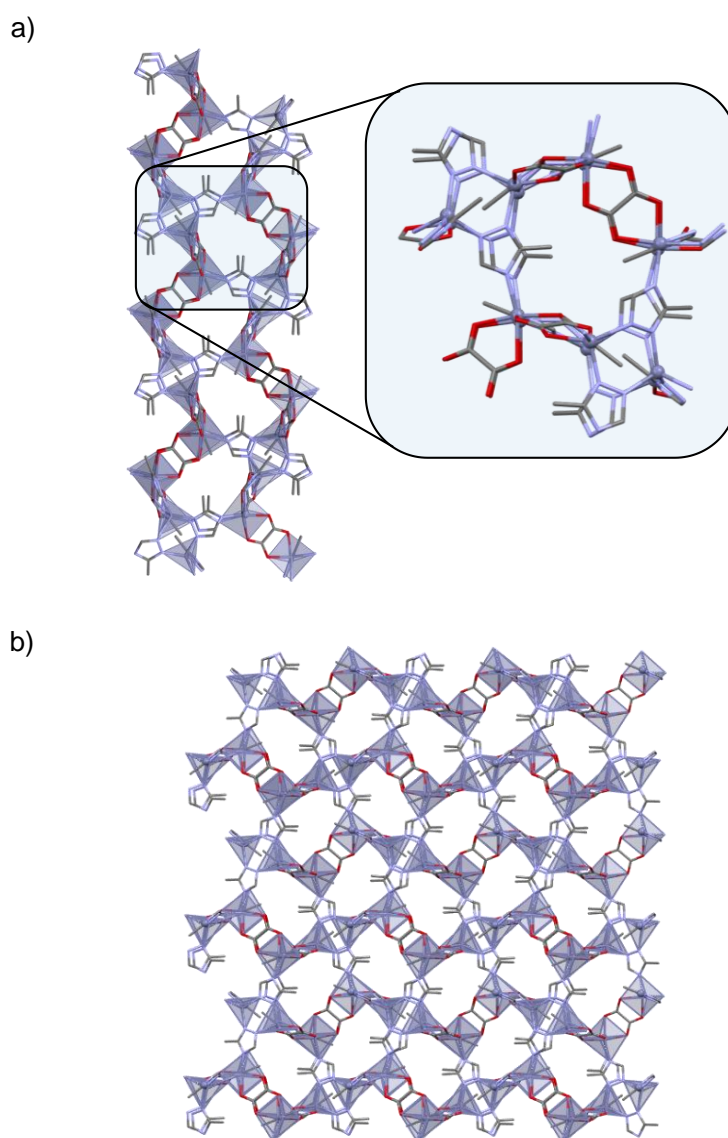
Figure 2.10. a) Details of the connectivity found in ZU-301, and b) crystal packing enhancing the cannel present in the crystal structure.

2.2.2 Characterization

The crystallinity and purity of the samples were assessed by powder X-ray diffraction (PXRD). PXRD patterns were collected on a Philips X'PERT powder diffractometer with Cu Kα radiation (λ = 1.5418 Å) over the 5 < 2θ° < 40° range with a step size of 0.02° and an acquisition time of 2.5 s per step at 25 °C. Scanning electron microscopy (SEM) was used in order to determine particle size and morphology. For that, samples were coated with a thin gold layer and measured on a Hitachi S-4800 scanning electron microscope (150 s, 20 mA, 10 kV, zoom at ×10.000). Dynamic light scattering measurement were conducted in a Malvern Zetasizer ZS equipment featuring a laser with the wavelength λ = 633 nm in order to determine the hydrodynamic radius of MOF NPs in suspension. Measurements were done in DMF (Zr-fumarate) and ethanol (UiO-66, ZIFs and MIL-88A).

2.3 RESULTS

2.3.1 Effect of synthesis parameters on the size and shape of MOF particles

In the first part of this work, some well-known MOFs (Zr-fumarate, UiO-66, NH_2-UiO-66, ZIF-8, ZIF-67 and MIL-88A) were chosen in order to analyse how different reaction parameters could affect MOF formation. This study allows us to tune size and shape of the particles and provide the reader with reliable protocols in order to choose the best synthesis conditions according to the requirements for a specific purpose where MOF particles needs to be homogeneous and well-defined. The reproducibility of some of the optimized synthesis was proved. Generally, power X-ray diffraction was used to ensure the crystallinity of the material, as well as to confirm the synthesis of MOFs, comparing the experimental diffraction pattern with the simulated one based on the reported crystal structure. In addition, scanning electron microscopy was used to determine the size and morphology of the particles and dynamic light scattering to calculate the hydrodynamic radius in solution of these particles or their aggregates.

2.3.1.1 Zr-fumarate

For the synthesis and optimization of Zr-fumarate different parameters were taken into account. Zr-fumarate MOF was synthesized solvothermally at 110 °C with different reaction times (4, 8, 12, 18, 24 h) using formic acid as a modulator. As observed in Figure 2.11, all samples showed high crystallinity confirming that after only 4 hours of reaction, Zr-fumarate was successfully synthesized. All samples presented octahedral morphology except after 24 h of reaction time, where particles did not have well-defined shapes. In addition, particle size was determined with SEM and DLS. On the one hand, particle sizes obtained from SEM images showed that for the first 8 hours of reaction, particle size was almost constant. Referring to the LaMer model, in the first hours nucleation took part, where crystal seeds begin to form rapidly. Afterwards, we observed an increase in particle size (after 12 h) where growth took part. Finally, particle size diminished until 38 nm particles were obtained after 24 hours of reaction, probably due to an excess basification of the reaction media due to the progressive decomposition of DMF that leads to a partial redissolution of the previously formed well-shaped particles. Furthermore, we observed that in all cases particle sizes determined from DLS measurements are higher compared to SEM demonstrating that Zr-fumarate tends to aggregate, at least in the solvent employed in this case, DMF.

	Zr-fum_4	Zr-fum_8	Zr-fum_12	Zr-fum_18	Zr-fum_24
Zr-fumarate (SEM)	224 ± 25 nm	220 ± 52 nm	369 ± 32 nm	279 ± 32 nm	37.5 ± 8 nm
Zr-fumarate (DLS)	1070 ± 213 nm PDI: 0.357	1317 ± 136 nm PDI: 0.324	1020 ± 8 nm PDI: 0.419	725 ± 4 nm PDI: 0.195	908 ± 31 nm PDI: 0.196
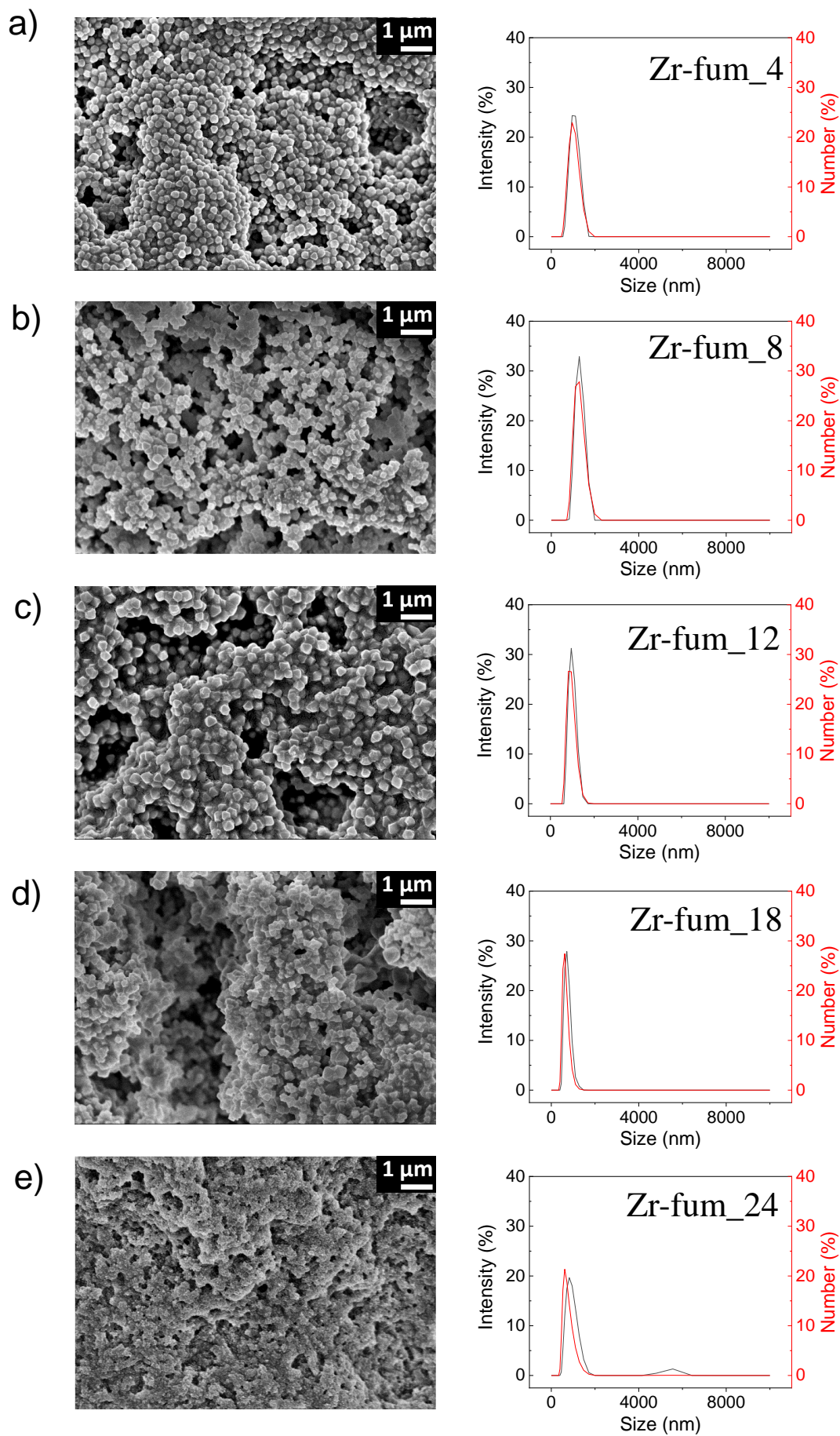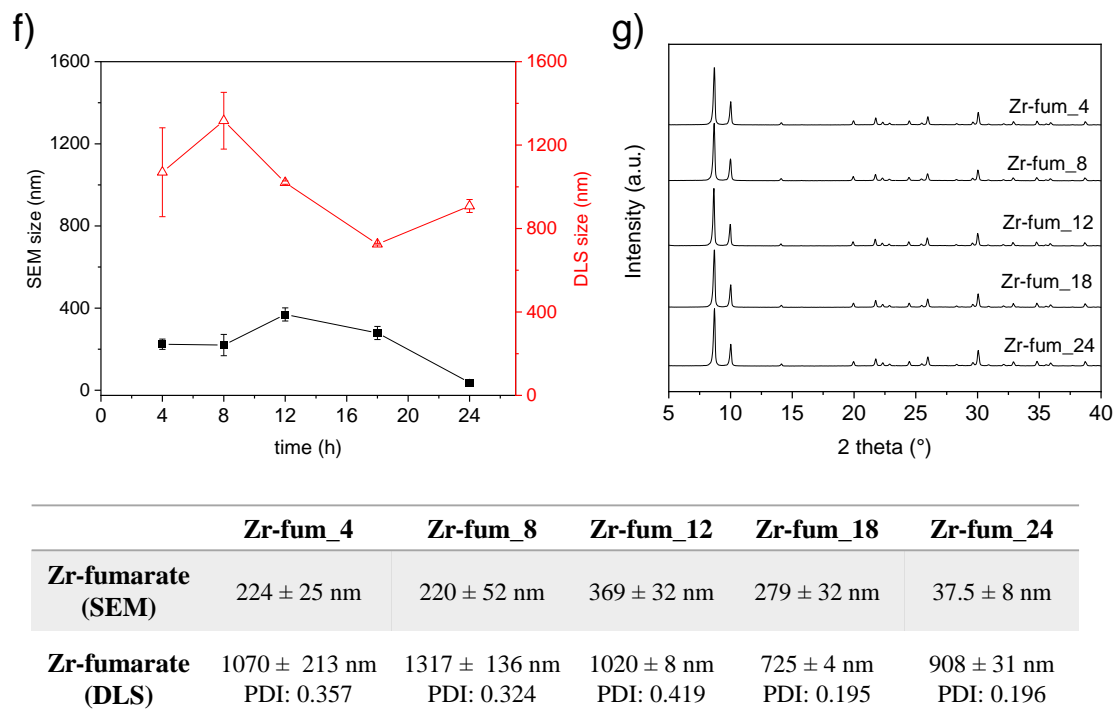
Figure 2.11. Characterization of Zr-fumarate MOF synthesized using different reaction times (4 h, 8 h, 12 h, 18 h and 24 h): a-e) SEM images and DLS measurements; f) particle size determined from SEM images (■) and DLS measurements (△) and g) PXRD.

2.3.1.2 UiO-66 and UiO-66-NH$_2$

For the synthesis and optimization of UiO-66, different parameters were taken into account. In a typical synthesis, UiO-66 is synthesized solvothermally at 120 °C using zirconium chloride (ZrCl$_4$) as a metal precursor, terephthalic acid and DMF as the solvent[23]. In this work, these parameters were kept constant in order to study the role of formic acid (FA), acetic acid (AA) and propionic acid (PA) as modulators as well as the effect of water (Figure 2.12). In all cases, a white crystalline powder was obtained, which corresponded to UiO-66. In addition, all particles had well-defined octahedron shapes. Regarding particle sizes calculated from SEM images it was observed that both the modulator and the added water influenced them. On the one hand, it was seen that the biggest particles were synthesized using acetic acid, while the smallest particles were obtained when propionic acid was used as a modulator. Moreover, particle size distribution was slightly broader when propionic acid was used. Zahn *et al.*[25] synthesized Zr-fumarate with different modulators (formic, acetic and propionic acid) and concentrations (0-100 eq) showing the effect on particle size

and morphology. They demonstrated that when formic acid was used, larger particles where formed, while when the same molar amount of acetic and propionic was added, the particles became smaller. On the contrary, Shearer *et al.*[26] showed that large particles could be obtained when acetic acid was used instead of formic acid. They speculated that this could be due to the acidity of the linkers. The more similar the pKa value of the modulator to the linker, the more competition there will be leading to bigger-size crystals since growth is promoted. The effect of water content in the formation of UiO-66 was also analysed and concluded that the addition of water led to bigger particles when formic acid was used as a modulator, which may result from the formation of defects[27]. Regarding particle sizes in suspension, we can conclude that all UiO-66 samples tend to aggregate while they are suspended in ethanol.
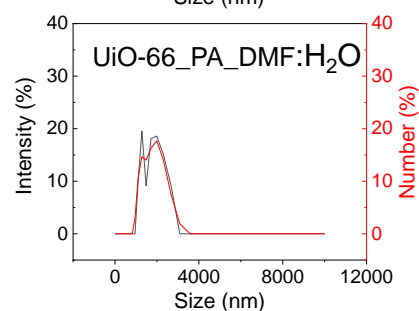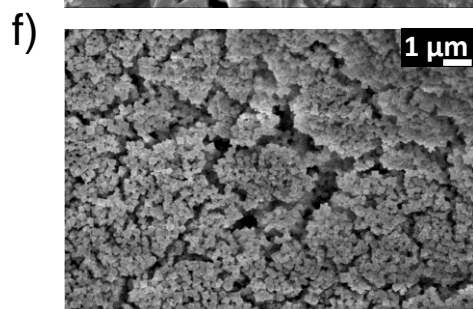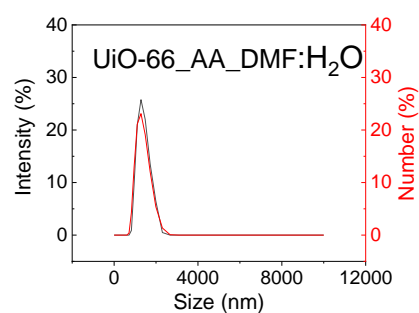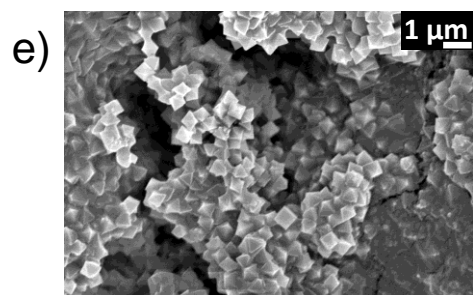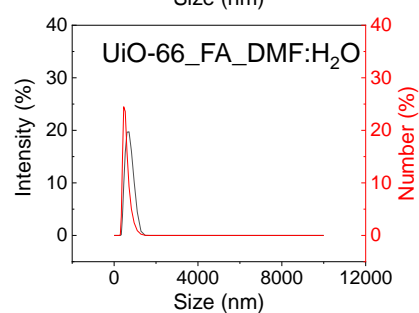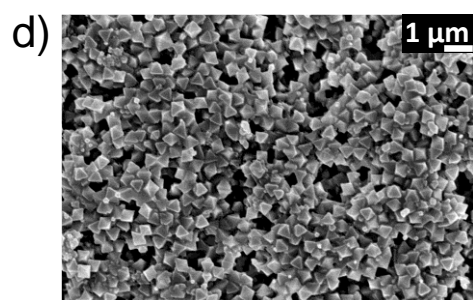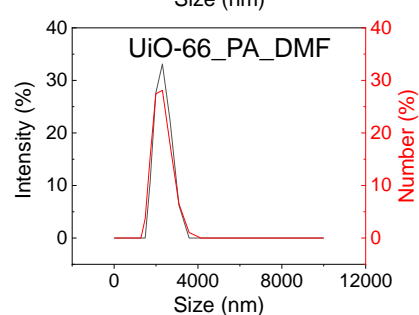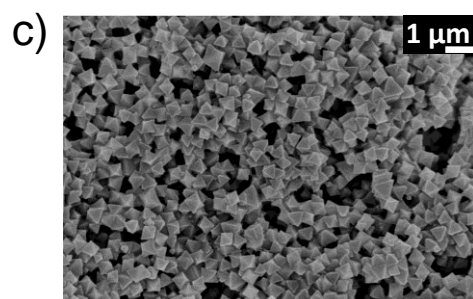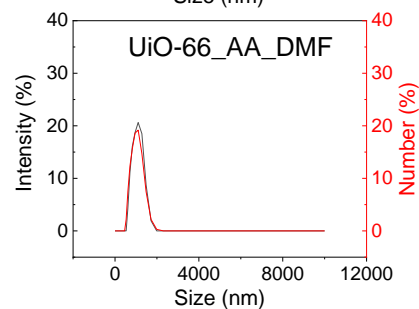
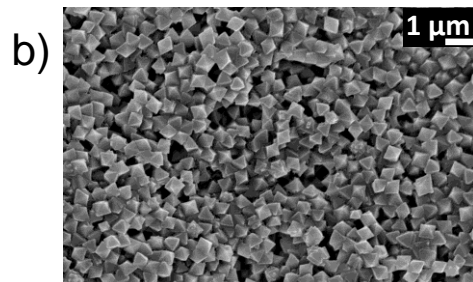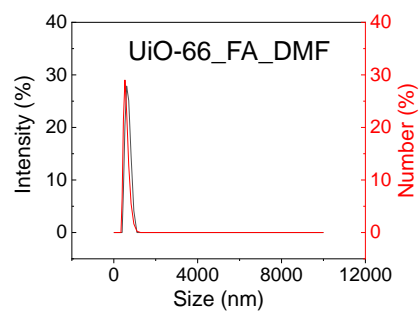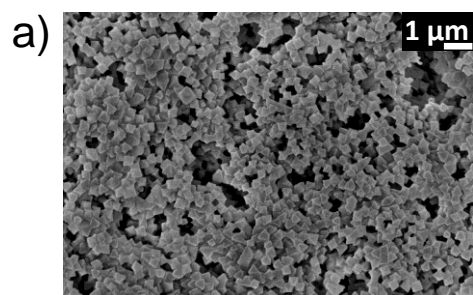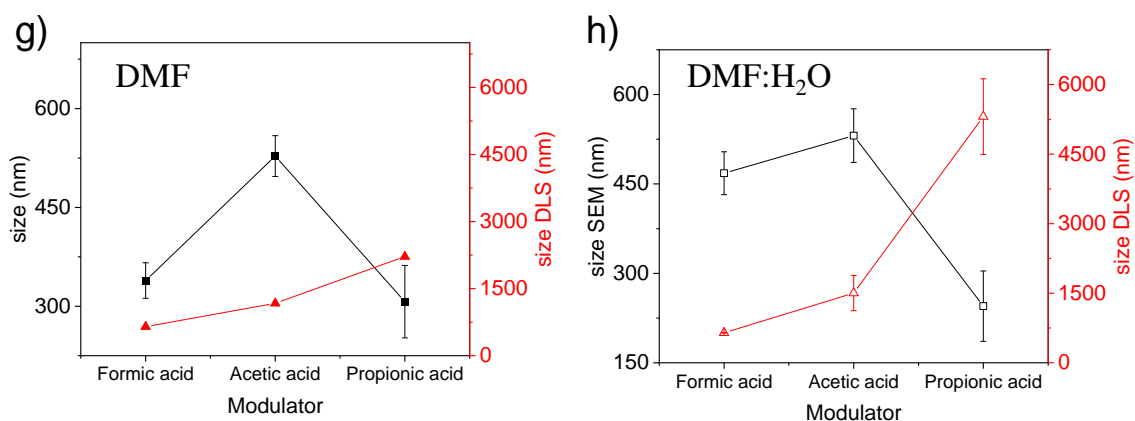| Solvent	Formic acid	Acetic acid	Propionic acid
DMF (SEM)	339 ± 27 nm	528 ± 31 nm	307 ± 55 nm
DMF (DLS)	649 ± 22 nm PDI: 0.11	1171 ± 223 nm PDI: 0.892	2217 ± 161 nm PDI: 0.215
DMF:H$_2$O (SEM)	468 ± 36 nm	531 ± 45 nm	245 ± 59 nm
DMF:H$_2$O (DLS)	647 ± 6 nm PDI: 0.051	1503 ± 380 nm PDI: 0.746	5310 ± 816 nm PDI: 0.525
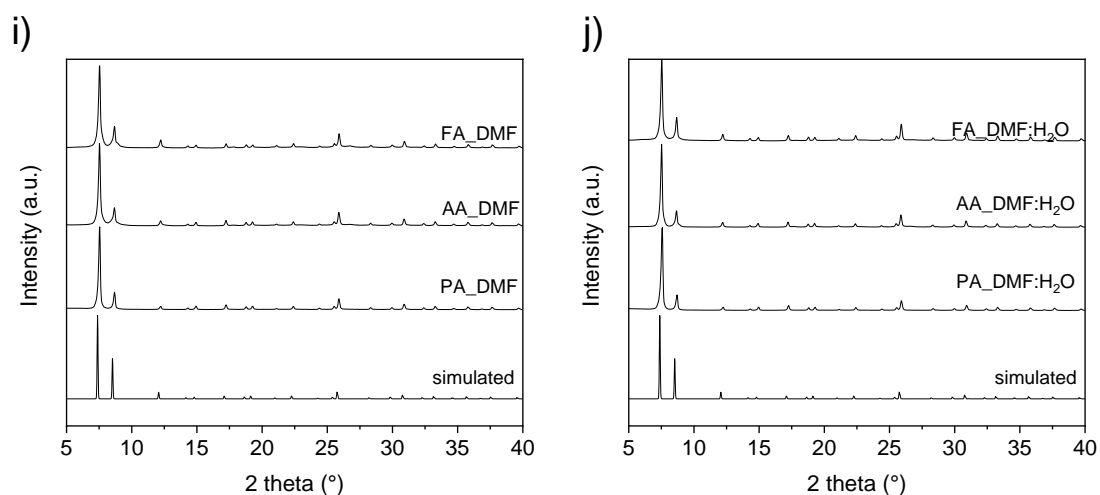
Figure 2.12. Characterization of UiO-66 MOF synthesized using different modulators (formic acid, acetic acid and propionic acid) and different solvents. SEM images and DLS measurements: a-c) in DMF and d-f) in DMF:H$_2$O. g-h) Particle size determined from SEM images (DMF: ■, DMF:H$_2$O: □) and DLS measurements (DMF: ▲, DMF:H$_2$O: △). PXRD of UiO-66: i) in DMF and j) in DMF:H$_2$O.

Once different parameters were studied, it was determined that the UiO-66 samples synthesized with formic acid and pure DMF (no water addition) were the best ones regarding smaller particle size, morphology and homogeneity. Microwave activation was studied in water in the optimized sample, this is UiO-66_FA_DMF, to eliminate the possible unreacted reagents and solvent (DMF) from the pores of the materials. As observed in Figure 2.13, it was also demonstrated that this activation procedure did not affect to the crystal structure and that UiO-66 was stable during the whole process, as the PXRD remained unaltered. After the activation procedure, particle size decreased slightly, probably due to the dissolution of unwashed reagents. Furthermore, DLS measurements showed that particles are more dispersed after activation, which could corroborate our hypothesis. Finally, termogravimetric analyses (TGA) demonstrated that MW activation was a very effective method to activate the sample. As-synthesized UiO-66 sample showed an initial weight loss of 30% of the initial mass up to 170 °C, which corresponds not only to the removal of the solvent in the pores (ethanol and DMF) but also to the dehydroxylation of the zirconium oxo-clusters[28]. Contrarily, activated sample showed a lowest weight loss of 25% of the initial mass up to 100 °C corresponding to the release of water molecules trapped in the pores. After this process, the activated sample does not show any further weight loss until 500 °C. These results suggest that DMF and hydroxides were eliminated in the activation process. The strongly exothermic process taking place at 500 °C is attributed to the linker decomposition.
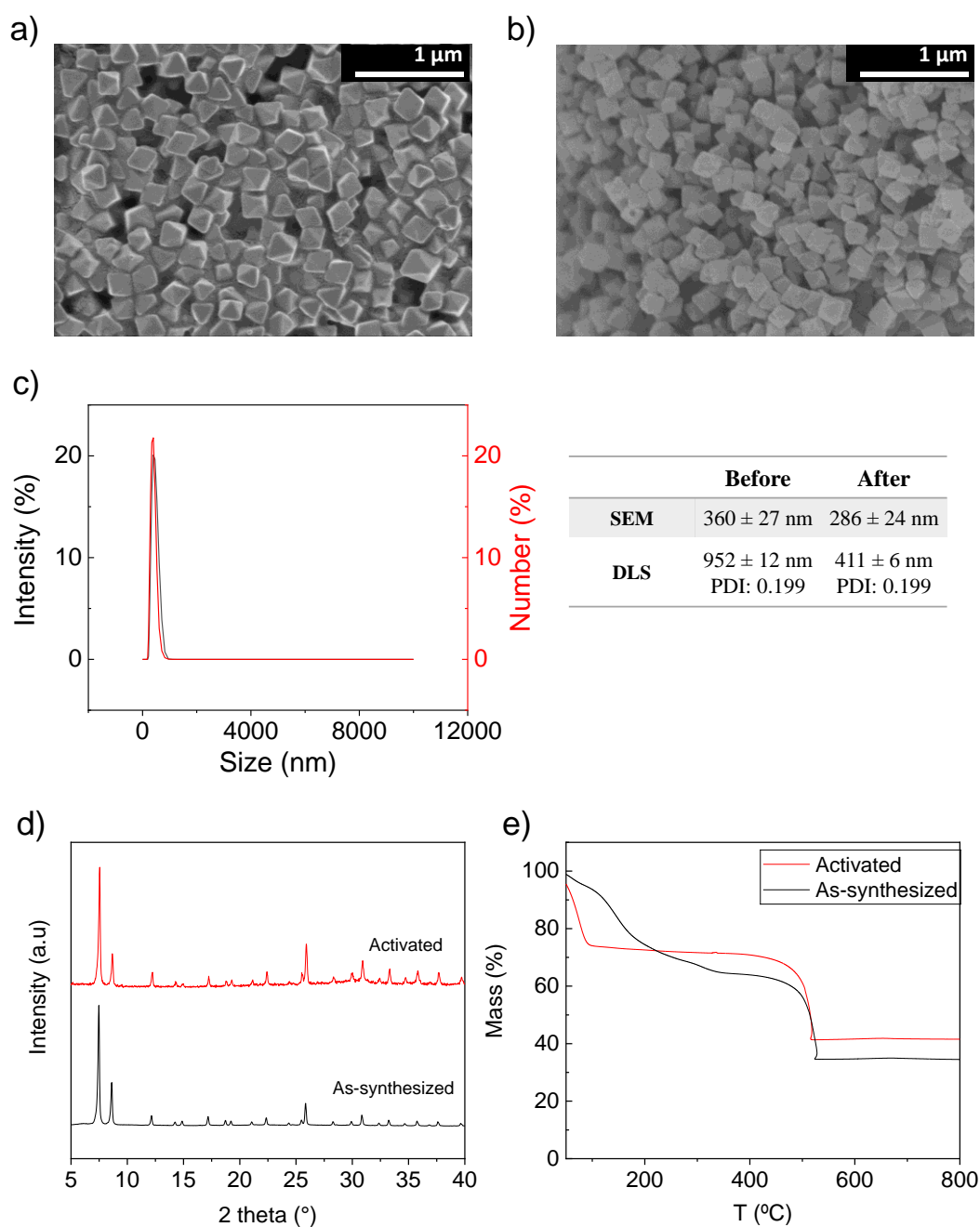
Figure 2.13. Characterization of the activated UiO-66: SEM pictures a) before and b) after activation, c) DLS measurements of the activated sample, d) PXRD and e) TGA.

In order to synthesize amino-functionalized UiO-66 (UiO-66-NH$_2$), optimized UiO-66 protocol (UiO-66_FA_DMF) was reproduced. After the reaction, a white-yellowish powder was obtained, which was confirmed to be UiO-66-NH$_2$ with powder X-ray diffraction. As observed in Figure 2.14, the particles had a well-defined octahedral morphology of 360 ± 27 nm, good size distribution and high crystallinity, demonstrating that the optimized protocol for UiO-66 served also for the synthesis of high quality UiO-66-NH$_2$ particles.

a)

b)

	UiO-66-NH$_2$
SEM	242 ± 42 nm
DLS	952 ± 12 nm PDI: 0.199

c)
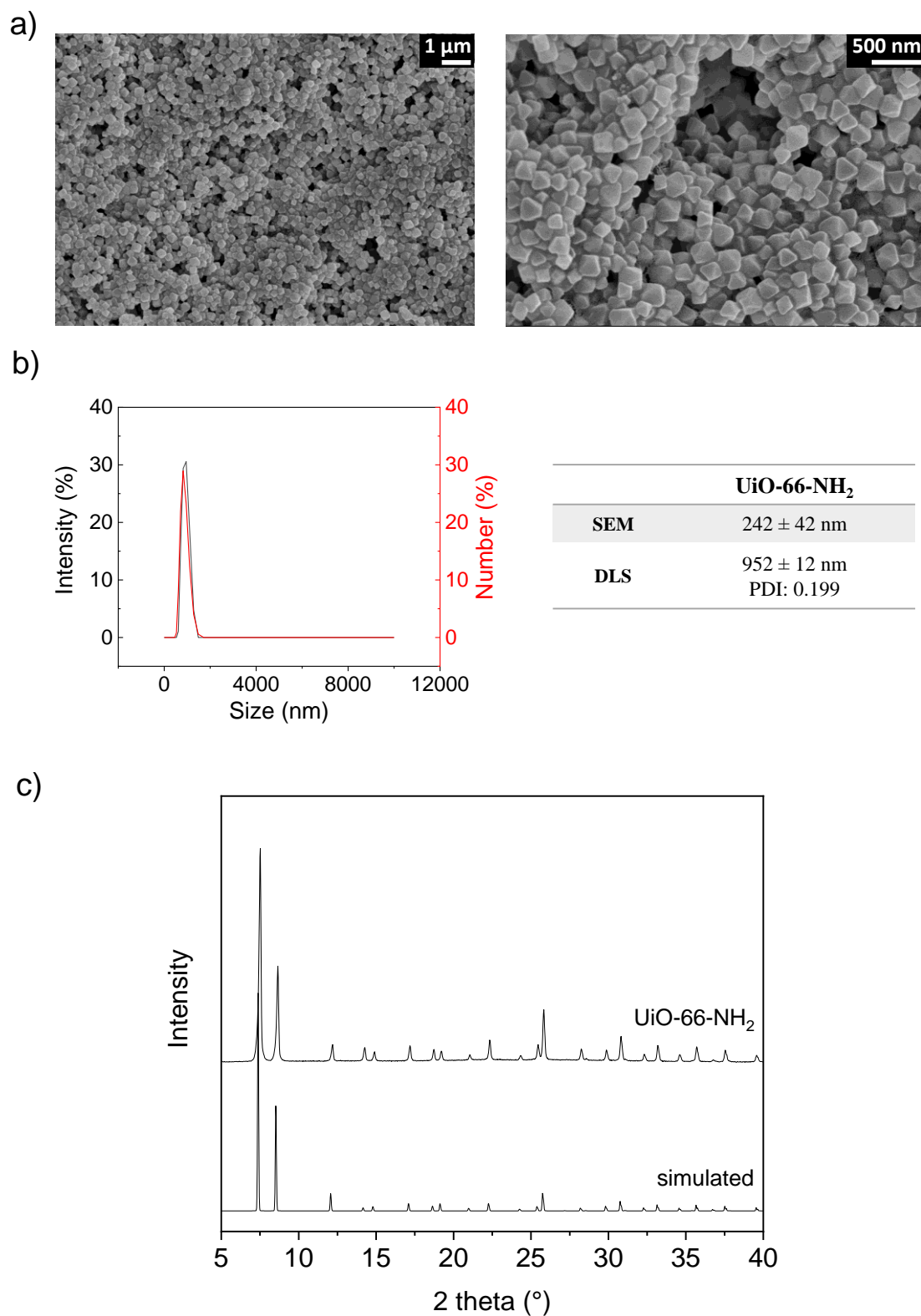
Figure 2.14. Characterization of UiO-66-NH$_2$ MOF: a) SEM pictures, b) DLS measurements and particle size determined from SEM images and DLS measurements and c) PXRD.

2.3.1.3 Zeolitic imidazole MOFs: ZIF-8 and ZIF-67

In the synthesis of zeolitic imidazole MOFs, different parameters like reaction times and CTAB content were analysed. Different morphologies and sizes could be obtained for ZIF-8 and ZIF-67, as shown in Figures 2.15 and 2.16, respectively. PXRD patterns showed high crystalline samples and all the peaks observed correspond to the characteristic reflections of isostructural ZIF-8 and ZIF-67, meaning that the syntheses were successfully completed.

For ZIF-8, it was observed that when procedure A and the same amount of CTAB (Zn^{2+}:CTAB 1:0.0011) was used, two morphologies were obtained: cubes or TC. CTAB acts as a capping agent that can be absorbed on the surface of the MOF, slowing down the growth rate and leading to the formation of cubic morphology, through the stabilization of the {100} facets[29,30]. When the reaction mixture was left undisturbed for 15 minutes, cubes with sharp edges were obtained, while for longer reaction times (2 h) morphology evolved and truncated cubes (TC) were obtained. These observations are in good agreement the with literature, as it is known that the growth of ZIF-8 evolves with time: in the early stages, cubes exposing 6 {100} faces are obtained, which evolve to intermediate shapes and finally, to the more stable rhombic dodecahedra (RD) exposing 12 {110} faces[31,32]. Moreover, it was observed that particle size decreased slightly with longer reaction times (from 448 nm to 360 nm, after 15 minutes and 2 h, respectively). When CTAB content was increased (Zn^{2+}:CTAB 1:0.011), after 2 h of reaction smaller particles were obtained and particles evolved to a truncated rhombic dodecahedron (TRD) morphology. These observations are also in good agreement with what Pan *et al.*[33] observed, obtaining smaller particles with an increasing amount of CTAB. Finally, we demonstrated how size and shape could be influenced, not only with molar ratios or synthesis times, but also with the preparation and addition order of precursor's solution. Morphology changed when procedures A or B were used, obtaining particles with a higher truncation degree in the latter, TC-TRD. For all synthesized ZIF-8 samples, DLS measurement showed that the particles do not aggregate and formed stable colloidal dispersions in ethanol.

e)
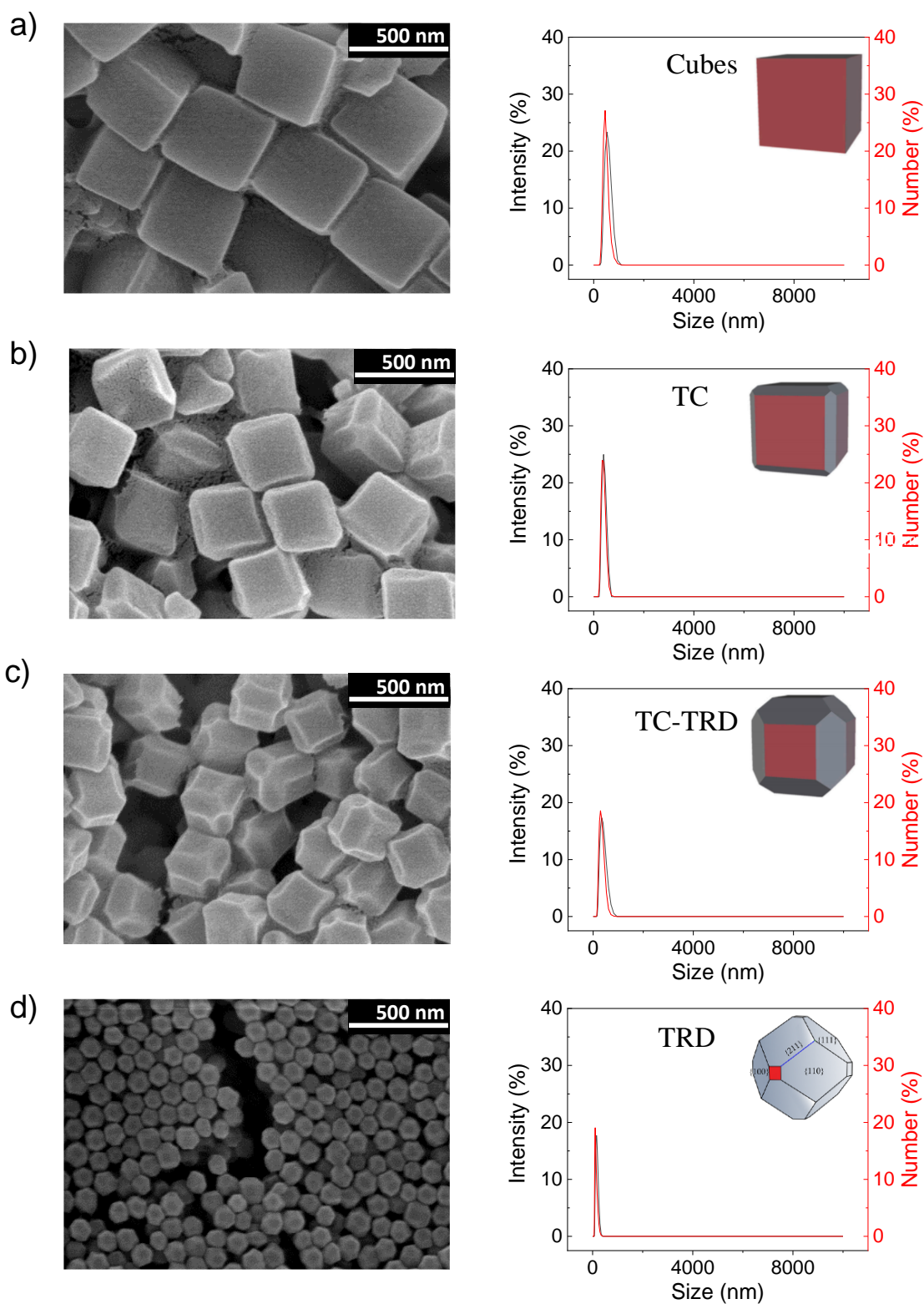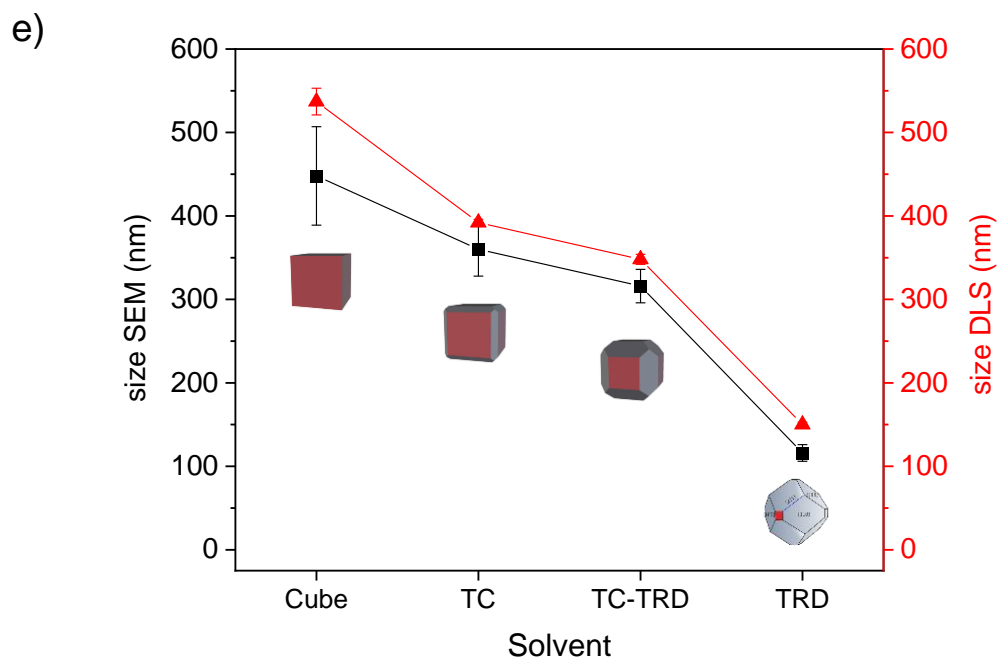
Sample	Cubes	TC	TC-TRD	TRD
Size (SEM)	448 ± 59 nm	360 ± 32 nm	316 ± 20 nm	116 ± 10 nm
Size (DLS)	537 ± 16 nm PDI: 0.117	392 ± 4 nm PDI: 0.02	348 ± 6 nm PDI: 0.116	150 ± 3 nm PDI: 0.079

f)
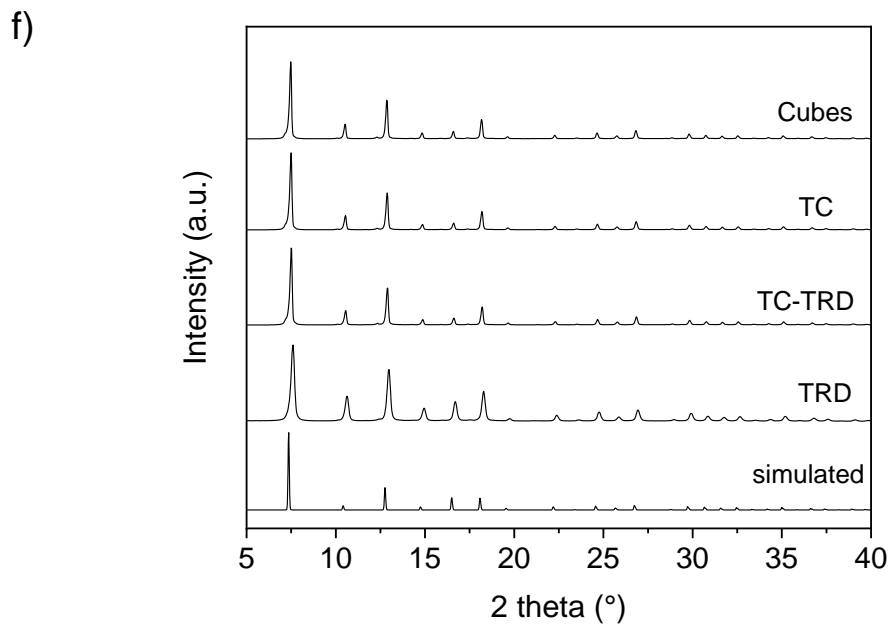
Figure 2.15. Characterization of ZIF-8 MOF synthesized with different morphologies (cubes, TC, TC-TRD, TRD): a-d) SEM images and DLS measurements and e) particle size determined from SEM images (■) and DLS measurements (▲) and f) PXRD.

In the optimization process of ZIF-67, similar observations as for ZIF-8 were made. On the one hand, when CTAB content was very small (Co^{2+}:CTAB 1:0.004) rhombic dodecahedron (RD) particles were obtained. On the contrary, when CTAB content was increased (Co^{2+}:CTAB 1:0.04), morphology evolve to cubic shape and smaller particle sizes were obtained. Following this data, one might assume a similar behaviour of the capping agent to what is observed for ZIF-8[34]. Furthermore, the concentration of the reagents was also altered and concluded that especially for short reaction times (3 h), the more diluted conditions the bigger the particles size. Finally, when reaction times are compared, it can be seen that particle size is reduced when longer reaction times are used (3 h vs 24 h), probably due to an excess acidification of the reaction media originated from the formation of nitric acid. Contrary to ZIF-8, ZIF-67 samples tend to aggregate in ethanol and therefore, hydrodynamic radius of the particles was significantly higher than that determined in the dried state.

a)

1:56:0.04, 8 mL

b)

1:56:0.04, 12 mL

c)

1:56:0.004, 12 mL

3 h

d)

1:56:0.04, 8 mL

e)

1:56:0.04, 12 mL

24 h

f)

g)

Time (h)	1:56:0.04, 8 mL	1:56:0.04, 12 mL	1:56:0.004, 12 mL
3 h (SEM)	75 ± 8 nm	170 ± 11 nm	1.4 ± 0.4 μ m
3 h (DLS)	592 ± 11 nm PDI = 0.378	318 ± 7 nm PDI = 0.287	1.62 ± 1.1 μm PDI = 0.121
24 h (SEM)	64 ± 7 nm	71 ± 6 nm	-
24 h (DLS)	397 ± 15 nm PDI = 0.381	3,1 ± 5 μm PDI = 0.538	-

h)

i)
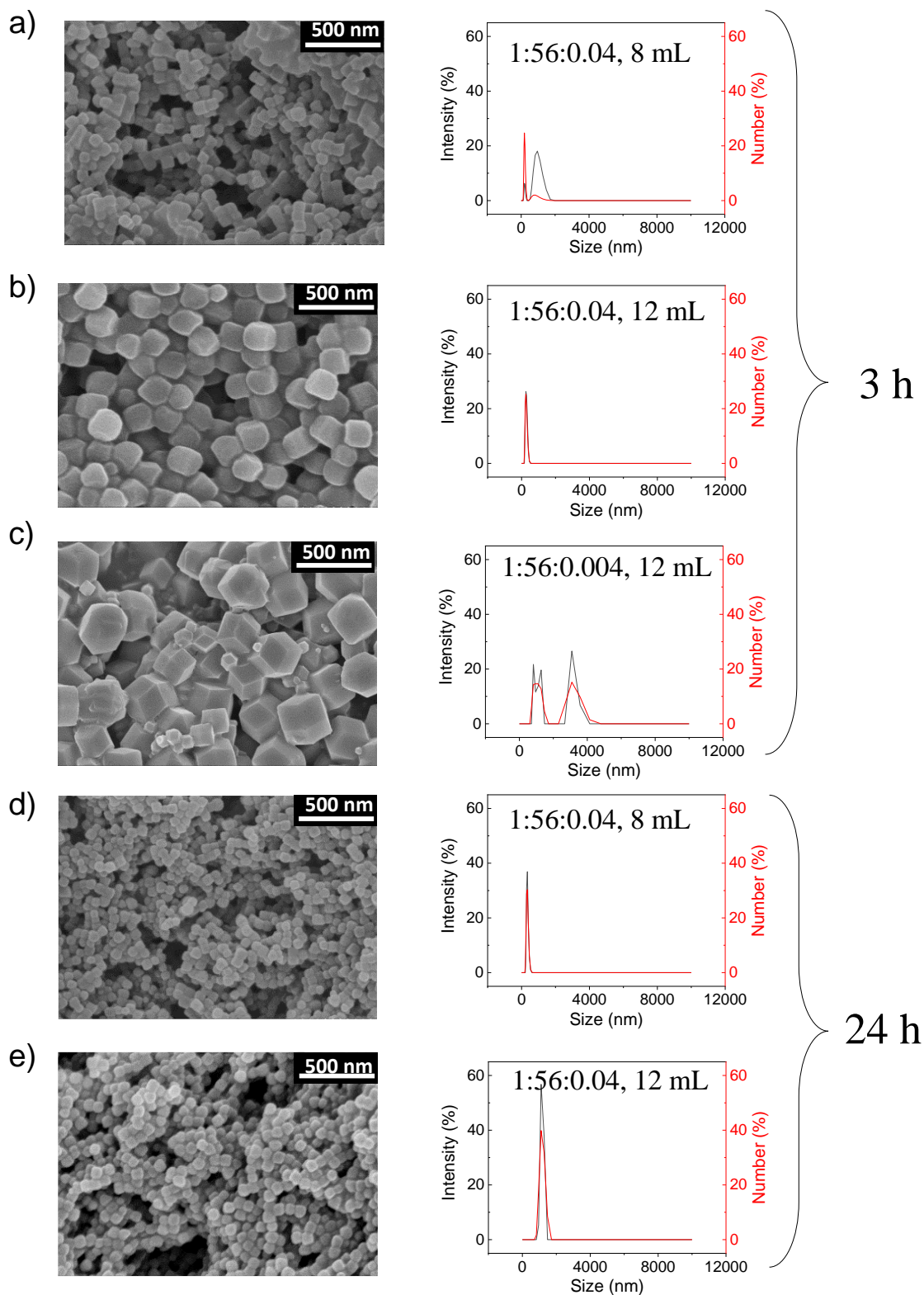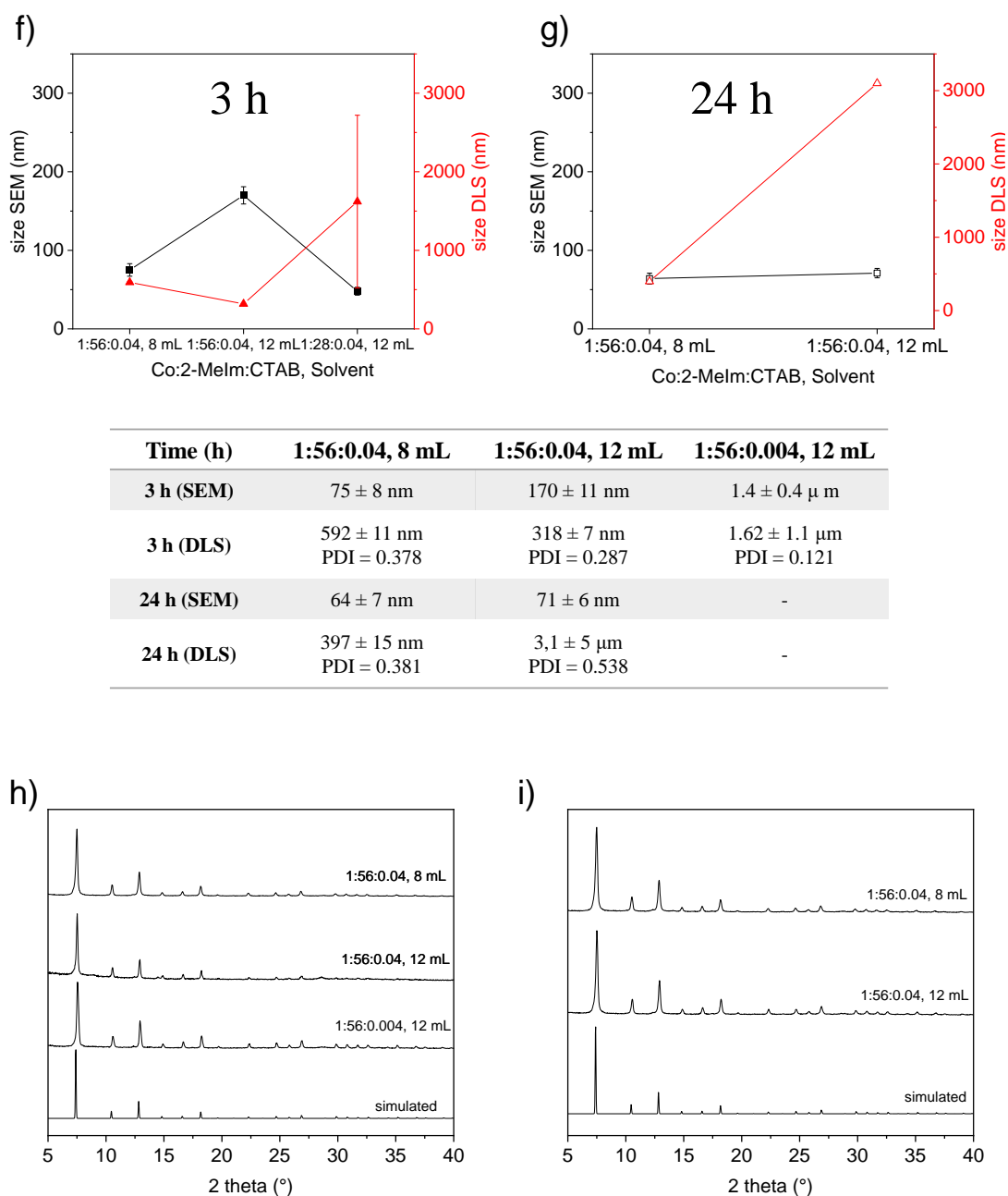
Figure 2.16. Characterization of ZIF-67 MOF synthesized with different size and morphologies at different reaction times and molar ratios: a-e) SEM images and DLS measurements, f-g) particle size determined from SEM images (3 h: ■, 24 h: □) and DLS measurements (3 h: ▲, 24 h: △) and h-i) PXRD.

2.3.1.4 MIL-88A

MIL-88A was synthesized using different solvents or solvent mixtures and reaction times that influenced the particle size and shape, as observed in Figure 2.17. When DMF was used as a solvent, (MIL-88A_DMF) rod-shape and big particles of 5.7 ± 2.0 μm length and 0.57 ± 1.96 μm width were obtained. When water was used (MIL-88A_H_2O), diamond-like particles of 1.5 ± 1.3 μm length and 0.9 ± 0.23 μm width were synthesized. Finally, with a mixture of both solvents (MIL-88A_DMF: H_2O), particles of 4.4 ± 0.54 μm length and 1.4 ± 0.16 μm width were obtained. The change in particles size can be assigned to the different polarity of solvents (μ_{DMF} = 3.86 D, μ_{H2O} = 1.85 D) since the solvation greatly influences nucleation growth. Therefore, DMF slowed down the nucleation growth giving large-size crystals. However, with the lower polarity solvent, water, nucleation is accelerated and smaller crystals are synthesized. When a mixture of both solvents was added, middle-sized crystals were generated[35].

d)

e)

	MIL-88A-DMF	MIL-88A-DMF:H2O	MIL-88A_H$_2$O
SEM	5.7 ± 2.0 μm (L) 0.57 ± 1.96 μm (W)	4.4 ± 0.5 μm (L) 1.4 ± 0.2 μm (W)	1.5 ± 1.3 μm (L) 0.9 ± 0.23 μm (W)
DLS	2.4 ± 0.4 μm PDI = 0.454	2.8 ± 0.1 μm PDI = 0.313	1.3 ± 0.1 μm PDI = 0.497
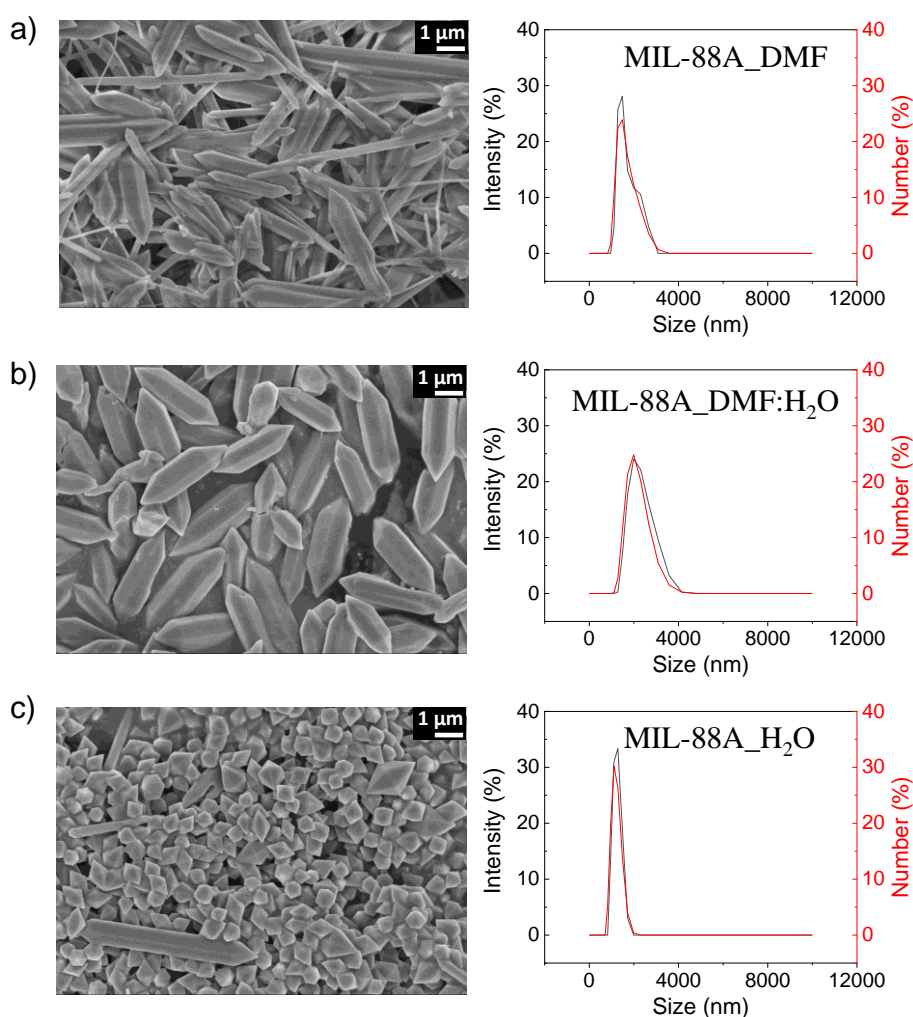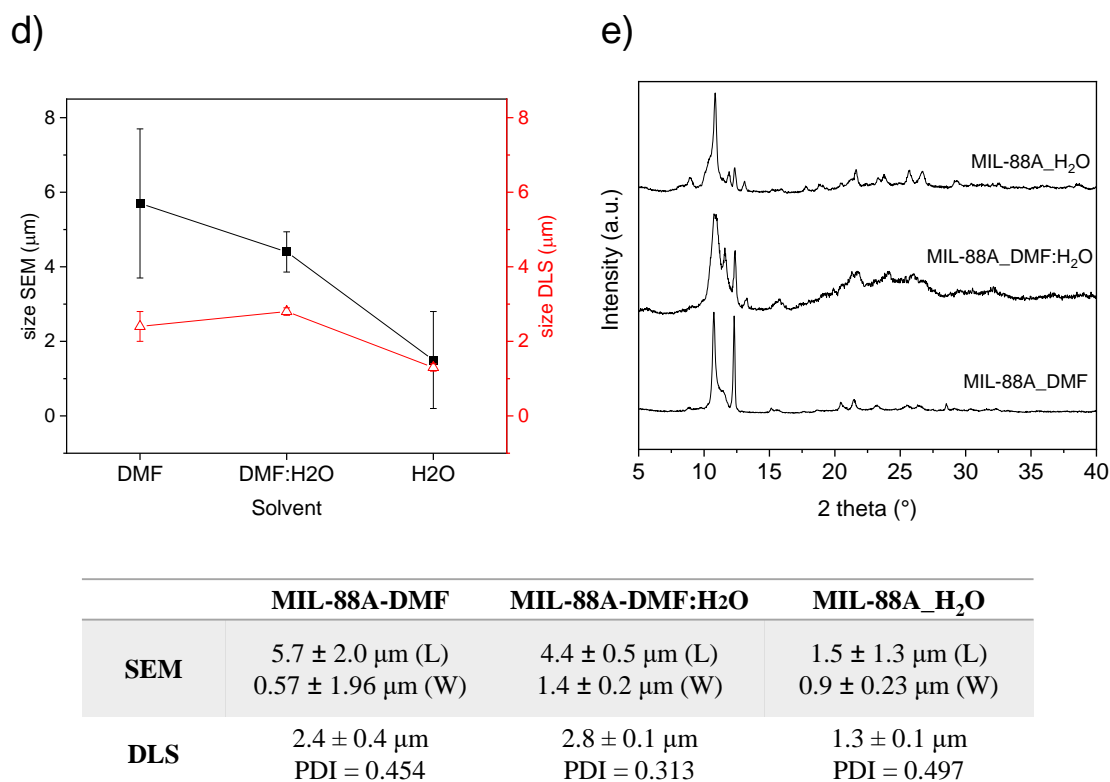
Figure 2.17. Characterization of MIL-88A(Fe) MOF with different size and morphologies synthesized using different times (4 h vs 12 h) and solvents: a-c) SEM images and DLS measurements; d) particle size determined from SEM images (■) and DLS measurements (▲) and e) PXRD.

2.3.2 Characterization of MOFs based on reported protocols

Isostructural MOF-74(Cu, Co, Ni), MIL-127(Fe), Cu-TDPAT, JUK-8 and ZU-301 were synthesized according to already reported protocols without further modifications. For the characterization, PXRD were performed in order to identify the most characteristic peaks of each MOF and compare to the simulated patterns in order to ensure the synthesis of the desire porous material. Moreover, all MOFs that were synthesized are crystalline, corroborated from the presence of narrow and high intensity diffraction peaks. SEM images were obtained in order to see the morphology and size of the obtained materials, *i.e.* cubic particles or needle-shape particles were obtained (Figures 2.18 and 2.19). These MOFs were specifically prepared for their use in *Chapter 3 and Chapter 5*.
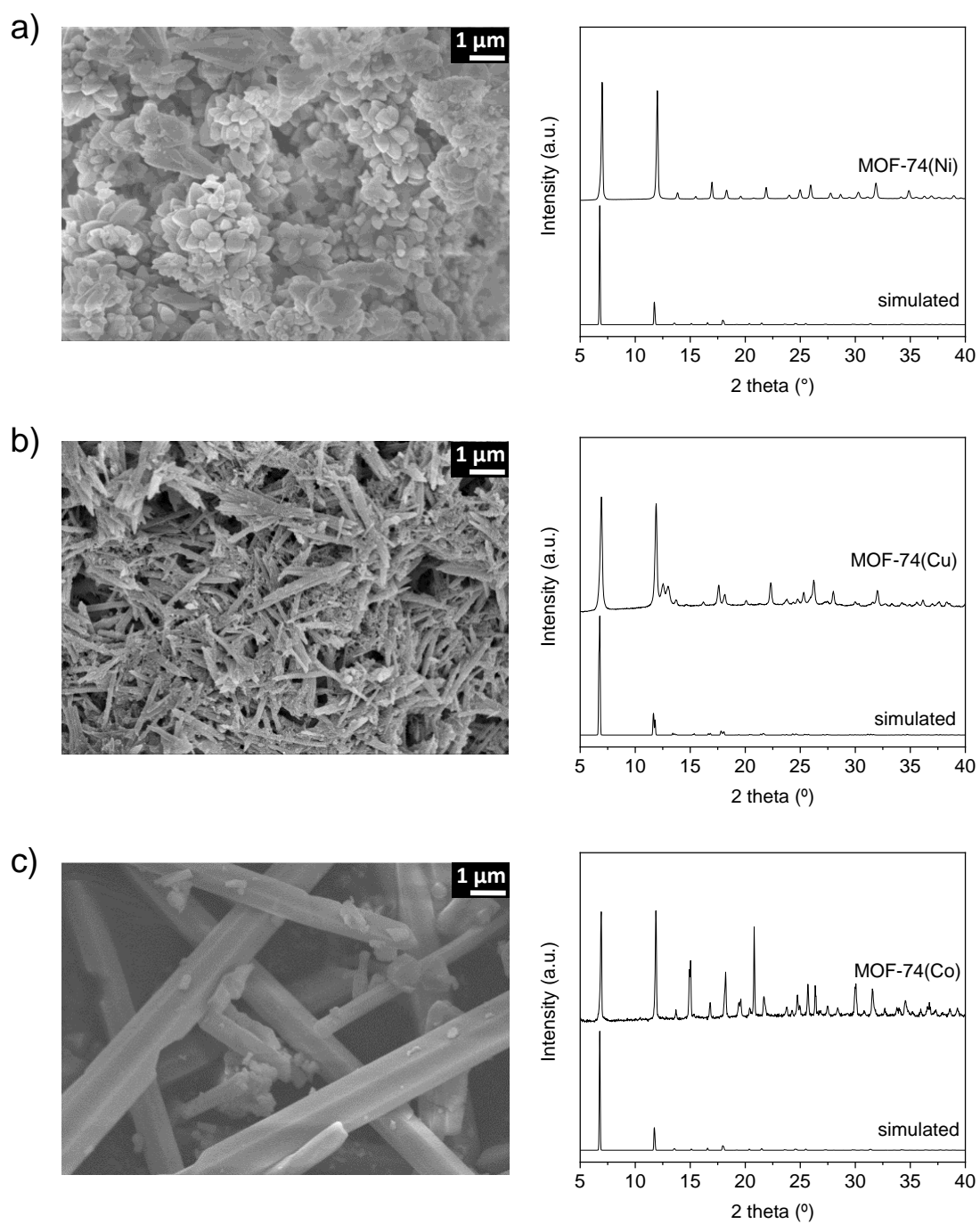
Figure 2.18. SEM pictures and PXRD patterns of isostructural M-MOF-74: a) Ni-MOF-74, b) Cu-MOF-74 and c) Co-MOF-74.
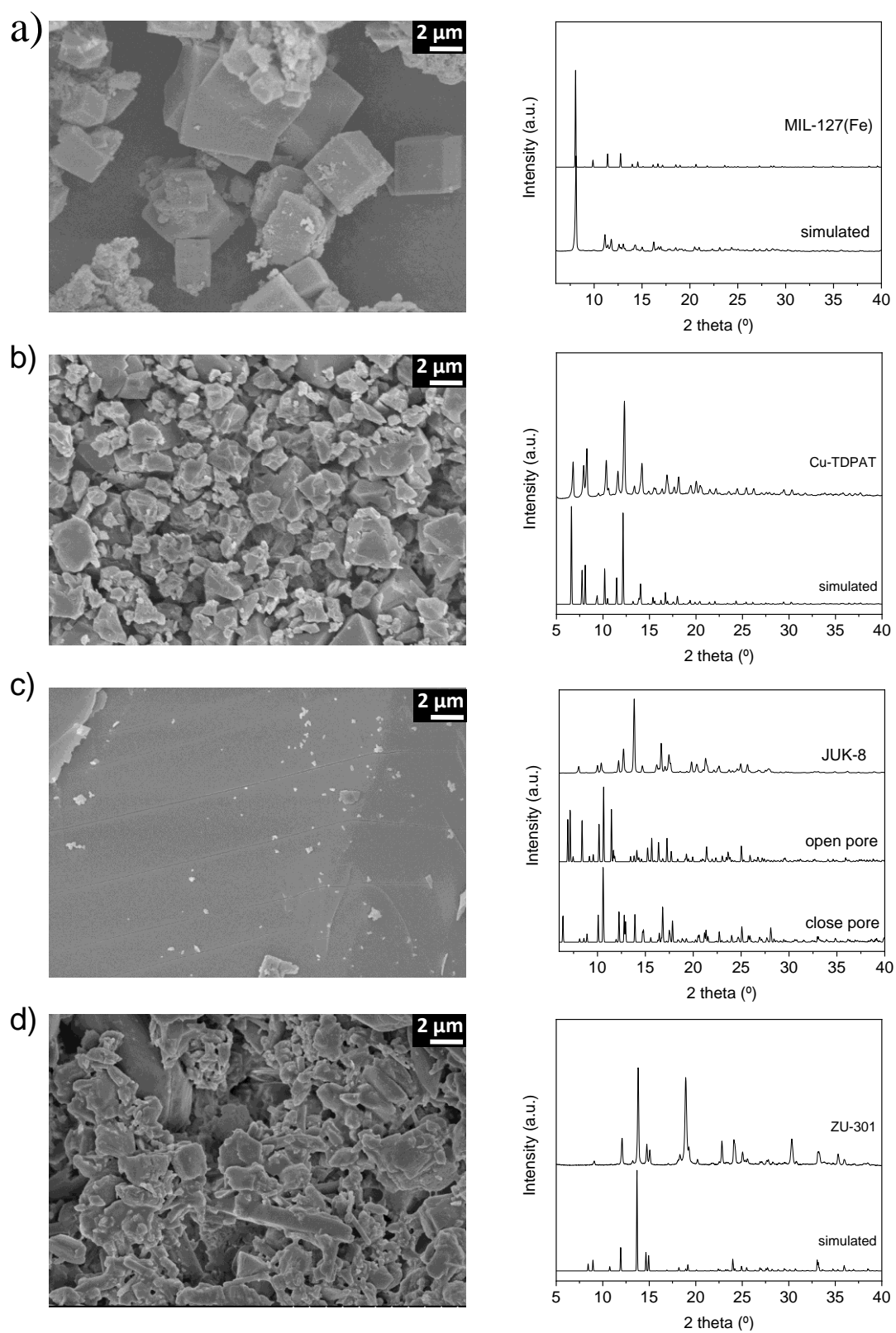
Figure 2.19. SEM pictures and PXRD patterns: a) MIL-127(Fe), b) Cu-TDPAT, c) JUK-8 and d) ZU-301.

2.4 CONCLUSIONS

In this chapter, we have shown how different synthetic parameters such as time, temperature, molar ratio of the reagents and the presence of modulators or surfactants can alter size and shape of the prepared metal-organic frameworks. It has been highlighted the lack of optimized protocols in the literature and the need to provide a feasible study on the synthetic parameters as they will change materials properties and thus, make them suitable for different applications. Different characterization techniques have been used along the chapter in order to provide a basic characterization for all MOFs, especially size, shape and crystallinity.

2.5 REFERENCES

(1) Ongari, D.; Talirz, L.; Smit, B. *ACS Cent. Sci*. **2020**, 6, 1890–1900.

(2) Li, H., Eddaoudi, M., O'Keeffe, M. & Yaghi, O. M. *Nature* **1999**, 402, 276–279.

(3) Stock, N.; Biswas, S. *Chem. Rev*. **2012**, 112, 933–969.

(4) Mai, Z.; Liu, D. *Cryst. Growth Des*. **2019**, 19, 7439–7462.

(5) Eddaoudi, M.; Kim, J.; Rosi, N.; Vodak, D.; Wachter, J.; O'Keeffe, M.; Yaghi, O. M. *Science* **2002**, 295, 469–472.

(6) Wang, Z.; Cohen, S. M. *Chem. Soc. Rev*. **2009**, 38, 1315–1329.

(7) Tanabe, K. K.; Cohen, S. M. *Chem. Soc. Rev*. **2011**, 40, 498–519.

(8) Andreo, J.; Ettlinger, R.; Zaremba, O.; Peña, Q.; Lächelt, U.; Luis, R. F. de; Freund, R.; Canossa, S.; Ploetz, E.; Zhu, W.; Diercks, C. S.; Gröger, H.; Wuttke, S. *J. Am. Chem. Soc*. **2022**, 144, 7531–7550.

(9) Haase, F.; Hirschle, P.; Freund, R.; Furukawa, S.; Ji, Z.; Wuttke, S. *Angew. Chem. Int. Ed*. **2020**, 59, 22350–22370.

(10) Ren, J.; Musyoka, N. M.; Langmi, H. W.; North, B. C.; Mathe, M.; Pang, W.; Wang, M.; Walker, *J. Appl. Surf. Sci*. **2017**, 404, 263–267.

(11) Feng, X.; Jena, H. S.; Krishnaraj, C.; Leus, K.; Wang, G.; Chen, H.; Jia, C.; van der Voort, P. *ACS Appl. Mater. Interfaces* **2021**, 13, 60715–60735.

(12) Pérez-Miana, M.; Reséndiz-Ordóñez, J. U.; Coronas, J. *Microporous Mesoporous Mater.* **2021**, 328, 111487.

(13) Xu, W.-T.; Ma, L.; Ke, F.; Peng, F.-M.; Xu, G.-S.; Shen, Y.-H.; Zhu, J.-F.; Qiu, L.-G.; Yuan, Y.-P. *Dalton Trans*. **2014**, 43, 3792–3798.

(14) Chalati, T.; Horcajada, P.; Gref, R.; Couvreur, P.; Serre, C. *J. Mater. Chem*. **2011**, 21, 2220–2227.

(15) Serre, C.; Mellot-Draznieks, C.; Surblé, S.; Audebrand, N.; Filinchuk, Y.; Férey, G. *Science* **2007**, 315, 1828–1831.

(16) Wongsakulphasatch, S.; Kiatkittipong, W.; Saupsor, J.; Chaiwiseshphol, J.; Piroonlerkgul, P.; Parasuk, V.; Assabumrungrat, S. *Greenhouse Gas Sci. Technol*. **2017**, 7, 383–394.

(17) Chevreau, H.; Permyakova, A.; Nouar, F.; Fabry, P.; Livage, C.; Ragon, F.; Garcia-Marquez, A.; Devic, T.; Steunou, N.; Serre, C.; Horcajada, P. *CrystEngComm* **2016**, 18, 4094–4101.

(18) Strauss, I.; Mundstock, A.; Treger, M.; Lange, K.; Hwang, S.; Chmelik, C.; Rusch, P.; Bigall, N. C.; Pichler, T.; Shiozawa, H.; Caro, J. *ACS Appl. Mater. Interfaces* **2019**, 11, 14175–14181.

(19) Zheng, H.; Wang, D.; Sun, X.; Jiang, S.; Liu, Y.; Zhang, D.; Zhang, L. *Chem. Eng. J*. **2021**, 411, 128524.

(20) Li, B.; Zhang, Z.; Li, Y.; Yao, K.; Zhu, Y.; Deng, Z.; Yang, F.; Zhou, X.; Li, G.; Wu, H.; Nijem, N.; Chabal, Y. J.; Lai, Z.; Han, Y.; Shi, Z.; Feng, S.; Li, J. *Angew. Chem. Int. Ed*. **2012**, 51, 1412–1415.

(21) Roztocki, K.; Formalik, F.; Krawczuk, A.; Senkovska, I.; Kuchta, B.; Kaskel, S.; Matoga, D. *Angew. Chem. Int. Ed*. **2020**, 59, 4491–4497.

(22) Roztocki, K.; Rauche, M.; Bon, V.; Kaskel, S.; Brunner, E.; Matoga, D. *ACS Appl. Mater. Interfaces* **2021**, 13, 28503–28513.

(23) Yu, C.; Ding, Q.; Hu, J.; Wang, Q.; Cui, X.; Xing, H. *Chem. Eng. J.* **2021**, 405, 126937.

(24) Polyzoidis, A.; Schwarzer, M.; Loebbecke, S.; Piscopo, C. G. *Mater. Lett.* **2017**, 197, 213–216.

(25) Zahn, G.; Schulze, H. A.; Lippke, J.; König, S.; Sazama, U.; Fröba, M.; Behrens, P. *Microporous Mesoporous Mater.* **2015**, 203, 186–194.

(26) Shearer, G. C.; Chavan, S.; Bordiga, S.; Svelle, S.; Olsbye, U.; Lillerud, K. P. *Chem. Mater.* **2016**, 28, 3749–3761.

(27) Song, X.; Yang, P.; Wu, D.; Zhao, P.; Zhao, X.; Yang, L.; Zhou, Y. *Chem. Phys.* **2020**, 531, 110655.

(28) Chavan, S. M.; Shearer, G. C.; Svelle, S.; Olsbye, U.; Bonino, F.; Ethiraj, J.; Lillerud, K. P.; Bordiga, S. *Inorg. Chem.* **2014**, 53, 9509–9515.

(29) Zheng, G.; Chen, Z.; Sentosun, K.; Pérez-Juste, I.; Bals, S.; Liz-Marzán, L. M.; Pastoriza-Santos, I.; Pérez-Juste, J.; Hong, M. *Nanoscale* **2017**, 9, 16645–16651.

(30) Jia, M.; Jin, Y.; Zhao, C.; Zhao, P.; Jia, M. *J. Alloys Compd.* **2020**, 831, 154749.

(31) Malekmohammadi, M.; Fatemi, S.; Razavian, M.; Nouralishahi, A. *Solid State Sci.* **2019**, 91, 108–112.

(32) Schejn, A.; Balan, L.; Falk, V.; Aranda, L.; Medjahdi, G.; Schneider, R. *CrystEngComm* **2014**, 16, 4493–4500.

(33) Pan, Y.; Heryadi, D.; Zhou, F.; Zhao, L.; Lestari, G.; Su, H.; Lai, Z. *CrystEngComm* **2011**, 13, 6937.

(34) Chen, Y.; Li, X.; Nisa, M. U.; Lv, J.; Li, Z. *Fuel* **2019**, 241, 802–812.

(35) Liao, X.; Wang, F.; Wang, F.; Cai, Y.; Yao, Y.; Teng, B.-T.; Hao, Q.; Shuxiang, L. *Appl. Catal., B* **2019**, 259, 118064.

Chapter 3

Magnetic Sustentation as an adsorption characterization technique for paramagnetic MOFs

3.1 INTRODUCTION

Adsorption is widely used for different purposes due to the advantages it offers, such as low-cost and high efficiency. For decades, many efforts have been made to develop suitable adsorbents, but few works have focused on developing suitable direct characterization techniques for adsorption processes in solution that do not rely on specific physicochemical properties of the adsorbate. The greatest advantages of adsorption in the removal and purification of chemicals are the low-cost, high efficiency and ease of operation compared to conventional methods such as chemical precipitation, ion exchange, liquid-liquid extraction or filtration[1] and the considerable variety of adsorbents available. For this reason, adsorption is a widely used process in different industrial and environmental protection applications such as catalysis, storage and purification of water and air[2]. Therefore, adsorption capacity, kinetics and enthalpy are widely studied in order to analyse and evaluate the performance of the adsorbents[3].

For the study of adsorption properties in the gas phase, there are reliable characterization techniques, particularly volumetric and gravimetric adsorption experiments[4–6]. Other techniques such as vapour adsorption[7,8], quartz crystal microbalance in gravimetry[9], ellipsometry[10], pycnometry[11] and X-ray reflectometry[12] have been proposed in order to study the sorption of gas molecules for thin film

characterization[13]. However, if the aim is to study adsorption processes in solution, the available techniques rely on the indirect characterization of the adsorption by measuring the adsorbate concentration remaining in solution. In this regard, conventional techniques like ultraviolet spectroscopy[14], chromatography[15] or nuclear magnetic resonance[16], among others, are employed. These techniques provide a direct measurement of the adsorbate molecules remaining in the solution, which is normally correlated with the amount captured by the adsorbent, but there are cases where this assumption is not so straightforward. This is the case for many drug molecules, which are aimed to be incorporated into an adsorbent (drug carrier) to develop a drug delivery system[17–20]. The adsorbent would capture targeted molecules but if the drug molecule is not completely soluble, its concentration in the solution would remain constant as there are in equilibrium with the solid form and the adsorbate[21,22]. Therefore, a simple and reliable characterization technique focused on the physicochemical properties of the adsorbent, suitable to be used under different chemical conditions, will be a major step towards the development of an inexpensive, accurate and reproducible technique for characterizing adsorption processes in solution.

Since the development of porous materials in the 1950s[23], a wide variety of adsorbents have been used such as activated carbons, carbonized polymers and resins, polymeric adsorbents, silica-based materials, clay materials or zeolites[24]. In this vast world of porous materials used as adsorbents, an interesting class with intrinsic properties that can be directly correlated with the amount of captured adsorbate are Metal-Organic Frameworks (MOFs). The outstanding properties of MOFs (already mentioned in *Chapter 1*) and the possibility to design and tune their properties with atomic precision is what become MOFs one of the most attractive materials[25–30].

During the last decades, different strategies have been developed in order to improve the efficiency of MOFs in adsorption processes. The most common approaches are carbonization[31], metal doping[32], functionalization[33], graphen-oxide modification[34] and magnetic functionalization of MOFs[35]. In order to prepare magnetic MOFs, encapsulating and embedding, layer-by-layer or mixing methods have been used to the detriment that they are time-consuming, energy-consuming and are not environmentally friendly[36].

In this chapter, a direct and low-cost characterization technique is presented taking advantage of the intrinsic magnetic properties of paramagnetic MOFs for the *in situ* studies of adsorption processes in solution. This method does not rely on the complex magnetic interactions that usually only emerge at temperatures well below room temperature. Instead, it is based on the weak attraction exerted by an external magnetic field on paramagnetic materials, as most MOFs are at room temperature[37]. The simple process (Figure 3.1) consists of the suspension of a droplet of dispersed MOF microparticles between the poles of an electromagnet. As the field is decreased, a critical value will be reached, in which the magnetic attraction of the paramagnetic MOF for the magnet is no longer sufficient to maintain the aggregate suspended, making it to fall to the bottom of the test tube. The guest molecules present in the pores of the material varies the critical field value, providing a direct reading of the material adsorption.
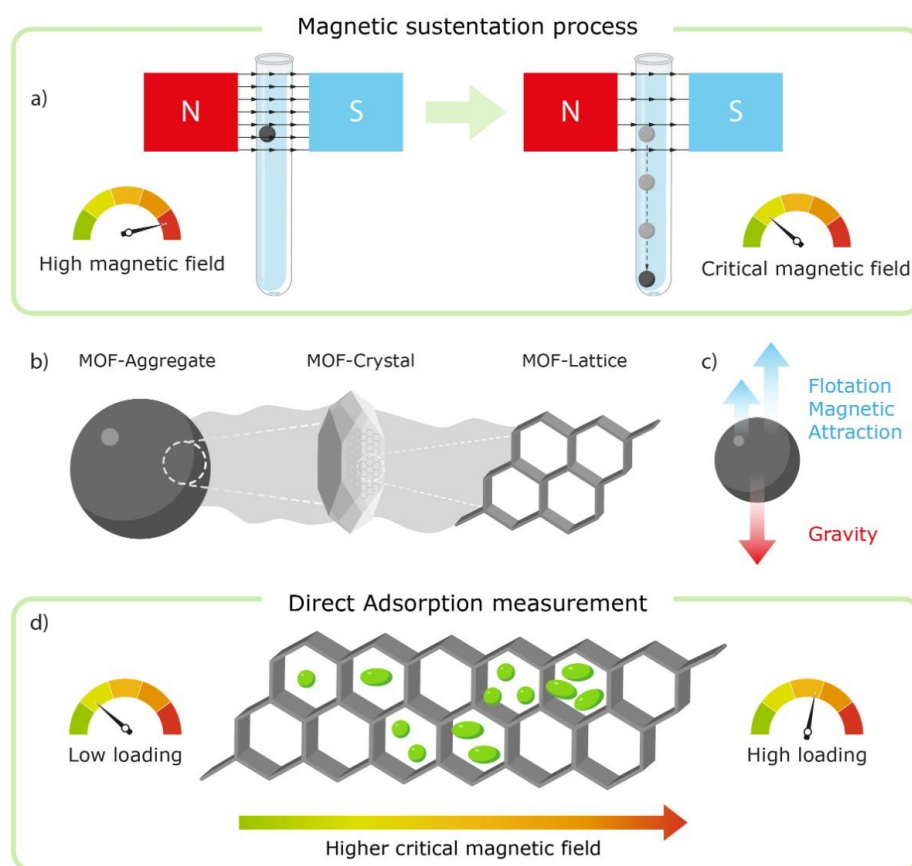
Figure 3.1. Magnetic Sustentation process: a) From the high magnetic field (suspended aggregate) to the critical magnetic field (aggregate dropping), b) the MOF aggregate composition, c) forces acting on the aggregate and d) the effect of the guest loading on the critical magnetic field.

Four MOFs have been selected containing Fe(III), Co(II) and Cu(II) as paramagnetic metal centres. MIL-88A(Fe) was chosen as an example of a water-stable MOF[38]. It contains Fe_3O trimers connected with fumarate linkers forming a flexible material with interconnected pores and cages of 5-7 Å[39,40]. ZIF-67(Co) is a zeolitic imidazole framework (ZIF) formed by bridging cobalt cations with imidazolate linker anions resulting in a sodalite-type topology (SOD) with a pore size of 3.4 Å[41,42]. Finally, two isostructural compounds were chosen, cobalt and copper MOF-74, in order to analyse the effect of the plasticity of the metal centre on their adsorption properties. This MOF contains unsaturated M^{2+} sites located at the edges of the 1D hexagonal channel of around 11 Å of diameter[43,44].

3.2 MAGNETIC SUSTENTATION EXPERIMENTAL SETTING

Magnetic Sustentation experiments (Figure 3.2) are performed using a parallel aligned dipole electromagnet. The procedure starts with the MOF crystals being added to a test tube full of pure solvent, located between the two poles of the electromagnet at their maximum magnetic field. The particles aggregate and are held suspended at the bottom of the magnet's poles. Once the system is stable, the magnetic field is slowly lowered and the particles start falling down in groups starting from those not directly attached to the glass walls of the test tube (the ones located further away from the magnetic pole). Finally, the last group of particles, those directly attached to the glass wall, fall down. The magnetic field at which this latter detachment happens is what we define as the critical magnetic field. This parameter corresponds to the value of the magnetic field necessary to retain the particles before gravity force overcomes magnetic attraction and the particles are not held suspended to the magnetic poles anymore.
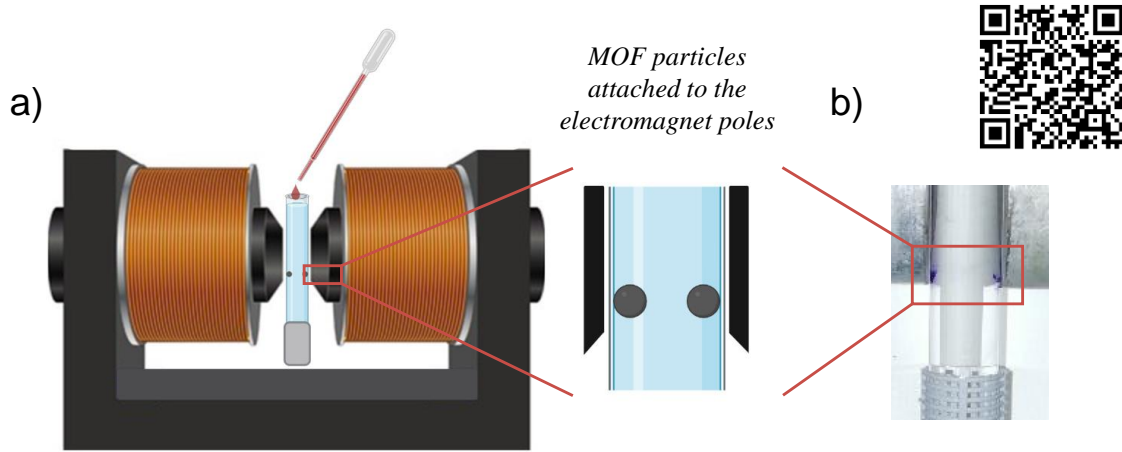
Figure 3.2. a) Scheme of the experimental set-up for Magnetic Sustentation experiment and b) an example of ZIF-67(Co) particles attached to the bottom part of the electromagnet poles. Inset: QR code (scan it to see the experimental set-up).

Different solvents were used in these experiments depending on the stability of the MOF, water was used for MIL-88A(Fe), while ethanol was used for MOF-74(Cu), MOF-74(Co) and ZIF-67(Co).

3.3 EQUATIONS GOVERNING THE FORCES BALANCE TAKING PLACE IN THE MAGNETIC SUSTENTATION EXPERIMENT

The Magnetic Sustentation experiment depicted in Figure 3.2, is the result of a fine balance between three forces acting on MOF particles: magnetic attraction, gravitation and flotation. Magnetic attraction is defined as the force that at the bottom of the magnetic pole pushes up the particles toward the maximum magnetic field central area (equation 3.1), gravitation is the force pushing down the particles (equation 3.2) and the flotation effect of the solvent is what keeps particles in suspension pushing up the particles (equation 3.3). The corresponding equations governing each force are depicted below:

$$F_{magnetism} = \nabla(m \cdot H) = m \cdot \nabla H = \frac{\chi_M}{MW_F} \cdot \rho_F \cdot V_F \cdot H \cdot \nabla H \qquad (3.1)$$

$$F_{gravity} = M \cdot g = (M_F + M_M) \cdot g = (V_F \cdot \rho_F + V_M \cdot \rho_M) \cdot g \qquad (3.2)$$

$$F_{flotation} = (V_F \cdot \rho_S + V_M \cdot \rho_S) \cdot g \qquad (3.3)$$

In these equations, we have made an arbitrary separation between the mass, volume and density corresponding to the MOF skeleton (M_F, V_F and ρ_F) and that corresponding to the adsorbed molecules (M_M, V_M and ρ_M). The other parameters are described as follows: χ_M corresponds to the molar susceptibility, H to the magnetic field, ∇H to the magnetic field gradient and g to the Earth magnetic attraction constant.

The critical magnetic field corresponds to the moment in which the forces pushing upwards and downwards the particle are equal (eq. 3.4):

$$F_{magnetism} = F_{gravity} - F_{flotation} \tag{3.4}$$

Replacing equations 3.1-3.3 into equation 3.4, equation 3.5 is achieved:

$$\frac{\chi_M}{MW_F} \cdot \rho_F \cdot V_F \cdot H \cdot \nabla H = (V_F \cdot \rho_F + V_M \cdot \rho_M) \cdot g - (V_F \cdot \rho_S + V_M \cdot \rho_S) \cdot g \tag{3.5}$$

Which can be rewritten as equation 3.6:

$$\frac{\chi_M}{MW_F} \cdot \rho_F \cdot H \cdot \nabla H = (\rho_F - \rho_S) \cdot g + (\rho_M - \rho_S) \cdot \frac{V_M}{V_F} \cdot g \tag{3.6}$$

On the other hand, V_F and V_M can be defined as: $V_F = \frac{M_F}{\rho_F} = \frac{n \cdot MW_F}{\rho_F}$ and $V_M = \frac{M_M}{\rho_M} = \frac{n \cdot x \cdot MW_M}{\rho_M}$, in order to provide the relation between the volumes of the adsorbed molecules (V_M) and MOF skeleton (V_F) as follows:

$$\frac{V_M}{V_F} = \frac{x \cdot MW_M \cdot \rho_F}{MW_F \cdot \rho_M} \tag{3.7}$$

Replacing it in equation (3.6) we obtain equation (3.8):

$$\frac{\chi_M}{MW_F} \cdot \rho_F \cdot H \cdot \nabla H = (\rho_F - \rho_S) \cdot g + (\rho_M - \rho_S) \cdot \frac{x \cdot MW_M \cdot \rho_F}{MW_F \cdot \rho_M} \cdot g \tag{3.8}$$

Which can be rewritten as equation (3.9):

$$x \cdot MW_M = \frac{\chi_M \cdot MW_F \cdot \rho_M}{MW_F \cdot (\rho_M - \rho_S) \cdot g} H \cdot \nabla H - \frac{(\rho_F - \rho_S) \cdot MW_F \cdot \rho_M}{(\rho_M - \rho_S) \cdot \rho_F} \tag{3.9}$$

Taking into account that all parameters except "$H \cdot \nabla H$" and "$x \cdot MW_M$" are constant and assuming that the density, ρ, of the different organic molecules is nearly the same, the above equation can be simplified to equation (3.10):

$$x \cdot MW_M = A \cdot H \cdot \nabla H - B \qquad (3.10)$$

We can define as $M_{M(F)} = x \cdot MW_M$, where, $M_{M(F)}$ is the mass of adsorbate molecules captured per formula of the framework compound we obtain equation (3.11), which defines a linear relationship between the adsorbed mass and the $H \cdot \nabla H$ parameter at which the particles are detached from the pole of the electromagnet.

$$M_{M(F)} = A \cdot H \cdot \nabla H - B \qquad (3.11)$$

On the other hand, the dependence of the $H \cdot \nabla H$ *vs* H in the parallel configuration of the electromagnet poles is not linear in the whole range but follows a quasi-linear dependence for more limited ranges as those taking place during the Magnetic Sustentation experiments (Figure 3.3). Therefore, the above equation can be rewritten as:

$$M_{M(F)} = A \cdot H - B \qquad (3.12)$$

a)

b)

c)

d)

e)
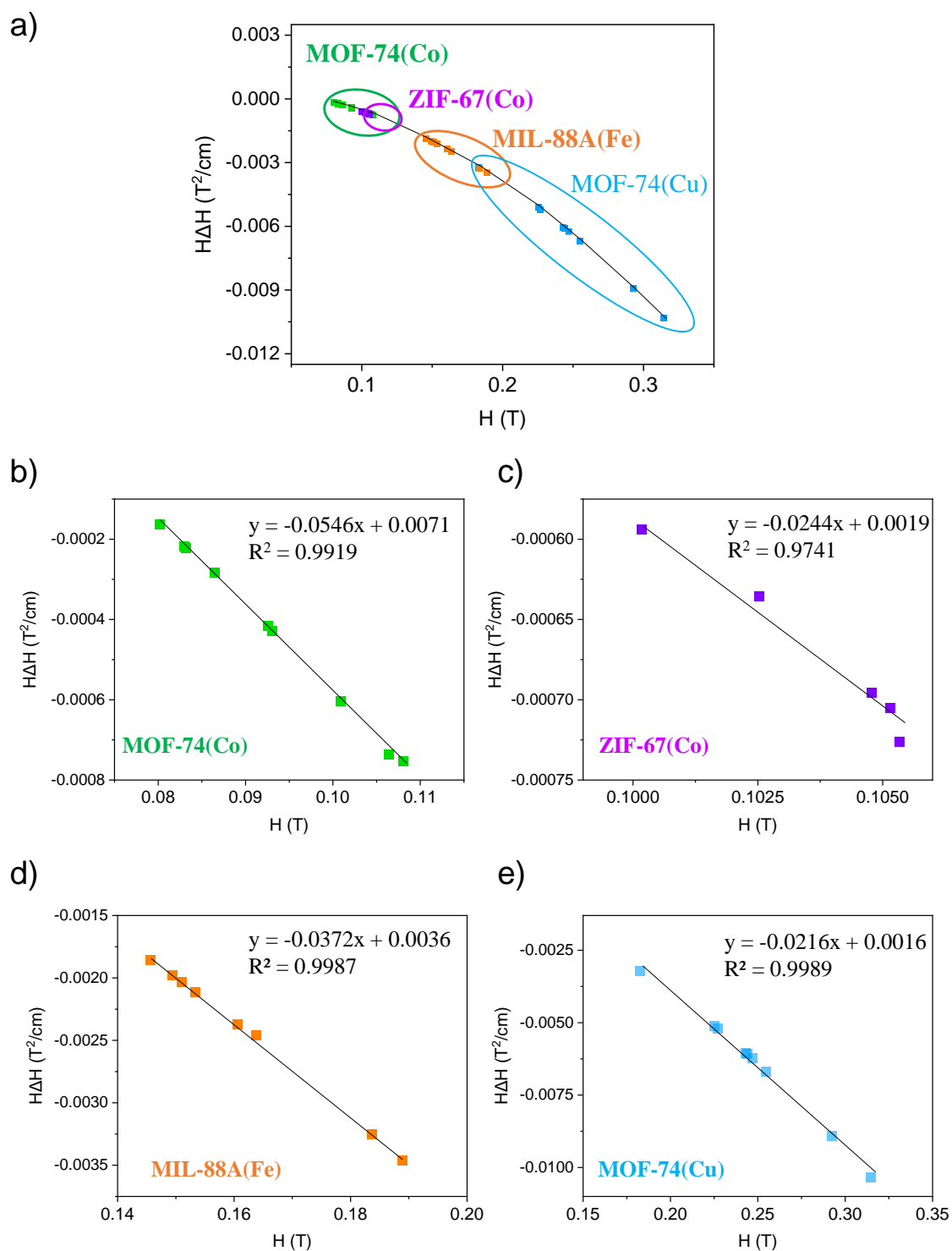
Figure 3.3. $H \cdot \nabla H$ dependence on the magnetic field, H, at the centre of the pole and linear fitting in the range at which the Magnetic Sustentation experiments are performed: a) all MOFs, b) MOF-74-Co, c) ZIF-67(Co), d) MIL-88A(Fe) and e) MOF-74(Cu).

3.4 RESULTS

3.4.1 Experimental verification of the absence of dependence concerning the particle size

Magnetic Sustentation experiments were performed over MIL-88A(Fe) samples with different particle sizes in order to analyse the influence of different particle sizes (1.5, 4.4 and 5.7 µm) on the critical magnetic field. As shown in Figure 3.4, there are no significant differences among the measured critical magnetic field for all samples, concluding there is no dependence with respect to the particle size in the range of ~ 1-6 µm in the considered morphologies. These experimental results agree with theoretical predictions indicating that there should not be such dependence.

Length: 5.7 ± 2.0 µm
Width: 0.57 ± 1.96 µm

Length: 4.4 ± 0.54 µm
Width: 1.4 ± 0.16 µm

Length: 1.5 ± 1.3 µm
Width: 0.9 ± 0.23 µm
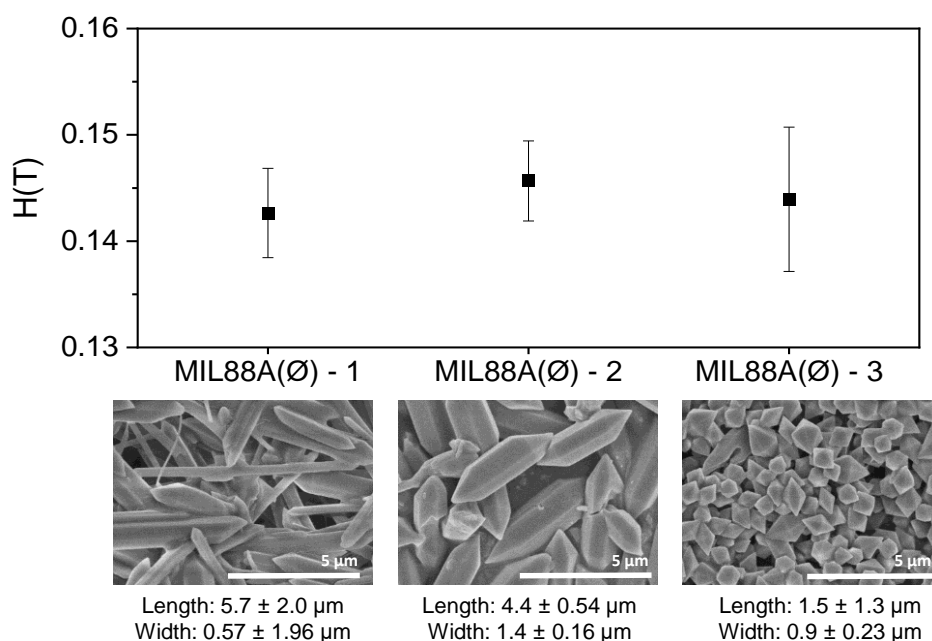
Figure 3.4. Determination of the critical magnetic field in water for the three as-synthesized MIL-88A(Fe) samples of different sizes.

3.4.2 Quantification experiments

In order to show the suitability of this approach to characterize adsorption processes, different adsorbates were selected, among them, some common organic solvents like DMSO or DMF and drug molecules such as acetylsalicylic acid or sodium naproxen (Figure 3.5). The critical magnetic field was determined in the same way as for plain MOFs. Briefly, 15 mg of the MOF were placed in 1.5 mL of the corresponding solvent

containing 50 mg of the corresponding adsorbate for 24 h at room temperature and under constant agitation before proceeding with the Magnetic Sustentation experiment.
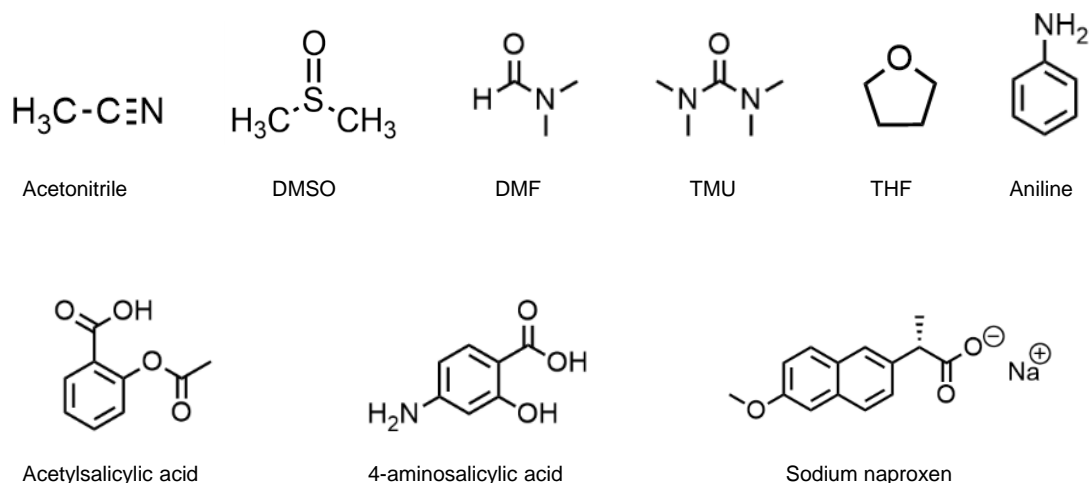
Figure 3.5. Selected organic compounds for the adsorption measurements.

In Figure 3.6, the measured critical magnetic field after the adsorption experiments can be seen for the selected MOFs. MIL-88A(Fe) and MOF-74(Cu, Co) were able to adsorb some of the tested compounds. More precisely, the smaller the size of the adsorbate, the higher the mass adsorbed and therefore, the magnetic field necessary to retain MOF particles attached to the poles. In that sense, while for smaller organic molecules such as acetonitrile and DMSO the adsorption is significant, bigger drug molecules present a more limited adsorption. On the contrary, for ZIF-67(Co), the adsorption of all adsorbate molecules was negligible due to the small size of the pore windows[41]. In the case of isostructural MOF-74, although a similar trend is shown for both metals in the adsorption of small organic molecules, slight differences are observed in the uptake of drugs. When the metallic centre is copper(II), MOF-74 provides a better adsorption for big-size drug molecules like acetylsalicylic acid and 4-aminosalicylic acid, compared to cobalt(II). This can be attributed to slight differences in the porosity of the two materials. Although cobalt MOF shows a bigger surface area (1327 m^2/g and 1126 m^2/g for cobalt and copper, respectively), MOF-74(Cu) has a bigger pore volume (0.57 cm^3/g for copper vs 0.52 cm^3/g for cobalt), which in combination with the well-known higher coordination sphere flexibility of copper(II) allows the MOF to accommodate bigger molecules in a more efficiently

way. Furthermore, the presence of defective positions in MOFs can also play a significant role on the adsorption selectivity due to the different coordination preferences of Co(II) and Cu(II). However, the observed high adsorption values for some of the adsorbates (in terms of mols per formula of MOF, as we will see later) seem to imply that physisorption is the main driving force in the capture of these adsorbates.
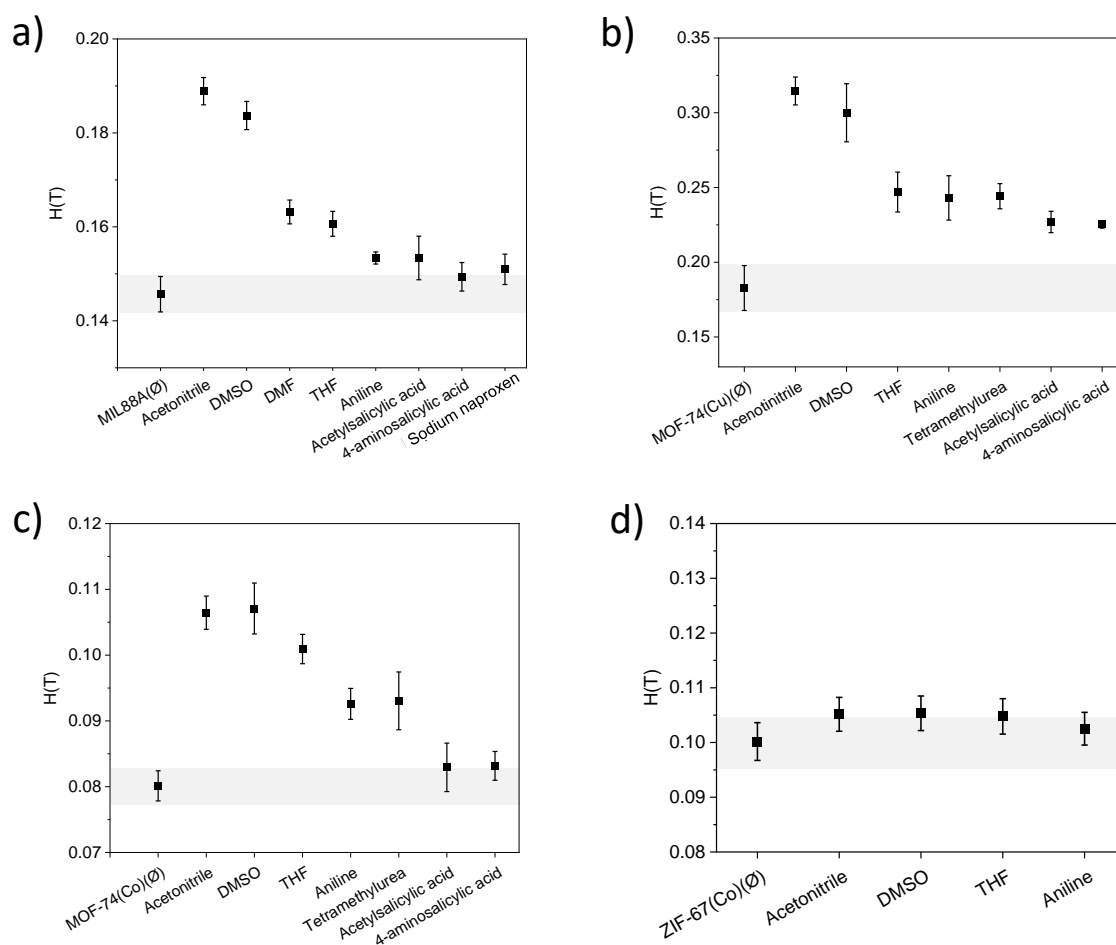
Figure 3.6. Determination of the critical magnetic field for a) MIL-88A(Fe), b) MOF-74(Cu), c) MOF-74(Co) and d) ZIF-67(Co) after being submerged 24 h and stirred in an aqueous (MIL-88A(Fe)) or ethanol (MOF-74(Cu), MOF-74(Co) and ZIF-67(Co)) solutions containing the adsorbate molecules. Samples labelled with Ø correspond to MOF samples not being exposed to any adsorbate.

Moreover, it has been experimentally proved that the magnetic field and the mass of captured adsorbate are linearly correlated, in agreement with equation (3.12). For that purpose, the adsorption experiments were reproduced with MIL-88A(Fe) and MOF-74(Cu, Co) and the adsorption was indirectly estimated from the concentration of the

adsorbate remaining in the solution using ultraviolet spectroscopy. Specifically, DMSO and DMF were chosen for MIL-88A(Fe) and DMSO and TMU for MOF-74(Cu, Co). The concentrations of these adsorbates were calculated with previously prepared regression lines (Figures 3.7).
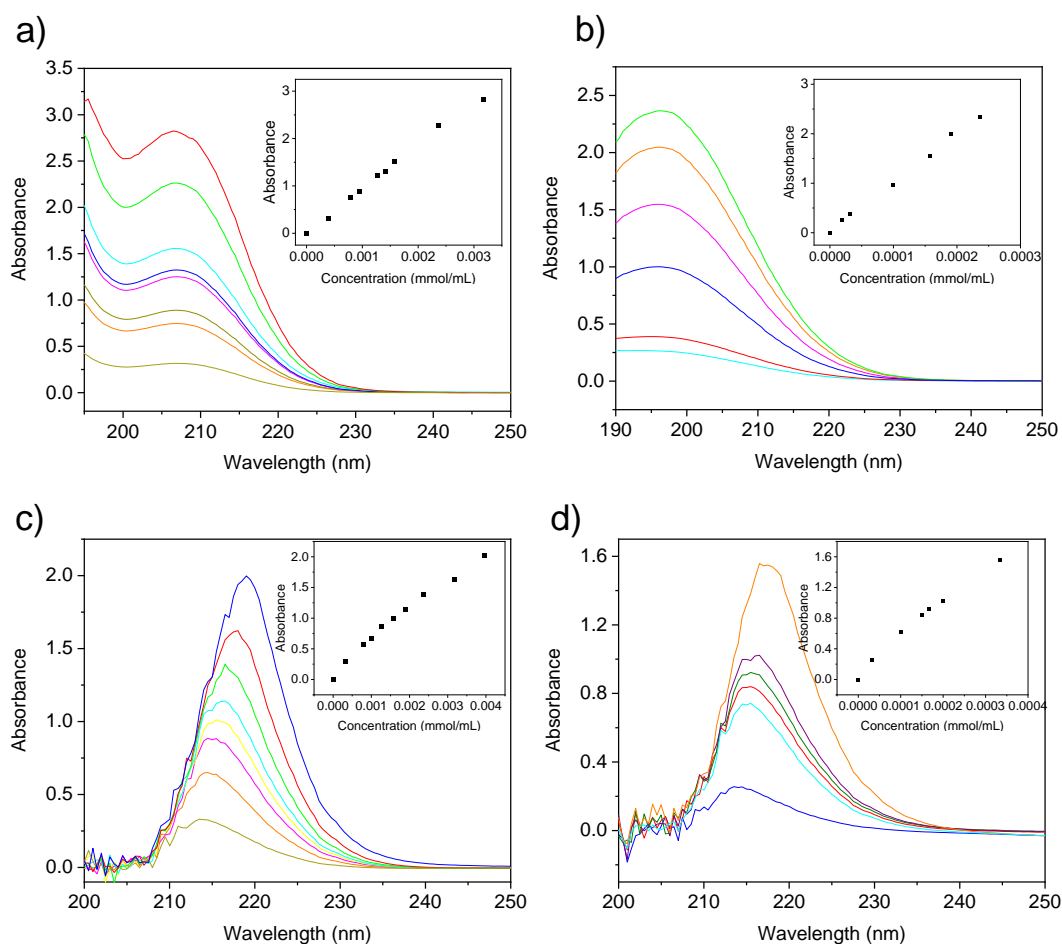
Figure 3.7. Ultraviolet spectra and regression lines in water: a) DMSO (y = 393.21x – 57.021; R^2 = 0.997), b) DMF (y = 9796.5x + 0.0412; R^2 = 0.996) and in ethanol c) DMSO (y = 488.63x + 0.1602; R^2 = 0.984) and d) TMU (y = 4578.1x + 0.099; R^2 = 0.985).

The obtained values represented in Figure 3.8 with their corresponding uncertainty corroborate the theoretically predicted linear correlation, and therefore, allows to directly quantify the mass adsorbed of the other molecules that are not UV active from the value of their critical magnetic field. Furthermore, it can also be observed that the slope of the linear fitting shows also dependence concerning the transition metal present in the MOF. The higher the number of unpaired electrons, the higher the magnetic susceptibility, and the steeper the slope. This becomes evident when

comparing MOF-74(Co) and MOF-74(Cu), where the other parameters appearing in equation (3.9) remain unchanged.

a) $y = 393.595x − 56.853; R^2 = 0.9945$

Calibration Curve - UV-VIS		H(T)	Adsorbed mass (%)	Adsorbed molecules/ MOF formula
□	MIL-88A(Ø)	0.146	0	0
○	DMF	0.164	7.9	0.62
◇	DMSO	0.184	15.9	1.11
Extrapolated values		H(T)	Adsorbed mass (%)	Adsorbed molecules/ MOF formula
Acetonitrile		0.189	17.3	2.43
THF		0.161	6.2	0.50
Aniline		0.153	3.3	0.20
Acetylsalicylic acid		0.153	3.3	0.11
4-aminosalicylic acid		0.149	1.7	0.07
Sodium naproxen		0.151	2.4	0.05

b) $y = 241.85x − 44.488; R^2 = 0.9982$

Calibration Curve - UV-VIS		H(T)	Adsorbed mass (%)	Adsorbed molecules/ MOF formula
□	MOF-74(Cu)(Ø)	0.183	0	0
○	TMU	0.244	13.9	0.39
◇	DMSO	0.293	26.3	1.10
Extrapolated values		H(T)	Adsorbed mass (%)	Adsorbed molecules/ MOF formula
Acetonitrile		0.315	31.6	2.75
THF		0.247	13.9	0.43
Aniline		0.243	15.2	0.75
Acetylsalicylic acid		0.227	14.3	0.55
4-aminosalicylic acid		0.225	10.4	0.21

c) $y = 750.38x − 59.365; R^2 = 0.9846$

Calibration Curve - UV-VIS		H(T)	Adsorbed mass (%)	Adsorbed molecules/ MOF formula
□	MOF-74(Co)(Ø)	0.08	0	0
○	TMU	0.09	11.9	0.32
◇	DMSO	0.107	20.3	0.82
Extrapolated values		H(T)	Adsorbed mass (%)	Adsorbed molecules/ MOF formula
Acetonitrile		0.106	20.5	1.57
THF		0.101	16.4	0.71
Aniline		0.093	10.1	0.34
Acetylsalicylic acid		0.083	2.9	0.05
4-aminosalicylic acid		0.083	3.0	0.06

Figure 3.8. Calibration curves obtained for quantifiable molecules (DMSO, DMF, TMU) by UV-VIS spectroscopy and the extrapolated values for the other adsorbates represented in a table. a) MIL-88A(Fe), b) MOF-74(Cu) and c) MOF-74(Co). For the calibration curves each measurement was repeated five times in order to provide the corresponding associated statistical error.

3.4.3 Adsorption isotherm curves

To illustrate all the opportunities this new technique offers, the adsorption isotherm curves (Figure 3.9a-c) were measured using different concentrations (0 – 40 mg/mL) of the selected adsorbate molecules for the Magnetic Sustentation experiments. Independently and for comparative purposes, the same adsorption isotherm curves were obtained by UV-Vis spectroscopy (Figure 3.9d-f) for quantifiable active adsorbates (DMSO, DMF, TMU). The results showed very similar results from both approaches. MIL-88A(Fe) adsorbs a maximum of 15% and 7% of DMSO and DMF, respectively, by the Magnetic Sustentation technique and 15% and 8% by UV-VIS spectroscopy. For MOF-74(Cu), the adsorption was calculated to be the same for both techniques, 27% and 14% of DMSO and TMU, respectively. Finally, for MOF-74(Co), adsorption of DMSO and TMU was 21% and 10 % determined by Magnetic Sustentation experiments and 20% and 12% with UV-Vis.

In all cases, it can be seen that adsorption isotherms calculated by Magnetic Sustentation experiments and ultraviolet spectroscopy are similar, showing this new approach as a versatile technique that allows not only the determination of the adsorbed mass in solution, but also offers the possibility to measure adsorption isotherms for any molecule. The advantage of the technique is on the one hand, that it offers a fast and direct way of obtaining the data due to the lack of sample preparation and dilutions, and on the other hand, the independence with respect to the chemical nature of the adsorbate. Conventional characterization techniques like UV-Vis spectroscopy are highly dependent on the adsorbate molecules as the adsorbate needs to be active (*i.e.* contain double bonds) reducing the adsorbates that can be quantified, while this new approach can be directly used with any molecule, independently of its physicochemical properties. Therefore and in order to prove this, adsorption isotherms for acetonitrile, a non-quantifiable molecule in UV-Vis spectroscopy, were also determined by Magnetic Sustentation experiment showing a maximum uptake of 17%, 31% and 21% for MIL-88A(Fe), MOF-74(Cu) and MOF-74(Co), respectively.
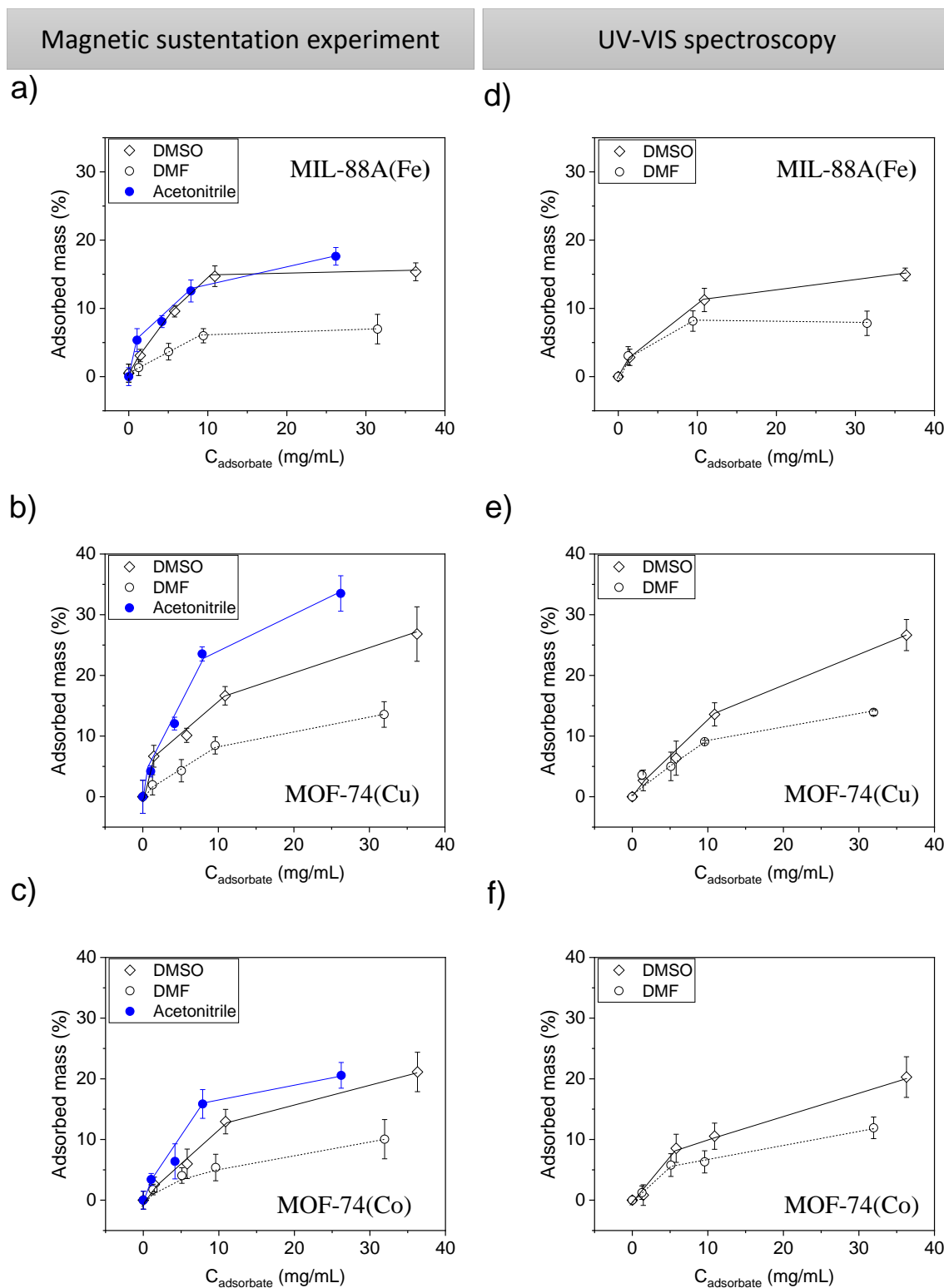
Figure 3.9. Adsorption isotherm curves of (a, d) MIL-88A(Fe), (b, e) MOF-74(Cu) and (c, f) MOF-74(Co) determined by Magnetic Sustentation experiments and ultraviolet spectroscopy for acetonitrile (●), DMSO (◇) and DMF(○).

3.4.4 Determination of the concentration of paramagnetic centres in solid-state solutions

In order to expand the possible uses of the technique, we decided to monitor also the incorporation of cobalt(II) in ZIF-8(Zn) with the Magnetic Sustentation technique. As a result, a solid-state solution between the ZIF-8(Zn) and ZIF-67(Co) isostructural MOFs with formula $[Zn_{1-x}Co_x(2\text{-methylimidazole})_2]_n$ was prepared. As Zn(II) is diamagnetic a decrease in the critical magnetic field should be observed with the incorporation of paramagnetic cobalt(II) metal centres in the framework. Later in this section, the equations governing the process will be developed.

Briefly, the protocols proposed by Linder-Patton *et al.*[45] for the synthesis of 10 and 100 µm-size particles (here, named as A and B, respectively) were modified in order to have a mixture of both cobalt(II) and zinc(II) nitrate in the initial mixture. The molar ratio between Zn and Co was varied in syntheses A and B to get a 25, 50 and 75% of cobalt(II) in the reaction mixture. Figure 3.10a and 3.10b show the PXRD of the synthesized samples, demonstrating that the structure of ZIF-8 (A_0% and B_0%) was kept after the incorporation of different amount of cobalt(II) in the framework. Figure 3.10c shows the captured pictures of the powder samples and SEM-EDS images. The colour of the MOF powder changed according to the loaded cobalt, suggesting a more intense purple colour for samples with a higher amount of cobalt. Furthermore, it was proven that both zinc and cobalt are homogeneously distributed in the particles proving that both metals were incorporated successfully in the framework, discarding the possibility of having segregated ZIF-8 and ZIF-67 particles.

Taking into account that the paramagnetic nature of the framework would be related to the presence of cobalt(II), the molar susceptibility, χ_M, can be defined as the resultant of the magnetic susceptibility of cobalt(II) per the fraction (x) of cobalt in the formula following equation (3.13):

$$\chi_M = x \cdot \chi_{Co} \qquad (3.13)$$

In these experiments, all the terms related to the adsorbed molecules used in the previous sections equations can be removed as no adsorption phenomena is taking place. Therefore, equation (3.5) can be simplified to equation (3.14):

$$\frac{\chi_M}{MW_F} \cdot \rho_F \cdot V_F \cdot H \cdot \nabla H = V_F \cdot \rho_F \cdot g - V_F \cdot \rho_S \cdot g \qquad (3.14)$$

Replacing equation (3.13) in equation (3.14) and simplifying it, we get:

$$x = \chi_{Co} \frac{MW_F \cdot g \cdot (\rho_F - \rho_S)}{\rho_F \cdot \chi_{Co}} \cdot \frac{1}{H \cdot \nabla H} \qquad (3.15)$$

The molecular weight [MW(ZIF-8) = 227.6 g/mol and MW(ZIF-67) = 221.1 g/mol], the molar susceptibility of cobalt(II) in this compound and the density of the framework can be considered nearly constant and therefore, we can rewrite equation (3.15) as follows:

$$x = A \cdot \frac{1}{H \cdot \nabla H} \qquad (3.16)$$

As we have demonstrated in section 3.3, $H \cdot \nabla H$ *vs* H follows a quasi-linear dependence for small variations on the critical magnetic field. Thus, equation (3.16) can be rewritten as equation (3.17):

$$x = A \cdot \frac{1}{H} \qquad (3.17)$$

For the determination of the critical magnetic field, ethanol was used as solvent and the procedure described in section 3.1 was applied. In addition, the amount of cobalt and zinc in the samples was determined by ICP-AES (Figure 3.10d). We proved that ZIF-8 needs less than a 5% of cobalt(II) in the structure to be attached to the electromagnet pole and thus, be quantifiable with the Magnetic Sustentation technique. Furthermore, the cobalt fraction calculated from ICP-AES (named as x_{CO}) in the sample was plotted against the inverse of the critical magnetic field. In Figure 3.10e, it can be observed that there is a linear relation between the inverse of the critical magnetic field and the paramagnetic contribution of cobalt in agreement with the theoretical predictions of equation (3.17).
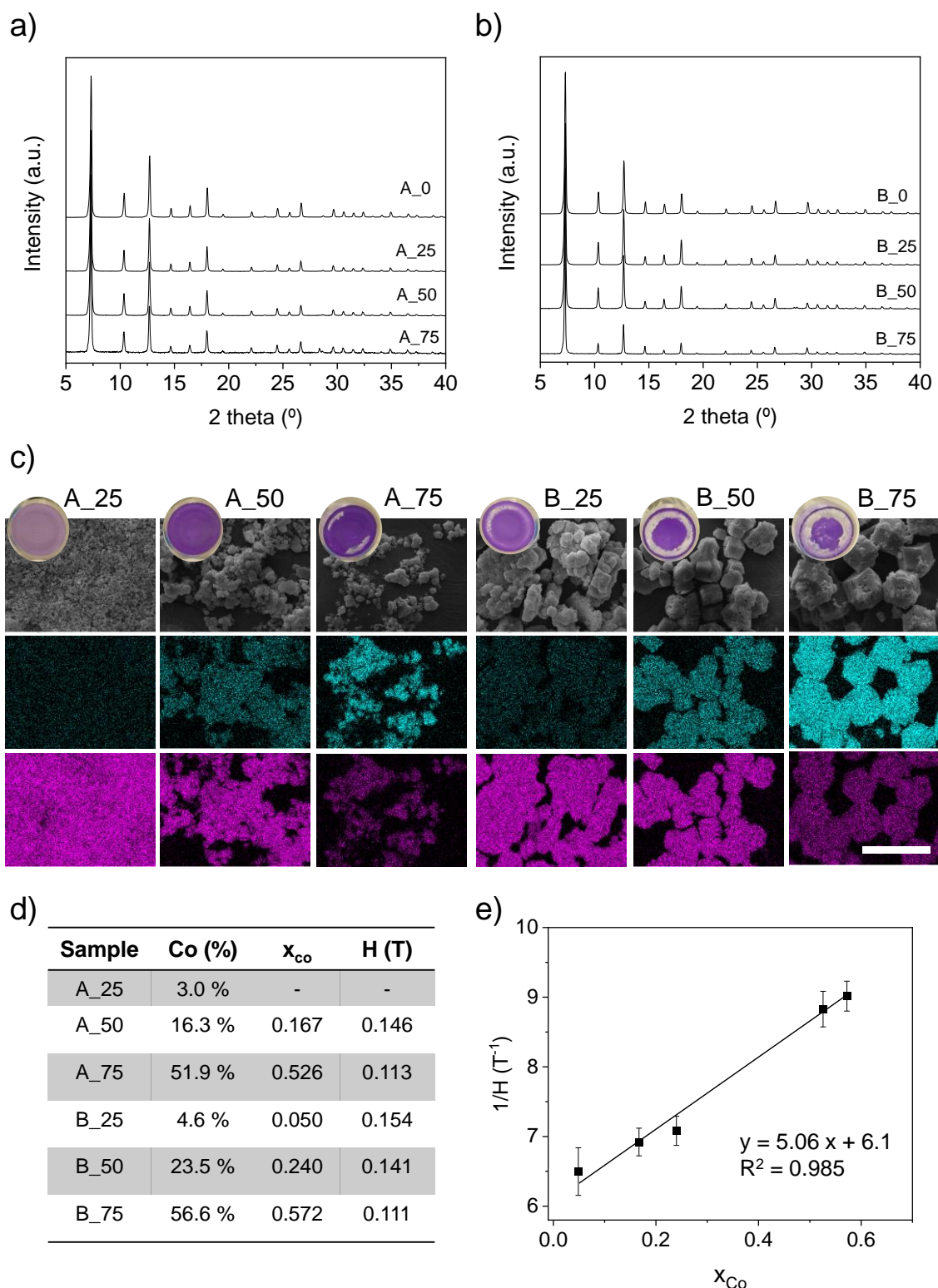
Figure 3.10. Powder X-Ray diffraction of the as synthesized samples synthesized following a) A procedure and b) B procedure. c) Captured images of the powder samples, SEM images and SEM-EDS images (blue for cobalt and pink for zinc. Scale bar 10 µm). d) Critical magnetic field, cobalt percentage (%) and fraction (x_{co}), where x_{co} refers to x in $[Zn_{1-x}Co_x(2\text{-methylimidazole})_2]_n$ determined with ICP-AES. d) 1/H vs cobalt fraction (x_{co}) in the ZIF-8/67 samples.

Sample	Co (%)	x_{co}	H (T)
A_25	3.0 %	-	-
A_50	16.3 %	0.167	0.146
A_75	51.9 %	0.526	0.113
B_25	4.6 %	0.050	0.154
B_50	23.5 %	0.240	0.141
B_75	56.6 %	0.572	0.111

$y = 5.06\,x + 6.1$
$R^2 = 0.985$

3.5 CONCLUSIONS

In this chapter, we have presented a fast and direct characterization technique for adsorption processes in solution based on the intrinsic magnetic properties – paramagnetic metal nodes- of MOFs at room temperature. We have developed the theoretical equations that guide Magnetic Sustentation experiments to better understand the process and experimentally verify its feasibility using four well-known MOFs. On the one hand, water-stable MIL-88A(Fe) was selected, demonstrating that the critical magnetic field it is not influenced by particles size in the range 1-6 μm. In addition, the adsorption of different organic molecules was quantified, and it was confirmed that there is a linear relationship between the critical magnetic field and captured mass. In order to prove the versatility of this new technique, the same experiments were recorded in ethanol using MOFs that are not water stable, isostructural Cu(II)- and Co(II)-MOF-74 and ZIF-67(Co). In addition, this technique allowed obtaining adsorption isotherms curves, which altogether provides the advantage of performing a direct and *in situ* measurement of captured molecules and without the need for any sample preparation that conventional techniques such as ultraviolet spectroscopy usually require. Finally, similar experiments were performed on ZIF-8(Zn)/ZIF-67(Co) solid state solutions to determine the amount of paramagnetic cobalt(II) incorporated.

3.6 REFERENCES

(1) Chakraborty, R.; Asthana, A.; Singh, A. K.; Jain, B.; Susan, A. B. H. *Int. J. Environ. Anal. Chem.* **2022**, 102, 342–379.

(2) Dabrowski, A. *Adv. Colloid Interface Sci*. **2021**, 93, 135–224.

(3) Qiu, H.; Lv, L.; Pan, B.-c.; Zhang, Q.-j.; Zhang, W.-m.; Zhang, Q.-x. *J. Zhejiang Univ. Sci. A* **2009**, 10, 716–724.

(4) Wang, J.-Y.; Mangano, E.; Brandani, S.; Ruthven, D. M. *Adsorption* **2021**, 27, 295–318.

(5) Sotomayor, F.; Cychosz, K.; Thommes, M. *Acc. Mater. Surf. Res* **2018**, 3, 34–50.

(6) Talu, O. *Adv. Colloid Interface Sci*. **1998**, 76-77, 227–269.

(7) Bettens, B.; Verhoef, A.; van Veen, H. M.; Vandecasteele, C.; Degrève, J.; van der Bruggen, B. *J. Phys. Chem. C* **2010**, 114, 9416–9423.

(8) Bosnick, K.; Ban, S.; Hiebert, W.; Shi, Z.; Huang, C.; Lister, R.; Mleczko, M. *Carbon* **2011**, 49, 3639–3644.

(9) Thoury-Monbrun, V.; Gaucel, S.; Rouessac, V.; Guillard, V.; Angellier-Coussy, H. *Carbohydr. Polym*. **2018**, 190, 307–314.

(10) Löbmann, P. *J. Sol-Gel Sci. Technol*. **2017**, 84, 2–15.

(11) Dral, A. P.; Elshof, J. E. ten. *Microporous Mesoporous Mater*. **2018**, 258, 197–204.

(12) Klotz, M.; Rouessac, V.; Rébiscoul, D.; Ayral, A.; van der Lee, A. *Thin Solid Films* **2006**, 495, 214–218.

(13) Rouessac, V.; van der Lee, A.; Bosc, F.; Durand, J.; Ayral, A. *Microporous Mesoporous Mater*. **2008**, 111, 417–428.

(14) Lv, S.-W.; Liu, J.-M.; Ma, H.; Wang, Z.-H.; Li, C.-Y.; Zhao, N.; Wang, S. *Microporous Mesoporous Mater*. **2019**, 282, 179–187.

(15) González-Hernández, P.; Gutiérrez-Serpa, A.; Lago, A. B.; Estévez, L.; Ayala, J. H.; Pino, V.; Pasán, *J. ACS Appl. Mater. Interfaces* **2021**, 13, 45639–45650.

(16) Luo, X.-Z.; Jia, X.-J.; Deng, J.-H.; Zhong, J.-L.; Liu, H.-J.; Wang, K.-J.; Zhong, D.-C. *J. Am. Chem. Soc*. **2013**, 135, 11684–11687.

(17) Kalepu, S.; Nekkanti, V. *Acta Pharmacol. Sin. B* **2015**, 5, 442–453.

(18) Mitchell, M. J.; Billingsley, M. M.; Haley, R. M.; Wechsler, M. E.; Peppas, N. A.; Langer, R. *Nat. Rev. Drug discovery* **2021**, 20, 101–124.

(19) Vargason, A. M.; Anselmo, A. C.; Mitragotri, S. *Nat. Biomed. Eng*. **2021**, 5, 951–967.

(20) Wang, N.; Cheng, X.; Li, N.; Wang, H.; Chen, H. *Adv. Healthcare Mater*. **2019**, 8, e1801002.

(21) Herrmann, I. K.; Wood, M. J. A.; Fuhrmann, G. *Nature Nanotechnol.* **2021**, 16, 748–759.

(22) Savjani, K. T.; Gajjar, A. K.; Savjani, J. K. *ISRN pharmaceutics* **2012**, 2012, 195727.

(23) Sing, K. S.W. *Colloids Surf.*, A **2004**, 241, 3–7.

(24) Thomas, W. J.; Crittenden, B. *Adsorption technology and design*; Butterworth-Heinemann: Oxford, **1998**.

(25) Yaghi, O. M. *J. Am. Chem. Soc.* **2016**, 138, 15507–15509.

(26) Gropp, C.; Canossa, S.; Wuttke, S.; Gándara, F.; Li, Q.; Gagliardi, L.; Yaghi, O. M. *ACS Cent. Sci.* **2020**, 6, 1255–1273.

(27) Freund, R.; Canossa, S.; Cohen, S. M.; Yan, W.; Deng, H.; Guillerm, V.; Eddaoudi, M.; Madden, D. G.; Fairen-Jimenez, D.; Lyu, H.; Macreadie, L. K.; Ji, Z.; Zhang, Y.; Wang, B.; Haase, F.; Wöll, C.; Zaremba, O.; Andreo, J.; Wuttke, S.; Diercks, C. S. *Angew. Chem. Int. Ed.* **2021**, 60, 23946–23974.

(28) Freund, R.; Zaremba, O.; Arnauts, G.; Ameloot, R.; Skorupskii, G.; Dincă, M.; Bavykina, A.; Gascon, J.; Ejsmont, A.; Goscianska, J.; Kalmutzki, M.; Lächelt, U.; Ploetz, E.; Diercks, C. S.; Wuttke, S. *Angew. Chem. Int. Ed*. **2021**, 60, 23975–24001.

(29) Ejsmont, A.; Andreo, J.; Lanza, A.; Galarda, A.; Macreadie, L.; Wuttke, S.; Canossa, S.; Ploetz, E.; Goscianska, *J. Coord. Chem. Rev*. **2021**, 430, 213655.

(30) Andreo, J.; Ettlinger, R.; Zaremba, O.; Peña, Q.; Lächelt, U.; Luis, R. F. de; Freund, R.; Canossa, S.; Ploetz, E.; Zhu, W.; Diercks, C. S.; Gröger, H.; Wuttke, S. *J. Am. Chem. Soc.* **2022**, 144, 7531–7550.

(31) Li, X.; Yuan, H.; Quan, X.; Chen, S.; You, S. *J. Environ*. Sci. **2018**, 63, 250–259.

(32) Jin, J.; Yang, Z.; Xiong, W.; Zhou, Y.; Xu, R.; Zhang, Y.; Cao, J.; Li, X.; Zhou, C. *Sci. Total Environ.* **2019**, 650, 408–418.

(33) Guo, X.; Kang, C.; Huang, H.; Chang, Y.; Zhong, C. *Microporous Mesoporous Mater.* **2019**, 286, 84–91.

(34) Sun, Y.; Chen, M.; Liu, H.; Zhu, Y.; Wang, D.; Yan, M. *Appl. Surf. Sci.* **2020**, 525, 146614.

(35) Moradi, S. E.; Haji Shabani, A. M.; Dadfarnia, S.; Emami, S. *J. Iran. Chem. Soc.* **2016**, 13, 1617–1627.

(36) Aghayi-Anaraki, M.; Safarifard, V. *Eur. J. Inorg. Chem.* **2020**, 1916–1937.

(37) Pérez-Aguirre, R.; Artetxe, B.; Beobide, G.; Castillo, O.; Pedro, I. de; Luque, A.; Pérez-Yáñez, S.; Wuttke, S. *Cell Rep. Phys. Sci* **2021**, 2, 100421.

(38) Hirschle, P.; Hirschle, C.; Böll, K.; Döblinger, M.; Höhn, M.; Tuffnell, J. M.; Ashling, C. W.; Keen, D. A.; Bennett, T. D.; Rädler, J. O.; Wagner, E.; Peller, M.; Lächelt, U.; Wuttke, S. *Chem. Mater.* **2020**, 32, 2253–2263.

(39) Serre, C.; Millange, F.; Surblé, S.; Férey, G. *Angew. Chem. Int. Ed.* **2004,** 43, 6285–6289.

(40) Chalati, T.; Horcajada, P.; Gref, R.; Couvreur, P.; Serre, C. *J. Mater. Chem.* **2011**, 21, 2220–2227.

(41) Qian, J.; Sun, F.; Qin, L. *Mater. Lett.* **2012**, 82, 220–223.

(42) Avci, C.; Ariñez-Soriano, J.; Carné-Sánchez, A.; Guillerm, V.; Carbonell, C.; Imaz, I.; Maspoch, D. *Angew. Chem. Int. Ed.* **2015**, 127, 14625–14629.

(43) Rosi, N. L.; Kim, J.; Eddaoudi, M.; Chen, B.; O'Keeffe, M.; Yaghi, O. M. *J. Am. Chem. Soc.* **2005**, 127, 1504–1518.

(44) Katz, M. J.; Howarth, A. J.; Moghadam, P. Z.; DeCoste, J. B.; Snurr, R. Q.; Hupp, J. T.; Farha, O. K. *Dalton Trans.* **2016**, 45, 4150–4153.

(45) Linder-Patton, O. M.; Prinse, T. J. de; Furukawa, S.; Bell, S. G.; Sumida, K.; Doonan, C. J.; Sumby, C. J. *CrystEngComm* **2018**, 20, 4926–4934.

Chapter

4

This chapter is based on an original research article (currently under review) of the same name

Chapter 4

Guest-induced breathing mediated size- and shape-selective alcohol recovery from water by MIL-88A(Fe)

4.1 INTRODUCTION

Global climate change along with rising fuel prices and depletion of natural fuel supplies have culminated in huge demand for green renewable energy production in order to meet the enormous energy demands worldwide[1–3]. In this regard, biofuels are considered one of the most promising viable and environmentally benign alternatives, which can also bring down the huge dependence on fossil energy sources[4,5]. Typically, biofuel products are obtained from dilute mixtures of alcohol in water, which are currently produced from agricultural feedstocks, fermentation of molasses and algae farms. This inevitably requires the recovery of those alcohols from such diluted mixtures, which usually relies on high energy demanding distillation and purification processes that also presents a poor net energy balance (NEB), *i.e.* the difference between the energy generated from the fuel and the production energy consumption is only ~25%[6–8]. Moreover, ethanol and water form an azeotropic mixture from which ~4% of the water is impossible to remove using the conventional distillation process[5]. Hence, recovery of alcohols from low-concentration aqueous solutions is still challenging and highly important from an energy-economic point of view[9]. Short-chain alcohols present many valuable applications and technological relevance. Apart from the ubiquitous ethanol, methanol is also a major alcoholic component having a

huge importance in various industrial sectors. For instance, methanol is an industrial feedstock in the production of insecticides. It is also employed as feedstock to manufacture several other industrial products such as methanal (formaldehyde), acetic acid, methyl esters of various acids and so on. However, because of its intrinsic toxic nature, methanol and its distillation wastes are classified as HW42 hazardous waste and possess high threat to the atmosphere, soil and groundwater[10]. Long-term ingestion of methanol contamination can lead to some diseases like blindness, chronic nerve damage and even death. Therefore, the development of novel porous materials for efficient methanol removal from water, even at low concentrations, is a pressing environmental need.

In this regard, adsorptive separation-based techniques have established themselves as green and cost-effective alternatives to the high-energy footprint of the traditional distillation processes[11]. In this context, metal-organic frameworks (MOFs) have attracted significant scientific attention as they offer superior sorption performance as well as enhanced selectivity toward targeted sorbate species[12–19]. All this together with the outstanding properties of MOFs make them very suitable materials, especially for volume specific applications such as purification, separation or adsorption processes[20–23]. Over the last decades MOF field have increased sharply, leading to a deep understanding of the field, which together with the discovery of many different structures such as breathing MOFs, have attracted great interest[24–29]. Unlike rigid frameworks, flexible MOFs exhibit structural dynamism arising from physical (temperature, pressure, light) or chemical (guest incorporation or elimination) external stimuli[30–37]. Among the flexible MOFs, MIL-88A outstands due to the large breathing transformation, cost effectiveness or easy synthesis. MIL-88A(Fe) presents a hexagonal-type structure built up from oxocentred iron(III) octahedral trimers connected by dicarboxylates groups from the fumarate anion, forming an interconnected 3D structure[38,39]. The O-O axis of the carboxylate groups allows the rotation of both metal clusters and organic linker[36], making MIL-88A one of the largest breathing MOF ever reported[27]. In this sense, the adsorption/desorption of guest molecules in the MOF is accompanied with an expansion/contraction of the unit cell, while the space group is maintained[40]. Such flexibility of MIL-88A series proven to be beneficial for various applications. For example, effect of flexible character of

MIL-88(Fe) was exploited for selective adsorption of n-akanes[41]. The guest-induced breathing of MIL-88 also have been employed toward adsorption of biologically active nitric oxide (NO) species[42]. The breathing effect was also exploited for remediation of various toxic water pollutants such as heavy metals[43], pharmaceuticals and personal care products (PPCPs)[44] and dyes[45]. Despite of these efforts, the potential of guest-induced framework adaptability of MIL-88A(Fe) toward liquid separation challenges such as the recovery of alcohols from aqueous environments is still untapped.

On the other hand, it is worth mentioning that although MOFs show good adsorptive performances due to their high surface areas and porosity, they are obtained as fine powders, which limits their practical applications[46,47]. Among the main disadvantages of using MOFs as powder limited packing densities, high diffusion barriers and difficulties to recover the material from solution can be found. In order to overcome these problems, the use of MOFs as fillers in polymeric mixed matrix membranes have been proposed[48–50]. Over the last years, polymer@MOF membranes have been widely reported for the removal of metal ions in water[51,52], capture of pharmaceuticals, dye wastewater[53,54] or oil pollution[55,56]. Although there are many different polymeric materials available, polyvinylidene fluoride (PVDF) has been widely used due to the high chemical and thermal stability, easy processing, high organic selectivity or hydrophobicity[57,58]. To the best of our knowledge, there are only very few examples of MOF or MOF-membrane based materials reported for the removal of alcohols from water, and none of them addresses the possible effect of using a breathing MOFs in this context.

In order to close this scientific gap, herein, the recovery of short-chain aliphatic alcohols from water has been studied with MIL-88A(Fe) MOF in order to address the challenge of alcohol-water separation (Figure 4.1). Specifically, 1 to 4 carbon-containing aliphatic alcohols has been used: methanol, ethanol, propyl alcohol (n- and iso- isomers) and butyl alcohol (n-, sec, iso- and *tert*-isomers), herein denoted as MeOH, EtOH, n-PrOH, i-PrOH, n-BuOH, s-BuOH, i-BuOH, and t-BuOH, respectively . The single-component alcohol adsorption experiments showed a linear tendency for the adsorption of linear alcohols, where the adsorption capacity of MIL-

88A(Fe) was found to be higher for smaller molecules (methanol), while branched alcohols showed more modest values. Theoretical studies corroborate well with the fact that such differential adsorption behaviour is attributed to the flexible nature of the MOF structure allowing the diffusivity of small molecules, while hindering the diffusion of branched alcohols. Interestingly, the competitive adsorption studies contrast with the single-component alcohol adsorption experiments, where a clear preference towards more hydrophobic molecules (*isopropyl alcohol* or *tert*-butyl alcohol) was observed over methanol. Difference in polarity of the incoming alcohol molecules found to dictate the sorption process in case of the multicomponent sorption studies. Finally, PVDF@MIL-88A(Fe) mixed matrix membranes were prepared to address the real-time applicability aspect of the MOF powders. The combination of guest-selective adaptable breathing effect along with selective host-guest interaction were proven to be highly potent for MIL-88A toward selective and efficient recovery of alcohols from water even in the low concentration liquid mixtures.
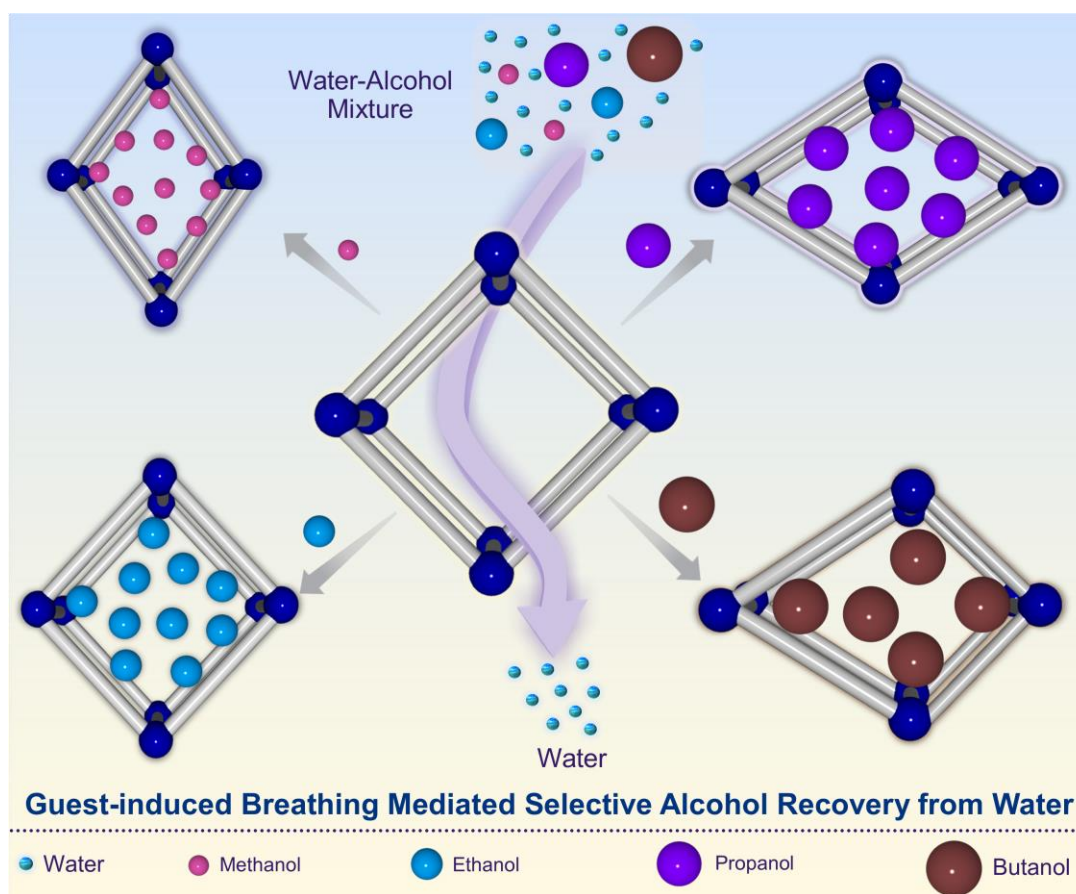
Figure 4.1. Schematic illustration of the guest-induced MOF breathing mediated alcohol recovery from aqueous solution.

4.2 EXPERIMENTAL DETAILS

4.2.1 Preparation of the materials

MIL-88A(Fe). For experimental details see *Chapter 2* (section 2.2.2).

PVDF@MIL-88A(Fe) membrane preparation. PVDF@MIL-88A(Fe) membranes with different MOF loadings (0, 10, 20 and 30 wt%) were prepared following doctor blade and NIPS procedure according to already reported protocols[59,60]. Briefly, to an initial suspension of MIL-88A(Fe) microparticles in DMF (6 mL), PVDF powder was gently added to prevent agglomeration while stirring (2 h) and ensuring its complete dissolution. The amount of MOF and polymer employed were adapted to obtain a total mass of 1 g. Then, the colloids were spread onto a glass substrate using a doctor blade with a fixed thickness of 250 μm in order to obtain thin films of the composite. The membrane was detached from the glass substrate by immersing it in a water bath at 75 °C and afterwards, it was left 30 min in another water bath at room temperature to remove all the DMF. Finally, membranes were allowed to dry overnight at room temperature.

4.2.2 Characterization

The crystallinity and purity of the samples were assessed by powder X-ray diffraction (PXRD). PXRD patterns were collected on a Philips X'PERT powder diffractometer with Cu Kα radiation (λ = 1.5418 Å) over the 5 < 2θ° < 40° range with a step size of 0.02° and an acquisition time of 2.5 s per step at 25 °C. Fourier transform infrared spectroscopy (ATR FT-IR) measurements were performed on a Bruker Alpha Series FT-IR spectrometer equipped with an attenuated total reflectance (ATR) module by collecting 16 scans of MIL-88A(Fe) in the ATR module to ensure the chemical stability of the sample after the cycling. Scanning electron microscopy (SEM) was used to determine particles size and morphology. For that, samples were coated with a thin gold layer and measured on a Hitachi S-4800 scanning electron microscope (150 s, 20 mA, 10 kV, zoom at ×10.000). Magnetic sustentation experiments were performed using a dipole electromagnet (Newport Pagnell England Electromagnet Type C sourced by a Hewlett Packard 6655A System DC Power Supply) in order to determine the critical magnetic field of MIL-88A(Fe). Briefly, 15 mg of MOF were

placed in a 1.5 mL water or alcohol containing aqueous solutions and were kept 2°
under rotating agitation. Afterwards, MIL-88A(Fe) crystals were placed in a 13 mm
diameter test tube filled with distilled water. The critical magnetic field of MIL-
88A(Fe) before and after the capture of the short chain alcohols from aqueous solution
was determined. Each measurement was repeated 5 times in order to provide the
corresponding associated error. In order to test the recyclability, MIL-88A(Fe)
samples were treated under high vacuum, after each cycle, to eliminate all the
molecules trapped in the pores. A series of additional adsorption experiments were
designed in which two consecutive single alcohol adsorption experiments were
performed (each one of 24 h) alternating between branched (t-BuOH and s-BuOH)
and small linear alcohols (MeOH and EtOH). The determination of the critical
magnetic field in the consecutive adsorption experiments was performed as previously
described. Kinetic adsorption curve was prepared similarly, but in this case, the same
methanol-water mixture employed for the adsorption procedure was used as the liquid
media. Pore-size distribution (PSD) data of MIL-88A(Fe) (open and close
configurations) were computed using Poreblaze 4.0 an open-source Fortran 90 code
to calculate structural properties of porous materials[61]. The structural models for the
MOF structures were taken from their crystallographic information files[62], from which
solvent molecules were removed prior to run the calculations. Force-field based Grand
Canonical Monte Carlo (GCMC) simulations of methanol and *tert*-butyl alcohol
adsorption were carried out using the SORPTION module included in the Accelrys
"Materials Studio" package[63]. The theoretical background of GCMC simulations is
described in detail elsewhere[64]. Dispersive and electrostatic interactions were
considered in all simulations. Dispersive interactions were modelled using a Lennard-
Jones 12–6 potential. Lorentz-Berthelot mixing rules were used to calculate the
parameters representing the interaction between different atom types. A cut-off radius
of 12.5 Å was set for dispersive interactions. Point charges were assigned to the atomic
sites in order to model the electrostatic interactions, while Ewald summation was
applied to consider the periodicity of the simulation box. All simulations were
performed using 2x2x2 supercells of MIL-88A(Fe). The LJ parameters for all the
atoms of the adsorbents were taken from the universal force field (UFF)[65]. The partial
charges to represent the electrostatic potential inside the pores were derived from DFT

calculations using the ESP method as described by Singh and Kollman[66], which is implemented in the DMOL3 code[67]. For this calculation, the DNP basis set and the PBE exchange-correlation functional were selected. The Lennard-Jones parameters and the point charges that model the adsorbate molecules were taken from the transferable potentials for phase equilibria-united atom (TraPPE-UA) force field developed for primary, secondary, and tertiary alcohols[68]. Fixed loading sorption simulations (single-molecule loading per calculation cell, 298 K) and fixed loading calculations (100 kPa, 298 K) involved 10 million equilibration steps and 10 million production steps.

^{1}H-NMR spectra were acquired in a Bruker AVANCE 5OO (one-bay; 500 MHz) at 293 K. For the competitive alcohol adsorption study, 100 mg of MIL-88A(Fe), 1.5 mL of deuterated water and 3.7×10^{-4} mol of each alcohol were placed in a vial (0.23 M of each alcohol). The samples were left under continuous rotation for 24 h at room temperature (25 ℃). The samples were filtered to separate the solid from the solution. To an aliquot of 650 µL of the supernatant 30 µL of sodium acetate deuterated water solution (0.45 g/L) were added. The same procedure was applied for each adsorbate but without adding the porous material (named as blank) in order to set the initial adsorbate amount in the adsorption experiment. The characteristic signals of the adsorbate and the sodium acetate obtained from ^{1}H-NMR measurement were employed to quantify the amount remaining in solution after 24 h of adsorption taking into account the difference with the blank. The same procedure was followed to quantify the alcohol adsorption in membranes. In this case, 12 mg of membrane were placed in a 0.1 wt% aqueous solution of methanol or ethanol and the same procedure as for the competitive adsorption studies on powder adsorbent was employed. Thermogravimetric analysis (TGA) was performed in a METTLER TOLEDO TGA/SDTA851 thermal analyser, under dynamic synthetic air atmosphere with a flow rate of 50 mL/min. The sample was heated at 5 °C/min in the temperature range 30–800 °C. Contact angle was determined using an Ossila L2004A1-UK optical system to study the hydrophobicity of the 0, 10, 20 and 30 wt% PVDF@MIL-88A(Fe) membranes.

4.3 RESULTS

4.3.1 Alcohols sorption from aqueous media

As mentioned in the introduction, the crystal structure of MIL-88A(Fe) can switch between open and closed forms (Figure 4.2a-d). The PXRD pattern of the as-synthetized micron-size rod-like shape samples revealed an intermediate state between the open and close forms (Figure 4.2e and 4.2f). This intermediate state was previously observed by Troyano *et al.*[69] when MIL-88A(Fe) was exposed to different humidity atmospheric conditions. In this study, the sorption experiments were performed in aqueous media and thus, the as-synthesized MIL-88A(Fe) sample transits to the open form configuration. Therefore, the results obtained in all the adsorption experiments must be understood regarding pore dimensions and connectivity of the open form.
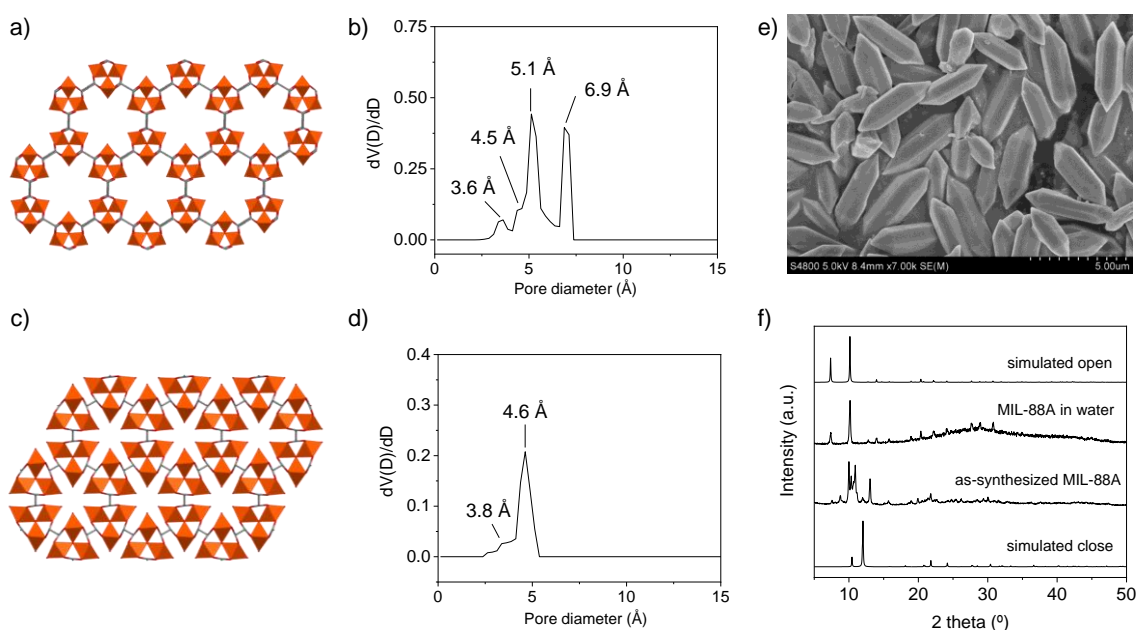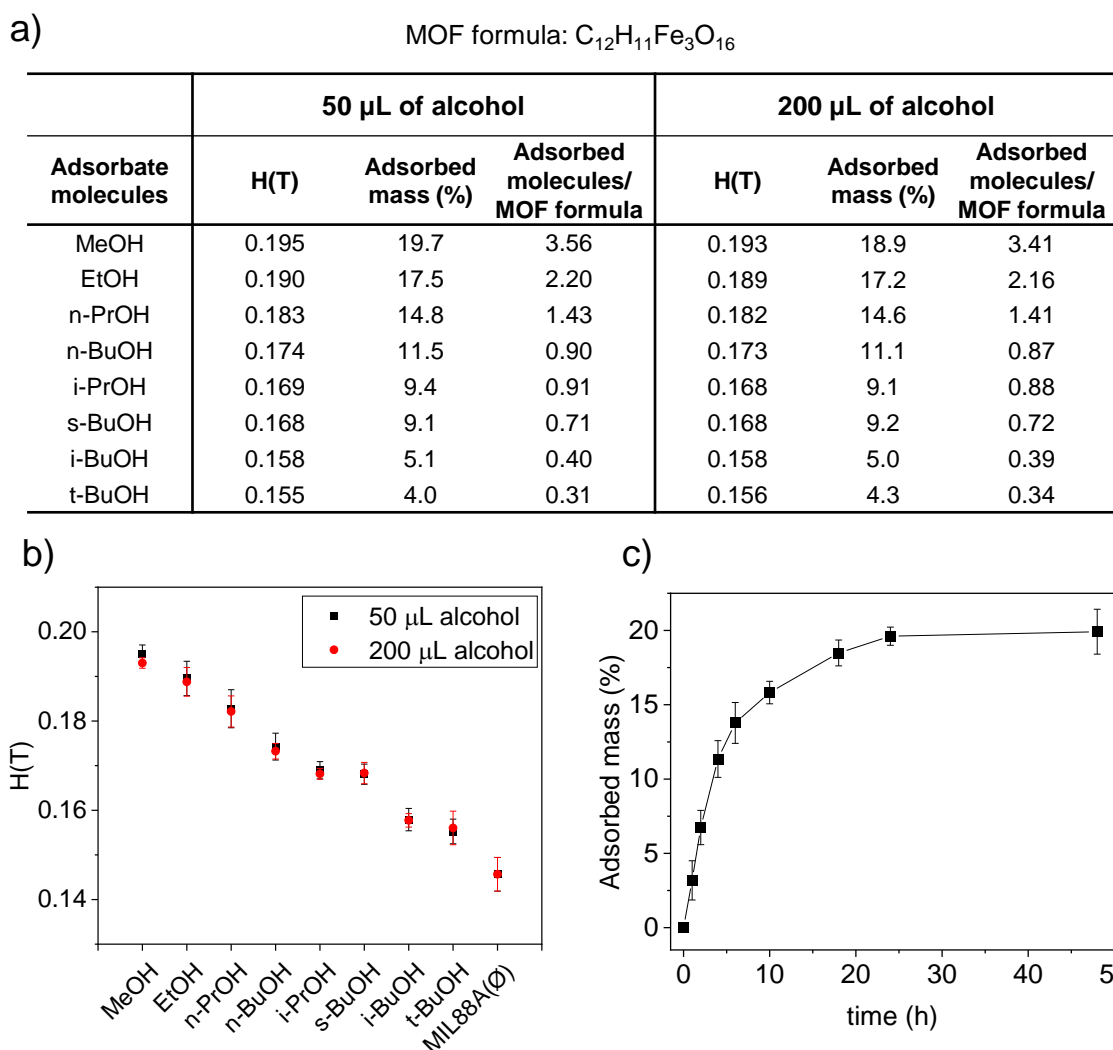

Figure 4.2. Schematic representation of the a) open and b) close forms of MIL-88A(Fe) viewed along c axis. Pore size distribution of the c) open and d) close forms computed using *Poreblaze 4.0*. e) FESEM images of as-synthesized MIL-88A(Fe). f) PXRD patterns of the as-synthesized dry and soaked in water sample and simulated open and close forms.

The quantification of the captured alcohols from aqueous media was performed using the Magnetic Sustentation technique[70] developed in *Chapter 3*. The critical magnetic field of paramagnetic MIL-88A(Fe) before and after the adsorption of the short chain alcohols (methanol, ethanol, n- and *isopropyl alcohol*, n-, sec-, iso- and *tert*-butyl alcohol) in water was determined (Figure 4.3). Briefly, MIL-88A(Fe) particles were dropped in a test tube located between the two poles of an electromagnet and subjected to its maximum magnetic field. The paramagnetic particles were attached to the walls of the test tube in the lower part of the electromagnet pole, where the magnetic force is maximum. Afterwards, the generated magnetic field is progressively reduced until the particles are detached. The magnetic field value at this point is denoted as the critical magnetic field.

The alcohol sorption experiments were performed placing MIL-88A(Fe) in an aqueous solution containing 50 µL of the corresponding alcohol. The resulting suspension was kept under agitation for 24 h. Later, MIL-88A(Fe) microcrystals were recovered by centrifugation and the captured amount of alcohol was quantified. The critical magnetic field of MIL-88A(Fe) before alcohol adsorption was labelled as Ø. As observed in Figure 4.3a, the critical magnetic field of MIL-88A(Fe) after adsorption of short chain alcohols increased comparing to the pristine MOF(Ø); the bigger the deviation from the pristine material the higher the mass percentage incorporated in the MOF suggesting that MIL-88A(Fe) can efficiently capture alcohols from water. The extrapolated adsorption values are represented in Figure 4.3b (the calibration curve can be seen in *Chapter 3*). As expected the smaller the adsorbate molecules the greater the adsorption showing the highest value for methanol (3.56 molecules per MOF formula) and the lowest for *tert*-butyl alcohol (0.31 molecules per MOF formula).

In addition, the adsorption experiments were repeated and quantified using 200 µL of the alcohols. The results indicated no significant differences in the adsorption values, suggesting that MIL-88A(Fe) was already saturated at 50 µL. Furthermore, a kinetic adsorption study was also completed for MeOH to ensure that the established 24 h for the adsorption procedure is enough for the system to have achieved the equilibrium state (Figure 4.3c).

a)

MOF formula: $C_{12}H_{11}Fe_3O_{16}$

| Adsorbate molecules	50 µL of alcohol			200 µL of alcohol		
	H(T)	Adsorbed mass (%)	Adsorbed molecules/ MOF formula	H(T)	Adsorbed mass (%)	Adsorbed molecules/ MOF formula
MeOH	0.195	19.7	3.56	0.193	18.9	3.41
EtOH	0.190	17.5	2.20	0.189	17.2	2.16
n-PrOH	0.183	14.8	1.43	0.182	14.6	1.41
n-BuOH	0.174	11.5	0.90	0.173	11.1	0.87
i-PrOH	0.169	9.4	0.91	0.168	9.1	0.88
s-BuOH	0.168	9.1	0.71	0.168	9.2	0.72
i-BuOH	0.158	5.1	0.40	0.158	5.0	0.39
t-BuOH	0.155	4.0	0.31	0.156	4.3	0.34

b)

c)

Figure 4.3. a) Quantification of the adsorbed alcohols: critical magnetic field, H(T), adsorbed mass (%) and adsorbed molecules per formula of MOF. b) Critical magnetic field of MIL-88A(Fe) after adsorption of alcohols (50 µl: ■, 200 µl: ●) determined by Magnetic Sustentation experiments. c) Kinetic of the adsorption of methanol.

This is indicative of the fact that the obtained values should reflect the complementarity between the shapes of the adsorbate molecules and the voids in the open form of MIL-88A(Fe). In this sense, we have performed a computational characterization, using the Materials Studio suite platform. The configuration for each alcohol was optimized to provide the less sterically hindered conformation (Figure 4.4a). The molecular volume and cross section of the alcohols on these optimized conformations were calculated using a 1.2 Å molecular probe. The same molecular probe was employed to characterize the big cavity and connecting windows dimensions. The pore system within the open form of MIL-88A(Fe) is composed of
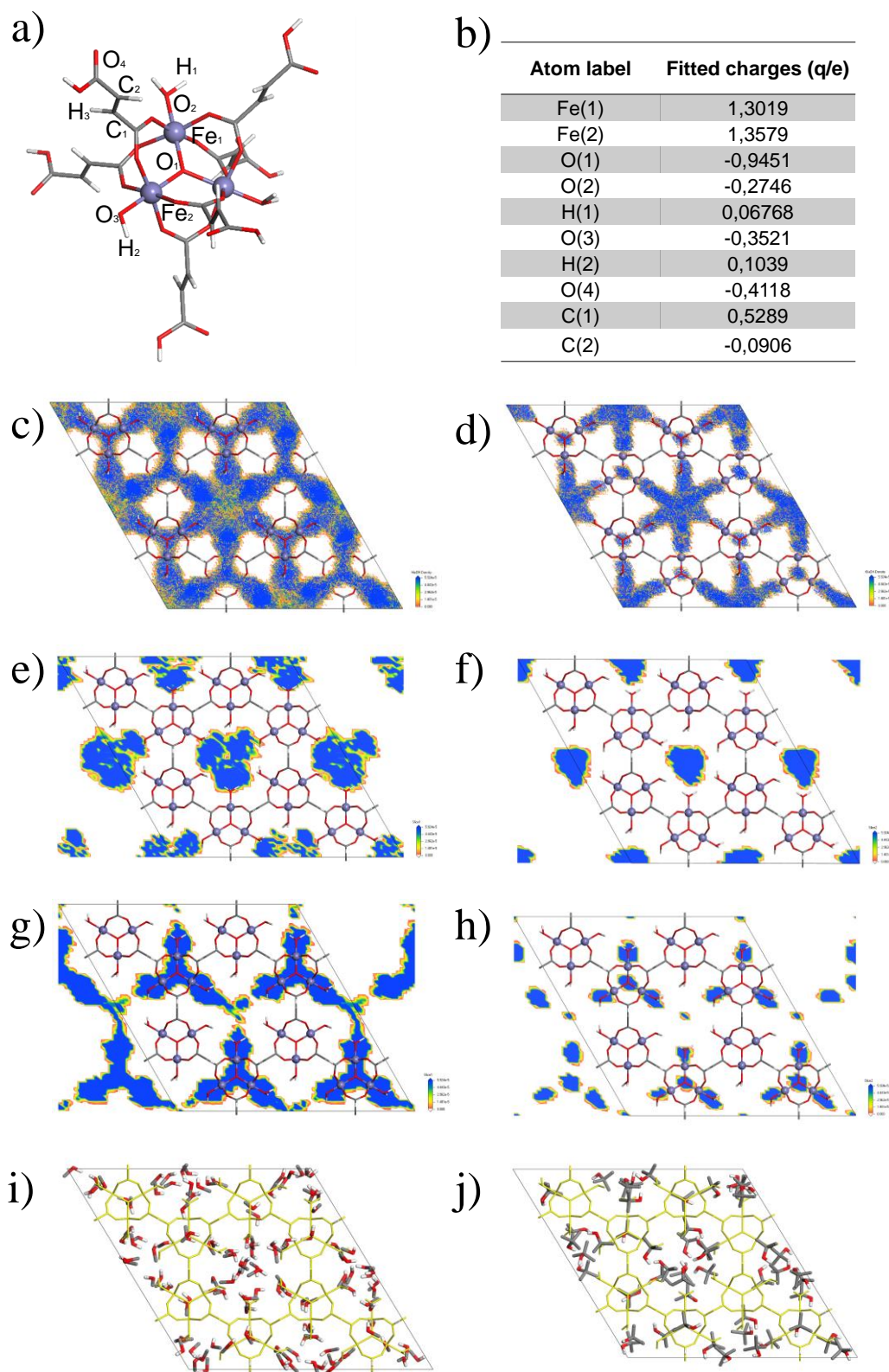
two big cavities around 6.9 and 5.1 Å connected by slightly narrower windows (diameter: 4.4 and 3.6 Å) to generate an interconnected 3D channel system. In a rigid crystal structure, the diffusion-limiting factor should be the cross sections of these windows. Nonetheless, the flexible nature of the crystal structure of MIL-88A(Fe) allows the diffusion of alcohol molecules with slightly greater cross-sections, as happened for linear alcohols. However, this structural flexibility is limited and above certain cross-section values, the diffusion of the alcohol molecules is hindered resulting in significantly lower adsorption values. The latter is the case of the branched alcohols. In Figures 4.4b and 4.4c, the adsorption values are plotted against the calculated molecular volume and cross section, respectively. A linear tendency can be observed between the captured mass and molecular volume of linear alcohols (methanol, ethanol, n-propanol and n-butyl alcohol), which can be attributed to a more efficient occupation of the voids by smaller molecules. On the contrary, the adsorbed mass of branched alcohols (isopropyl alcohol, sec-butanol, isobutyl alcohol and *tert*-butyl alcohol) shows a linear dependence with respect to the cross-section, which in this case is the limiting factor as the diffusion of the molecules seems to play a crucial role. Although the molecular volumes of isopropyl alcohol and sec-butyl alcohol are significantly different, they have similar cross sections, which results in similar adsorption values. In addition, the similar cross-section for iso- and *tert*-butyl alcohols give rise to similar adsorption values. Overall, it can be concluded that the molecular volume of the alcohols is the key factor determining the adsorption of linear alcohols (relatively small cross-section), while for branched alcohols, where bigger cross-sections are shown, this latter parameter becomes the dominant one.

a)

b)

c)
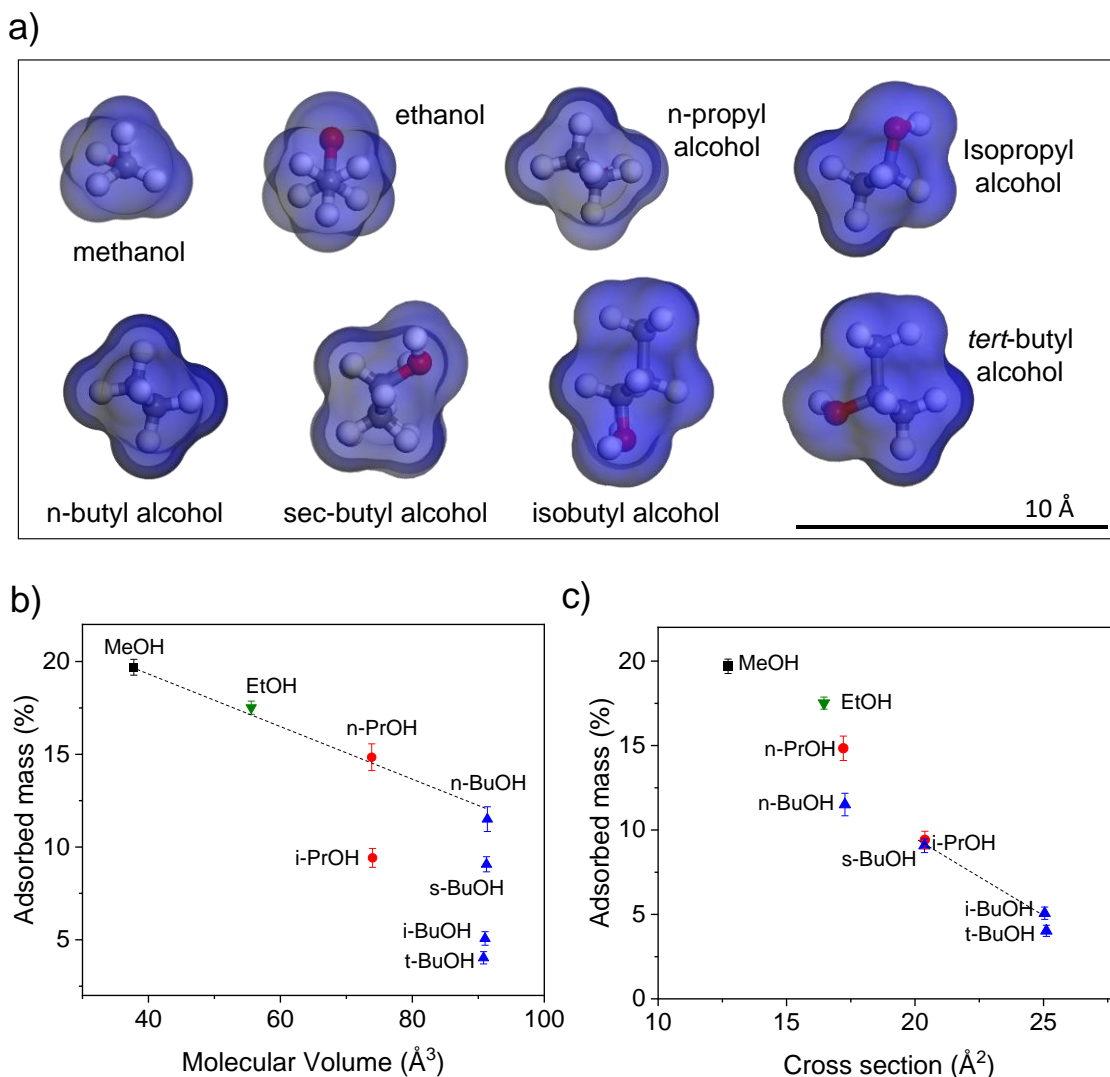
Figure 4.4. a) Optimised configuration of the alcohols drawn with "Materials Studio Suite. Adsorbed mass (%) for each alcohol plotted against b) molecular volumes and c) cross sections.

In order to provide more evidence to support this explanation, further computational studies were carried out. The pore structure was analysed by GCMC calculations (Figure 4.5a and 4.5b) using methanol and *tert*-butyl alcohol as molecular probes. Figure 4.5c-h showed the probability density maps probed by a single-molecule (*i.e.* fixed loading calculations) in a 2x2x2 supercell of the open form of MIL-88A(Fe) computed at 298 K. Methanol molecule shows percolation along the entire three-dimensional pore network. Despite *tert*-butyl alcohol can also fit into the bigger cavities of the open form structure, it shows occupational discontinuities in the vicinity of the windows that create the above explained diffusional problem of the branched alcohols. On the other hand, the calculations performed at fixed pressure

(100 kPa at 298 K) led to loadings of 130 methanol molecules and 49 *tert*-butyl alcohol molecules per supercell, which correspond to approximately 8 methanol molecules and 3 *tert*-butyl alcohol molecules per formula. These values are higher than the experimental ones (3.5 and 0.3 molecules of methanol and *tert*-butyl alcohol, respectively). In the case of methanol, this discrepancy can be attributed to the fact that the experimental adsorption experiment involves a competition between water and alcohol molecules to occupy the pores of the compound. In the experimental, this competition reaches the equilibrium, in which probably a mixture of water and alcohol molecules occupies the pores. However, for the computational studies only the occupation of the voids by alcohol molecules is considered. As consequence, a greater adsorption capacity is computed comparing to the experimental results. Regarding *tert*-butyl alcohol, the difference between the experimental and theoretical calculations relies on diffusion. Briefly, the employed GCMC simulations place the alcohol molecules directly inside the voids without requiring them to diffuse from the outside of the crystal structure. Therefore, the reduced adsorption of *tert*-butyl alcohol obtained from the experimental results must be understood as a probe of the presence of a diffusion problem and not due to an absence of big enough pores that could fit *tert*-butyl alcohol. Finally, Figure 4.5i and 4.5j shows a low energy distribution of guest alcohol molecules at MIL-88A(Fe), where both alcohols show similar adsorption preferential sites. On the whole, it can be concluded that even if similar preferential adsorption sites are observed for both molecules, the flexibility of the structure is what limits the diffusion and thus, the loading of *tert*-butyl alcohol.

a)

b)

Atom label	Fitted charges (q/e)
Fe(1)	1,3019
Fe(2)	1,3579
O(1)	-0,9451
O(2)	-0,2746
H(1)	0,06768
O(3)	-0,3521
H(2)	0,1039
O(4)	-0,4118
C(1)	0,5289
C(2)	-0,0906

c)

d)

e)

f)

g)

h)

i)

j)

Figure 4.5. a) MOF fragment used for the DFT calculations and b) resulting ESP-fitted charges (q/e) upon the atoms of the structure models of the adsorbents. Fixed loading calculations (1 molecule per cell at 298 K) for methanol (left) and *tert*-butyl alcohol (right): probability density distribution and its projection: c,d) for plane (001), e,f) at z = 0.5 and g, h) z = 0.375. Lowest energy frames for fixed pressure calculation (100 kPa at 298 K) for i) methanol and j) *tert*-butyl alcohol.

The MIL-88A(Fe) samples resulting from the adsorption experiments were further characterized by PXRD while they were still wet, which to the best of our knowledge it was not previously studied. The wet samples were subjected to a series of consecutive scans with an interval of 10 min in order to observe the evolution of their PXRD patterns upon the release of the adsorbed alcohol molecules (Figure 4.6). In all cases, the initial diffractogram show the amorphous contribution of water wetting the solid particles, together with the typical diffraction peaks of the open form of MIL-88A(Fe). Over time, the amorphous contribution decreases in agreement with the expected evaporation of the solvent (water). Finally, after the drying of the sample (water evaporation) and the release of the captured alcohols molecules, the diffractogram evolve to the initial intermediate structure of MIL-88A(Fe).
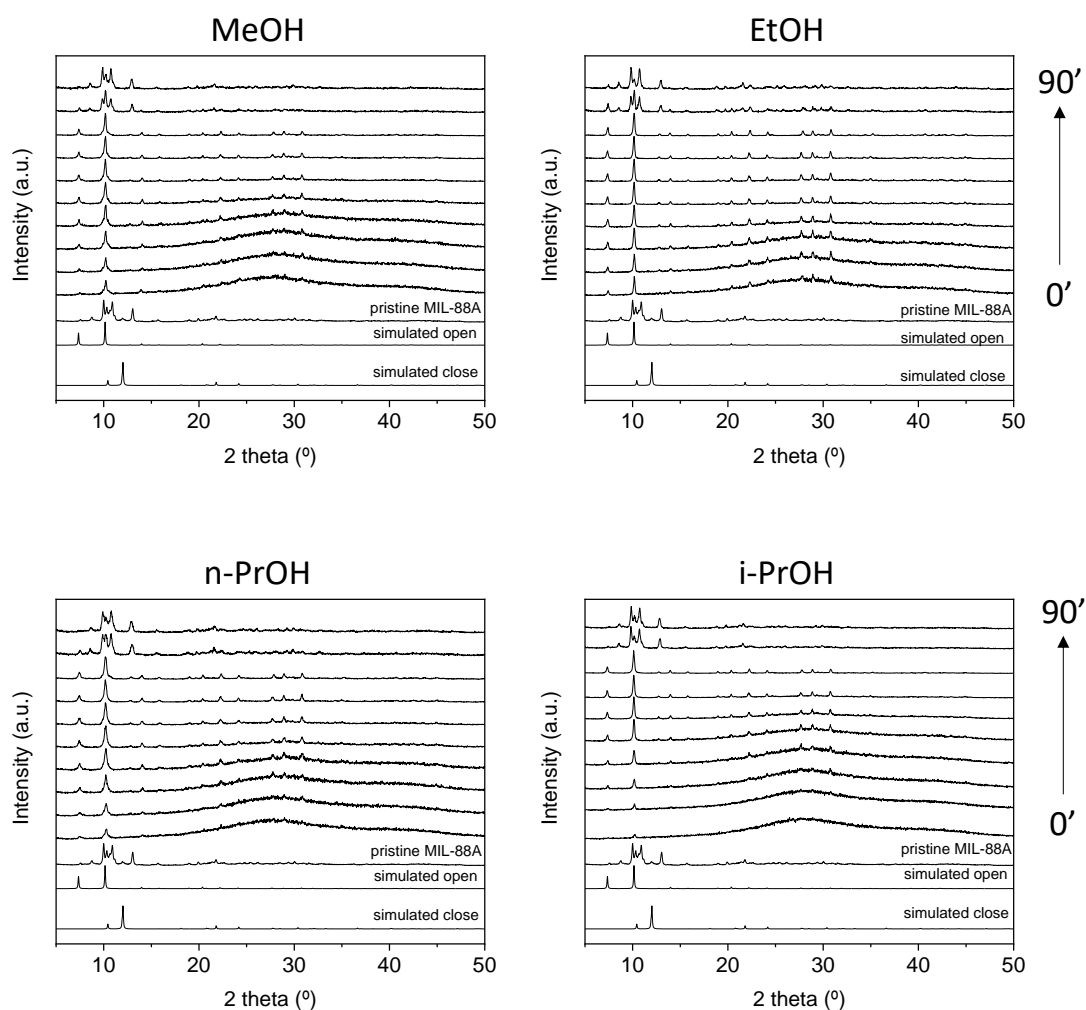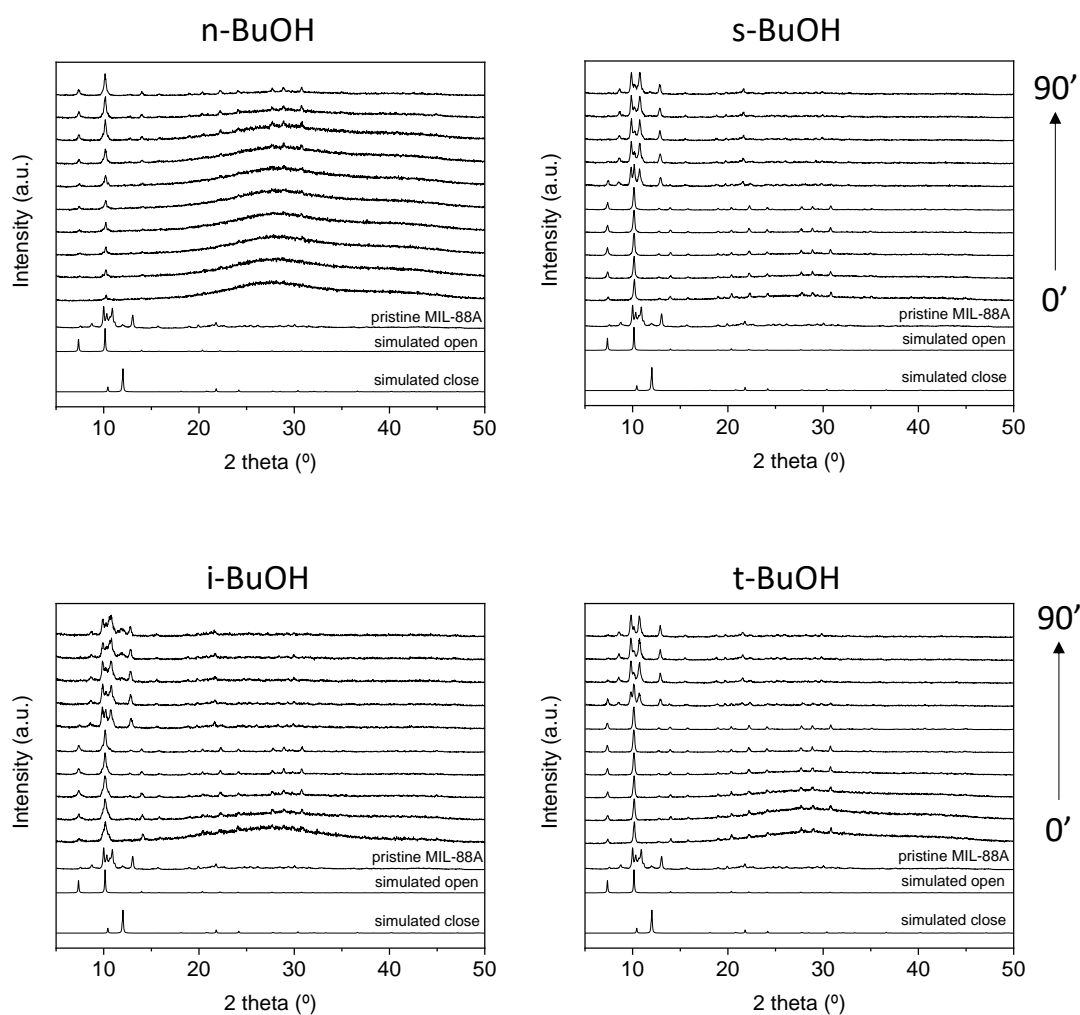
Figure 4.6. PXRD scans showing the evolution of wet MIL-88A(Fe) after 24 h of immersion in aqueous solutions of different alcohols with an interval of 10 minutes between each.

The recyclability and stability of MIL-88A(Fe) were studied measuring the adsorption capacity of the material up to four cycles, where the alcohol molecules were desorbed in between the cycles under high vacuum. Overall, it can be concluded that there is no significant change on its adsorption capacity. PXRD and ATR FT-IR measurements were performed after the first and last cycle to ensure the structural and chemical stability of MIL-88A(Fe), showing no significant change (Figure 4.7).
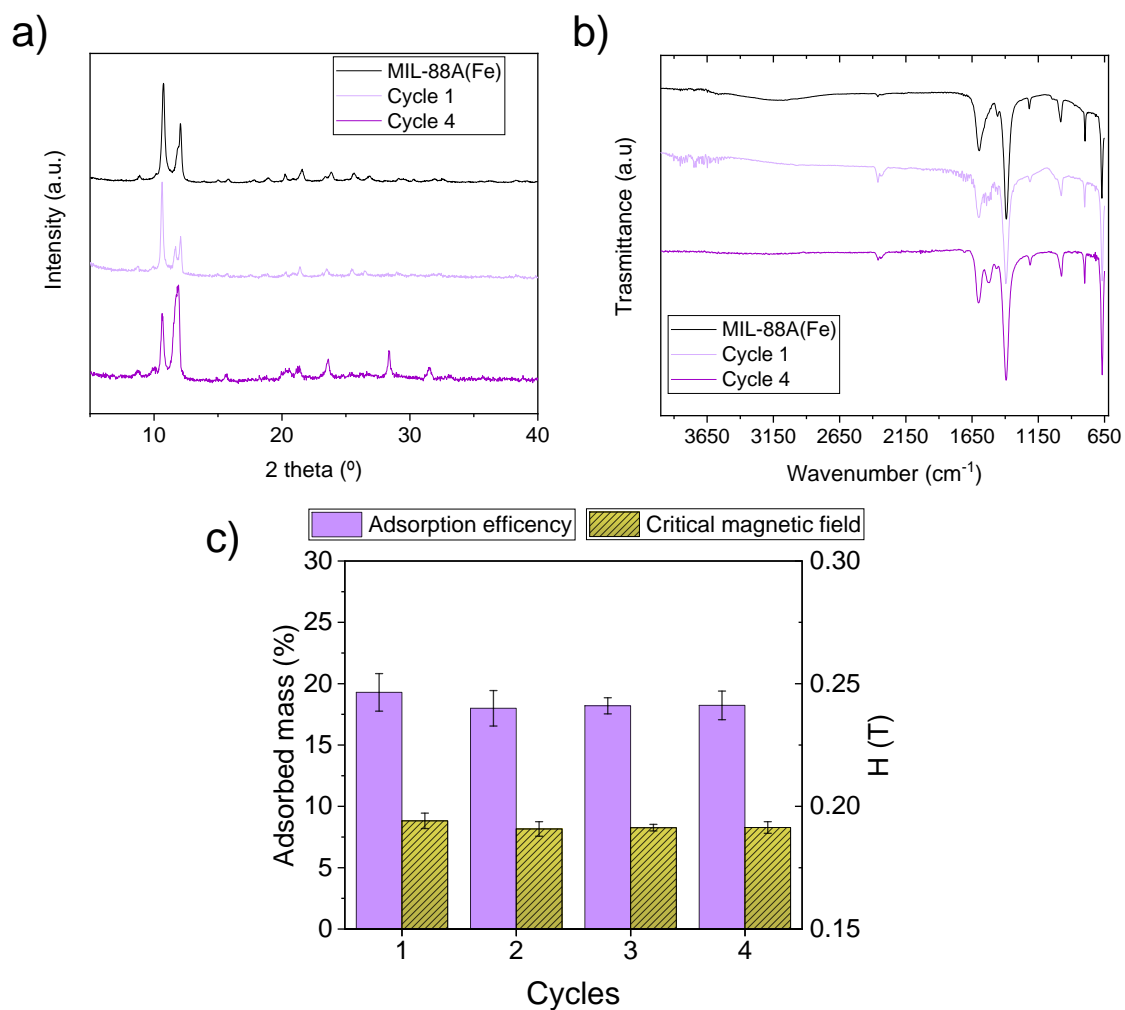
Figure 4.7. a) PXRD and b) FT-IR measurements of the pristine MIL-88A(Fe) and after the first and the fourth cycle. c) Recyclability of the material determined with the Magnetic Sustentation technique. Each measurement was repeated five times in order to provide the corresponding associated statistical error.

4.3.2 Competitive adsorption studies

Simultaneous and consecutive adsorption studies were performed to further study the behavior of MIL-88A(Fe) (Figure 4.8).
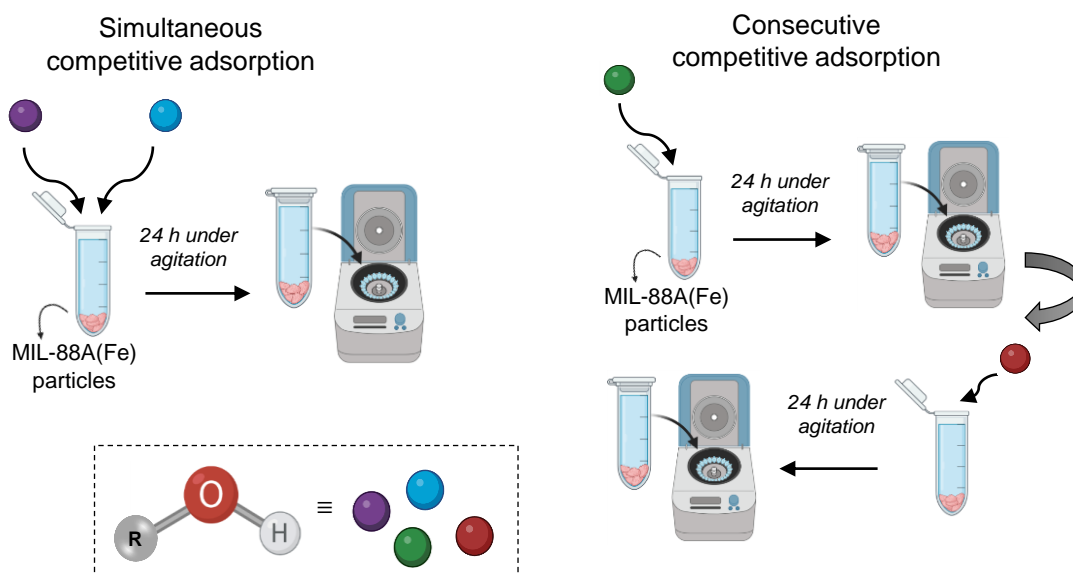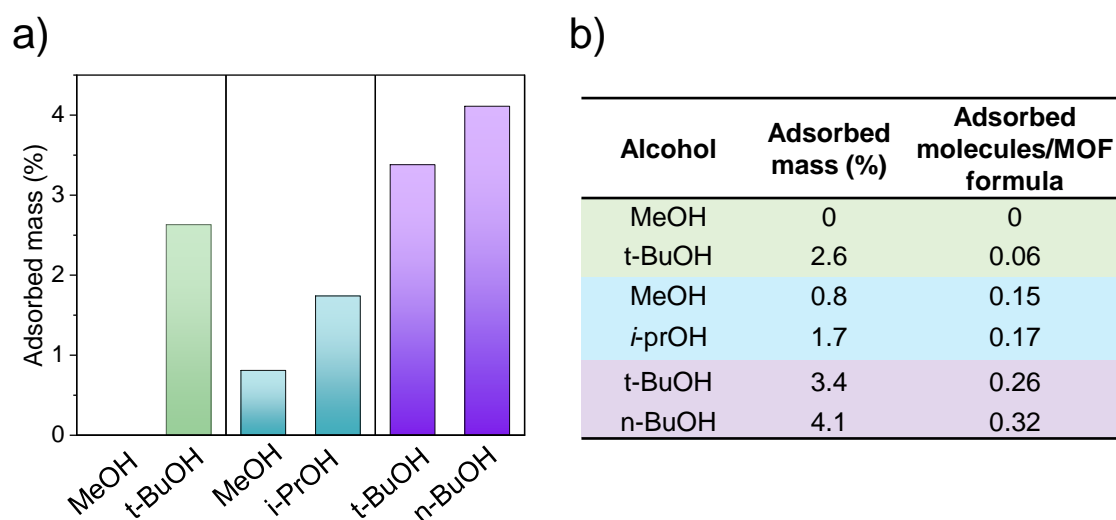

Figure 4.8. Schematic representation of the simultaneous and consecutive competitive adsorption.

Selectivity studies were performed to study the affinity of MIL-88A(Fe) towards different alcohols. Three different mixtures were prepared containing an equimolar amount of each alcohol: (A) combination of the two most diverse alcohols (methanol/*tert*-butyl alcohol), (B) combination of the two widely employed alcohols (methanol/isopropyl alcohol) and (C) combination of the linear and branched alcohols with the same number of carbons (n-butyl alcohol/*tert*-butyl alcohol). ^{1}H-NMR was used to quantify the remaining amount of alcohol in solution after 24 h of adsorption. The amount of alcohol in solution was reduced from the employed in the Magnetic Sustentation experiments in order to ensure that the variation of the alcohol in the remaining liquid could be reliably quantified by ^{1}H-NMR (see section 4.2.1). This fact also explains the relatively lower adsorption values obtained in these latter experiments. The obtained values from the competitive adsorption experiments are depicted in Figure 4.9.

The results of the competitive studies indicate that the adsorption preference is directed by the hydrophobicity of the alcohol and not by size or shape factor as

observed from the single alcohol adsorption experiments. Although methanol showed the highest adsorption in the single adsorbate experiments, there is a clear preference for more hydrophobic molecules, *tert*-butyl alcohol and isopropyl alcohol. In addition to that, the amount of captured *tert*-butyl alcohol is very modest, in agreement with the results from the single alcohol experiments, which implies that there is still a lot of free space in the pore system of the open form of MIL-88A(Fe) that apparently are not further accessible after the incorporation of *tert*-butyl alcohol molecules. The explanation for this phenomenon relies again on the diffusional problems of *tert*-butyl alcohol (and to a lower extent, isopropyl alcohol) within the pore system of MIL-88A(Fe). The diffusion problems do not only affect the adsorption values of *tert-butyl alcohol*, which are quite modest, but also the adsorption of any other molecules that have to deal with increasing diffusion difficulties arising from those branched alcohol molecules clogging the pore system. Moreover, it also implies that the more hydrophobic molecules are the first ones coming out from the aqueous solution to start interacting with the MIL-88A(Fe) particles. Finally, n-butyl alcohol and *tert*-butyl alcohol isomers, with similar affinity towards MIL-88A(Fe), have similar adsorption values as both alcohols compete in relatively equal terms.

a)

b)

Alcohol	Adsorbed mass (%)	Adsorbed molecules/MOF formula
MeOH	0	0
t-BuOH	2.6	0.06
MeOH	0.8	0.15
i-prOH	1.7	0.17
t-BuOH	3.4	0.26
n-BuOH	4.1	0.32

Figure 4.9. Competitive adsorption studies for MIL-88A(Fe): a) adsorbed mass (%) of alcohols and b) values of the adsorbed mass (%) and adsorbed molecules per formula of MOF in equimolar mixtures (A (methanol/*tert*-butyl alcohol), B (methanol/isopropyl alcohol) and C (*tert*-butyl alcohol/n-butyl alcohol)).

In order to get further insight into this clogging phenomenon that the branched alcohols seem to create, a series of additional adsorption experiments were designed in which two 24 h consecutive single alcohol adsorption experiments were performed alternating between branched (t-BuOH and s-BuOH) and small linear alcohols (MeOH and EtOH). The results showed a striking difference depending on the order of the addition of alcohols (Figure 4.10). The high adsorption values observed in the single alcohol adsorption experiments for MeOH and EtOH showed a slight increase when the branched alcohols are added in the second step. However, the very modest adsorption values of the branched alcohols are retained even after the exposure to the short chain alcohols in the second step. This behavior can also be attributed to the clogging of the pore system of MIL-88(Fe) caused by the branched alcohols, which hinders the adsorption of MeOH or EtOH leading to a far smaller amount incorporated in the framework.

Another feature that seems to agree with the hypothesis of pores clogging is that the small increase observed after the second addition follows the expected order. The overall increase after the second step is higher when, in the first step, the less hindering s-BuOH is employed over t-BuOH. On the other hand, the increase after the second addition is in both cases higher for the smaller MeOH than for the bigger EtOH.
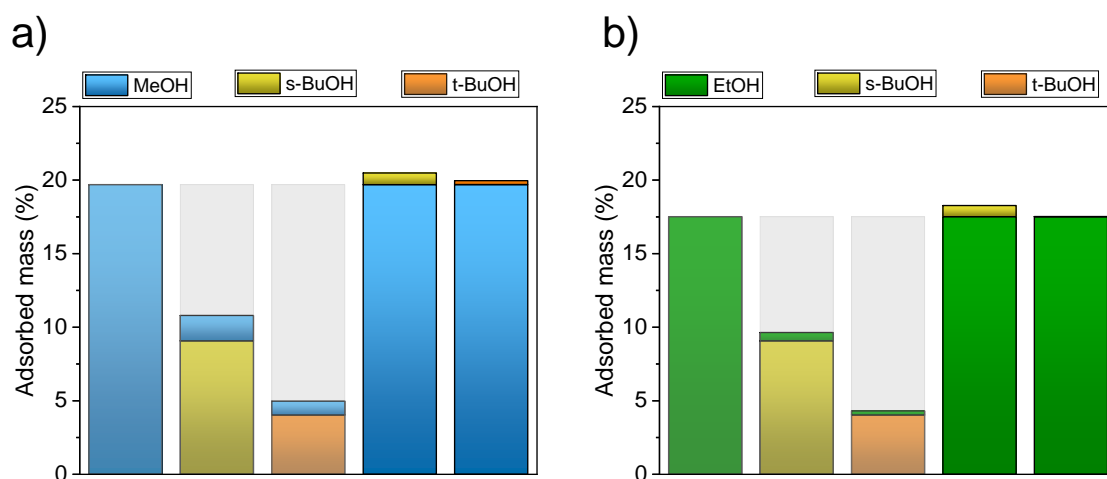
Figure 4.10. Consecutive adsorption studies for MIL-88A(Fe): a) methanol, branched alcohols + methanol and methanol + branched alcohols and b) ethanol, branched alcohols + ethanol and ethanol + branched alcohols.

Moreover, the hypothesis of the clogging effect was validated determining the kinetic desorption curves of linear (MeOH) and branched alcohol (t-BuOH), together with the consecutively adsorbed alcohols, where the linear alcohol was adsorbed first (MeOH+t-BuOH). To confirm the diffusional problem generated by t-BuOH, a significant decrease on the desorption rate of MeOH+t-BuOH should be observed compared to the desorption rate of MeOH. In other words, the clogging effect should hinder both the incorporation (as proved before) and the release. Figure 4.11, shows the desorption curves, in which the above predicted behaviour is clearly observed. In addition to that, the desorption rate of MeOH+t-BuOH samples during the first 4 hours of the experiments shows a similar behaviour to t-BuOH, indicating that the branched alcohols is the determining factor dictating the slower release due to the clogging.
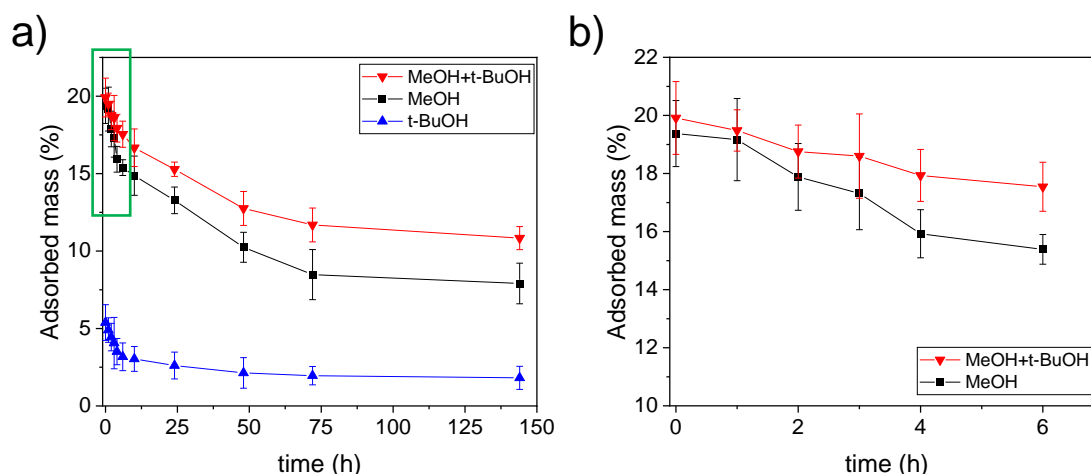

Figure 4.11. Desorption kinetic for t-BuOH (▲), MeOH (■) and consecutive MeOH+t-BuOH (▼): a) complete desorption curve and b) zoom of the desorption curve in the range 0-6 h.

4.3.3   PVDF@MIL-88A(Fe) composite membranes

Generally, MOFs are obtained as fine powder, which limits their practical applications. In order to overcome the main disadvantages mentioned before, the use of MOFs as fillers in polymeric mixed matrix membranes have been proposed[48,50]. Therefore, to overcome one of the limiting factors of MOF powders in practical applications, *i.e.* the processability, the use of MIL-88A(Fe) as filler in a polymeric matrix was explored. PVDF@MIL-88A(Fe) composite membranes with different MOF loadings (0, 10, 20, 30 wt%) were prepared according to the procedure described in the experimental section.

SEM images (surface and cross-section) of the membranes confirm that MIL-88A(Fe) microcrystals were homogeneously dispersed within the porous PVDF matrix without any sign of agglomeration (Figure 4.12). The dimensions of the macropores within the polymeric matrix changed with the loaded amount of MIL-88A(Fe) showing an average pore size of 0.49 ± 0.11 μm, 0.96 ± 0.39 μm, 1.51 ± 0.47 μm, and 0.51 ± 0.26 μm, for the 0, 10, 20 and 30 wt% MOF-loaded membranes, respectively. Higher content of MOF in the PVDF membranes up to a 20 wt% increased the size of the pores, except for the 30 wt% MOF-loaded membrane, whose pores are comparable to those of the 0 wt% membrane.
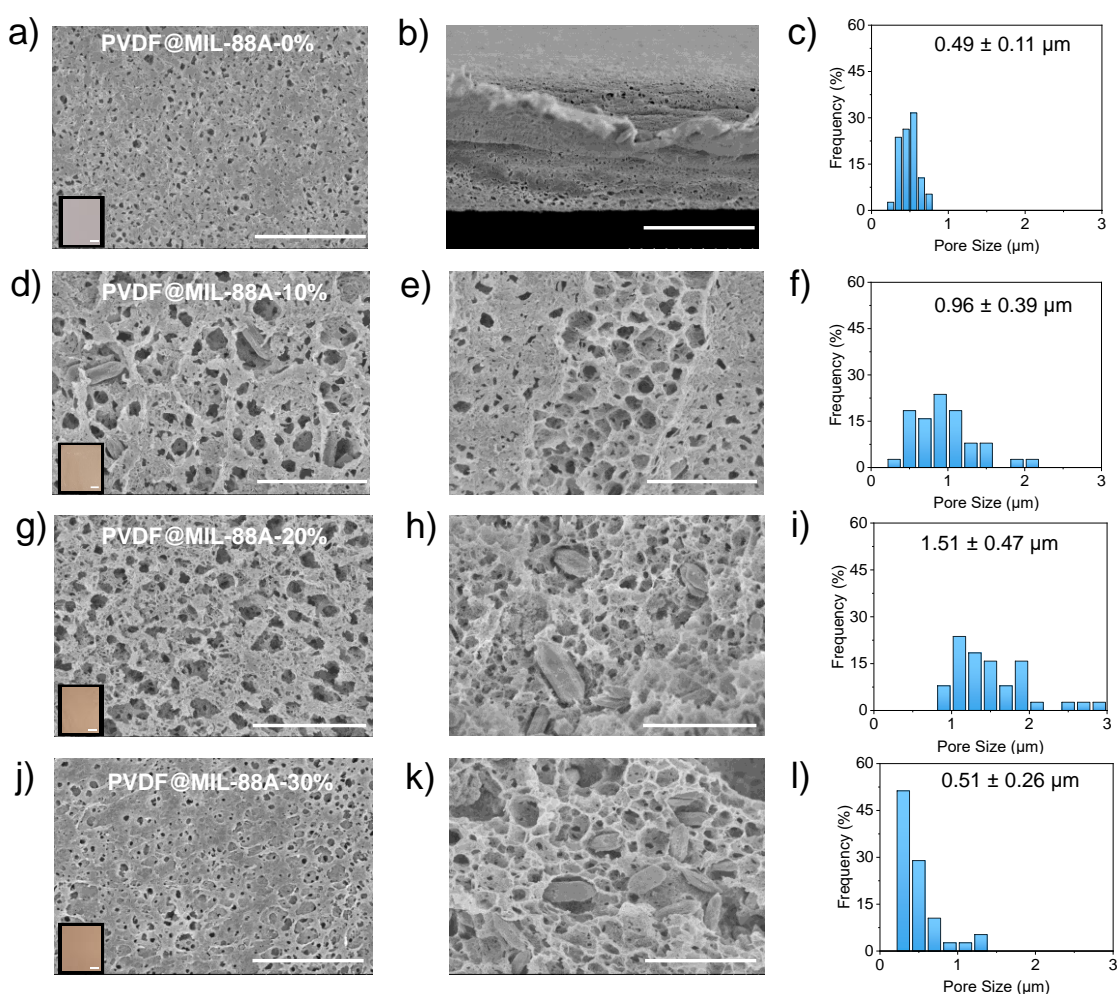

Figure 4.12. SEM images (scale bar: 10 μm) for pore size and morphology characterization of PVDF@MIL-88A(Fe) membranes and captured images (inset figure, scale bar: 1 cm) with different MOF loadings: a, d, g, j) surface, b, e, h, k) cross section and c, f, i, l) pore-size distribution and average pore size of 0, 10, 20 and 30wt% MOF-loaded membranes, respectively.

In addition, PXRD patterns of the membranes also confirm the successful incorporation of MIL-88A(Fe) into the matrix as no significant changes were appreciated between the different MOF loadings (Figure 4.13a). The membranes were further characterized by thermogravimetric and contact angle analyses (Figures 4.13b and 4.13c). TGA measurements of the membranes show the expected mass loss around 215 ℃ corresponding to MIL-88A(Fe) and a more pronounced mass loss around 315 ℃ corresponding to PVDF. The latter appears at a lower temperature compared to the pure PVDF (370 ℃), which can be attributed to the increased porosity of the MOF-incorporated membranes. This trend has also been previously reported for other PVDF composites[60,71,72]. The mass percentage of the residue at 800 ℃, corresponding to Fe_2O_3 (PDF 89-0597), was employed to confirm the MOF content in the membrane. Furthermore, contact angle measurements showed that the hydrophilic nature of the PVDF membranes is decreased after the incorporation of MIL-88A(Fe), which is in agreement with the greater preference towards the more hydrophobic alcohols observed in the competitive adsorption studies.

The methanol and ethanol adsorption performances of the PVDF@MIL-88A(Fe) membranes were analysed by ^{1}H-NMR spectroscopy. The experiments were performed using a very dilute aqueous solution (0.1 wt%) of both alcohols in order to study the removal capacity of low-concentration alcohols from water (Figures 4.13d and 4.13e). In both cases, the higher adsorption was observed for the 20 wt% MOF-loaded membrane: 17% and 12% for methanol and ethanol, respectively. This excellent performance of the 20 wt% membrane could be attributed to the intrinsic adsorptive properties of MIL-88A(Fe) as well as the higher porosity of the polymeric PVDF matrix that ensures better accessibility for the adsorbate molecules. The sharp decrease of the porosity in the polymeric matrix can be the reason for the poor adsorptive performance of the membrane with a 30 wt% of MOF. On the other hand, the results obtained for the 20 wt% loaded PVDF@MIL-88A(Fe) membrane clearly exceed the expected adsorption capacity based on the MIL-88A(Fe) adsorption results on single alcohols and the adsorption of the pure PVDF membrane. This fact is indicative of the synergetic contribution from both the MIL-88A(Fe) microcrystals

and PVDF matrix which in combination result in the higher porosity as well as the more hydrophobic nature of the membrane.
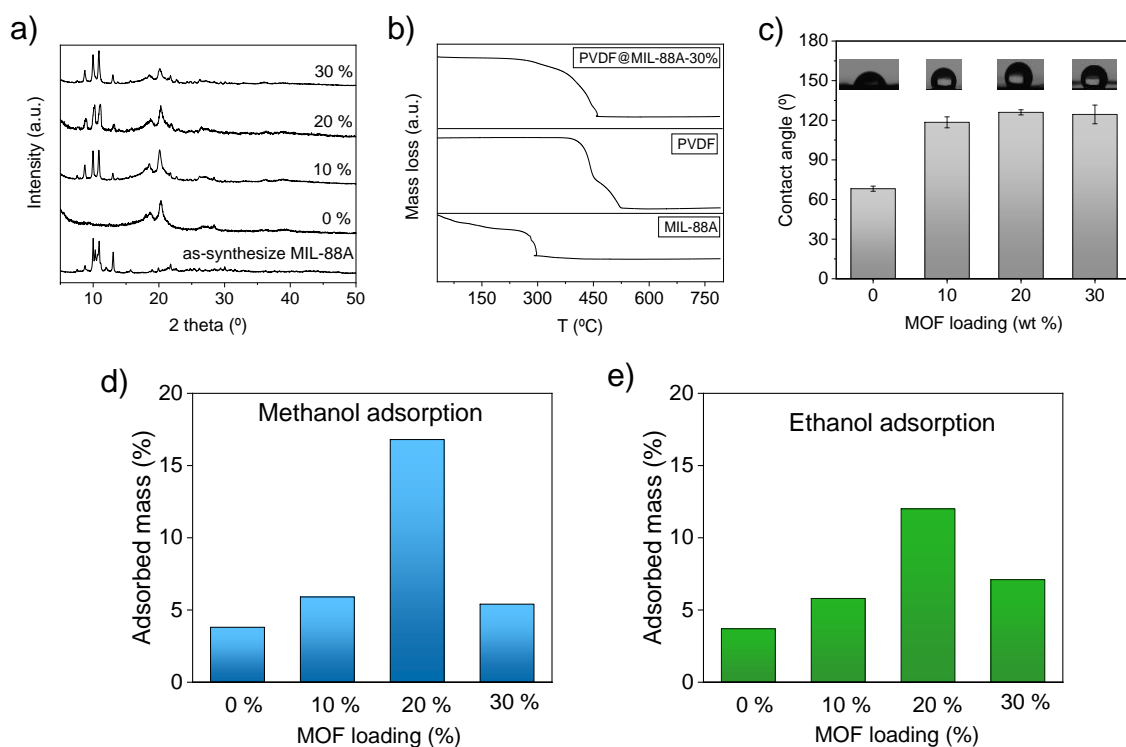
Figure 4.13. a) PXRD of MIL-88A(Fe) and prepared membranes, b) TGA analyses and c) contact angle measurements. Adsorption of alcohols from water in PVDF@ MIL-88A(Fe) membranes: d) methanol and e) ethanol.

4.4 CONCLUSIONS

In this work we have analysed how the flexible nature of the crystal structure of MIL-88A(Fe) impacts on its adsorptive performance for the recovery of alcohols from water. Taking advantage of the paramagnetic nature of MIL-88A(Fe), the Magnetic Sustentation technique described in the previous chapter was employed for the quantification of the captured alcohol mass. The results show the tendency for the linear alcohols, in which greater adsorption values are shown for the smaller alcohol molecule (methanol) due to a more efficient occupation of the void volume. However, this trend is not observed for the branched alcohols, where more modest adsorption values are shown. In this case, the adsorption is related to the cross-section (contrary to linear alcohols, where molecular volume is the limiting factor), suggesting an

adsorption phenomenon dominated by diffusional aspects. In fact, the computational analysis of the pore system in the open form of MIL-88A(Fe) revealed that although the windows connecting these cavities are narrow, the cavities are big enough to accommodate these branched alcohols. In addition, considering the cross-section of the adsorbate molecules, even the linear alcohols with the smaller cross-section would not be able to go through them if the crystal structure would be rigid. However, the flexible structure of MIL-88A(Fe) is able to overcome this apparent diffusional problem in the case of the linear alcohols but hardly for branched alcohols. These diffusional challenge also play a crucial role on the adsorption selectivity, as the hydrophobic nature of MIL-88A(Fe) favours a stronger interaction with the *tert*-butyl alcohol molecules on the outer surface of the adsorbent. These molecules start diffusing through the pore system of MIL-88A(Fe) but the mentioned diffusional problem leads to a clogging effect that hinders the entering of methanol molecules, a counterintuitive result based on the data coming from the single alcohol adsorption experiments but confirmed through consecutive single alcohol adsorption experiments.

Overall, MIL-88A(Fe) was strategically utilized in this work for selective alcohol recovery from water owing to its guest-induced breathing mediated structural adaptability. Furthermore, the sorption properties of MIL-88A(Fe) found to vary depending upon the nature of the sorbent solution, *i.e.* single-component or mixture alcohol solution. Such important findings are further supported by the theoretical and experimental studies revealing that the framework flexibility and diffusion play a key role in alcohol adsorption for MIL-88A(Fe). Furthermore, processability aspect of the power MOF materials has been addressed by preparing PVDF@MIL-88A(Fe) membranes. The synergistic effect of the polymeric matrix and the incorporated MIL-88A(Fe) microcrystals resulted in an increment in the adsorption capacity of the PVDF@MIL-88A(Fe) composite material comparing to the performance of each component, independently. We believe that the results acquired in this work can open new avenues toward rational designing and potential utilization of flexible MOF-based systems offering enhanced selectivity and sorption performance toward the challenging liquid-liquid separation. Such adaptive systems can be extremely crucial

and even a potential game changer towards designing of multipurpose standalone sorbent materials for size selective separation applications.

4.5 REFERENCES

(1) Al-Sabawi, M.; Chen, J.; Ng, S. *Energy Fuels* **2012**, 26, 5355–5372.

(2) Balat, M.; Balat, H.; Öz, C. *Prog. Energy Combust. Sci.* **2008**, 34, 551–573.

(3) Balat, M.; Balat, H. *Energy Convers. Manage*. **2008**, 49, 2727–2741.

(4) Xu, L.-H.; Li, S.-H.; Mao, H.; Li, Y.; Zhang, A.-S.; Wang, S.; Liu, W.-M.; Lv, J.; Wang, T.; Cai, W.-W.; Le Sang; Xie, W.-W.; Pei, C.; Li, Z.-Z.; Feng, Y.-N.; Zhao, Z.-P. *Science* **2022**, 378, 308–313.

(5) Shigematsu, A.; Yamada, T.; Kitagawa, H. *J. Am. Chem. Soc*. **2012**, 134, 13145–13147.

(6) Nalaparaju, A.; Zhao, X. S.; Jiang, J. W. *Energy Environ. Sci*. **2011**, 4, 2107.

(7) Huang, H.-J.; Ramaswamy, S.; Tschirner, U. W.; Ramarao, B. V. *Sep. Purif. Technol*. **2008**, 62, 1–21.

(8) Hill, J.; Nelson, E.; Tilman, D.; Polasky, S.; Tiffany, D. *PNAS* **2006**, 103, 11206–11210.

(9) Lee, S. C.; Oh, H. W.; Woo, H. C.; Kim, Y. H. *Biomass Conv. Bioref*. **2021**, 56, 289.

(10) Ma, Y. Q.; Ma, H. Z.; Zheng, L.; Yang, J.; Liu, Y. F.; Wang, Q. H. *Appl. Mech. Mater* **2013**, 448-453, 540–544.

(11) Mukherjee, S.; Sensharma, D.; Qazvini, O. T.; Dutta, S.; Macreadie, L. K.; Ghosh, S. K.; Babarao, R. *Coord. Chem. Rev.* **2021**, 437, 213852.

(12) Zhou, H.-L.; Lin, R.-B.; He, C.-T.; Zhang, Y.-B.; Feng, N.; Wang, Q.; Deng, F.; Zhang, J.-P.; Chen, X.-M. *Nat. Commun*. **2013**, 4, 2534.

(13) Blake, A. J.; Champness, N. R.; Hubberstey, P.; Li, W.; Withersby, M. A.; Schröder, M. *Coord. Chem. Rev.* **1999**, 183, 117–138.

(14) Mueller, U.; Schubert, M.; Teich, F.; Puetter, H.; Schierle-Arndt, K.; Pastré, J. J. *Mater. Chem.* **2006**, 16, 626–636.

(15) Safaei, M.; Foroughi, M. M.; Ebrahimpoor, N.; Jahani, S.; Omidi, A.; Khatami, M. *TrAC, Trends Anal. Chem.* **2019**, 118, 401–425.

(16) Moghadam, P. Z.; Li, A.; Wiggin, S. B.; Tao, A.; Maloney, A. G. P.; Wood, P. A.; Ward, S. C.; Fairen-Jimenez, D. *Chem. Mater.* **2017**, 29, 2618–2625.

(17) Zhou, H.-C. J.; Kitagawa, S. *Chem. Soc. Rev.* **2014**, 43, 5415–5418.

(18) Freund, R.; Lächelt, U.; Gruber, T.; Rühle, B.; Wuttke, S. *ACS nano* **2018**, 12, 2094–2105.

(19) Ahmadijokani, F.; Molavi, H.; Tajahmadi, S.; Rezakazemi, M.; Amini, M.; Kamkar, M.; Rojas, O. J.; Arjmand, M. *Coord. Chem. Rev.* **2022**, 464, 214562.

(20) Ji, Z.; Wang, H.; Canossa, S.; Wuttke, S.; Yaghi, O. M. *Adv. Funct. Mater.* **2020**, 30, 2000238.

(21) Freund, R.; Canossa, S.; Cohen, S. M.; Yan, W.; Deng, H.; Guillerm, V.; Eddaoudi, M.; Madden, D. G.; Fairen-Jimenez, D.; Lyu, H.; Macreadie, L. K.; Ji, Z.; Zhang, Y.; Wang, B.; Haase, F.; Wöll, C.; Zaremba, O.; Andreo, J.; Wuttke, S.; Diercks, C. S. *Angew. Chem. Int. Ed.* **2021**, 60, 23946–23974.

(22) Freund, R.; Zaremba, O.; Arnauts, G.; Ameloot, R.; Skorupskii, G.; Dincă, M.; Bavykina, A.; Gascon, J.; Ejsmont, A.; Goscianska, J.; Kalmutzki, M.; Lächelt, U.; Ploetz, E.; Diercks, C. S.; Wuttke, S. *Angew. Chem. Int. Ed.* **2021**, 60, 23975–24001.

(23) Czaja, A. U.; Trukhan, N.; Müller, U. *Chem. Soc. Rev.* **2009**, 38, 1284–1293.

(24) Virmani, E.; Beyer, O.; Lüning, U.; Ruschewitz, U.; Wuttke, S. *Mater. Chem. Front.* **2017**, 1, 1965–1974.

(25) Yot, P. G.; Ma, Q.; Haines, J.; Yang, Q.; Ghoufi, A.; Devic, T.; Serre, C.; Dmitriev, V.; Férey, G.; Zhong, C.; Maurin, G. *Chem. Sci.* **2012**, 3, 1100.

(26) Devic, T.; Horcajada, P.; Serre, C.; Salles, F.; Maurin, G.; Moulin, B.; Heurtaux, D.; Clet, G.; Vimont, A.; Grenèche, J.-M.; Le Ouay, B.; Moreau, F.; Magnier, E.; Filinchuk, Y.; Marrot, J.; Lavalley, J.-C.; Daturi, M.; Férey, G. *J. Am. Chem. Soc.* **2010**, 132, 1127–1136.

(27) Férey, G.; Serre, C. *Chem. Soc. Rev.* **2009**, 38, 1380–1399.

(28) Serre, C.; Millange, F.; Thouvenot, C.; Noguès, M.; Marsolier, G.; Louër, D.; Férey, G. *J. Am. Chem. Soc.* **2002**, 124, 13519–13526.

(29) Kitaura, R.; Fujimoto, K.; Noro, S.-i.; Kondo, M.; Kitagawa, S. *Angew. Chem. Int. Ed.* **2002**, 41, 133–135.

(30) Parent, L. R.; Pham, C. H.; Patterson, J. P.; Denny, M. S.; Cohen, S. M.; Gianneschi, N. C.; Paesani, F. *J. Am. Chem. Soc.* **2017**, 139, 13973–13976.

(31) Wang, Z.; Cohen, S. M. *J. Am. Chem. Soc.* **2009**, 131, 16675–16677.

(32) Zhang, J.-P.; Chen, X.-M. J. *Am. Chem. Soc.* **2008**, 130, 6010–6017.

(33) Salles, F.; Maurin, G.; Serre, C.; Llewellyn, P. L.; Knöfel, C.; Choi, H. J.; Filinchuk, Y.; Oliviero, L.; Vimont, A.; Long, J. R.; Férey, G. *J. Am. Chem. Soc.* **2010**, 132, 13782–13788.

(34) Cheng, X.-N.; Zhang, W.-X.; Lin, Y.-Y.; Zheng, Y.-Z.; Chen, X.-M. *Adv. Mater.* **2007**, 19, 1494–1498.

(35) Chang, Z.; Yang, D.-H.; Xu, J.; Hu, T.-L.; Bu, X.-H. *Adv. Mater.* **2015**, 27, 5432–5441.

(36) Seth, S.; Jhulki, S. Mater. Horiz. **2021**, 8, 700–727.

(37) Lee, J. H.; Jeoung, S.; Chung, Y. G.; Moon, H. R. *Coord. Chem. Rev.* **2019**, 389, 161–188.

(38) Hirschle, P.; Hirschle, C.; Böll, K.; Döblinger, M.; Höhn, M.; Tuffnell, J. M.; Ashling, C. W.; Keen, D. A.; Bennett, T. D.; Rädler, J. O.; Wagner, E.; Peller, M.; Lächelt, U.; Wuttke, S. *Chem. Mater.* **2020**, 32, 2253–2263.

(39) Chalati, T.; Horcajada, P.; Gref, R.; Couvreur, P.; Serre, C. *J. Mater. Chem*. **2011**, 21, 2220–2227.

(40) Horcajada, P.; Salles, F.; Wuttke, S.; Devic, T.; Heurtaux, D.; Maurin, G.; Vimont, A.; Daturi, M.; David, O.; Magnier, E.; Stock, N.; Filinchuk, Y.; Popov, D.; Riekel, C.; Férey, G.; Serre, C. *J. Am. Chem. Soc*. **2011**, 133, 17839–17847.

(41) Ramsahye, N. A.; Trung, T. K.; Scott, L.; Nouar, F.; Devic, T.; Horcajada, P.; Magnier, E.; David, O.; Serre, C.; Trens, P. *Chem. Mater*. **2013**, 25, 479–488.

(42) McKinlay, A. C.; Eubank, J. F.; Wuttke, S.; Xiao, B.; Wheatley, P. S.; Bazin, P.; Lavalley, J.-C.; Daturi, M.; Vimont, A.; Weireld, G. de; Horcajada, P.; Serre, C.; Morris, R. E. *Chem. Mater*. **2013**, 25, 1592–1599.

(43) Wu, H.; Ma, M.-D.; Gai, W.-Z.; Yang, H.; Zhou, J.-G.; Cheng, Z.; Xu, P.; Deng, Z.-Y. *Environ. Sci. Pollut. Res. Int*. **2018**, 25, 27196–27202.

(44) Zhang, Z.; Chen, Y.; Wang, Z.; Hu, C.; Ma, D.; Chen, W.; Ao, T. *Appl. Surf. Sci*. **2021**, 542, 148662.

(45) Xu, W.-T.; Ma, L.; Ke, F.; Peng, F.-M.; Xu, G.-S.; Shen, Y.-H.; Zhu, J.-F.; Qiu, L.-G.; Yuan, Y.-P. *Dalton Trans*. **2014**, 43, 3792–3798.

(46) Yu, S.; Pang, H.; Huang, S.; Tang, H.; Wang, S.; Qiu, M.; Chen, Z.; Yang, H.; Song, G.; Fu, D.; Hu, B.; Wang, X. *Sci. Total Environ*. **2021**, 800, 149662.

(47) Ren, J.; Musyoka, N. M.; Langmi, H. W.; Swartbooi, A.; North, B. C.; Mathe, M. *Int. J. Hydrogen Energy* **2015**, 40, 4617–4622.

(48) Datta, S. J.; Mayoral, A.; Bettahalli, N.; Bhatt, P. M.; Karunakaran, M.; Carja, I. D.; Fan, D.; Mileo, P.; Semino, R.; Maurin, G.; Terasaki, O.; Eddaoudi, M. *Science* **2022**, 376, 1–8.

(49) Jia, Z.; Wu, G. *Microporous Mesoporous Mater*. **2016**, 235, 151–159.

(50) Zhou, S.; Shekhah, O.; Jia, J.; Czaban-Jóźwiak, J.; Bhatt, P. M.; Ramírez, A.; Gascon, J.; Eddaoudi, M. *Nat. Energy* **2021**, 6, 882–891.

(51) Efome, J. E.; Rana, D.; Matsuura, T.; Lan, C. Q. *ACS Appl. Mater. Interfaces* **2018**, 10, 18619–18629.

(52) Wang, X.; Zhai, L.; Wang, Y.; Li, R.; Gu, X.; Di Yuan, Y.; Qian, Y.; Hu, Z.; Zhao, D. *ACS Appl. Mater. Interfaces* **2017**, 9, 37848–37855.

(53) Li, Z.; Yang, P.; Gao, Z.; Song, M.; Fang, Q.; Xue, M.; Qiu, S. *Chem. Commun.* **2019,** 55, 3505–3508.

(54) Makhetha, T. A.; Moutloali, R. M. *J. Membr. Sci.* **2018**, 554, 195–210.

(55) Gu, J.; Fan, H.; Li, C.; Caro, J.; Meng, H. *Angew.Chem. Int. Ed.* **2019**, 58, 5297–5301.

(56) Deng, Y.; Wu, Y.; Chen, G.; Zheng, X.; Dai, M.; Peng, C. *Chem. Eng. J.* **2021**, 405, 127004.

(57) Valverde, A.; Gonçalves, R.; Silva, M. M.; Wuttke, S.; Fidalgo-Marijuan, A.; Costa, C. M.; Vilas-Vilela, J. L.; Laza, J. M.; Arriortua, M. I.; Lanceros-Méndez, S.; Fernández de Luis, R. *ACS Appl. Energy Mater.* **2020**, 3, 11907–11919.

(58) Otitoju, T. A.; Ahmad, A. L.; Ooi, B. S. *J. Water Process Eng.* **2016**, 14, 41–59.

(59) Ribeiro, C.; Costa, C. M.; Correia, D. M.; Nunes-Pereira, J.; Oliveira, J.; Martins, P.; Gonçalves, R.; Cardoso, V. F.; Lanceros-Méndez, S. *Nat. Protoc.* **2018**, 13, 681–704.

(60) Barbosa, J. C.; Gonçalves, R.; Valverde, A.; Martins, P. M.; Petrenko, V. I.; Márton, M.; Fidalgo-Marijuan, A.; Fernández de Luis, R.; Costa, C. M.; Lanceros-Méndez, S. *Chem. Eng. J.* **2022**, 443, 136329.

(61) Sarkisov, L.; Bueno-Perez, R.; Sutharson, M.; Fairen-Jimenez, D. *Chem. Mater.* **2020**, 32, 9849–9867.

(62) Serre, C.; Mellot-Draznieks, C.; Surblé, S.; Audebrand, N.; Filinchuk, Y.; Férey, G. *Science* **2007**, 315, 1828–1831.

(63) Accelrys Inc. Materials Studio, 2011.

(64) Allen, M. P.; Tildesley, D. J. *Computer simulation of liquids*; Clarendon Press; Oxford University Press: Oxford England, New York, **1987**.

(65) Rappe, A. K.; Casewit, C. J.; Colwell, K. S.; Goddard, W. A.; Skiff, W. M. *J. Am. Chem. Soc.* **1992**, 114, 10024–10035.

(66) Singh, U. C.; Kollman, P. A. *J. Comput. Chem.* **1984,** 5, 129–145.

(67) Delley, B. The Journal of Chemical Physics **2000**, 113, 7756–7764.

(68) Chen, B.; Potoff, J. J.; Siepmann, J. I. *J. Phys. Chem. B* **2001**, 105, 3093–3104.

(69) Troyano, J.; Carné-Sánchez, A.; Pérez-Carvajal, J.; León-Reina, L.; Imaz, I.; Cabeza, A.; Maspoch, D. *Angew. Chem. Int. Ed.* **2018**, 130, 15646–15650.

(70) Barroso, N.; Andreo, J.; Beobide, G.; Castillo, O.; Luque, A.; Perez-Yáñez, S.; Wuttke, S. *Commun. Chem.* **2023**, 6, 1-9.

(71) Thakur, P.; Kool, A.; Bagchi, B.; Das, S.; Nandy, P. Phys. *Chem. Chem. Phys.* **2015**, 17, 1368–1378.

(72) Martins, P.; Lopes, A. C.; Lanceros-Mendez, S. *Prog. Polym. Sci.* **2014**, 39, 683–706.

Chapter 5

Chapter 5

MOFs for the capture of dissolved CO_2 and generated carbonate ions from water

5.1 INTRODUCTION

Over the past 250 years, the level of the most abundant greenhouse gas on earth, carbon dioxide (CO_2), have increased by ~40% from the preindustrial era primarily due to human fossil fuel combustion and deforestation[1,2]. While the atmospheric CO_2 level was measured to be just ~280 ppm in the 1800s, it was recently recorded at over ~400 ppm and is projected to reach ~950 ppm by 2100[3–5]. Anthropogenic CO_2 emissions have caused (and will continue to cause) serious environmental issues such as global warming, ocean acidification, melting of snow cover and ice caps, elevated sea levels, and species extinction[6,7]. Natural hydrological cycles cause atmospheric CO_2 to be absorbed by the ocean and other bodies of water[8–10]. Approximately, 30% of carbon that humans have released into the atmosphere has been absorbed by the oceans; without this sink, atmospheric CO_2 would be approximately 450 ppm today. The absorption of CO_2 in the water dramatically alters the chemistry of oceans, lowering their pH and fundamentally changing seawater carbonate chemistry, which is commonly referred to as "other CO_2 problems"[11,12]. Since the pre-industrial era, surface ocean pH has decreased by ~0.1, a change, which has occurred approximately ten times faster than at any other occasion in the last 300 million years. Consequently, the oceans are experiencing unprecedented catastrophes like marine heat waves, widespread habitat destruction, ocean acidification and so on[13,14] (Figure 5.1).

Carbon capture and storage (CCS) is widely accepted as a critical part of any solution to reverse the effects of climate change, and a great deal of technology has been developed to perform this task[7,15–17]. CO_2 capture methods include adsorption (physisorption and chemisorption), physical/chemical absorption, cryogenic fractionation, membrane-based separation, etc. Among these, physisorption with porous materials is perhaps the most efficient method, with a much smaller energy footprint than any others mentioned[18,19].
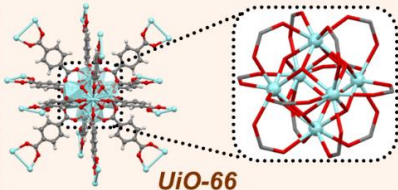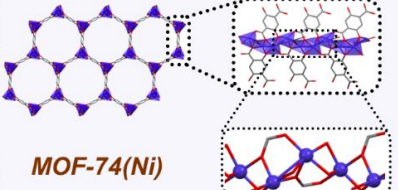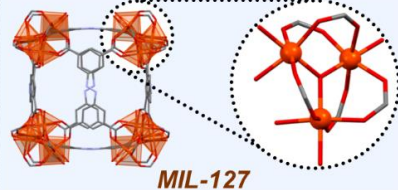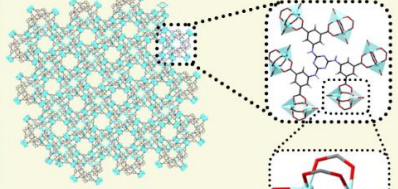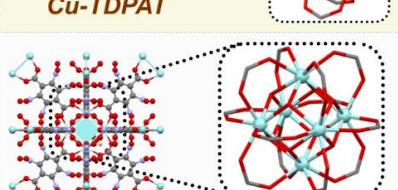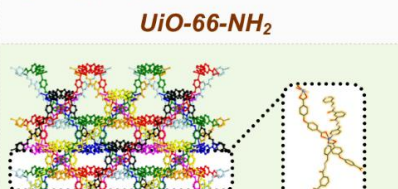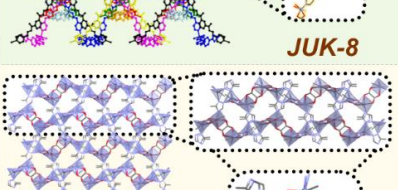
Over the last two decades, metal-organic frameworks (MOFs) have been designed and optimized specifically for the capture of gasses; including atmospheric CO_2[20–23]. Of all of the adsorbents available today, MOFs stand out as particularly advantageous[24–27]. As a consequence, they have become popular sorbent materials and have been widely studied[1,28,29] for the capture of different gas molecules including volatile organic compounds (VOCs)[30], hydrogen[31], methane[32], and CO_2[33] as well as common water pollutants like dyes[34], heavy metals[35], and pharmaceuticals[36]. MOFs have broken records for CO_2 gas capture and storage. Surprisingly, despite the excellent performance of these materials toward CO_2 capture and their reliable performance in aqueous environments for other applications, MOFs have never been utilized for CO_2 removal from aqueous environments (Figure 5.1). This creates a serious scientific knowledge gap and a window of opportunities for both chemical and material scientists to introspect the area of aqueous CO_2 sequestration by such materials.
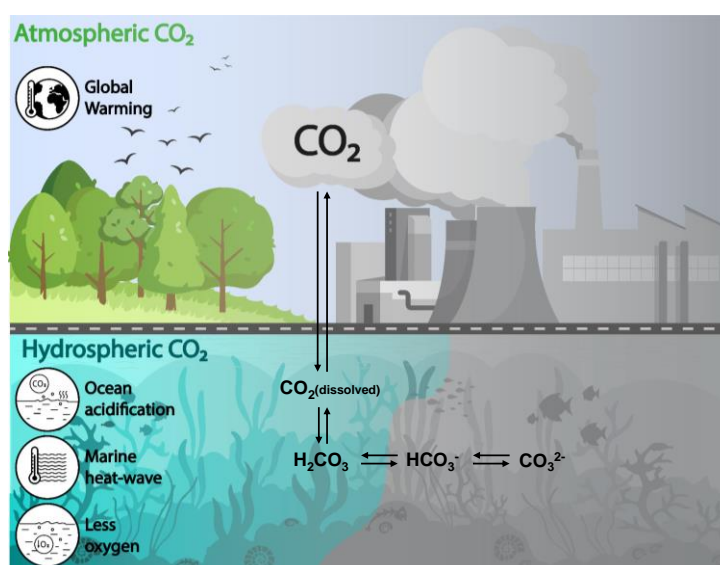
Figure 5.1. Schematic representation of synergic CO_2 absorption between atmosphere and hydrosphere.

In this chapter, we present a first benchmark study that explores and characterizes the potentials of various MOF systems for capturing CO_2 and other carbonate species from water, to provide a possible solution to alleviate/address the aforementioned problem. We selectively chose seven representative MOF systems that were extensively studied for the CO_2 capture in the gas phase before, and tested their performance for CO_2 capture and uptake of other carbonic species from water at different pH levels (Figure 5.2). The MOF systems were selected according to their high adsorption capacity, such as MIL-127(Fe)[37], Cu-TDPAT[38], MOF-74(Ni)[39], UiO-66(Zr)[40,41], UiO-66-NH₂(Zr)[41], and JUK-8[42] or high selectivity (ZU-301)[43], while providing a broad selection of material properties simultaneously such as chemical composition, structure, porosity, and functionality. Their relative performances provide key information about chemical and structural prerequisites for this task as different MOFs exhibits diverse sorption behaviour in different pH conditions. Finally, all MOFs systems were deployed for uptake studies of carbonate species (carbonic acid, H_2CO_3; hydrogen carbonate, HCO_3^- and carbonate, CO_3^{2-}) from real-world water samples of varying compositions to explore their potential in real-world applications. The water samples were collected from diverse natural water bodies (the Mediterranean Sea, Foix Reservoir, Pletero Lagoon, Colomers Weir and Tordera River), which differ in water composition (salt) and pH.

MOFs	Key Properties
UiO-66	• **Micropore channels with high stability** • *Bi-porous cage systems: tetrahedral cages ~8 Å and octahedral cages ~11 Å* • *Pre-adsorption and co-adsorption of water molecules in octahedral cage promotes CO_2 uptake in less favourable space than tetrahedral cages.*
MOF-74(Ni)	• *Narrow micropore channels* • ***Abundant Ni open metal sites*** • ***Preferential coordination of CO_2 to Ni^{2+} metal centers, forming $Ni^{2+}\cdots O=C=O$ adducts*** • *Oxygen lone pair orbitals of CO_2 can interact with the cations*
MIL-127	• *3D microporous system* • *Hydrophilic and hydrophobic groups* • *Accessible channel system of varying size and cages around 10 Å diameter* • ***Fe open metal sites, greater impact on interacting with CO_2 molecules***
Cu-TDPAT	• *Rigid framework* • *Cu-paddlewheel metal units along with rht topology* • ***Abundant unsaturated Cu metal sites*** • *Electronically polarized secondary amine groups in triazine ligands*
UiO-66-NH$_2$	• *Micropore channels with high stability* • ***NH_2 functionalized MOF*** • ***Higher selectivity*** *for CO_2 due to presence of NH_2-functionalities*
JUK-8	• ***Eightfold interpenetrated*** *structure* • ***Guest-dependent flexibility*** • *Switchable pore configuration* • *Presence of **secondary amide and carboxylate functional groups***
ZU-301	• **Ultramicroporous** *pore channels* • **Hydrophobic pore-surface** • *Rigid framework* • **High selectivity** *toward CO_2*

Figure 5.2. The key physiochemical properties related to CO_2 adsorption are summarized on the right column for each MOF. Crystal data information was obtained from: UiO-66[44], MOF-74(Ni)[45], MIL-127(Fe)[46], Cu-TDPAT[47], UiO-66-NH2[48], JUK-8[42], ZU-301[43].

5.2 EXPERIMENTAL DETAILS

5.2.1   Synthesis of MOFs

The synthesis and basic characterization (PXRD, SEM) for all MOFs chapter can be found in *Chapter 2*.

5.2.2   Characterization

Powder X-Ray Diffraction (PXRD). The stability of the crystal structure was monitored after exposure to carbonate solutions by powder X-ray diffraction using the D8 Advance Diffractometer (Bruker) with the copper Kα1 radiation ($\lambda = 1.5406$ Å). The XRD profiles of MOFs were obtained in the 2θ range of 6–80°, using a 0.05° step size per 1 s at RT. The analysis was conducted for as-synthesized MOFs and materials recovered after CO_2 adsorption from aqueous solutions.

Adsorption of CO₂ and other carbonate species from aqueous solutions. The MOF materials were applied as adsorbents for CO_2 adsorption from aqueous solutions. Depending on the pH, different forms of CO_2 occur in aqueous solutions, *i.e.*, at pH 2.0: gaseous CO_2; pH 6.3: CO_2 /HCO_3^-; pH 8.0: HCO_3^-; and pH 10.0: HCO_3^- /CO_3^{2-}. The adsorption processes were carried out as follows: 41.5 mL of $NaHCO_3$ aqueous solutions with concentrations varying from 5 to 640 mg/l were added to 25 mg of each MOF (UiO-66, MOF-74, MIL-127, CuTDPAT, UiO-66-NH₂, JUK-8, and ZU-301). The pH of initial solutions of $NaHCO_3$ was 8.0. The sorption capacities of the materials at pH 2.0, 6.3, and 10.0 were also tested. The pH of the mixtures was adjusted in the closed system by adding HCl (5 mol/L for pH 2.0 and 0.1 mol/L for pH 6.3) or NaOH (0.1 mol/L for pH 10.0) solutions. Concentrations of $NaHCO_3$ solutions before adjusting to a proper pH varied and were in the range of 40–640 mg/l (for pH 2.0), 5–150 mg/l (for pH 6.3 and 8.0), and 10–150 mg/l (for pH 10.0). Afterward, all samples were placed in IKA KS 4000i control incubator shaker for 4 h. In the next step, MOF materials were separated, and residual total inorganic carbon (TIC) analysis was performed.

Total Inorganic Carbon (TIC) analysis. Carbon dioxide dissolves and reacts in water to carbonic acid, followed by dissociation to hydrogen carbonate and carbonate.

We determined the Total Carbon (TC), Total Organic Carbon (TOC), and Total Inorganic Carbon (TIC) concentration in the liquid phase using catalytic high-temperature combustion by means of a TOC-L analyzer (Shimadzu; Japan) equipped with an additional nondispersive infrared (NDIR) sensor for CO_2 detection. This method relies on the catalytic oxidation of samples by combustion at 680°C inside the tubes filled with a platinum catalyst. We carried out experiments on solutions before/after the adsorption of inorganic carbon species to MOFs. TC and TOC values were measured directly via the TOC-L analyzer. We determined TIC values (derived from the difference between the two others) before and after the adsorption processes in order to determine their maximum uptake capacity.

To establish the amount of the adsorbed inorganic carbon species (q_e) from aqueous solutions in various conditions, the following formula was applied:

$$q_e = \frac{(C_0 - C_e) \cdot V}{m}$$
(5.1)

where, C_0 is initial inorganic carbon species concentration (mmol/l), C_e is the inorganic carbon species concentration (mmol/l) remaining after the adsorption process, V is the volume of the adsorbate solution and m is the mass of the MOF material (g).

For the real-world water samples, the removal efficiency (R) was calculated, where R is the ratio between the final and initial TIC concentration, *i.e.*, the TIC values of the collected water and the water after exposure to the various MOF samples.

$$R = \frac{\text{TIC}_{final}}{\text{TIC}_{initial}}$$
(5.2)

Correlative two-photon microscopy with *in-situ* Raman spectroscopy. Spatially resolved Raman spectra inside single MOF crystals and confocal two-photon fluorescence images on MOF particles by nonlinear microscopy were recorded on a recently published setup dedicated to multi-modal optical spectroscopy and image correlation analysis (MOSAIC)[49]. Briefly, the setup is based on a confocal scanning microscope (TE 300; Nikon) with mounted brightfield illumination and a camera. A fiber-based, frequency-doubled erbium laser (FemtoFiber dichro bioMP; Toptical Photonics) running at 774 nm as the excitation source for two-photon imaging of MOF

particles was used. The excitation laser line for Raman spectroscopy was as DPSS CW laser at 532 nm (Cobolt Samba, 04-01, 100 mW; Sweden). The laser powers amounted to 9.7 mW at 774 nm and 10.6 mW at 532 nm and were determined at the backport of the microscope body. The laser light was coupled into the microscopy via a dichroic mirror (zt532NIRrpc; AHF Analysetechnik) that separates the excitation from the detection path. The excitation light was focused onto the specimens using a water immersion objective with 1.2 NA (CFI Plan Apo VC 60x water; Nikon) while positioning or scanning of the sample was done using an XYZ piezo stage (BIO3.200; PiezoConcept). The sample response, *i.e.*, the two-photon induced emission during imaging or inelastically scattered light during Raman spectroscopy, was collected by the same objective and guided and detected on two different detection paths. For two-photon imaging, the emission was recorded on an APD detector (Count Blue; Laser Components) after filtering the emission using a dichroic mirror (BS 647 SP; AHF Analysetechnik), a bandpass filter (630/50; AHF Analysetechnik), and a 750-nm short-pass (FES0750; Thorlabs) to block the 774 nm laser line. The experiments were controlled using a home-written program in C#. The confocal data was afterward extracted and evaluated by PAM[50] and Image J2[51]. For spontaneous Raman spectroscopy, a movable silver mirror guided the scattered light to a spectrograph (Kymera 328i; Oxford instruments) equipped with an emCCD camera (iXon 897; Andor). Two filters before the spectrometer served to block shorter wavelengths, including Rayleigh scattering at 532 nm (RET 537 LP; AHF Analysetechnik / 532 nm Notch filter, OD6; Edmund Optics). The spectral resolution amounted to 7.2 cm^{-1} (Grating with 600 l/mm and blaze at 500 nm). Raman spectra were recorded using *Andor Solis for Imaging V4.30* (Oxford Instruments) between 280-4500 cm^{-1}. The acquisition time per pixel was set to 25 sec with 6 repeats (UiO-66) and 5 sec with 6 repeats (JUK-8) with an excitation density of 46.3 mW/µm^2 at the sample plane.

Measurement of alkalinity and electrical conductivity. The brine salinity, *i.e.*, the electrical conductivity, was measured in-field immediately after collection using a WTW Multi 3630 IDS sensor. The total alkalinity was measured by potentiometric titration with a Methrom, 848 Titrion plus system using the Gran method to calculate it from acidic volumes. The titration acid was 0.05 M HCl. Duplicate measurements were made for each sample, and the precision error was ±1 µmol/kg.

5.3 RESULTS AND DISCUSSION

5.3.1 CO₂ and Carbonic acid species in water

Carbonic acid is a diprotic acid that converts into different forms depending on the pH (pk_{a1} = 6.532 and pk_{a2} = 10.329)[52]. In acidic conditions (pH < pK_{a1}), the dominant form is CO_2, while in basic conditions (pH > pK_{a2}), the majority remains as CO_3^{2-}. At intermediate pHs, *i.e.* pK_{a1} < pH < pK_{a2}, the most abundant form is hydrogen carbonate (HCO_3^-). The concentration of carbonic acid is considered to be negligible compared to the concentration of the other species in all pH ranges. Hence, to study the adsorption behavior of the selected MOFs towards CO_2 capture in water, four different pH values (namely pH 2.0, 6.3, 8.0 and 10.0) were selected. These were chosen according to the dominant species, which are CO_2, CO_2/HCO_3^-, HCO_3^-/CO_3^{2-} and CO_3^{2-}, respectively.

5.3.2 MOFs selection criterion

The primary criterion for selecting the MOFs was a good track record of CO_2 adsorption in the gas phase, which will allow us to compare and correlate their adsorption phenomenon depending upon the matrix (air and water). Further, our aim was to include MOFs with structural diversity (different topology, porosity, structural flexibility, etc.) and MOFs with diverse chemical functionalities (presence of open metal sites (OMS), basic groups, etc.). To cover a wide spectrum, seven MOFs were chosen (Figure 5.3), which can be primarily categorized into two: MOFs with high CO_2 adsorption capacity, and MOFs with high selectivity toward CO_2. The first category consists of six MOFs, namely UiO-66, MOF-74(Ni), MIL-127, Cu-TDPAT, UiO-66-NH₂, and JUK-8, while ZU-301 was chosen as the representative of MOF for CO_2 selectivity. ZU-301 presents optimum pore size and geometry to sieve larger molecules and selectively adsorb CO_2 over water and other small molecules. The six high-capacity MOFs can be further subdivided into three categories depending on the structural characteristics: *i*) MOFs with undercoordinated metal sites, *ii*) MOFs with basic groups and *iii*) MOFs with a flexible framework, all of them are well known to assist in high CO_2 uptake. MOF-74(Ni), MIL-127, and Cu-TDPAT were chosen to understand the role of open metal sites and different coordination environments for

CO_2 capture from water. In MOF-74(Ni), the undercoordinated site in the apical position of the coordination sphere and the neutral ligand in this position (DMF in the material we synthesized) is easily exchanged. MIL-127 presents as a metal SBU a trimeric iron(III) cluster, and the apical position is occupied by a chloride anion which is easily exchangeable. Cu-TDPAT presents a copper paddlewheel cluster, and the free apical position of the coppers is coordinated by an exchangeable DMF molecule. UiO-66 and UiO-66-NH_2 were chosen as the representative well-studied, robust MOF and functionalized MOF with basic groups, which in comparison can highlight the role of basic groups toward CO_2 affinity. JUK-8 was selected as a flexible MOF, which is well known for its structural dynamism depending upon the incoming guest molecules. For example, it is found to transform from its closed form to open form in the presence of water or carbon dioxide, which make it interesting and promising to study this MOF for CO_2 capture in water.
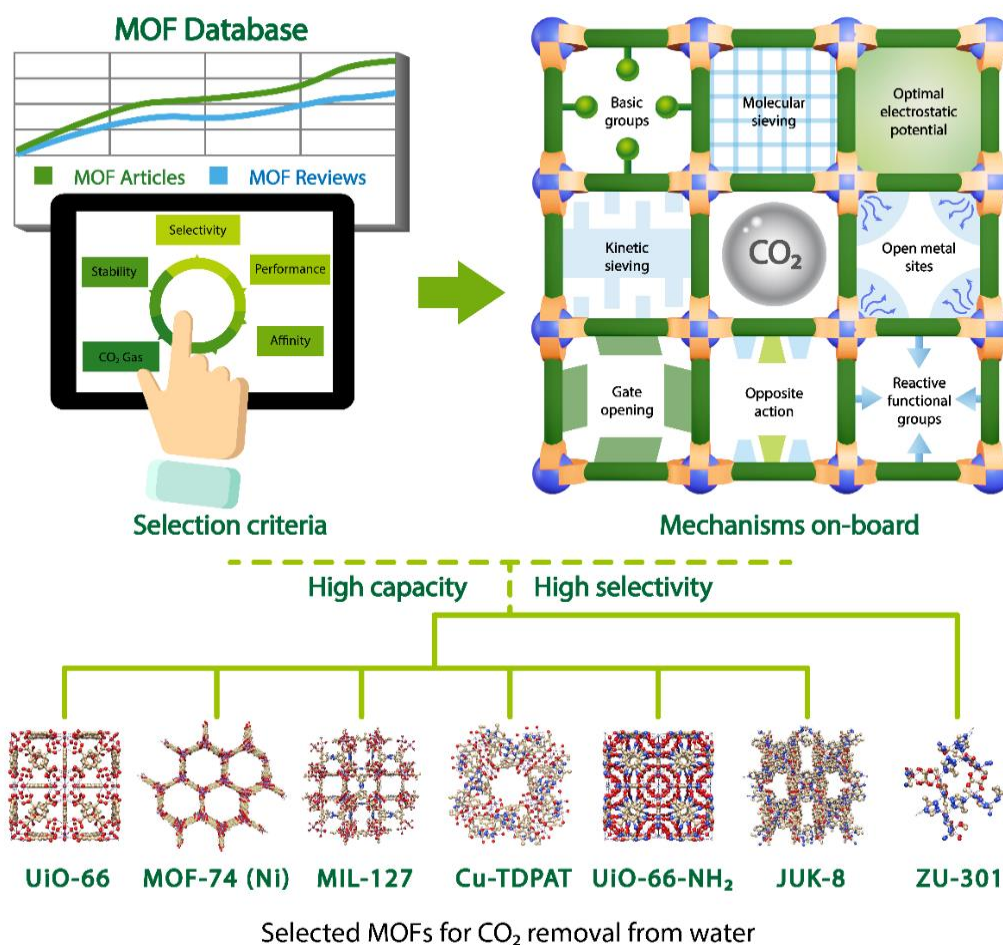
Figure 5.3. Selection criterion of MOFs offering various CO_2 interaction mechanism.

5.3.3 Stability of MOFs

Prior to evaluating their adsorption performance for different carbonate species in aqueous solutions, the stability of MOFs at the above-mentioned four pHs was monitored in order to study their structural stability. For those experiments, all the MOFs were dipped into the corresponding carbonate aqueous solutions for 4 h, subsequently filtered and dried in air. Afterward, their structural integrity was evaluated via PXRD experiments (Figure 5.4). All the MOFs exhibited good stability at pH 8.0 and pH 10.0, while high acidity frequently led to instability. In particular, JUK-8 and Cu-TDPAT showed structural instability at pH 2.0, while ZU-301(Zn) showed structural instability at both pH 2 and 6.3. In addition, Cu-TDPAT exhibited partial instability during adsorption experiments at pH 6.3, which was found to be dependent on the carbonate concentration in the solution. This phenomenon can be correlated to the ability of carbonate ions to replace the carboxylate groups coordinating the copper paddlewheel in the MOF structure[53]. According to these stability performances, we further employed the MOFs for the adsorption studies in different pH conditions.
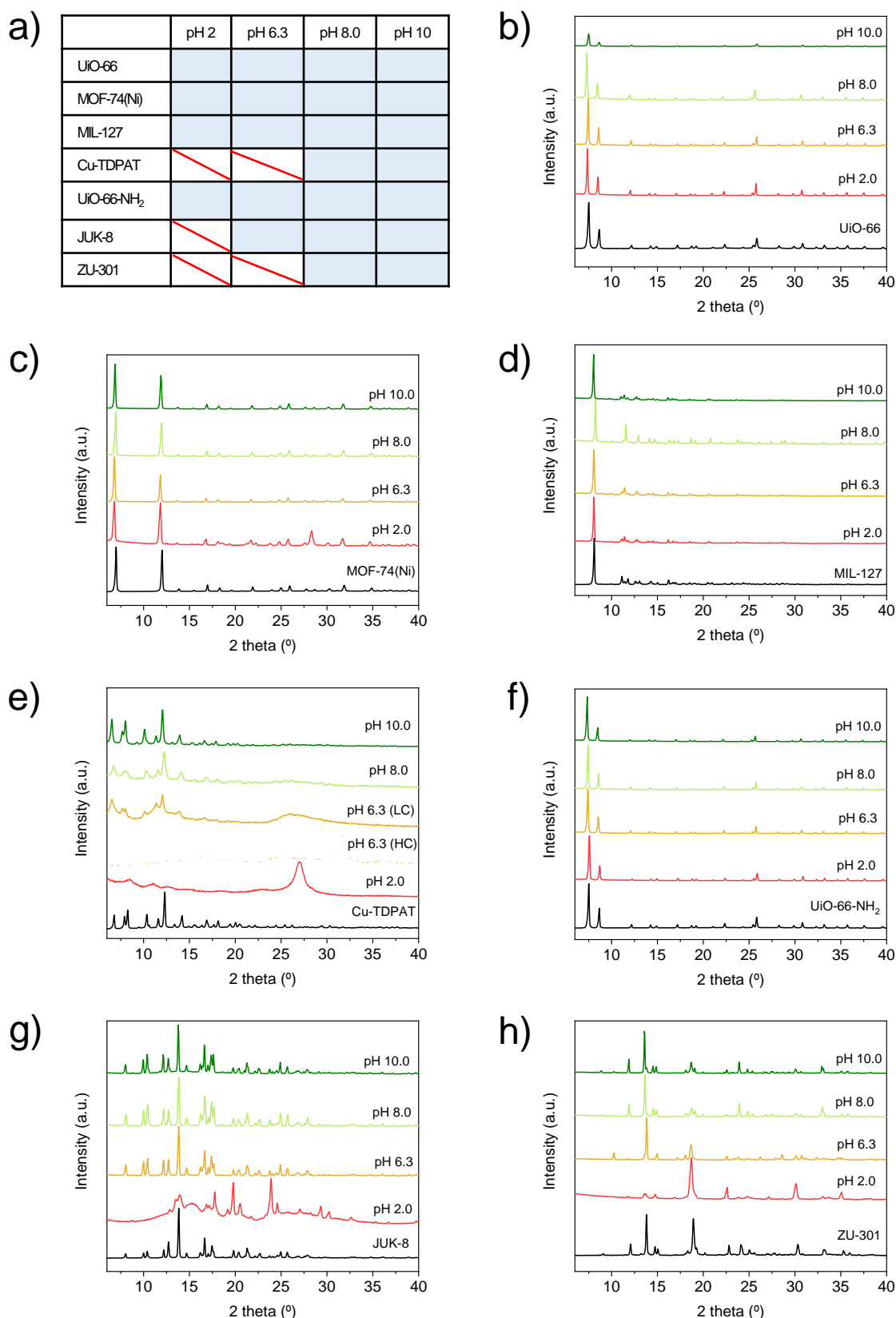
Figure 5.4. PXRD measurements of MOF samples before and after inorganic carbon adsorption at pH 2.0, 6.3, 8.0 and 10.0: a) Table summarizing stability of MOFs (blue: stable, red bar: not stable). b) UiO-66, c) MOF-74(Ni), d) MIL-127, e) Cu-TDPAT, f) UiO-66-NH$_2$, g) JUK-8, and h) ZU-301. (LC = 150 mg/l of HCO$_3^-$ solution at pH 6.3 and HC = 1000 mg/L of HCO$_3^-$ solution at pH 6.3).

5.3.4   Uptake studies

Adsorption experiments revealed remarkable differences in the MOF performances, depending strongly on the nature of the species and the pH of the medium (Figure 5.5 and 5.6). Different MOFs were found to exhibit diverse sorption trends toward different species. In particular, at pH 2.0, where only neutral species, CO_2 and H_2CO_3 are present, MOFs with open metal sites exhibited the highest sorption efficiency (MOF-74(Ni) with 1.84 mmol/g and MIL-127 with 2.78 mmol/g). UiO-66 and UiO-66-NH_2, the only other stable MOFs at this pH showed lower adsorption capacities (0.84 mmol/g and 1.23 mmol/g, respectively). All MOFs showed relatively similar saturation concentrations at this pH, ranging from 3.53 mmol/g for MIL-127 to 2.39 mmol/l for MOF-74(Ni).

At pH 6.3, at which both neutral species and HCO_3^- are present, all MOFs discussed for pH 2.0 showed lower adsorption capacities. In particular, MOF-74(Ni) showed a reduced capacity of 0.36 mmol/g, while the other MOF with open metal sites, MIL-127, was found to exhibit 1.42 mmol/g of capacity. UiO-66 and UiO-66-NH_2 showed 0.69 mmol/g and 0.90 mmol/g respectively. JUK-8, on the other hand, presents a staggering 6.79 mmol/g of adsorption corresponding to 30% in weight. Overall, all MOFs presented similar saturation concentration ranges, although the measured concentrations are lower at this pH than pH 2. The saturation concentrations were calculated to be 2.11 mmol/l for MOF-74(Ni) and 2.53 mmol/l for MIL-127 and higher for UiO-66 (3.15 mmol/l) and UiO-66-NH_2 (2.78 mmol/l). Expectedly, JUK-8 showed a much higher saturation concentration (7.87 mmol/l), which could be correlated to the conformational switch in structure –flexibility- between its partially open and completely open pores. Further in-depth experimental analysis has been carried out to better understand this unique phenomenon which will be discussed later in more detaill later.

Adsorption at pH 8.0, where only hydrogen carbonate is present, revealed similar results as pH 6.3 for UiO-66, UiO-66-NH_2, and MOF-74(Ni) (0.64 mmol/g, 0.88 mmol/g and 0.33 mmol/g, respectively). MIL-127 presented a further decrease in capacity (0.55 mmol/g), as did JUK-8 (0.63 mmol/g) with a ten-fold decrease in adsorption. Cu-TDPAT presented an adsorption capacity in line with the other open

metal site materials (0.44 mmol/g). Unsurprisingly, ZU-301 exhibited lower uptake, with a capacity of only 0.17 mmol/g. This lower sorption behavior can be explained by the presence of small pores in ZU-301, which are not suited to accommodate the solvation sphere of the carbonate ions present in aqueous solution. Carbonate saturation occurred at 0.84 mmol/l for Cu-TDPAT and 1.23 mmol/l for ZU-301. All other materials were saturated at lower concentrations if compared with pH 6.3, with values comprised between 1.63 mol/l for UiO-66 and 1.32 mol/l for MOF-74(Ni). JUK-8 also followed this trend, although its saturation concentration remained much higher at 5.67 mmol/l.
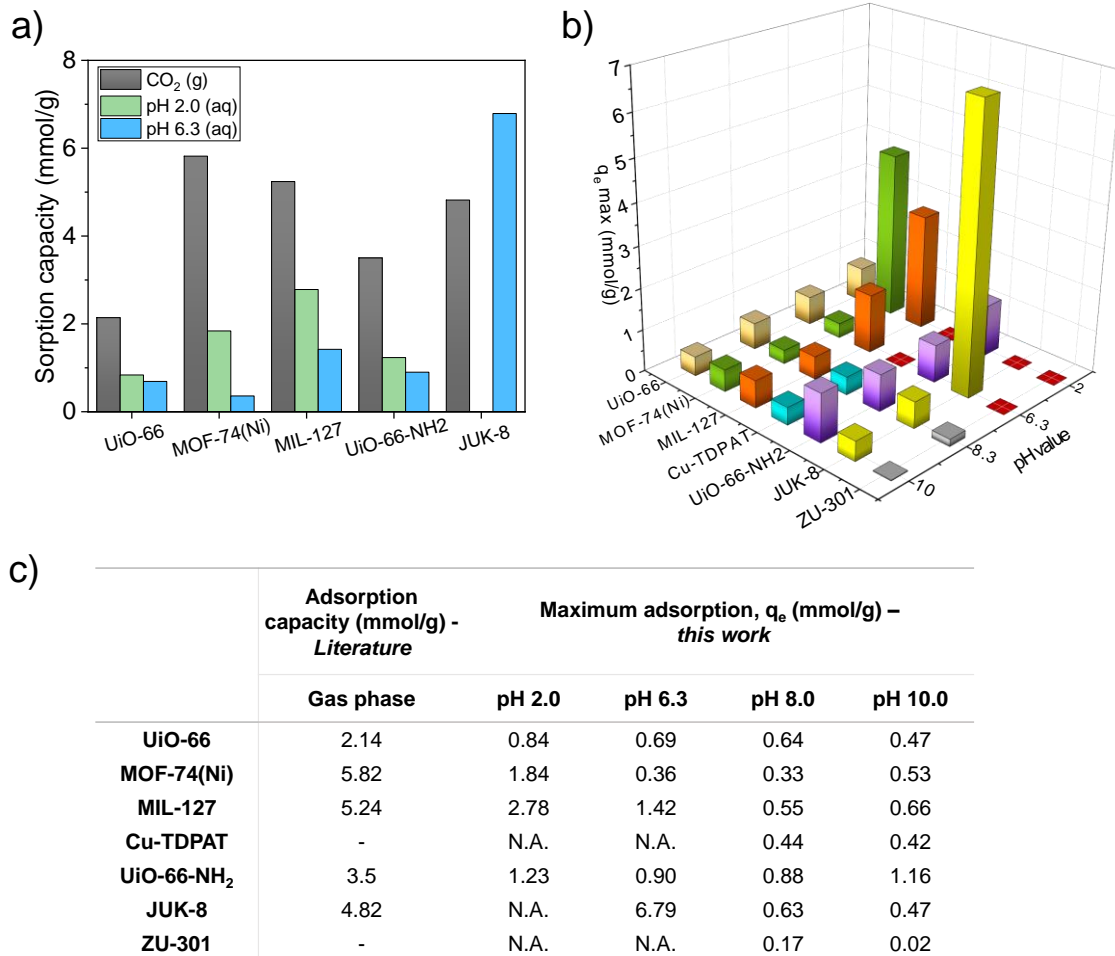
At the most basic pH (pH 10), the species present in the solution are both HCO_3^- and CO_3^{2-}, and two distinct behaviors emerge in the materials: UiO-66, JUK-8 and ZU-301 exhibited a decrease in adsorption capacity, while UiO-66-NH₂, MOF-74(Ni) and MIL-127 showed an increment in their respective uptake capacities. Interestingly, Cu-TDPAT was found to almost retain its performance, with a difference of less than 0.1 mmol/g in adsorption. In particular, UiO-66-NH₂ adsorption capacity increases to 1.15 mmol/g, better than pH 6.3 and 8.0, while ZU-301 drops at 0.02 mmol/g. Material saturation is reached at higher concentrations for almost all materials, with the only exception of ZU-301 and JUK-8, for which it dropped to 1.70 mmol/l.

Among all the chosen MOFs, JUK-8 demonstrated the best adsorption performance at pH 6.3, registering the highest uptake capacity (6.79 mmol/g) and 30% in weight of adsorbed CO_2. Alike other MOFs, JUK-8 also showed better performance in acidic conditions than basic ones (pH 6.3 (6.79 mmol/g) > pH 8.0 (0.63 mmol/g) > pH 10.0 (0.47 mmol/g)), while the material proved to be unstable at pH 2.0. The saturation concentration were found to be as high as 7.87 mmol/l at pH 6.3, followed by 5.67 mmol/l at pH 8.0 and 1.7 mmol/l at pH 10. It is worth noticing that much higher CO_2 or carbonate concentrations are needed to reach the saturation capacity of JUK-8 in comparison to the other MOFs tested. In addition, the adsorption isotherm of JUK-8 at pH 6.3 showed multistep sorption behavior with a clear step around 3.5 mol/g of CO_2. This is indicative of significant interaction between the incoming carbonate molecules with the MOF framework and potential structural alteration of the flexible JUK-8 sharing a peculiar interpenetrated structure, with three different possible pore-opening configurations (closed, partially open, and fully open) depending on the

exposure matrix, where nitrogen does not have enough affinity for the framework to force the pores open compared to water and CO_2 that are reported to open the MOF pores[42].
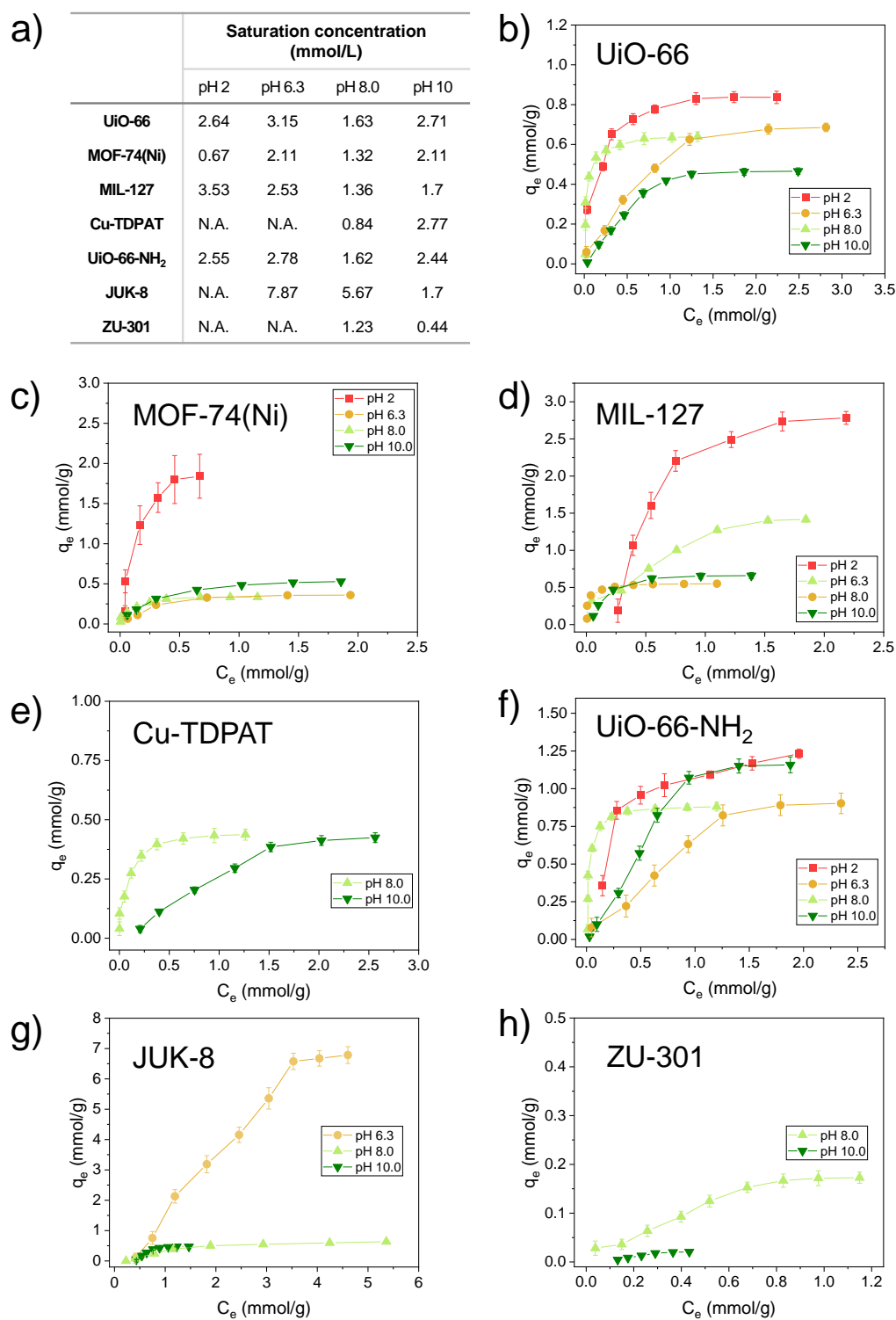
Figure 5.5. Adsorption isotherms of carbon inorganic species from solution by MOFs: a) Summary of the saturation concentration detected for the 7 MOF samples at different pHs. Adsorption isotherms for b) UiO-66, c) MOF-74(Ni), d) MIL-127, e) Cu-TDPAT, f) UiO-66-NH₂, g) JUK-8, and h) ZU-301.

a)

b)

c)

	Adsorption capacity (mmol/g) - *Literature*	Maximum adsorption, q$_e$ (mmol/g) – *this work*			
	Gas phase	pH 2.0	pH 6.3	pH 8.0	pH 10.0
UiO-66	2.14	0.84	0.69	0.64	0.47
MOF-74(Ni)	5.82	1.84	0.36	0.33	0.53
MIL-127	5.24	2.78	1.42	0.55	0.66
Cu-TDPAT	-	N.A.	N.A.	0.44	0.42
UiO-66-NH$_2$	3.5	1.23	0.90	0.88	1.16
JUK-8	4.82	N.A.	6.79	0.63	0.47
ZU-301	-	N.A.	N.A.	0.17	0.02

Figure 5.6. a) Comparison between CO$_2$ adsorption in gas phase (data obtained from literature: UiO-66[40], MOF-74[39], MIL-127[37], UiO-66-NH$_2$[41] and JUK-8[42]) and experimental data at pH 2.0 and pH 6.3 obtained in this work. b) Maximum adsorption values (q$_e$) of carbon inorganic species from solution for the 7 MOF samples after exposure to aqueous carbonate solutions at pH 2, 6.3, 8 and 10 for 4 hours. c) Summary table with detailed data.

Overall, these results highlight several trends among the MOFs and the nature of the sorbate species. MOFs with open metal sites (MOF-74(Ni), Cu-DTPAT, and MIL-127) show a decreasing trend in CO$_2$ adsorption capacity from acidic to basic pHs. UiO-66 was also found to follow this trend with a lesser pronounced difference between the high and low pHs. ZU-301, featuring the small pore-apertures, showed low or negligible adsorption. JUK-8 presented remarkable adsorption at pH 6.3, in line with its strong affinity of this material with CO$_2$ and UiO-66-NH$_2$ proved to be the material with the most constant performance, maintaining good adsorption over all pHs. Due to their efficient and interesting sorption behavior, we further carried out in-depth studies with UiO-66-NH$_2$ and JUK-8 via *transient* vibrational spectroscopy.

5.3.5 Characterization by vibrational spectroscopy

FTIR and Raman spectra where recorded for each MOF (Figure 5.7), where the most characteristics bands where assigned comparing to the literature. Moreover, the two MOF systems were investigated by confocal imaging as well as transient and spatially resolved vibrational spectroscopy to elucidate the complex adsorption process. At first, we characterized both MOF systems in water using two-photon-excited fluorescence scanning microscopy (Figure 5.8a). As expected from SEM imaging, JUK-8 consists of well-separated crystals of least 50 µm with clean surfaces. The synthesized UiO-66-NH$_2$ nanoparticles, however, are assembled into micron-sized clusters, which partially dissolve over time providing a large surface-to-volume ratio available for the adsorption of carbonate species.
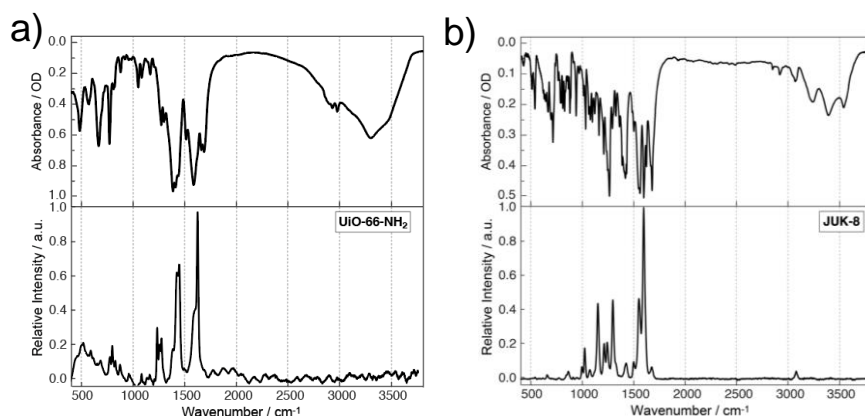
Figure 5.7. FTIR (top) and Raman (bottom) spectra for a) UiO-66-NH$_2$ and b) JUK-8.

To follow the uptake of carbonate species over time, we employed transient ATR-FTIR spectroscopy on MOF-coated ATR substrates as shown in Figure 5.8b. Experiments were carried out in a flow cell, which was first filled with water only. Upon exposure to a 150 mmol/l solution of NaHCO$_3$ at pH 8.0, new vibrational resonances were observed compared to the pristine host material. The resulting ATR-FTIR difference spectrum of UiO-66-NH$_2$ (Figure 5.8c) exhibited significant differences in presence of NaHCO$_3$. Negative bands were formed around 1400 cm^{-1} and 1583 cm^{-1} coinciding with the carboxylate stretching modes of the amino terephthalic acid coordinated to the Zr-clusters. This is indicative of an interaction between hydrogen carbonate ions HCO$_3^-$ and the MOF structure, which is in strong contrast to gas-phase CO$_2$ adsorption, where no perturbation of the MOF framework

is observed in line with the literature[54]. Moreover, the significant broadening of the stretching vibrations of the carboxyl group around 1583 cm^{-1} (v_{as}(COO$^-$)) and 1383 cm^{-1} (v_s(COO$^-$)) and the appearance of a shoulder around 1340 cm^{-1} can be correlated with the structural change of the MOF framework. Here, the rise at 1360 cm^{-1} and 1668 cm^{-1} can be assigned to the incorporation of hydrogen carbonate HCO$_3^-$ and carbonate CO$_3^{2-}$ ions. Noteworthy, a small positive signal at 2345 cm^{-1} is observed corresponding to gaseous CO$_2$[55], whose intensity is less intense in comparison to samples where gaseous CO$_2$ was adsorbed. The presence of this low-intesity band can be attributed to the presence of carbon dioxide in the measurement chamber, which in aqueous solutions is strongly reduced, if not suppressed by the competitive binding of water molecules to the Zr nodes.

Next, *transient* ATR-FTIR experiments were carried out to probe the adsorption behavior of JUK-8 for carbon species from water. Figure 5.8d shows the difference spectrum for JUK-8 upon exposure to 150 mmol/l NaHCO$_3$ solution, which shows additional bands around 1275 cm^{-1}, 1400 – 1500 cm^{-1}, 1580 cm^{-1} and 1660 cm^{-1}. This bands has been previously assigned as characteristic bands of polydentate carbonate (1400 – 1500 cm^{-1}) and hydrogen carbonate species (1660 cm^{-1})[56], and bidentate carbonate (1580 and 1274 cm^{-1})[57–59]. This is indicative of intermolecular interaction between hydrogen carbonate and the Zn metal nodes of JUK-8 during the uptake process. The appearance of minor negative bands at 1245 cm^{-1} and 1597 cm^{-1} indicate insignificant perturbation of the MOF during hydrogen carbonate uptake.

Knowing that carbonate and hydrogen carbonate ions interact with both frameworks, we consecutively evaluated how fast this process is happening by filling the flow chamber with 150 mmol/l NaHCO$_3$ at pH 8.0. As shown in Figure 5.8e, the maximum concentration is already reached within less than 2 minutes, after exchanging water against 150 mmol/l carbonate solution inside the ATR crystal. The presence of MOF inside the chamber delays the local influx of carbonate species, while both MOF samples show a nearly identical, temporal profile. In both cases, the IR signature reaches the saturation level observed for the carbonate solution within less than 5 min. It is also noteworthy that both MOFs lead to an increase in carbonate bands compared to the measurements obtained on blank ATR crystals (Figure 5.8f). This means,

although aqueous solutions are replaced by the MOF powders on the surface, carbonate species are enriched.
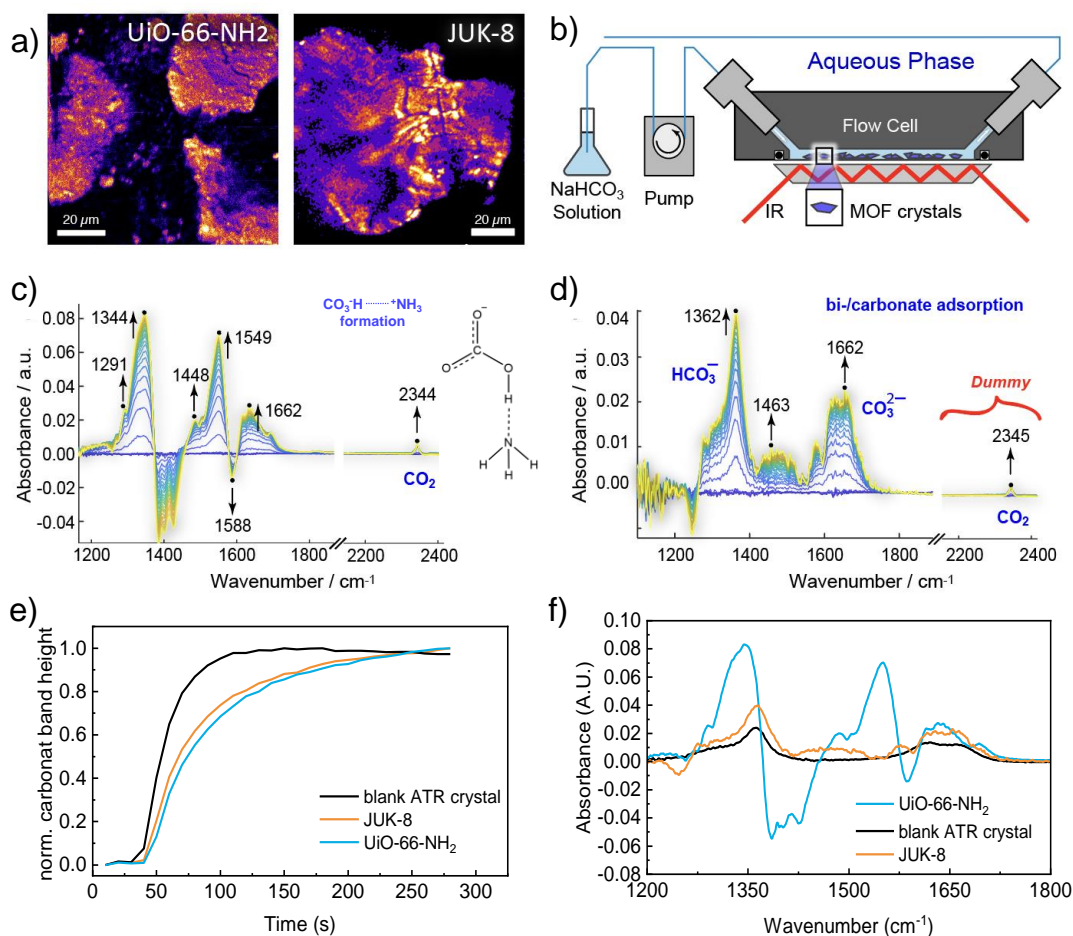
Figure 5.8. Spectroscopic evaluation of CO_2 adsorption by UiO-66-NH$_2$ and JUK-8 in an aqueous environment: a) Two-photon excitation-induced fluorescence microscopy reveals that UiO-66-NH$_2$ particles are formed by aggregated nanoparticles while JUK-8 was synthesized as large-sized crystals. b) Schematic ATR-FTIR experiment to follow CO_2 adsorption to MOFs in solution by transient spectroscopy. c-d) Difference ATR-FTIR spectra after the addition of 150 mM $NaHCO_3$ (pH 8.0) show an increased uptake of adsorption of carbonate species to the Si ATR crystal coated with c) UiO-66-NH$_2$ and d) JUK-8. The reference/background spectrum was recorded for MOFs exposed to water in the flow cell. e) ATR-FTIR spectra were obtained after flushing the flow chamber for 250 sec with 150 mM $NaHCO_3$ solution in the absence and presence of UiO-66-NH$_2$ and JUK-8. f) Comparison of FTIR-ATR spectra obtained after flushing hydrogen carbonate solution for 250 s.

5.3.6 Real-world sample testing

Adsorption performance in the real-world complex matrixes is one of the crucial criteria to evaluate true potential of any sorbent materials. Encouraged from the above-mentioned results, we have further performed preliminary experiments for CO$_2$ removal from real-world water samples, collected from lakes, rivers and the Mediterranean Sea. As different natural water bodies consist of diverse chemical constituents such as dissolved gases (CO$_2$, O$_2$, etc.), inorganic ions, organic compounds and so on, this set of experiments is not to be intended as a direct applicability of MOFs as adsorbers in water treatment for water solubilized carbon capture, but as a preliminary way to gage the material behaviour in more complex environments. Real-world water samples were collected at 5 different locations along the east coast of Spain (Figure 5.9; Table 5.1), in particular, along the coast of the Mediterranean Sea, *i.e.*, around Mataró and in the Pletera lagoon, the Tordera river and the water reservoirs of the Foix and Colomers rivers. The locations were chosen such that samples from salt and fresh water were taken into account, as well as conditions of free (ocean), flowing (river), and retained (reservoirs) water in a similar climatic region could be incorporated into the study.
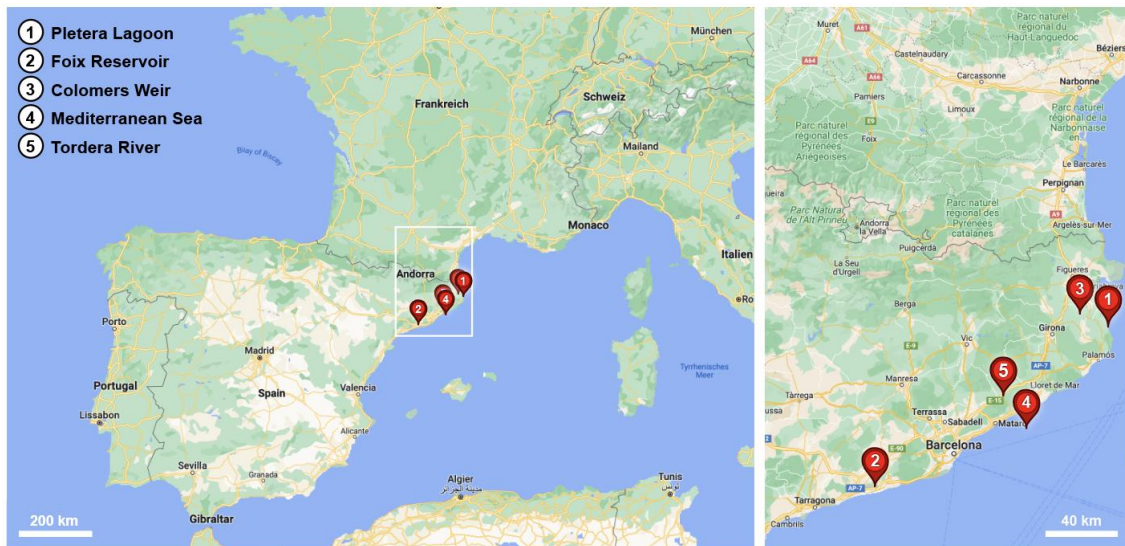
Figure 5.9. Selected sampling sites along the east coast of Spain. Water samples were collected in the Mediterranean Sea, at the coast at Mataró (4) and the Pletera lagoon (1), in the Tordera River (5) and reservoirs of the Foix (2) and Colomers River (3). The locations are numbered and marked in red.

All samples were characterized via in-field measurements, together with their location and environmental conditions such as the temperature, atmospheric pressure, and the partial pressure of CO_2. The parameters are summarized in Table 5.1.

Table 5.1. Collection sites and environmental parameters. Samples were collected and characterized in-field. NA: not applicable.

#	Sample	Latitude	Longitude	Temperature	Atmospheric pressure	CO_2 partial pressure
				(°C)	(mm Hg)	(µ-atm)
1	Pletera Lagoon	42.0312135	3.1906245	15.3	769.5	289
2	Foix Reservoir	41.2544287	1.6440742	11.6	760.6	2352
3	Colomers Weir	42.0769462	2.9915725	13.1	767.3	2541
4	Mediterranean Sea	41.5780474	2.5506917	NA	NA	NA
5	Tordera River	41.6858087	2.4972243	11.2	758.7	884

5.3.6.1 Composition of collected water samples

To link our findings to the chemical composition of ions and elements dissolved in the collected water samples, we characterized various physicochemical parameters. Samples were collected at different locations and filtered through an isopore membrane with a 200-µm cut-off. The brin salinity (expressed electrical conductivity), the pH and dissolved oxygen concentration were measured in-field. In addition, alkalinity titrations and HTC measurements were carried out in the lab to derive the alkalinity and the total inorganic carbon (TIC) concentration of the collected samples. From Table 5.2 is clear that, as expected, all these variables are correlated, and that the sample with the highest inorganic carbon concentration is also the most alkaline, the most basic and the best conductor, with the only exception of the Mediterranean Sea sample, that due to the high salinity presented the best conductivity although it ranked only fourth in terms of inorganic carbon. Thus, salted water samples (collected in the Pletera Lagoon and the Mediterranean Sea) contain more ions and hence show a higher electrical conductivity compared to freshwater samples. While the pH is fairly constant around pH 8, the alkalinity varies at

maximum by a factor of 5, similar to the total amount of measured hydrogen carbonate HCO_3^-, which is the most abundant species in a moderate basic environment.

Table 5.2. Physicochemical parameter of collected water samples. Since the addition of the CO_2 to water lowers the pH, while the alkalinity is not affected, we further quantified the electrical conductivity and the amount of dissolved CO_2 species.

| #	Sample	Alkalinity	pH	Electrical conductivity	TIC
		(meq/L)		@25ºC (µS / cm)	(mmol/l of HCO_3^-)
1	Pletera Lagoon	7.086	8.38	43000.0	4.73
2	Foix Reservoir	4.636	8.26	1187.0	3.90
3	Colomers Weir	3.072	8.28	533.0	2.50
4	Mediterranean Sea	2.756	8.03	52100.0	2.11
5	Tordera River	1.201	7.99	219.0	0.95

5.3.6.2 Carbonate adsorption from different bodies of water

Lastly, we investigated the uptake capacities of MOFs for carbon species from real-world water samples. For this, we exposed UiO-66, MOF-74(Ni), MIL-127, Cu-TDPAT, UiO-66-NH₂, JUK-8 and ZU-301 to different water samples, by adding 25 mL of water to 25 mg of MOF powder. The mixtures were shaken for 4 h after water addition, followed by materials separation. A strong dependency on the water composition is observed, nevertheless, all tested MOF systems lead to a reduction of the dissolved carbon content (Figure 5.10, Table 5.3). While JUK-8, ZU-301, and MOF-74(Ni) show an average removal efficiency below 5%, all other MOF systems reduce the carbon concentration on average by around 30%, with up to 48 and 59% even in the case of UiO66-NH₂ and MIL-127, respectively. Empirically, we observed that the removal efficiency strongly depends on the ion composition of the water, as represented by the alkalinity of the water: the lower these parameters are, the higher the removal efficiency is. The electrical conductivity, and as such the brine salinity, follows the same trend, except for water from the Mediterranean Sea.

Adsorption experiments revealed interesting trend in the performance of the MOFs in terms of % efficiency in TIC removal, arguably the most important parameter for material applicability. MIL-127, Cu-TDPAT, UiO-66 and UiO-66-NH₂ followed the

same trend, presenting higher removal efficiencies in samples with lower TIC. This is expected, as all samples present concentrations higher (or, in the case of the Tordera river, comparable) than the material saturation. Overall, these four MOFs presented the best adsorptions, with removal efficiencies between 9 and 23% for the Pletera Lagoon (eq. concentration of HCO_3^-: 4.73 mmol/l) and from 19 to 30% for the Foix Reservoir (3.90 mmol/l). The Colomers Weir and the Mediterranean Sea samples present a similar TIC concentration (2.50 mmol/l and 2.11 mmol/l, respectively), but very different conductivities (533.0 μScm^{-1} and 52100.0 μScm^{-1} respectively). Interestingly, MIL-127 and Cu-TDPAT showed very similar adsorptions in the two samples (38% and 40% respectively for MIL-127, 38% and 41% for Cu-TDPAT) while UiO-66 and UiO-66-NH_2 adsorption increased substantially for the Mediterranean Sea sample (19% and 30% for the two MOFs in Colomers Weir and 28% and 39% respectively for the Mediterranean Sea). This increase in adsorption is most likely due to a lower competition of water for the materials adsorption sites, as the higher concentration of ions in the sea sample, mainly due to sodium and chloride, forces the water molecules in solvation spheres and thus lowering their availability to enter the pores and, at the same time, it weakens the solvation spheres of the carbonic species, allowing an easier adsorption in the materials. Lastly, these four materials presented adsorption efficiencies between 31% and 59% for the Tordera river, the sample with the lowest TIC (0.95 mmol/l).

MOF-74(Ni), JUK-8 and ZU-301, on the other hand, presented much lower adsorptions for the real-world samples. In particular, MOF-74(Ni) presented a very low adsorption only for the three samples with the highest concentrations, while no adsorption was detected for the Mediterranean Sea and the Tordera River. JUK-8 presented no adsorption for the Pletera lagoon sample, while its efficiency for the other four varied between 1% and 9%, with no clear trend between different samples. ZU-301 was able to adsorb small amounts of TIC in all samples, but never exceeding 4% of the sample concentration. Most likely, the high affinity of JUK-8 and ZU-301 for CO_2 over HCO_3^- and CO_3^{2-}, allowed these MOFs to adsorb only the dissolved gaseous CO_2 present in the sample and the little that could be formed by tipping the complex equilibria in play in the samples.
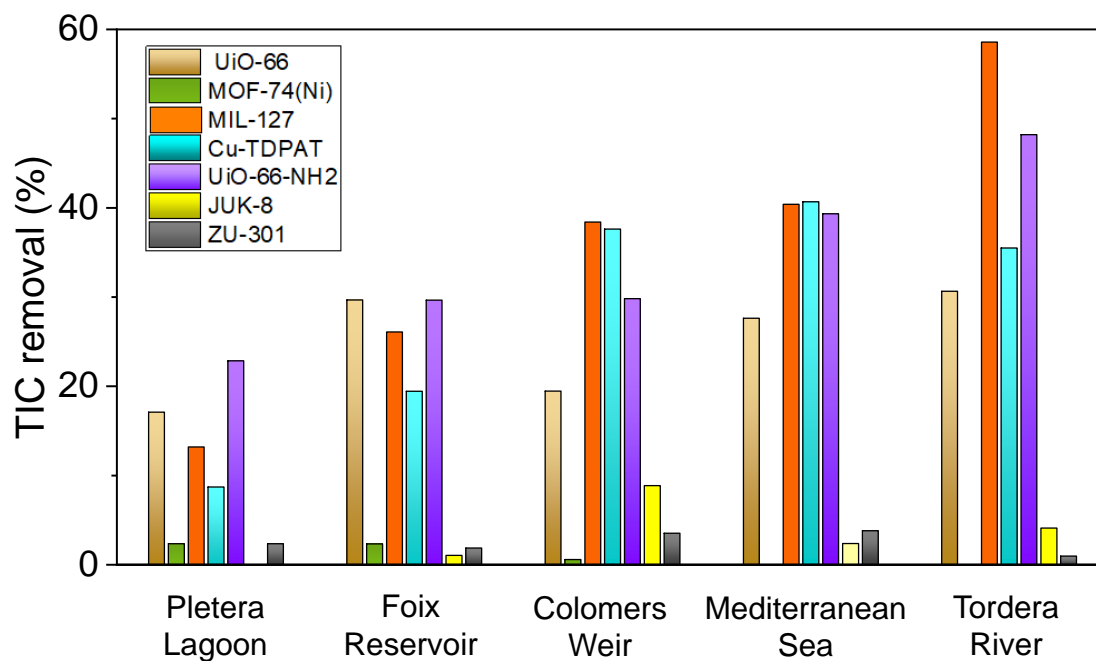
Figure 5.10. Adsorption capacity of MOFs in the different real-world water samples.

Table 5.3. Uptake of carbon species from real-world water samples. The removal efficiency is given in percent %. N.D. – not detectable.

Material	Removal efficiency in %				
	Pletera Lagoon	Foix Reservoir	Colomers Weir	Mediterranean Sea	Tordera River
UiO-66	17.10	29.66	19.45	27.62	30.64
MOF-74(Ni)	2.34	2.33	0.57	N.D.	N.D.
MIL-127	13.20	26.09	38.41	40.40	58.58
Cu-TDPAT	8.69	19.43	37.61	40.67	35.50
UiO-66- NH₂	22.84	29.65	29.81	39.33	48.19
JUK-8	N.D.	1.05	8.86	2.37	4.12
ZU-301	2.34	1.86	3.53	3.79	0.96
Alkalinity	7.086	4.636	3.072	2.756	1.201
Electrical Conductivity	43000	1187	533	52100	219

5.4 CONCLUSIONS

In this chapter, the removal of carbon dioxide and the generated species from water has been studied in order to address a worldwide problem caused by the ocean acidification and worsened by climate changed. The design of adsorbents for water remediation is not trivial due to the many and different requirements of the materials; although some MOFs have shown good adsorption capacities in aqueous environments, they are still far from the best scenario. However, this preliminary study on carbon dioxide and carbonate ions adsorption from water with MOFs allows us to highlight the key contributing properties and to lay a few points for the future development of the field. Structural stability of the MOFs is, clearly, a crucial prerequisite for this application. The materials must be stable not only in pure water, but also in aqueous solutions with diverse chemical composition at high concentration of ions and in a range of different pH values. In addition, the material pores should have sufficiently large apertures to allow a good diffusion of the different species through them. Moreover, they should present high affinity not only for carbon dioxide, but also for carbonates, the main specie present in natural water environments, as this leads to higher adsorption efficiency. In this regard, both the basic groups in UiO-66-NH_2 and open metal sites seems to contribute substantially to the material TIC adsorption, although not all metal sites appear to have the same effect.

5.5 REFERENCES

(1) Boyd, P. G.; Chidambaram, A.; García-Díez, E.; Ireland, C. P.; Daff, T. D.; Bounds, R.; Gładysiak, A.; Schouwink, P.; Moosavi, S. M.; Maroto-Valer, M. M.; Reimer, J. A.; Navarro, J. A. R.; Woo, T. K.; Garcia, S.; Stylianou, K. C.; Smit, B. *Nature* **2019**, *576*, 253–256.

(2) MacDowell, N.; Florin, N.; Buchard, A.; Hallett, J.; Galindo, A.; Jackson, G.; Adjiman, C. S.; Williams, C. K.; Shah, N.; Fennell, P. *Energy Environ. Sci.* **2010**, *3*, 1645.

(3) Mikkelsen, M.; Jørgensen, M.; Krebs, F. C. *Energy Environ. Sci.* **2010**, *3*, 43–81.

(4) Zhang, L.; Zhao, Z.-J.; Gong, J. *Angew. Chem. Int. Ed.* **2017**, *56*, 11326–11353.

(5) Intergovernmental Panel on Climate Change (ipcc). Carbon Dioxide: Projected emissions and concentrations.

(6) Gruber, N.; Clement, D.; Carter, B. R.; Feely, R. A.; van Heuven, S.; Hoppema, M.; Ishii, M.; Key, R. M.; Kozyr, A.; Lauvset, S. K.; Lo Monaco, C.; Mathis, J. T.; Murata, A.; Olsen, A.; Perez, F. F.; Sabine, C. L.; Tanhua, T.; Wanninkhof, R. *Science* **2019**, *363*, 1193–1199.

(7) McDonald, T. M.; Mason, J. A.; Kong, X.; Bloch, E. D.; Gygi, D.; Dani, A.; Crocellà, V.; Giordanino, F.; Odoh, S. O.; Drisdell, W. S.; Vlaisavljevich, B.; Dzubak, A. L.; Poloni, R.; Schnell, S. K.; Planas, N.; Lee, K.; Pascal, T.; Wan, L. F.; Prendergast, D.; Neaton, J. B.; Smit, B.; Kortright, J. B.; Gagliardi, L.; Bordiga, S.; Reimer, J. A.; Long, J. R. *Nature* **2015**, *519*, 303–308.

(8) Bronselaer, B.; Zanna, L. *Nature* **2020**, *584*, 227–233.

(9) Hurd, C. L.; Lenton, A.; Tilbrook, B.; Boyd, P. W. *Nat. Clim. Change* **2018**, *8*, 686–694.

(10) Intergovernmental Panel on Climate Change (ipcc). Climate Change 2013: The Physical Science Basis. Contribution of Working Group I to the Fifth Assessment Report of the Intergovernmental Panel on Climate Change.

(11) Doney, S. C.; Fabry, V. J.; Feely, R. A.; Kleypas, J. A. *Annu. Rev. Mar. Science* **2009**, *1*, 169–192.

(12) Feely, R. A.; Doney, S. C. *Limnol. Oceanogr. e-Lect.* **2011**.

(13) Orr, J. C.; Fabry, V. J.; Aumont, O.; Bopp, L.; Doney, S. C.; Feely, R. A.; Gnanadesikan, A.; Gruber, N.; Ishida, A.; Joos, F.; Key, R. M.; Lindsay, K.; Maier-Reimer, E.; Matear, R.; Monfray, P.; Mouchet, A.; Najjar, R. G.; Plattner, G.-K.; Rodgers, K. B.; Sabine, C. L.; Sarmiento, J. L.; Schlitzer, R.; Slater, R. D.; Totterdell, I. J.; Weirig, M.-F.; Yamanaka, Y.; Yool, A. *Nature* **2005**, *437*, 681–686.

(14) Pelejero, C.; Calvo, E.; Hoegh-Guldberg, O. *Trends Ecol. Evol.* **2010**, *25*, 332–344.

(15) Boot-Handford, M. E.; Abanades, J. C.; Anthony, E. J.; Blunt, M. J.; Brandani, S.; Mac Dowell, N.; Fernández, J. R.; Ferrari, M.-C.; Gross, R.; Hallett, J. P.; Haszeldine, R. S.; Heptonstall, P.; Lyngfelt, A.; Makuch, Z.; Mangano, E.; Porter, R. T. J.; Pourkashanian, M.; Rochelle, G. T.; Shah, N.; Yao, J. G.; Fennell, P. S. *Energy Environ. Sci.* **2014**, *7*, 130–189.

(16) Oschatz, M.; Antonietti, M. *Energy Environ. Sci.* **2018**, *11*, 57–70.

(17) Flaig, R. W.; Osborn Popp, T. M.; Fracaroli, A. M.; Kapustin, E. A.; Kalmutzki, M. J.; Altamimi, R. M.; Fathieh, F.; Reimer, J. A.; Yaghi, O. M. *J. Am. Chem. Soc.* **2017**, *139*, 12125–12128.

(18) Sumida, K.; Rogow, D. L.; Mason, J. A.; McDonald, T. M.; Bloch, E. D.; Herm, Z. R.; Bae, T.-H.; Long, J. R. *Chem. Rev.* **2012**, *112*, 724–781.

(19) Yu, J.; Xie, L.-H.; Li, J.-R.; Ma, Y.; Seminario, J. M.; Balbuena, P. B. *Chem. Rev.* **2017**, *117*, 9674–9754.

(20) Banerjee, R.; Phan, A.; Wang, B.; Knobler, C.; Furukawa, H.; O'Keeffe, M.; Yaghi, O. M. *Science* **2008**, *319*, 939–943.

(21) Chen, K.-J.; Yang, Q.-Y.; Sen, S.; Madden, D. G.; Kumar, A.; Pham, T.; Forrest, K. A.; Hosono, N.; Space, B.; Kitagawa, S.; Zaworotko, M. J. *Angew. Chem. Int. Ed.* **2018**, *57*, 3332–3336.

(22) Kim, E. J.; Siegelman, R. L.; Jiang, H. Z. H.; Forse, A. C.; Lee, J.-H.; Martell, J. D.; Milner, P. J.; Falkowski, J. M.; Neaton, J. B.; Reimer, J. A.; Weston, S. C.; Long, J. R. *Science* **2020**, *369*, 392–396.

(23) Lin, L.-C.; Kim, J.; Kong, X.; Scott, E.; McDonald, T. M.; Long, J. R.; Reimer, J. A.; Smit, B. *Angew. Chem. Int. Ed.* **2013**, *52*, 4410–4413.

(24) Chae, H. K.; Siberio-Pérez, D. Y.; Kim, J.; Go, Y.; Eddaoudi, M.; Matzger, A. J.; O'Keeffe, M.; Yaghi, O. M. *Nature* **2004**, *427*, 523–527.

(25) Furukawa, H.; Ko, N.; Go, Y. B.; Aratani, N.; Choi, S. B.; Choi, E.; Yazaydin, A. O.; Snurr, R. Q.; O'Keeffe, M.; Kim, J.; Yaghi, O. M. *Science* **2010**, *329*, 424–428.

(26) Hirai, K.; Furukawa, S.; Kondo, M.; Uehara, H.; Sakata, O.; Kitagawa, S. *Angew. Chem. Int. Ed.* **2011**, *50*, 8057–8061.

(27) Wang, K.; Feng, D.; Liu, T.-F.; Su, J.; Yuan, S.; Chen, Y.-P.; Bosch, M.; Zou, X.; Zhou, H.-C. *J. Am. Chem. Soc.* **2014**, *136*, 13983–13986.

(28) Mukherjee, S.; Sensharma, D.; Qazvini, O. T.; Dutta, S.; Macreadie, L. K.; Ghosh, S. K.; Babarao, R. *Coord. Chem. Rev.* **2021**, *437*, 213852.

(29) Rieth, A. J.; Wright, A. M.; Dincă, M. *Nat. Rev. Mater.* **2019**, *4*, 708–725.

(30) Takashima, Y.; Martínez, V. M.; Furukawa, S.; Kondo, M.; Shimomura, S.; Uehara, H.; Nakahama, M.; Sugimoto, K.; Kitagawa, S. *Nat. Commun.* **2011**, *2*, 168.

(31) Jaramillo, D. E.; Jiang, H. Z. H.; Evans, H. A.; Chakraborty, R.; Furukawa, H.; Brown, C. M.; Head-Gordon, M.; Long, J. R. *J. Am. Chem. Soc.* **2021**, *143*, 6248–6256.

(32) Mason, J. A.; Oktawiec, J.; Taylor, M. K.; Hudson, M. R.; Rodriguez, J.; Bachman, J. E.; Gonzalez, M. I.; Cervellino, A.; Guagliardi, A.; Brown, C. M.; Llewellyn, P. L.; Masciocchi, N.; Long, J. R. *Nature* **2015**, *527*, 357–361.

(33) Ding, M.; Flaig, R. W.; Jiang, H.-L.; Yaghi, O. M. *Chem. Soc. Rev.* **2019**, *48*, 2783–2828.

(34) Rojas, S.; Horcajada, P. *Chem. Rev.* **2020**, *120*, 8378–8415.

(35) Zhu, L.; Sheng, D.; Xu, C.; Dai, X.; Silver, M. A.; Li, J.; Li, P.; Wang, Y.; Wang, Y.; Chen, L.; Xiao, C.; Chen, J.; Zhou, R.; Zhang, C.; Farha, O. K.; Chai, Z.; Albrecht-Schmitt, T. E.; Wang, S. *J. Am. Chem. Soc.* **2017**, *139*, 14873–14876.

(36) Lin, S.; Zhao, Y.; Yun, Y.-S. *ACS Appl. Mater. Interfaces* **2018**, *10*, 28076–28085.

(37) Wongsakulphasatch, S.; Kiatkittipong, W.; Saupsor, J.; Chaiwiseshphol, J.; Piroonlerkgul, P.; Parasuk, V.; Assabumrungrat, S. *Greenhouse Gas Sci. Technol.* **2017**, *7*, 383–394.

(38) Li, B.; Zhang, Z.; Li, Y.; Yao, K.; Zhu, Y.; Deng, Z.; Yang, F.; Zhou, X.; Li, G.; Wu, H.; Nijem, N.; Chabal, Y. J.; Lai, Z.; Han, Y.; Shi, Z.; Feng, S.; Li, J. *Angew. Chem. Int. Ed.* **2012**, *124*, 1441–1444.

(39) Caskey, S. R.; Wong-Foy, A. G.; Matzger, A. J. *J. Am. Chem. Soc.* **2008**, *130*, 10870–10871.

(40) Koutsianos, A.; Kazimierska, E.; Barron, A. R.; Taddei, M.; Andreoli, E. *Dalton Trans.* **2019**, *48*, 3349–3359.

(41) Huang, A.; Wan, L.; Caro, J. *Mater. Res. Bull.* **2018**, *98*, 308–313.

(42) Roztocki, K.; Rauche, M.; Bon, V.; Kaskel, S.; Brunner, E.; Matoga, D. *ACS Appl. Mater. Interfaces* **2021**, *13*, 28503–28513.

(43) Yu, C.; Ding, Q.; Hu, J.; Wang, Q.; Cui, X.; Xing, H. *Chem. Eng. J.* **2021**, *405*, 126937.

(44) Øien, S.; Wragg, D.; Reinsch, H.; Svelle, S.; Bordiga, S.; Lamberti, C.; Lillerud, K. P. *Cryst. Growth Des.* **2014**, *14*, 5370–5372.

(45) Wong-Ng, W.; Kaduk, J. A.; Wu, H.; Suchomel, M. *Powder Diffr.* **2012**, *27*, 256–262.

(46) Drake, H. F.; Day, G. S.; Vali, S. W.; Xiao, Z.; Banerjee, S.; Li, J.; Joseph, E. A.; Kuszynski, J. E.; Perry, Z. T.; Kirchon, A.; Ozdemir, O. K.; Lindahl, P. A.; Zhou, H.-C. *Chem. Commun.* **2019**, *55*, 12769–12772.

(47) Trickett, C. A.; Gagnon, K. J.; Lee, S.; Gándara, F.; Bürgi, H.-B.; Yaghi, O. M. *Angew. Chem. Int. Ed.* **2015**, *54*, 11162–11167.

(48) Chevreau, H.; Permyakova, A.; Nouar, F.; Fabry, P.; Livage, C.; Ragon, F.; Garcia-Marquez, A.; Devic, T.; Steunou, N.; Serre, C.; Horcajada, P. *CrystEngComm* **2016**, *18*, 4094–4101.

(49) Fuchs, A.; Mannhardt, P.; Hirschle, P.; Wang, H.; Zaytseva, I.; Ji, Z.; Yaghi, O.; Wuttke, S.; Ploetz, E. *Adv. Mater.* **2022**, *34*, e2104530.

(50) Schrimpf, W.; Barth, A.; Hendrix, J.; Lamb, D. C. *Biophys. J.* **2018**, *114*, 1518–1528.

(51) Schneider, C. A.; Rasband, W. S.; Eliceiri, K. W. *Nat. Methods* **2012**, *9*, 671–675.

(52) Pedersen, O.; Colmer, T. D.; Sand-Jensen, K. *Front. Plant Sci.* **2013**, *4*, 140.

(53) Jia, M.; Su, J.; Su, P.; Li, W. *Nanoscale* **2021**, *13*, 5069–5076.

(54) Kandiah, M.; Nilsen, M. H.; Usseglio, S.; Jakobsen, S.; Olsbye, U.; Tilset, M.; Larabi, C.; Quadrelli, E. A.; Bonino, F.; Lillerud, K. P. *Chem. Mater.* **2010**, *22*, 6632–6640.

(55) Li, J.; Guo, J.; Dai, H. *Sci. Adv.* **2022**, *8*, eabo0399.

(56) Wang, X.; Bürgi, T. *Angew. Chem. Int. Ed.* **2021**, *60*, 7860–7865.

(57) Saussey, J.; Lavalley, J.-C.; Bovet, C. *J. Chem. Soc., Dalton Transac.* **1982**, *78*, 1457.

(58) Buchholz, M.; Weidler, P. G.; Bebensee, F.; Nefedov, A.; Wöll, C. *Phys. Chem. Chem. Phys.* **2014**, *16*, 1672–1678.

(59) Pokrovski, K.; Jung, K. T.; Bell, A. T. *Langmuir* **2001**, *17*, 4297–4303.

6

Chapter 6

Conclusions and future trends

6.1 CONCLUSIONS

In this thesis, the use of Metal-Organic Frameworks as adsorption platforms for solution adsorption processes has been assessed from the point of view of their performance towards different adsorbates (organic and inorganic). Furthermore, a new characterization approach was established in order to study these adsorption process into the porous scaffold of MOFs. As a result of all the work done, the following main conclusions can be drawn:

- The synthesis parameters have been proven to be crucial in order to control the size and shape of MOF particles. Moreover, the importance of determining the size of the particles using different techniques (SEM, DLS) that measure in different states, e.g. solid and liquid, has been highlighted. It has been shown that in most cases the size of wet (DLS) or dry (SEM) forms of the particles do not match attributing the difference to the agglomeration of the particles and therefore, this has to be considered for the targeted MOF nanoparticle application.

- The suitability of MOFs for adsorption processes in solution has been demonstrated. In detail, adsorption experiments have been performed in ethanol and water, two of the most common solvents. Furthermore, inorganic and organic species have been used as target molecules in order to demonstrate the great versatility of MOF as sorbent materials.

- A new characterization technique, named Magnetic Sustentation has been established. Theoretical equations have been developed and the first experimental setting has been done with MIL-88A(Fe), MOF-74(Cu, Co) and ZIF-67(Co). In detail, the experiments have been performed in water and ethanol proving a great example of the opportunities afforded by the technique as it can be used with a wide variety of sorbents and/or solvents.

- The Magnetic Sustentation technique opens a new possibility for the characterization of paramagnetic MOFs for adsorption processes in solution. It offers direct and quick measurements and is independent towards the chemical nature of the analyte, which is often difficult to quantify with traditional techniques. In line with this, adsorption isotherms curves have been determined for DMSO, DMF and acetonitrile. Concretely, it was possible to prepare the isotherms for acetonitrile, which was not possible with UV-VIS spectroscopy.

- Taking advantage of the paramagnetic and flexible nature of MIL-88A(Fe), the removal of alcohols from aqueous solutions has been tested as an alternative to more traditional techniques, where high-energy demanding processes are needed. For that, short-chain aliphatic alcohols have been selected: methanol ethanol, n-propanol, isopropyl alcohol, n-butyl alcohol, sec-butyl alcohol, isobutyl alcohol and *tert*-butyl alcohol.

- MOF powder has been used for testing the adsorption capacity of single alcohols aqueous solutions, as well as to perform competitive studies. Single-component alcohol adsorption experiments demonstrated that the adsorption capacity of MIL-88A(Fe) is higher for smaller molecules (methanol), while more modest values are shown for branched alcohols. Theoretical studies corroborate that the flexibility of the framework is responsible for this, allowing the diffusivity of smaller molecules while hindering the diffusion of branched alcohols. In fact, it has been found that there is a dependence of the adsorbed mass percentage with the linear alcohols with respect to their molecular volume. This fact has been attributed to a better occupation of the space for smaller molecules, but a cross section dependence for the branched alcohols, related to a diffusion controlled adsorption process.

- On the contrary, competitive adsorption studies have shown a clear preference towards more hydrophobic molecules (isopropyl alcohol or *tert*-butyl alcohol) over methanol.

- In addition, PVDF@MIL-88A(Fe) membranes have been successfully prepared to improve the handling and applicability of the material. It has been proven that the MOF content greatly impacts the porosity of the membrane, where the 20 wt% MOF-loaded membranes show the highest porosity.

- All the prepared membranes have been tested for the adsorption of low-concentration alcohols (0.1 wt%). The experiments have shown that the 20 wt% PVDF@MIL-88A(Fe) membrane outperforms, in agreement with the highest porosity. Overall, the synergetic effect between the polymeric matrix and the porous material has been demonstrated with adsorption values far above the expected ones based on the performance of each component alone.

- Carbon dioxide and generated carbonate ions capture from water has been studied for the first time with different MOFs. For that, MOFs with high adsorption capacity for $CO_2(g)$ containing open-metal sites, flexible structure or basic functional groups (amines) and high selective MOFs have been chosen.

- Taking into account the speciation of carbon dioxide at different pH values, all MOFs have been tested at pH 2, 6.3, 8.0 and 10.0, where the main species are CO_2, HCO_3^-/CO_2, HCO_3^- and HCO_3^-/ CO_3^{2-}, respectively. Moreover, real-world water samples were employed to gage the material behaviour in more complex environments.

- The preliminary study on carbon dioxide and carbonate ions adsorption from water allows us to highlight the key contributing properties and to lay a few points for the future development of the field such as the stuctural stability, adecuate pore size or affinity for carbonates, which is the main specie present in natural water environments.

6.2 FUTURE TRENDS

The advances made throughout this work have opened the way for developing a new characterization technique as an alternative to more traditional ones. The need for reproducible and well-characterized synthesis protocols has also been highlighted, in addition to the great potential that these materials present for the adsorption of organic and inorganic species in solution.

In order to expand our research in the near future, some of the points that we have considered of great interest are listed below:

- In the short term and related to the Magnetic Sustentation technique that has been developed, one of the aspects to improve would be the experimental setup. In order to facilitate the determination of the critical magnetic field the possibility of including some image or video device that monitors the experiment in real time should be considered.

- In addition to this, it would be of great benefit to be able to control the temperature of the vial in which the measurements are performed. In this way, possible heating effects induced by the applied magnetic field of the electromagnet could be avoided, as well as expanding the possibilities offered by the technique, since the viscosity of the solvent can be altered with the temperature of the vial.

- Regarding the flexible nature of MIL-88A(Fe), it would be interesting to study the ability to deform the structure using longer-chain alcohols or aromatics, such as pentanol or phenol, respectively. Besides, it would be crucial to go a step further in the theoretical studies to take into account the flexibility of the structure or the alcohol/water mixture.

- Among the innumerable possibilities of preparing polymer@MOF membranes, this work has studied a narrow window: PVDF was chosen as the polymeric matrix and the thick of the membrane was fixed at 250 μm. Considering other polymers or changing the thickness of the membrane would be of great interest in order to see if the adsorption of alcohols from water could be enhanced.

- The study of the capture of carbon dioxide and carbonates from water has been a pioneer study in the area and therefore, there is still a long way to go. Among other things, Reticular Chemistry could be used with the aim of designing materials with greater stability at different pH values, the appropriate pore size to increase the selectivity of CO_2 with respect to other species (*i.e.* water) or including adequate functional groups to be able to increase the adsorption capacity. The latter could be performed using linkers with the desired functional groups or making post-synthetic modifications.

- Furthermore, there is the possibility of assembling MOFs with different properties, *i.e.* high adsorption capacity and selectivity, in hierarchical structures, in order to study the possible synergy between them and thus, expand the field of study.

Annex

Annex

Curriculum Vitae and contributions

A.1. Education

2022-2023	Master's Degree in Teaching in Secondary Education (UEU)
2019-2023	PhD, "A study of Metal-Organic Framework sorption phenomena in solution" (BCMaterials and UPV/EHU)
2018-2019	Master in New Materials (UPV/EHU and UC)
2014-2018	Bachelor's Degree in Chemistry

A.2. Contribution to conferences

- 8th International Conference on Metal-Organic Framework Compounds. Dresden, Germany (4th-7th of September, 2022) – Poster Contribution.
  A rapid and direct method to sense the capture of pollutants in water by magnetic MOFs.
  N. Barroso, J. Andreo, O. Castillo and S. Wuttke.

- B&B 2021: BCMaterials – University of Bourdeaux symposium on bilateral cooperation in advanced materials and applications. Leioa, Spain – Online (22th of June, 2021) – Poster Contribution.
  Synthesis of MOFs and their synergistic effect on hierarchical framework materials.
  N. Barroso, J. Andreo, O. Castillo and S. Wuttke.

- 2nd International School on Porous Materials: MOFschool2021. Como, Italy – Online (21st-25th of June, 2021) – Poster Contribution.
  Hierarchical Framework Materials for CO_2 capture.
  N. Barroso, J. Andreo, Aleksander Ejsmont, Joanna Goscianska, O. Castillo and S. Wuttke.

A3. Training courses

- Fundamentos para la caracterización de materiales mediante técnicas de difracción de Rayos X (muestra policristalina y monocristal) y Fluorescencia de Rayos X. Leioa, Spain (28th of March to 1st of April, 2022). 20 hours.
- Gestión de Riesgo Químico. Prevor – webinar (14th of January, 2022). 2 hours.
- Introducción a la Microscopía Electrónica: Fundamentos, Accesorios y Aplicaciones. IESMAT S.A. - webinar (June 11th 2021). 1 hour.
- Buenas Prácticas en el Laboratorio (I): Prevención de Riesgos. Leioa, Spain – Online (11th of January to 31st of March, 2021). 25 hours.
- Buenas Prácticas en el Laboratorio (II): Gestión de Residuos. Leioa, Spain – Online (23rd of February to 24th of March, 2020). 25 hours.
- 5th edition of the course Structural analysis from powder diffraction data using FulProf Suite of programs – Level: Beginners. Miñano, Spain (29th-30th of October, 2019).

A.4. Publications

Part of the Thesis

- Barroso, N.; Andreo, J.; Beobide, G.; Castillo, O.; Luque, A.; Perez-Yáñez, S.; Wuttke, S. Magnetic Sustentation as an adsorption characterization technique for paramagnetic metal-organic frameworks. *Commun. Chem.* **2023**, 6(4), 1-9. DOI: 10.1038/s42004-022-00799-w.
- Barroso, N.; Dutta, S.; Andreo, J.; Beobide, G.; Castillo, O.; Luque, A.; Perez-Yáñez, S.; Wuttke, S. Guest-induced breathing mediated size- and shape-selective alcohol recovery from water by MIL-88A(Fe). *Submitted*.
- Barroso, N.; Andreo, J.; Dutta, S.; Ejsmont, A.; Baumgartner, B.; Jankowska, A.; Titteld, J.; Marcé, R.; Frankowski, M.; Weckhuysen, B.; Ploetz, E.; Goscianska, J.; Wuttke, S. MOFs for the capture of dissolved CO_2 and generated carbonate ions from water. To be *submitted*.

Other Publications

- Maiz-Fernández, S.; <u>Barroso, N.</u>; Pérez-Álvarez, L.; Silván, U.; Vilas-Vilela, J. L.; Lanceros-Méndez, S. 3D printable self-healing hyaluronic acid/chitosan polycomplex hydrogels with drug release capability. *Int. J. Biol. Macromol.* **2021**, 188, 820-832. DOI: 10.1016/j.ijbiomac.2021.08.022.

- <u>Barroso, N.</u>; Guaresti, O.; Pérez-Álvarez, L.; Ruiz.Rubio, L; Gabilondo, N.; Vilas-Vilela, J. L. Self-healable hyaluronic acid/chitosan polyelectrolyte complex hydrogels and multilayers. *Eur. Polym. J.* **2019**, 120. DOI: 10.1016/j.eurpolymj.2019.109268.

- <u>Barroso, N.</u>; Moreno, M. I.; Pérez-Álvarez, L. Gainazal-topografiak naturan duen eragina. *EKAIA*, **2019**, 35. DOI: 10.1387/ekaia.19722

A.4. Research Stays

- Research stay at Ludwig Maximilians Universität, Munich from the 25th of September to the 10th of October, 2021.